

## Two Blocking Sites of Amino-Adamantane Derivatives in Open *N*-Methyl-D-Aspartate Channels

Alexander Sobolevsky and Sergey Koshelev

Institute of General Pathology and Pathophysiology, 125315 Moscow, Russia

**ABSTRACT** Using whole-cell patch-clamp techniques, we studied the blockade of open *N*-methyl-D-aspartate (NMDA) channels by amino-adamantane derivatives (AADs) in rat hippocampal neurons acutely isolated by the vibrodissociation method. The rapid concentration-jump technique was used to replace superfusion solutions. A kinetic analysis of the interaction of AAD with open NMDA channels revealed fast and slow components of their blockade and recovery. Mathematical modeling showed that these kinetic components are evidence for two distinct blocking sites of AADs in open NMDA channels. A comparative analysis of different simplest models led us to conclude that these AAD blocking sites can be simultaneously occupied by two blocker molecules. The voltage dependence of the AAD block suggested that both sites were located deep in the channel pore.

### INTRODUCTION

Earlier it was shown that the interaction of certain compounds with *N*-methyl-D-aspartate (NMDA) channels is complex and cannot be described by a simple one binding site model. The existence of two blocking sites in NMDA channels was established for long-chain adamantane derivatives (Antonov and Johnson, 1996) and *n*-alkyl diamines (Subramaniam et al., 1994). Intracellular and extracellular  $Mg^{2+}$  ions blocked the channels interacting with different binding sites (Johnson and Ascher, 1990). Mutagenesis experiments on NMDA receptor subunits showed that  $Ca^{2+}$  and  $Mg^{2+}$  were likely to bind to multiple sites within the pore that were contributed by both the NMDAR1 and NR2 subunits (MacBain and Mayer, 1994). Spermine and spermidine were suggested to act at distinct sites on NMDA receptors, thereby producing potentiation and block (Rock and MacDonald, 1992; Benveniste and Mayer, 1993; Aranedo et al., 1993). The high value of the Hill coefficient ( $n_{Hill} > 1$ ) characterizing the concentration dependence of the block by tetraalkylammonium derivatives (Koshelev and Khodorov, 1992) and bepridil (Sobolevsky et al., 1997) can be considered as evidence in favor of the existence of more than one blocking site for these compounds in NMDA channels. Antonov and Johnson (1996) found that the apparent fractional electrical depth,  $\delta$ , of the site at which IEM-1754 and IEM-1460 bound to the channel was different for two different ranges of the membrane potential. These different values of  $\delta$  allowed them to hypothesize the existence of deep and shallow blocking sites for these drugs in NMDA channels. The same assumption could be made

for  $Mg^{2+}$ , which demonstrated high values of  $\delta$ : 1.0 (Ascher and Nowak, 1988) and 0.8 (Jahr and Stevens, 1990).

Both parameters,  $n_{Hill}$  and  $\delta$ , proved to have high values for amino-adamantane derivatives (AADs) used in the present study. This fact led us to analyze the AAD-induced kinetics of open channels to verify the hypothesis about the multisite interaction of these compounds with NMDA channels. We actually revealed fast and slow components of channel blockade and recovery, which was in agreement with the two components of recovery from block by memantine and amantadine observed earlier by Johnson et al. (1995). The kinetic analysis described in the present study allowed us to conclude that the AAD-induced block of open NMDA channels was mediated by two distinct blocking sites. These sites are located in the depth of the channel pore and can be simultaneously occupied by two blocking molecules.

### MATERIALS AND METHODS

Pyramidal neurons were acutely isolated from the CA-1 region of rat hippocampus by "vibrodissociation techniques" (Vorobjev, 1991). The experiments were begun not earlier than after 3 h of incubation of the hippocampal slices in a solution containing (in mM) 124 NaCl, 3 KCl, 1.4  $CaCl_2$ , 2  $MgCl_2$ , 10 glucose, 26  $NaHCO_3$ . The solution was bubbled with carbogen at 32°C. During the whole period of isolation and current recording, nerve cells were washed with a  $Mg^{2+}$ -free solution (in mM): 140 NaCl, 5 KCl, 2  $CaCl_2$ , 15 glucose, 10 HEPES (pH 7.3). Fast replacement of superfusion solutions ( $\tau < 30$  ms) was achieved using the concentration-jump technique (Benveniste et al., 1990b; Vorobjev, 1991). The currents were recorded at 18°C in the whole-cell configuration, using micropipettes made from Pyrex tubes and filled with an "intracellular" solution (in mM): 140 CsF; 4 NaCl; 10 HEPES (pH 7.2). Electric resistance of filled micropipettes was 3–7 M $\Omega$ . Analog current signals were digitized at 1-kHz frequency.

Statistical analysis was performed using the scientific and technical graphics computer program Microcal Origin (version 3.5 for Windows). All of the data presented are mean  $\pm$  SE; comparisons were made using a paired Student's *t*-test.

Kinetic models used to simulate the AAD action were based on the conventional rate theory and used independent forward and reverse rate constants to simultaneously solve first-order differential equations repre-

Received for publication 10 July 1997 and in final form 20 November 1997.

Address reprint requests to Dr. Sergey Koshelev, Institute of General Pathology and Pathophysiology, Baltiyskaya str. 8, 125315 Moscow, Russia. Tel.: 7-095-155-47-42; Fax: 7-095-151-04-21; E-mail: rans@rans.msk.ru.

© 1998 by the Biophysical Society

0006-3495/98/03/1305/15 \$2.00

sensing the transitions between all possible states of the channel. The rate constants,  $k_i$  ( $i = 1, \dots, 4$ ), were calculated by the method described in Appendix B with the help of Mathcad (version 5.0). Differential equations were solved numerically by using the algorithm analogous to that described previously (Benveniste et al., 1990a).

Amino-adamantane derivatives were synthesized by MERZ (Eckenhäuser Landstr. 100–104, 60318 Frankfurt-am-Main, Germany) (see Table 1).

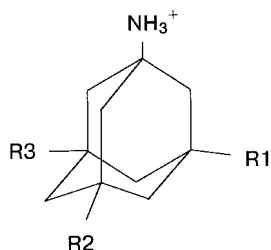
## RESULTS

### Concentration dependence

Ionic currents through NMDA channels were elicited by fast application of 100  $\mu\text{M}$  aspartate (ASP) in a  $\text{Mg}^{2+}$ -free, 3  $\mu\text{M}$  glycine-containing solution. At a holding potential of  $-100$  mV, ASP induced an inward current which, after its initial fast rise ( $\tau < 30$  ms) up to the value,  $I_0$ , indicating the opening of NMDA channels, decreased gradually ( $\tau_D = 449 \pm 27$  ms,  $n = 21$ ) down to a certain plateau level,  $I_S$  (Fig. 1, *inset*). Such a current decay under continued action of the agonist is a result of desensitization of the receptor-channel complex. The fraction of desensitized channels,  $d = 1 - I_S/I_0$ , varied between the cells in a wide range of 0.08 to 0.75 and was, on the average,  $0.35 \pm 0.03$  ( $n = 23$ ). AAD inhibited the ASP-induced currents in a concentration-dependent manner. Two-second coapplications of ASP with the blocker were repeated every 3 s up to the point where the plateau current reached its stationary level ( $I_B$ ). Stationary current responses to MRZ 2/178 at different concentrations are shown in Fig. 1 A. The degree of the stationary open-channel block ( $I_B/I_S$ ) was fitted by the logistic equation (Fig. 1 B)

$$\frac{I_B}{I_S} = \frac{A}{1 + ([B]/IC_{50})^{n_{\text{Hill}}}} + \frac{1 - A}{1 + ([B]/IC_{50})^{n_{\text{Hill}}}} \quad (1)$$

**TABLE 1** Chemical structures of the amino-adamantane derivatives used in the study



Compound	R1	R2	R3
Memantine	-CH <sub>3</sub>	-CH <sub>3</sub>	-H
Amantadine	-H	-H	-H
MRZ 2/150	-C <sub>2</sub> H <sub>5</sub>	-C <sub>2</sub> H <sub>5</sub>	-H
MRZ 2/151	-C <sub>2</sub> H <sub>5</sub>	-CH <sub>3</sub>	-CH <sub>3</sub>
MRZ 2/177	-C <sub>3</sub> H <sub>7</sub> (-isopropyl)	-H	-H
MRZ 2/178	-C <sub>3</sub> H <sub>7</sub> (-propyl)	-H	-H
MRZ 2/184	-C <sub>6</sub> H <sub>5</sub>	-C <sub>2</sub> H <sub>5</sub>	-H
MRZ 2/239	-C <sub>3</sub> H <sub>7</sub> (-propyl)	-C <sub>3</sub> H <sub>7</sub> (-propyl)	-H
MRZ 2/372	-C <sub>3</sub> H <sub>7</sub> (-isopropyl)	-C <sub>3</sub> H <sub>7</sub> (-isopropyl)	-H
MRZ 2/457	-C <sub>2</sub> H <sub>5</sub>	-CH <sub>3</sub>	-H

where  $A = 0.79 \pm 0.01$  is the constant,  $IC_{50} = 8.7 \pm 0.8$   $\mu\text{M}$  and  $IC_{50}^1 = 0.010 \pm 0.004$   $\mu\text{M}$  are the apparent half-blocking concentrations,  $n_{\text{Hill}} = 1.26 \pm 0.08$  and  $n_{\text{Hill}}^1 = 1.83 \pm 0.99$  are the Hill coefficients, and  $[B]$  is the blocker concentration. The concentration dependencies of other AADs were studied at the blocker concentrations in approximately the following range: from 10 times lower to 10 times higher than  $IC_{50}$ . The degree of the stationary open-channel block ( $I_B/I_S$ ) for these blockers was fitted by the following logistic equation:

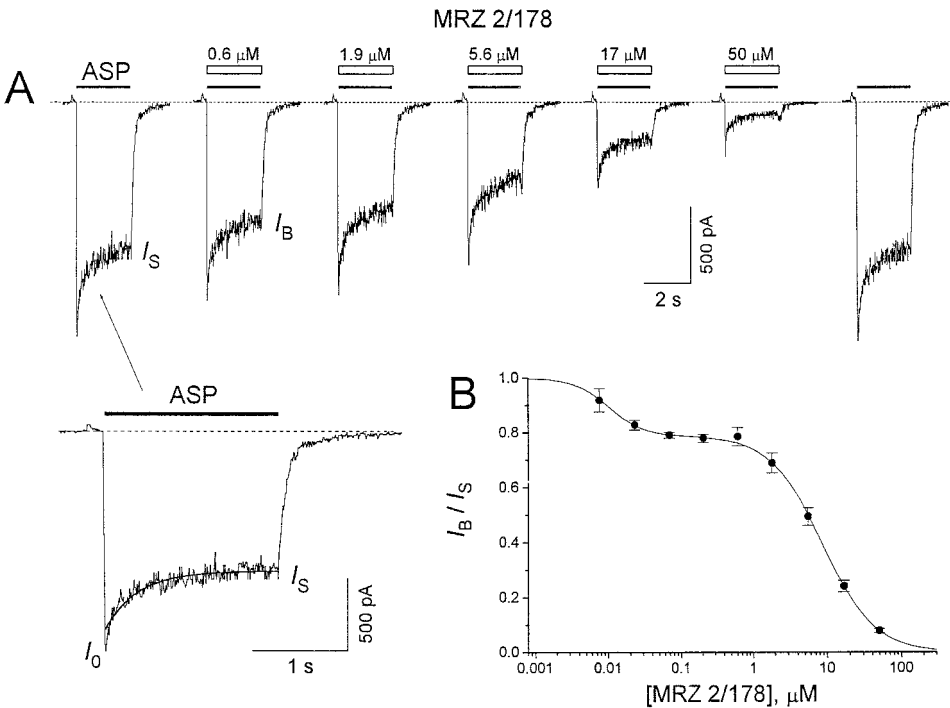
$$\frac{I_B}{I_S} = \frac{A}{1 + ([B]/IC_{50})^{n_{\text{Hill}}}} \quad (2)$$

The values of the fitting parameters  $A$ ,  $IC_{50}$ , and  $n_{\text{Hill}}$  are presented in Table 2. It is interesting that the value of  $A$  for all AADs proved to be lower than 1. Taking into account the heterogeneity of NMDA channels, this finding can be explained by the existence of another qualitatively different high-affinity binding of AAD to NMDA channels, due to which some of these channels become inactive or blocked.

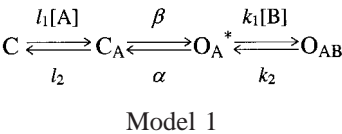
The kinetics of the open-channel blockade were studied by applying AAD in the continuous presence of ASP (100  $\mu\text{M}$ ). Only the cells with parameter  $d$  smaller than 0.33 were selected for these experiments. The current traces in response to 5-s applications of MRZ 2/178 at different concentrations are shown in Fig. 2. The blocking as well as the recovery kinetics of current responses were poorly fitted with single exponential functions (Fig. 2 A). In contrast, the fittings with double-exponential functions proved to be quite satisfactory (Fig. 2 B). The mean values of the amplitude of the fast component, fast and slow time constants, for the blocking ( $A_{\text{fast}}^{\text{on}}$ ,  $\tau_{\text{fast}}^{\text{on}}$ , and  $\tau_{\text{slow}}^{\text{on}}$ , respectively) and recovery kinetics ( $A_{\text{fast}}^{\text{off}}$ ,  $\tau_{\text{fast}}^{\text{off}}$ , and  $\tau_{\text{slow}}^{\text{off}}$ , respectively) of memantine (MEM) and MRZ 2/178 are shown in Fig. 3. Both time constants,  $\tau_{\text{fast}}^{\text{on}}$  and  $\tau_{\text{slow}}^{\text{on}}$ , decreased with the blocker concentration (Fig. 3, A and C), whereas  $\tau_{\text{fast}}^{\text{off}}$  and  $\tau_{\text{slow}}^{\text{off}}$  were practically concentration-independent (Fig. 3, B and D). The values of the amplitude of the fast component at any two different concentrations were significantly different:  $A_{\text{fast}}^{\text{on}}$  increased ( $p < 0.03$ ) and  $A_{\text{fast}}^{\text{off}}$  decreased with a rise in the blocker concentration ( $p < 0.0002$ ) (Fig. 3, E and F). For all AADs, in 67% of cells ( $n = 69$ )  $A_{\text{fast}}^{\text{off}}$  was equal to zero at high blocker concentrations. This fact provides direct evidence that the two components observed in the AAD-induced kinetics cannot be explained by the existence of two different populations of NMDA channels. Otherwise we would observe some fast component, even at infinitely high blocker concentrations. Moreover, two kinetic components were observed in the recovery kinetics of MEM and amantadine in homogeneous NR1a/NR2A and NR1a/NR2B populations of NMDA channels (Blanpied et al., 1997).

According to previous reports (Chen et al., 1992; Parsons et al., 1993, 1995), AADs are uncompetitive NMDA chan-

FIGURE 1 Concentration dependence of the stationary NMDA open-channel blockade by MRZ 2/178. MRZ 2/178 at different concentrations was coapplied with ASP (100  $\mu$ M) for 2 s at  $-100$  mV. (A) Stationary NMDA responses in the absence (*first and last traces*) and presence of MRZ 2/178 (0.6, 1.9, 5.6, 16.7, and 50  $\mu$ M). The inset shows the control response to ASP application on an expanded time scale. The current decrease from  $I_0$  to  $I_S$  was fitted with the exponent,  $\tau_D = 320$  ms. (B) Plateau current responses ( $I_B$ ) divided by the control plateau value ( $I_S$ ) were plotted against the MRZ 2/178 concentration. The solid line shows the fitting of the experimental data to Eq. 1. The fitting parameters are  $A = 0.79 \pm 0.01$ ,  $IC_{50} = 8.7 \pm 0.8$   $\mu$ M,  $n_{Hill} = 1.26 \pm 0.08$ ,  $IC_{50}^1 = 0.010 \pm 0.004$   $\mu$ M, and  $n_{Hill}^1 = 1.83 \pm 0.99$  ( $n = 6$ ).

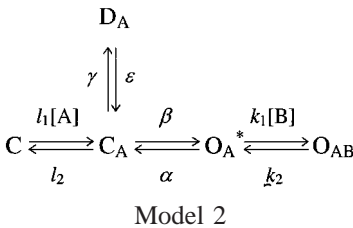


nel antagonists. Their action can be illustrated by a simple one-site model:



where C,  $C_A$ ,  $O_A$ , and  $O_{AB}$  represent the channel in closed agonist-unbound, closed agonist-bound, open, and open blocked states, respectively. The asterisk indicates the conducting state;  $l_1$ ,  $l_2$ ,  $\alpha$ ,  $\beta$ ,  $k_1$  and  $k_2$  are the kinetic constants.  $[A]$  is the agonist concentration. Model 1 is a priori unable to explain the existence of two components observed in the open-channel blocking kinetics, because the time constants of the transitions between the C,  $C_A$ , and  $O_A^*$  states (see Appendix A) are much higher than even fast time constants of the AAD-induced kinetics (Fig. 3, A–B).

Is it possible to explain the two components in the open-channel blocking kinetics without the addition to model 1 of another blocked state? Obviously it could be done by taking into account the existence of desensitized states of the channel. For the sake of simplicity, let us consider the model with only one desensitized state ( $D_A$ ):



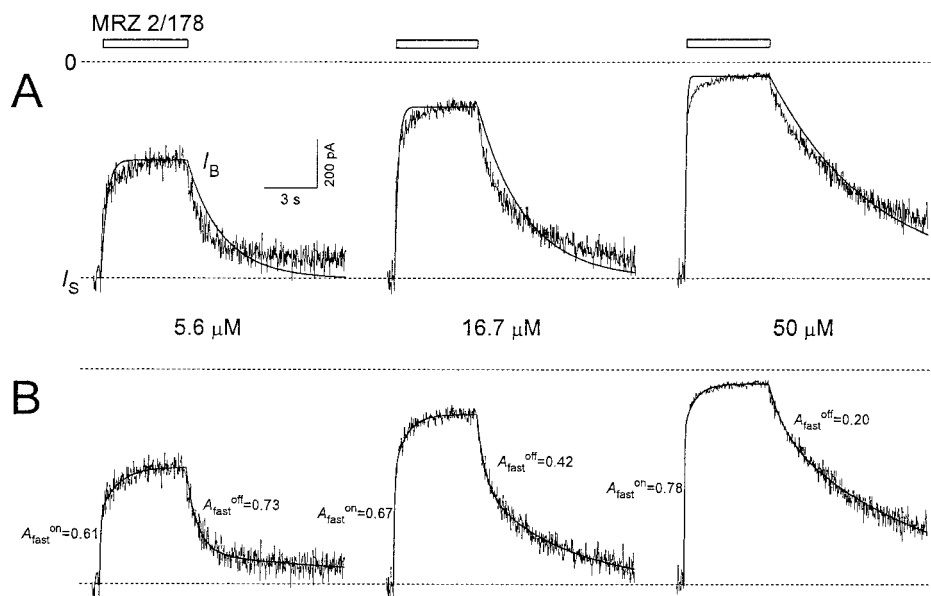
The kinetic constants  $l_1$ ,  $l_2$ ,  $\alpha$ , and  $\beta$  were determined by using the data from literature; and  $k_1$  and  $k_2$  were found

TABLE 2 The concentration and voltage-dependence parameters for AAD

Compound	Concentration dependence			Voltage dependence		
	$n_{Hill}$	$IC_{50}$ $\mu$ M	$A$	$\delta$	$Kd(0)$ $\mu$ M	$A$
Memantine	$0.92 \pm 0.06$	$0.80 \pm 0.21$	$0.79 \pm 0.07$	$0.73 \pm 0.03$	$18.5 \pm 2.7$	$0.99 \pm 0.04$
Amantadine	$1.02 \pm 0.13$	$14.5 \pm 4.4$	$0.83 \pm 0.10$	$0.92 \pm 0.02$	$737 \pm 36$	$0.99 \pm 0.01$
MRZ 2/150	$1.28 \pm 0.13$	$0.37 \pm 0.11$	$0.79 \pm 0.08$	$0.73 \pm 0.07$	$8.4 \pm 2.6$	$1.04 \pm 0.12$
MRZ 2/151	$1.19 \pm 0.15$	$0.70 \pm 0.14$	$0.75 \pm 0.05$	$1.03 \pm 0.12$	$36.1 \pm 14.8$	$0.83 \pm 0.07$
MRZ 2/177	$1.03 \pm 0.07$	$0.43 \pm 0.07$	$0.85 \pm 0.05$	$0.82 \pm 0.03$	$12.8 \pm 1.4$	$0.95 \pm 0.03$
MRZ 2/178	$1.26 \pm 0.08$	$8.7 \pm 0.8$	$0.79 \pm 0.01$	$0.82 \pm 0.08$	$102 \pm 33$	$0.90 \pm 0.09$
MRZ 2/184	$1.39 \pm 0.14$	$2.49 \pm 0.36$	$0.84 \pm 0.04$	$0.87 \pm 0.08$	$39.3 \pm 13.0$	$1.01 \pm 0.10$
MRZ 2/239	$1.34 \pm 0.20$	$2.78 \pm 0.61$	$0.88 \pm 0.04$	$0.89 \pm 0.09$	$39.2 \pm 12.3$	$0.98 \pm 0.08$
MRZ 2/372	$1.19 \pm 0.07$	$0.72 \pm 0.08$	$0.85 \pm 0.02$	$0.90 \pm 0.06$	$25.6 \pm 6.1$	$0.90 \pm 0.05$
MRZ 2/457	$1.14 \pm 0.08$	$0.39 \pm 0.06$	$0.80 \pm 0.03$	$0.88 \pm 0.06$	$13.4 \pm 2.6$	$0.98 \pm 0.05$

The values presented are mean  $\pm$  SE.  $n = 4$ –14 cells.

FIGURE 2 The fast and slow components in the kinetics of the NMDA open-channel blockade by MRZ 2/178. ASP (100  $\mu$ M) was applied continuously. MRZ 2/178 at various concentrations was coadministered for 6 s with ASP. (A) Original NMDA responses at the 5.6, 16.7, and 50  $\mu$ M MRZ 2/178 concentrations were fitted with single exponential functions. (B) The same responses were fitted with double exponential functions. The amplitude of the fast component increased with a rise in the blocker concentration for the channels blockade ( $A_{fast}^{on}$ ) and decreased for their recovery ( $A_{fast}^{off}$ ).

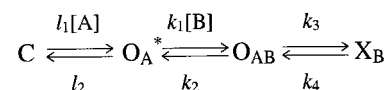


from the analysis of mean values of  $\tau_{slow}^{on}$  and  $\tau_{slow}^{off}$  (Fig. 3, C and D) for open-channel blockade by MEM and MRZ 2/178 (see Appendix A). The values of  $\gamma$  and  $\epsilon$ , the rate constants of transitions into and out of  $D_A$ , respectively, were defined from the results of studies of control current responses to 2-s ASP application (Fig. 1, inset). We found the numerical solutions at different values of  $d$  (Fig. 4 A) and fitted them in the same way as the experimental curves. The modeling values of  $\tau_{fast}^{on}$ ,  $\tau_{fast}^{off}$ ,  $\tau_{slow}^{on}$ , and  $\tau_{slow}^{off}$  were of the same range as the experimental ones.  $A_{fast}^{off}$ , however, remained constant at different AAD concentrations, irrespective of the  $d$  value (Fig. 4 B). Moreover, at a comparatively low value of  $d$  (but an extremely high value for kinetic experiments) of 0.32, the fast component of the recovery kinetics was negligible ( $A_{fast}^{off} = 0.014$  for MEM and  $A_{fast}^{off} = 0.045$  for MRZ 2/178). The Hill coefficient for model 2 is exactly equal to 1 (see Appendix C) and thus cannot explain the experimentally observed values of  $n_{Hill}$  exceeding 1.

Thus we failed in our attempt to explain the two components in the open-channel blocking kinetics of AAD by an addition of the desensitized state to one-site model 1. So it is necessary to increase the number of blocked states of the channel. Let us consider the appropriate simplest kinetic models. As the behavior of other parameters predicted by model 2 was qualitatively the same as the experimental one, the main object of our observation will be the behavior of  $A_{fast}^{off}$  for the channel recovery from the AAD-induced blockade depending on the blocker concentration. Therefore we have no need to take into account the desensitized states of the channel because, as shown above, the addition of these states to the kinetic model not only leaves  $A_{fast}^{off}$  constant at different blocker concentrations but, in our experimental range of  $d$ , it also allows one to consider it as practically zero. For the sake of simplicity and without any loss for our analysis due to the high value of the opening probability

(see Appendix A), the processes of the agonist binding and the subsequent channel opening are represented as a straight transition from the closed state (C) to the open state ( $O_A$ ).

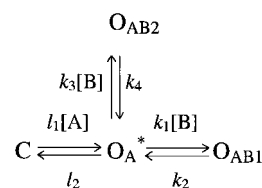
When only one blocker molecule binds to the channel, there are two simplest possibilities to add one new blocked state to Model 1. The first one can be expressed by a sequential kinetic model:



Model 3

$X_B$  can represent the second open ( $O'_{AB}$ ), desensitized ( $D_{AB}$ ), or closed ( $C_B$ ) blocked states of the channel. In the latter case, the blocker can be trapped in the closed channel. The trapping block of NMDA channels by memantine and amantadine was reported earlier (Johnson et al., 1995; Chen and Lipton, 1997). In this case,  $X_B$  can be designated as  $C_B$ , and the kinetic constant  $k_4$  can be written in more detail as  $k_4 = l_1 \cdot [A]$ . However, under our conditions of the continuous presence of ASP at a constant concentration (100  $\mu$ M), this more accurate definition is unimportant. Thus all three possible representations of the sequential model are kinetically equivalent.

Another simplest possibility, adding the second blocking site when only one blocker molecule binds to the channel, can be expressed in the form of a parallel kinetic model:



Model 4

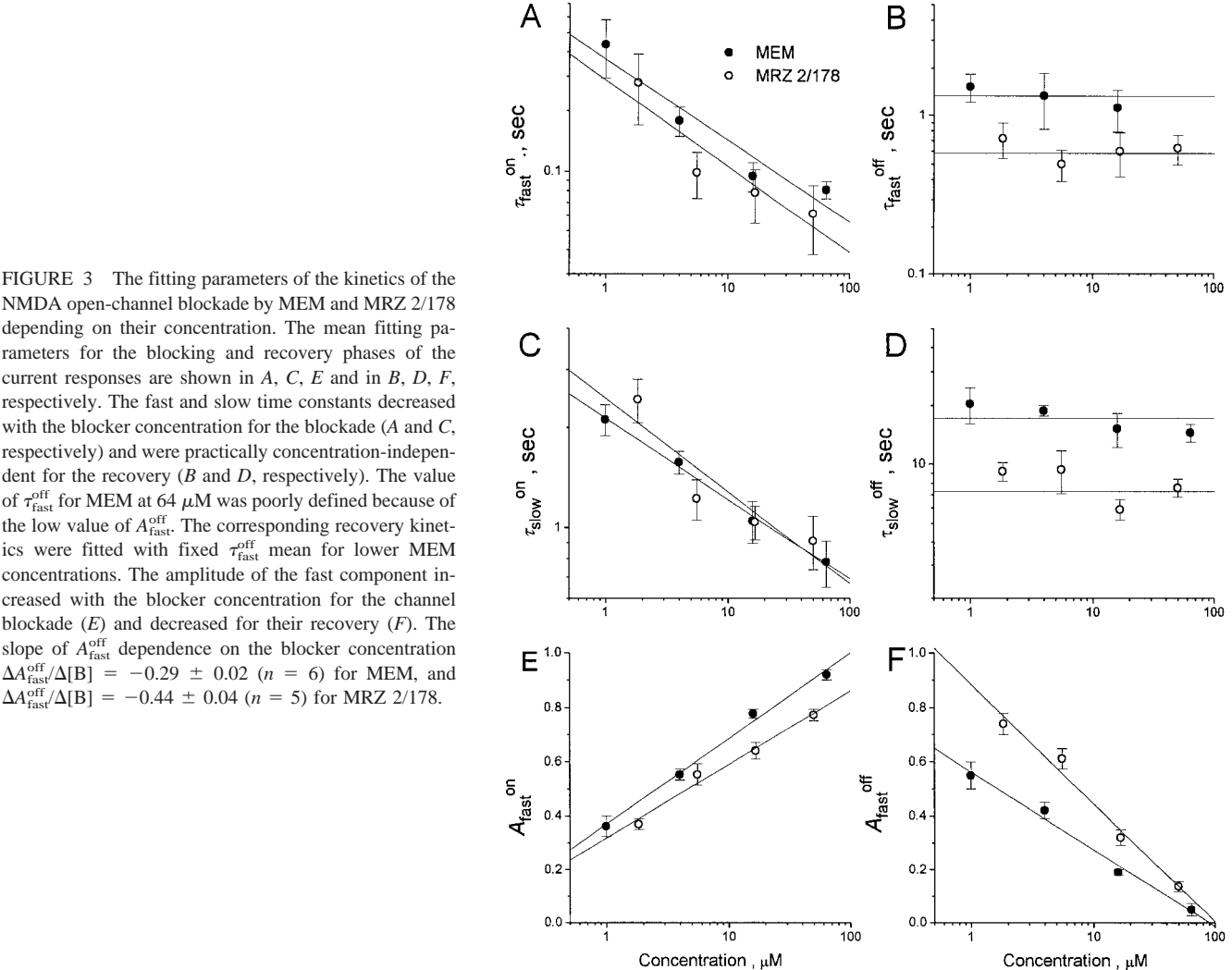
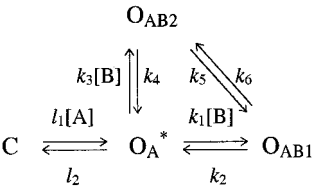


FIGURE 3 The fitting parameters of the kinetics of the NMDA open-channel blockade by MEM and MRZ 2/178 depending on their concentration. The mean fitting parameters for the blocking and recovery phases of the current responses are shown in A, C, E and in B, D, F, respectively. The fast and slow time constants decreased with the blocker concentration for the blockade (A and C, respectively) and were practically concentration-independent for the recovery (B and D, respectively). The value of  $\tau_{fast}^{off}$  for MEM at 64  $\mu$ M was poorly defined because of the low value of  $A_{fast}^{off}$ . The corresponding recovery kinetics were fitted with fixed  $\tau_{fast}^{off}$  mean for lower MEM concentrations. The amplitude of the fast component increased with the blocker concentration for the channel blockade (E) and decreased for their recovery (F). The slope of  $A_{fast}^{off}$  dependence on the blocker concentration  $\Delta A_{fast}^{off}/\Delta[B] = -0.29 \pm 0.02$  ( $n = 6$ ) for MEM, and  $\Delta A_{fast}^{off}/\Delta[B] = -0.44 \pm 0.04$  ( $n = 5$ ) for MRZ 2/178.

According to model 4, the blocker binds to one or another blocking site in the channel. The jumps from one blocking site to another are impossible. The kinetic constants for models 3 and 4 (Table 3) were defined unambiguously from the analysis of mean values of  $\tau_{fast}^{on}$ ,  $\tau_{fast}^{off}$ ,  $\tau_{slow}^{on}$ , and  $\tau_{slow}^{off}$  (Fig. 3, A-D) for the open-channel blockade by MEM and MRZ 2/178 (see Appendix B). Most of the kinetic parameters for both models changed qualitatively in the same way as in the experiment; however, the modeling values of  $A_{fast}^{off}$  for the channel recovery from the AAD-induced blockade did not change with the blocker concentration (cf. Figs. 5 and 3 F). The inadequacy of these models can also be seen in their inability to explain high experimental values of  $n_{Hill}$

(Table 2), because they predict the value of the Hill coefficient as being exactly equal to 1 (see Appendix C).

Model 4 can be complicated by the transition between  $O_{AB1}$  and  $O_{AB2}$ :



Model 5

TABLE 3 The modeling kinetic constants for MEM and MRZ 2/178

	MEM				MRZ 2/178			
	$k_1 \mu M^{-1} s^{-1}$	$k_2 s^{-1}$	$k_3 \mu M^{-1} s^{-1}$	$k_4 s^{-1}$	$k_1 \mu M^{-1} s^{-1}$	$k_2 s^{-1}$	$k_3 \mu M^{-1} s^{-1}$	$k_4 s^{-1}$
Model 3	$1.92 \pm 0.28$	$0.23 \pm 0.02$	$0.37 \pm 0.01$	$0.158 \pm 0.005$	$0.98 \pm 0.42$	$0.88 \pm 0.17$	$0.73 \pm 0.03$	$0.29 \pm 0.06$
Model 4	$0.24 \pm 0.18$	$0.77 \pm 0.07$	$1.29 \pm 0.28$	$0.056 \pm 0.005$	$0.50 \pm 0.27$	$1.76 \pm 0.13$	$0.48 \pm 0.15$	$0.136 \pm 0.019$
Model 7	$1.15 \pm 0.24$	$0.77 \pm 0.07$	$0.33 \pm 0.22$	$0.056 \pm 0.005$	$0.89 \pm 0.37$	$1.76 \pm 0.13$	$0.080 \pm 0.043$	$0.136 \pm 0.019$



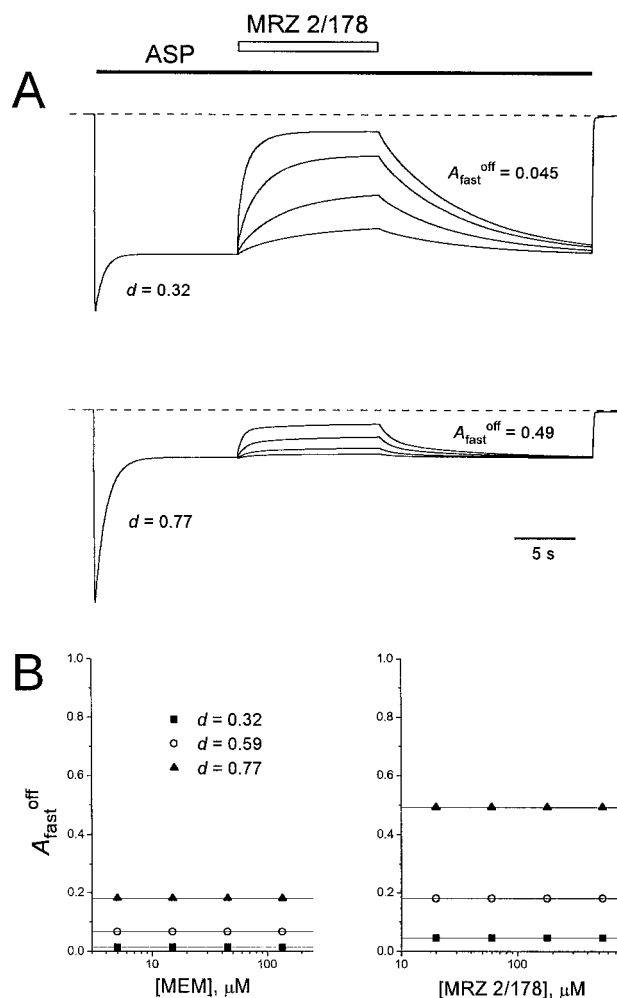


FIGURE 4 The kinetics of responses predicted by model 2. (A) MRZ 2/178 at different concentrations (20, 60, 180, and 540  $\mu\text{M}$ ) was coapplied with ASP (100  $\mu\text{M}$ ) after the agonist-induced current had reached its stationary level. The modeling current traces are presented for two values of the fraction of the desensitized channels,  $d$ . In both cases the amplitude of the fast component,  $A_{\text{fast}}^{\text{off}}$ , did not depend on the MRZ 2/178 concentration, but increased from 0.045 to 0.49 when  $d$  rose from 0.32 to 0.77, respectively. (B) The values of  $A_{\text{fast}}^{\text{off}}$  for MEM and MRZ 2/178 at different  $d$  (0.32, 0.59, and 0.77) are plotted against the blocker concentration. Despite the common independence of  $A_{\text{fast}}^{\text{off}}$  on the concentration for MEM and MRZ 2/178, MEM, the blocker slower than MRZ 2/178, demonstrated a lower increase in  $A_{\text{fast}}^{\text{off}}$  with  $d$ .

Model 5 describes the situation in which either blocking site can be occupied at first and the blocker can jump from one site to another. As a combination of models 3 and 4, it cannot simulate the experimentally observed kinetics either (Fig. 6). Furthermore, in the framework of the simplest models with two blocked states, the kinetic model can also be complicated by the appearance of two open states of the channel. The existence of two to five conductance levels was shown in experiments with native and recombinant NMDA channels (Gibb and Colquhoun, 1992; Wyllie et al., 1996). This complication of the model can be represented

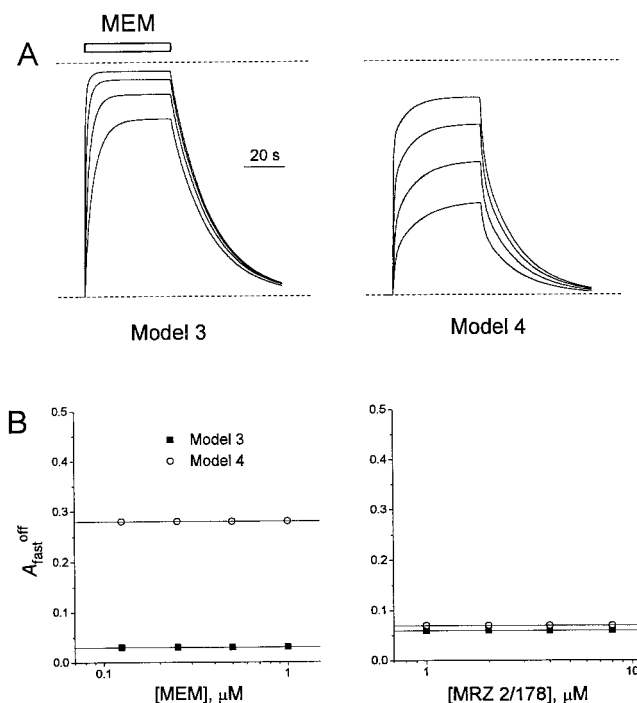
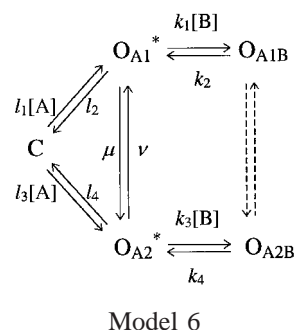


FIGURE 5 The kinetics of responses predicted by models 3 and 4. (A) The modeling current traces for models 3 and 4. MEM at different concentrations (0.125, 0.25, 0.5, and 1  $\mu\text{M}$ ) was applied in the continuous presence of ASP (100  $\mu\text{M}$ ). (B) The values of the amplitude of the fast component for the recovery from the block by MEM and MRZ 2/178 for models 3 and 4 were plotted against the blocker concentration. For both models  $A_{\text{fast}}^{\text{off}}$  did not depend on the blocker concentration.

by the following scheme:



where  $O_{A1}$  and  $O_{A2}$  are the two different open states of the channel and  $O_{A1B}$  and  $O_{A2B}$  are its blocked states, respectively. Thus the two blocked states in model 6 can correspond to only one binding site of the blocker. The transitions  $C \rightarrow O_{A1}$  and  $C \rightarrow O_{A2}$  are not slower than the transition between  $C$  and  $O_A$  in model 4 because the mean open time distribution was not shown to contain any components with  $\tau > 10$  ms; the transition between  $O_{A1}$  and  $O_{A2}$  is very fast ( $\tau \ll 1$  ms) and, in the majority of NMDA channels, symmetrical (Gibb and Colquhoun, 1992). To our knowledge, the existence of temporal asymmetry was found only for NMDA NR1a/NR2D recombinant channels (Wyllie et al., 1996). Despite the possible asymmetry of the transitions between  $C$ ,  $O_{A1}$ , and  $O_{A2}$  with respect to the transitions

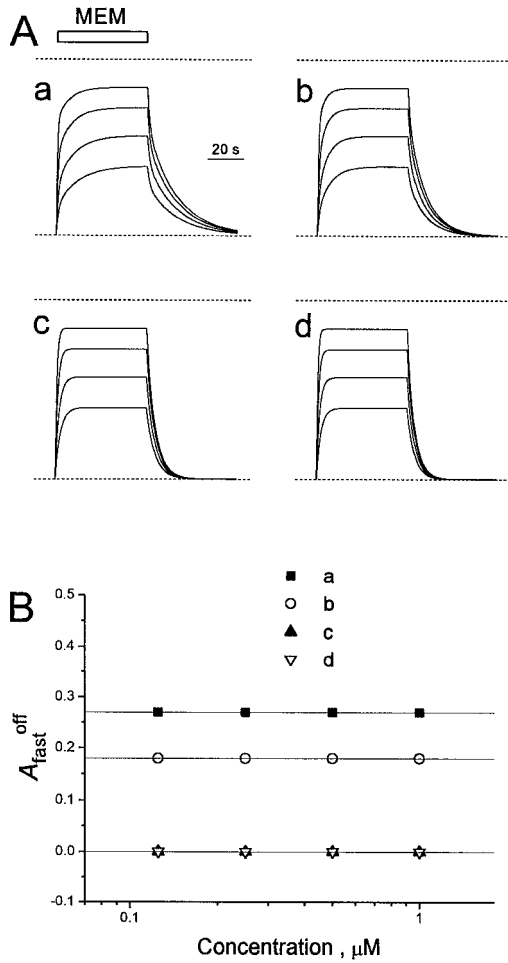


FIGURE 6 The kinetics of responses predicted by model 5. All of the kinetic constants except  $k_5$  and  $k_6$  are the same as for model 4 (see Table 3). The constants  $k_5$  and  $k_6$  are mutually dependent according to the equation  $k_1 \cdot k_4 \cdot k_6 = k_2 \cdot k_3 \cdot k_5$ . (A) The modeling current traces in the cases when the transition between  $O_{AB1}$  and  $O_{AB2}$  states was (a) slower than both  $O_A-O_{AB1}$  and  $O_A-O_{AB2}$  transitions,  $k_5 = 0.006 \text{ s}^{-1}$ ,  $k_6 = 0.0153 \text{ s}^{-1}$ ; (b) comparable to the slow one,  $k_5 = 0.06 \text{ s}^{-1}$ ,  $k_6 = 0.153 \text{ s}^{-1}$ ; (c) comparable to the fast one,  $k_5 = 0.6 \text{ s}^{-1}$ ,  $k_6 = 1.53 \text{ s}^{-1}$ ; and (d) faster than both of them,  $k_5 = 6 \text{ s}^{-1}$ ,  $k_6 = 15.3 \text{ s}^{-1}$ . MEM at different concentrations (0.125, 0.25, 0.5, and 1 μM) was applied in the continuous presence of ASP (100 μM). The recovery kinetics in a are practically the same as shown in Fig. 5 for model 4,  $\tau_{fast}^{off} = 1.46 \pm 0.01 \text{ s}$ ,  $\tau_{slow}^{off} = 16.3 \pm 0.1 \text{ s}$ . In b the kinetics are faster,  $\tau_{fast}^{off} = 1.32 \pm 0.01 \text{ s}$ ,  $\tau_{slow}^{off} = 9.7 \pm 0.1 \text{ s}$ . In c and d, the recovery kinetics are single exponential, with the time constants intermediate between the time constants in a and b. These time constants can be defined as slow; their values were  $\tau_{slow}^{off} = 4.69 \pm 0.01 \text{ s}$  and  $\tau_{slow}^{off} = 4.09 \pm 0.01 \text{ s}$  for c and d, respectively. (B) The values of the amplitude of the fast component for the recovery from the block by MEM for all four cases described in A were plotted against the blocker concentration; it decreased from  $0.28 \pm 0.01$  in a to  $0.19 \pm 0.01$  in b and became equal to zero in c and d.

$O_{A1}-O_{A1B}$  and  $O_{A2}-O_{A2B}$  due to the different conductance of  $O_{A1}$  and  $O_{A2}$  states or the temporal asymmetry between them, the rapidity of these transitions provides qualitatively the same kinetics as in the case of models 2–5, i.e.,  $A_{fast}^{off}$  is concentration-independent (Fig. 7). Model 6 also predicts the value of the Hill coefficient as being exactly equal to 1 (see Appendix C).

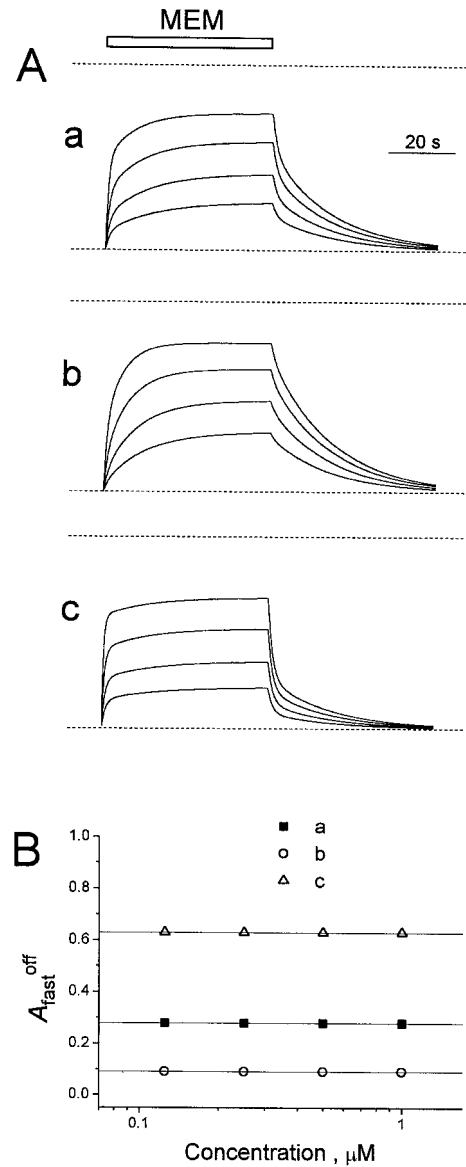
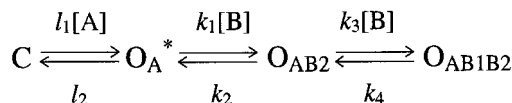


FIGURE 7 The kinetics of responses predicted by model 6. The kinetic constants  $l_1$ ,  $l_2$ ,  $k_1$ ,  $k_2$ ,  $k_3$ , and  $k_4$  are the same as those for model 4 (see Table 3). The constants  $\mu$  and  $\nu$  were taken to be high enough to ensure the rapidity of the transition between the  $O_{A1}$  and  $O_{A2}$  states with respect to the other transitions in model 6 and not too high to simplify the modeling process. The constants  $l_3$  and  $l_4$  were of the same range as  $l_1$  and  $l_2$  and were changed symmetrically with  $\mu$  and  $\nu$  to comply with the equation  $l_1 \cdot l_4 \cdot \mu = l_2 \cdot l_3 \cdot \nu$ . (A) The modeling current traces in the cases when the dynamic equilibrium along the transition  $O_{A1}-O_{A2}$  was (a) symmetrical,  $\mu = \nu = 1000 \text{ s}^{-1}$ ,  $l_3 = l_1$ ,  $l_4 = l_2$ ; (b) shifted to  $O_{A1}$ ,  $\mu = 4 \cdot \nu = 2000 \text{ s}^{-1}$ ,  $l_3 = 2 \cdot l_1$ ,  $l_4 = 0.5 \cdot l_2$ ; (c) shifted to  $O_{A2}$ ,  $\mu = 0.25 \cdot \nu = 500 \text{ s}^{-1}$ ,  $l_3 = 0.5 \cdot l_1$ ,  $l_4 = 2 \cdot l_2$ . MEM at different concentrations (0.125, 0.25, 0.5, and 1 μM) was applied in the continuous presence of ASP (100 μM). The values of  $\tau_{fast}^{off}$  and  $\tau_{slow}^{off}$  were practically the same as for model 4 and did not depend on the blocker concentration. (B) The values of the amplitude of the fast component for the recovery from the block by MEM for all three cases described in A were plotted against the blocker concentration.  $A_{fast}^{off}$  did not depend on the blocker concentration and was the same ( $A_{fast}^{off} = 0.28 \pm 0.01$ ) in a, smaller ( $A_{fast}^{off} = 0.09 \pm 0.01$ ) in b, and larger ( $A_{fast}^{off} = 0.63 \pm 0.01$ ) in c than for model 4 (see Fig. 5 B).

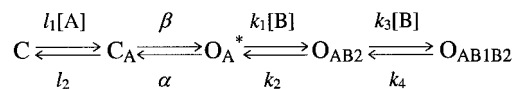
Thus no models considered above can qualitatively describe the kinetics of NMDA channel recovery from the AAD blockade. The only way to solve this problem within the framework of simplest models with two blocked states is to suppose that not one, but at least two blocking molecules can simultaneously bind to open NMDA channels. In a kinetic model this fact will be expressed by the appearance of the double-blocked state,  $O_{AB1B2}$ . The resulting kinetic model with a double-blocked open-channel state is sequential:



Model 7

Model 7 suggests the strong order for the blocker molecules to occupy their binding sites: site 2 is occupied first, site 1 is occupied thereafter. The constants  $k_1$ ,  $k_2$ ,  $k_3$ , and  $k_4$  (Table 3) were defined unambiguously according to the experimental kinetics (see Appendix B). Finally, in this case  $A_{fast}^{off}$  depends on the blocker concentration qualitatively in the same way as in the experiment: it decreased with concentration for both MEM and MRZ 2/178 (Fig. 8 A). It should be noted, however, that the slope of the  $A_{fast}^{off}$  dependence on the blocker concentration (Fig. 8 B,  $\Delta A_{fast}^{off}/\Delta[B] = -0.53 \pm 0.04$  for MEM and  $\Delta A_{fast}^{off}/\Delta[B] = -0.61 \pm 0.03$  for MRZ 2/178) was much steeper than that observed in the experiment (Fig. 3 F,  $\Delta A_{fast}^{off}/\Delta[B] = -0.29 \pm 0.02$  for

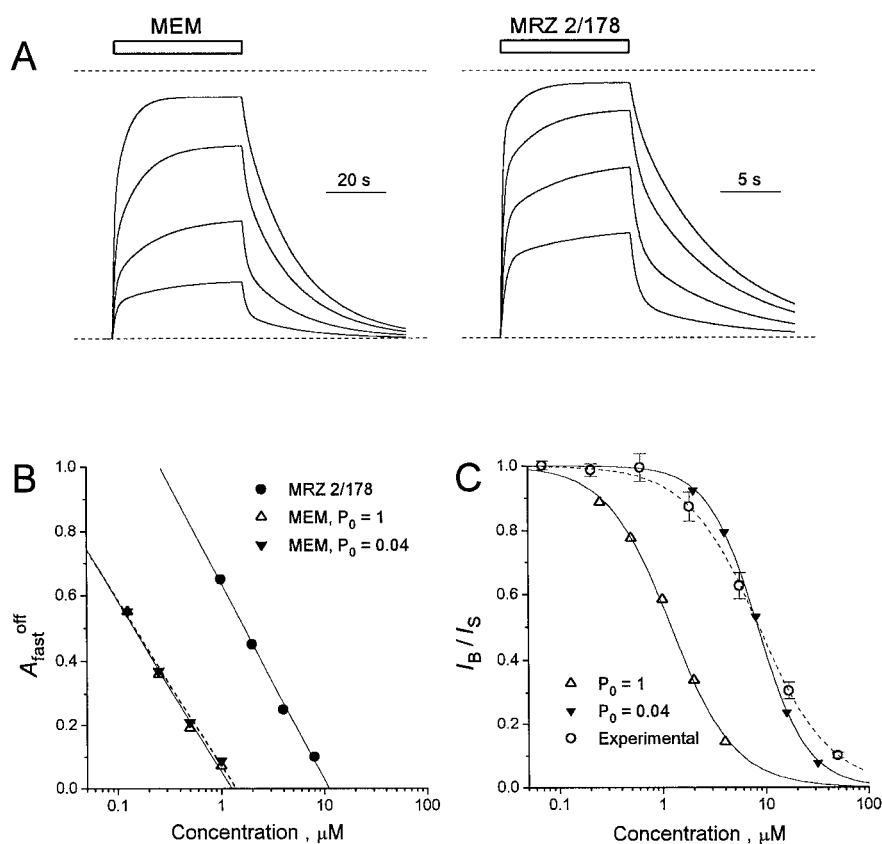
MEM and  $\Delta A_{fast}^{off}/\Delta[B] = -0.44 \pm 0.04$  for MRZ 2/178). It is interesting that taking into account the open probability of less than 1 by involving the closed agonist-bound state of the channel in model 7,



Model 7a

we did not change considerably the recovery kinetics (the values of  $P_0$  were varied by means of variation in  $\beta$  at  $\alpha = 200 \text{ s}^{-1}$ ; see Appendix A). Thus the kinetic constants  $\tau_{fast}^{off}$  and  $\tau_{slow}^{off}$  remained the same at different  $P_0$ .  $A_{fast}^{off}$  changed a little with a change in the open probability. The slope of the  $A_{fast}^{off}$  dependence on the blocker concentration changed within the error limits (cf. for MEM  $\Delta A_{fast}^{off}/\Delta[B] = -0.53 \pm 0.04$  at  $P_0 = 1$ , model 7, *solid line* in Fig. 8 B; and  $\Delta A_{fast}^{off}/\Delta[B] = -0.51 \pm 0.03$  at  $P_0 = 0.04$ , model 7a, *dashed line* in Fig. 8 B). Contrary to the kinetics, the concentration dependence of the stationary blockade predicted by model 7a strongly depended on the open probability (Fig. 8 C).  $n_{Hill}$  increased for MRZ 2/178 from  $1.43 \pm 0.05$  at  $P_0 = 1$  (model 7) to  $1.81 \pm 0.04$  at  $P_0 = 0.04$  (for MEM  $n_{Hill} = 1.60 \pm 0.04$  at  $P_0 = 1$  and  $n_{Hill} = 1.90 \pm 0.02$  at  $P_0 = 0.04$ ). Thus, in accordance with theoretical predictions (see Appendix C), the modeling kinetics gave  $n_{Hill}$  values within the interval from 1 to 2, despite being con-

FIGURE 8 The kinetics of responses and the concentration dependence of the stationary blockade predicted by model 7 (7a). (A) The modeling current traces predicted by model 7. MEM at concentrations 0.125, 0.25, 0.5, and 1  $\mu\text{M}$  and MRZ 2/178 at concentrations 1, 2, 4, and 8  $\mu\text{M}$  were applied in the continuous presence of ASP (100  $\mu\text{M}$ ). (B) The amplitude of the fast component predicted by model 7 (7a) at different blocker concentrations.  $A_{fast}^{off}$  decreased with the blocker concentration for both MEM and MRZ 2/178. The slope of  $A_{fast}^{off}$  dependence on the blocker concentration predicted by model 7 ( $P_0 = 1$ ) was  $\Delta A_{fast}^{off}/\Delta[B] = -0.53 \pm 0.04$  for MEM and  $\Delta A_{fast}^{off}/\Delta[B] = -0.61 \pm 0.03$  for MRZ 2/178 (shown by *solid lines*).  $A_{fast}^{off}$  dependence on the blocker concentration did not practically change when the open probability was decreased according to model 7a (for MEM  $\Delta A_{fast}^{off}/\Delta[B] = -0.51 \pm 0.03$  at  $P_0 = 0.04$ , shown by *dashed line*). (C) Concentration dependencies of the stationary blockade by MRZ 2/178 predicted by model 7 ( $P_0 = 1$ ) and model 7a at  $P_0 = 0.04$  were superimposed on the normalized concentration dependence observed in the experiment (all of the points except for the two left ones shown in Fig. 1 B are represented here). The fittings to Eq. 2 with  $A = 1$  of the modeling and experimental data are shown by solid and dashed lines, respectively. The dose-response curve predicted by model 7a was shifted to the right with a decrease in  $P_0$ .





siderably larger than those observed in the experiment (Table 2). The value of  $IC_{50}$  differed considerably at low and high values of  $P_0$ . Thus, for MRZ 2/178,  $IC_{50}$  increased from  $1.22 \pm 0.03$  to  $8.42 \pm 0.10 \mu\text{M}$  with a decrease in  $P_0$  from 1 to 0.04 (for MEM,  $IC_{50} = 0.28 \pm 0.01$  at  $P_0 = 1$  and  $IC_{50} = 1.63 \pm 0.01$  at  $P_0 = 0.04$ ), and at the low open probability was approximately the same as in the experiment ( $8.7 \pm 0.8 \mu\text{M}$ ).

### Potential dependence

The current responses to AAD application in the continuous presence of ASP (100  $\mu\text{M}$ ) were different at different membrane potentials (Fig. 9, *inset*). The voltage dependence of the stationary blockade of open NMDA channels by MEM and MRZ 2/178 is shown in Fig. 9. The fitting was done using the equation

$$I_B/I_S = A/(1 + [B]/Kd(0) \times \exp(\delta FE_h/RT)) \quad (3)$$

where  $A$  is the constant,  $E_h$  is the membrane potential, and  $Kd(0)$  is the equilibrium dissociation constant at  $E_h = 0$ .  $F$ ,  $R$ , and  $T$  have their usual meanings. The values of  $\delta$ , the fraction of the electric field that contributed to the energy of AAD at the blocking sites, proved to be very high (Table 2). The values of  $A$  were close to 1.

The double-exponential fit of the 10  $\mu\text{M}$  MEM-induced blocking kinetics (Fig. 10) showed that  $A_{\text{fast}}^{\text{on}}$  decreased at first from 0.79 to 0.54 with an increase in the holding potential from  $-100$  to  $-40$  mV and then was enhanced to 0.65 with a rise in  $E_h$  to  $-20$  mV.  $A_{\text{fast}}^{\text{off}}$  for the channel recovery from the MEM blockade increased from 0.27 to 0.79 with an increase in  $E_h$  from  $-100$  to  $-20$  mV. The mean values of the amplitude of the fast component, the fast

and slow time constants for the blocking, and the recovery kinetics of MEM and MRZ 2/178 depending on  $E_h$  are shown in Fig. 11. It should be noted that both time constants,  $\tau_{\text{fast}}^{\text{off}}$  and  $\tau_{\text{slow}}^{\text{off}}$ , in the kinetics of recovery from MRZ 2/178 decreased with membrane depolarization (Fig. 11, *B* and *D*), whereas in the case of MEM,  $\tau_{\text{fast}}^{\text{off}}$  was practically voltage-independent (Fig. 11 *B*). We modeled the kinetics of the AAD interaction with open NMDA channels depending on the membrane potential according to the simplest model 7. As the agonist binding site is considered to be located near the surface of the neuronal membrane, the transition from C to  $O_A$  was assumed to be voltage-independent. This assumption can be confirmed by the fact that the whole-cell current-voltage dependence curve in  $\text{Mg}^{2+}$ -free solutions for NMDA channels is practically linear (Nowak and Wright, 1992; Parsons et al., 1993, 1995) and by the observation that the inhibition of NMDA responses by the competitive antagonists was not voltage-dependent (Benveniste and Mayer, 1991a). The other constants depending on  $E_h$  are defined according to the following equations:

$$k_{1(3)} = k_{1(3)}^{-100\text{mV}} \exp\left(-\frac{\delta_{1(2)} F \Delta E_h}{2RT}\right) \quad (4)$$

$$k_{2(4)} = k_{2(4)}^{-100\text{mV}} \exp\left(\frac{\delta_{1(2)} F \Delta E_h}{2RT}\right) \quad (5)$$

where  $k_i^{-100 \text{ mV}}$  is the  $i$ th kinetic constant at the holding potential of  $-100$  mV,  $\delta_1$  and  $\delta_2$  are the fractions of the electric field corresponding to the first (from  $O_A$  to  $O_{AB1}$ ) and second (from  $O_{AB1}$  to  $O_{AB1B2}$ ) blocking transitions, and  $\Delta E_h$  is the difference between  $E_h$  and  $-100$  mV. All of the values of the kinetic constants at  $-100$  mV were the same

FIGURE 9 The voltage dependence of the stationary NMDA open-channel block by MEM (10  $\mu\text{M}$ ) and MRZ 2/178 (80  $\mu\text{M}$ ). The stationary current values in the presence of the blocker ( $I_B$ ) divided by the corresponding control current values ( $I_S$ ) were plotted against the membrane potential ( $E_h$ ). The solid lines show the fitting of the experimental data with Eq. 3. The fitting parameters are  $A = 0.99 \pm 0.04$ ,  $Kd(0) = 18.5 \pm 2.7 \mu\text{M}$ ,  $\delta = 0.73 \pm 0.03$  ( $n = 5$ ) for MEM, and  $A = 0.90 \pm 0.09$ ,  $Kd(0) = 102 \pm 33 \mu\text{M}$ ,  $\delta = 0.82 \pm 0.08$  ( $n = 6$ ) for MRZ 2/178. The inset shows the original current traces at various membrane potentials (from  $-100$  to  $40$  mV). MRZ 2/178 was applied for 6 s in the continuous presence of ASP (100  $\mu\text{M}$ ).

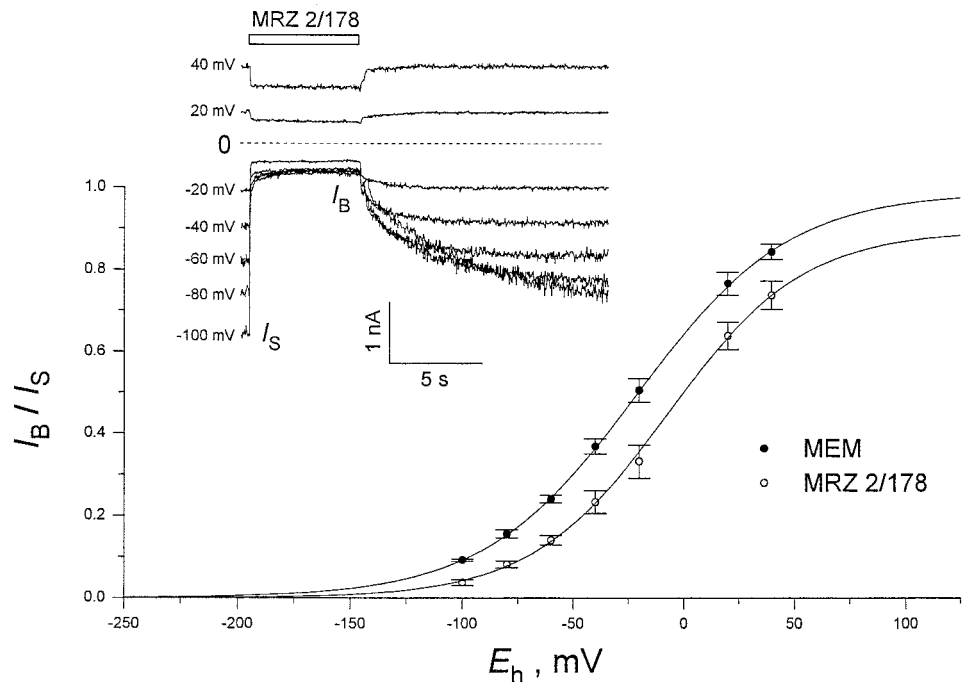
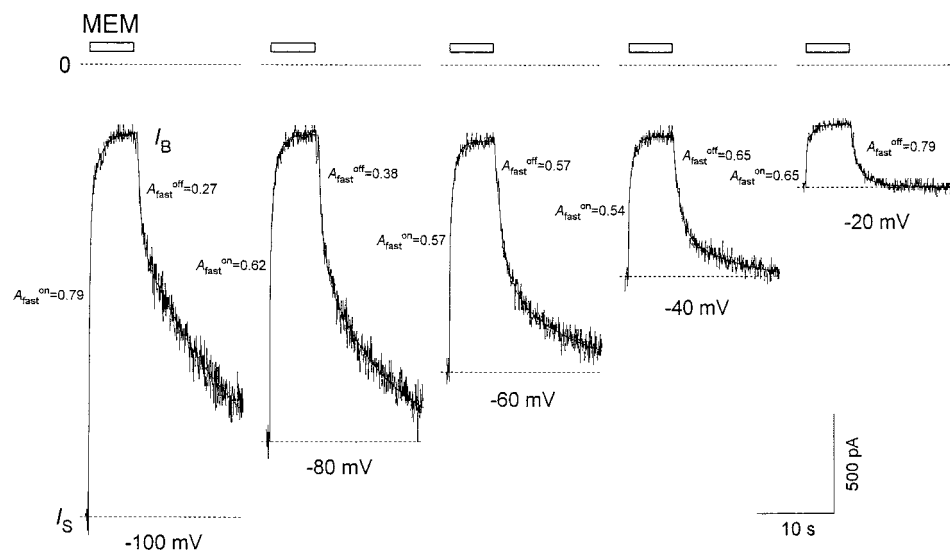


FIGURE 10 The kinetics of the NMDA open-channel block by MEM depending on the membrane potential. ASP (100  $\mu$ M) was applied continuously. MEM (10  $\mu$ M) was coadministered for 6 s with ASP at various membrane potentials (from  $-100$  to  $-20$  mV) ( $E_h$ ). The solid lines show the fitting of the current traces with double exponential functions. The amplitude of the fast component for the channels blockade,  $A_{fast}^{on}$ , decreased from 0.79 to 0.54 with an increase in  $E_h$  from  $-100$  to  $-40$  mV and then was enhanced to 0.65 with a rise in  $E_h$  to  $-20$  mV.  $A_{fast}^{off}$  increased from 0.27 to 0.79 with a rise in  $E_h$  from  $-100$  to  $-20$  mV.



as in previous experiments with model 7 (Table 3). We considered three different situations for a qualitative kinetic analysis depending on the membrane potential when 1) both the first and second blocking transitions of model 7 ( $\delta_1 = 0.45$ ,  $\delta_2 = 0.45$ ), 2) only the first transition ( $\delta_1 = 0.9$ ,  $\delta_2 = 0$ ), and 3) only the second transition ( $\delta_1 = 0$ ,  $\delta_2 = 0.9$ ) were voltage-dependent. The results of modeling experiments with MRZ 2/178 are shown in Fig. 12 (for MEM the results are qualitatively similar). In the first situation both the fast and slow time constants ( $\tau_{fast}^{off}$  and  $\tau_{slow}^{off}$ ) for the recovery kinetics decreased with the membrane potential (Fig. 12, *B* and *D*). In the second situation this decrease was observed only for  $\tau_{fast}^{off}$ , and in the third one, only for  $\tau_{slow}^{off}$ . A comparison of the  $\tau_{slow}^{off}$  behavior for the model (Fig. 12 *D*) and the experiment (Fig. 11 *D*) allows one to reject the second situation and to conclude that the second transition in model 7 for both MRZ 2/178 and MEM is potential-dependent. As for the first transition (cf. Fig. 12 and Fig. 11 *B*), the kinetics of MRZ 2/178 indicates that it is strongly voltage-dependent, whereas in the case of MEM the situation remains unclear. A comparison of other kinetic parameters (Fig. 12 and Fig. 11, *A*, *C*, *E*, and *F*) suggests that most probably the first transition for MEM depends on the membrane potential, although to a much smaller degree than for MRZ 2/178.

The voltage dependence of the stationary block by MEM and MRZ 2/178 for model 7 in the three situations mentioned above is shown in Fig. 13. The fit with Eq. 3 gave high values of the integral fraction of the membrane electric field,  $\delta$ : 0.70 for MEM and 0.66 for MRZ 2/178 in the first situation and 0.90 in the second and third situations for both MEM and MRZ 2/178. Contrary to the first and second cases, in the third case the essential decrease in the limit fraction of unblocked channels at an infinitely high positive potential (parameter  $A$  in Eq. 3) is observed for both MEM (Fig. 13 *A*,  $A = 0.65$ ) and MRZ 2/178 (Fig. 13 *B*,  $A = 0.43$ ), although in the experiment this value was close to 1 (Table 2). This fact can be considered strong evidence that for all

AADs, not only second but also the first transition in model 7 is potential-dependent. Therefore two blocking sites of AADs are located in the depth of the channel pore.

## DISCUSSION

In our experiments we studied the concentration- and voltage-dependent blockade of open NMDA channels by AAD. The kinetics of AAD-induced responses in the continuous presence of ASP contained fast and slow components (Fig. 2). This fact is not due to the existence of two different populations of NMDA channels. We made an attempt to explain the appearance of the second kinetic component by the process of desensitization (models 2 and 3), the ability of the channels to close with the blocker inside (model 3), the existence of two different AAD blocking sites on condition that only one blocker molecule can bind to the channel (models 3, 4, and 5), as well as by taking into account multiple open states of the channel (Model 6). However, these attempts failed to model the experimentally observed decrease in  $A_{fast}^{off}$  with an increase in the blocker concentration (Fig. 3 *F*). Moreover, the Hill coefficient higher than 1 for practically all AADs (Table 2) cannot be predicted by these models (see Appendix C). The low value of  $n_{Hill}$  for MEM can be explained by its ability not only to block NMDA channels but also to potentiate agonist-induced responses (Koshelev et al., 1997). It is clear that any combination of models 2–6 cannot simulate the dependence of  $A_{fast}^{off}$  on the blocker concentration or a Hill coefficient higher than 1. Thus the addition of any states to the model will not explain the experimentally observed kinetics on condition that only one blocker molecule can bind to the channel.

The ability of two blocking molecules to bind simultaneously to a NMDA channel and, correspondingly, the appearance in model 7 of the “double-blocked” state allowed us to resolve qualitatively the difficulties mentioned

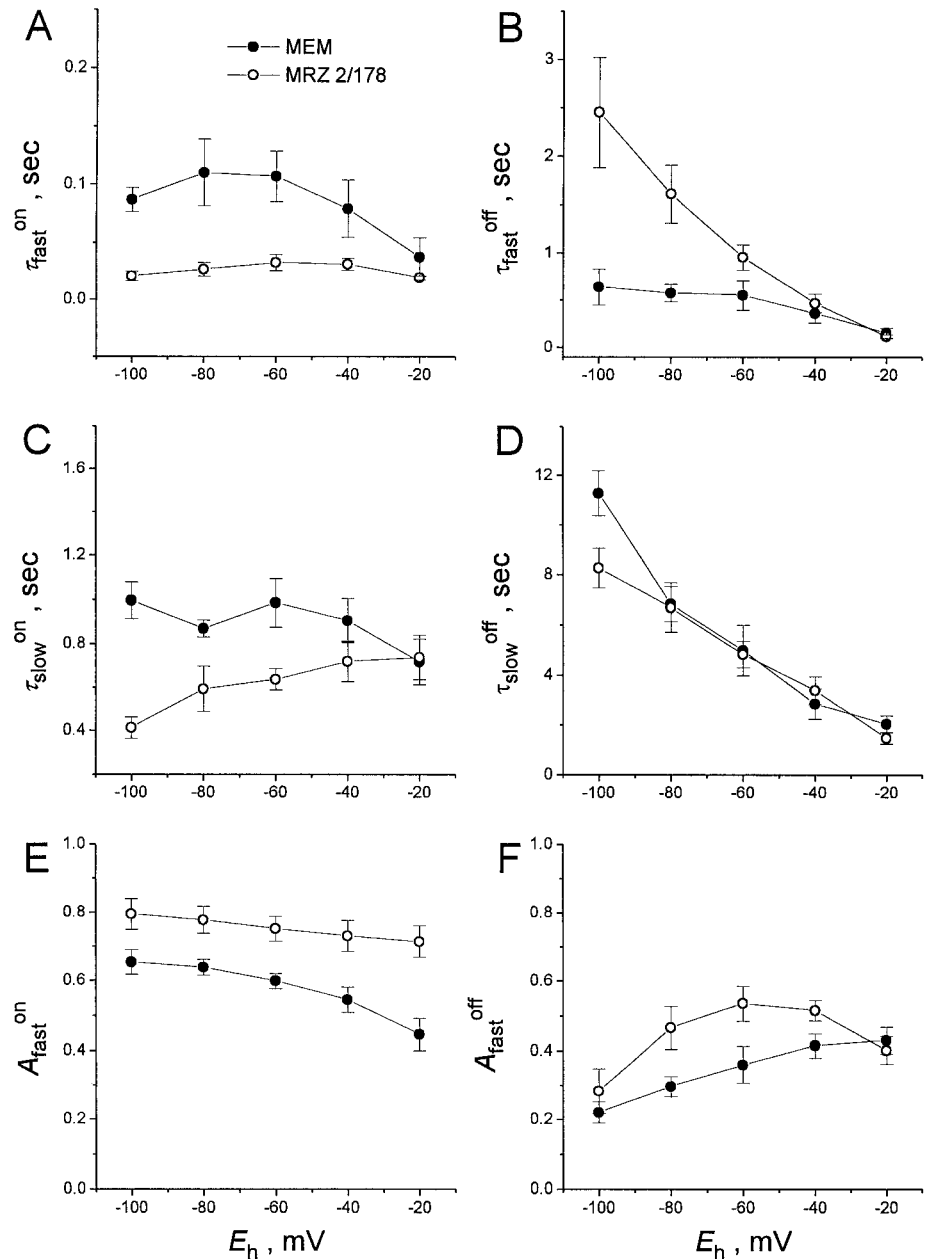
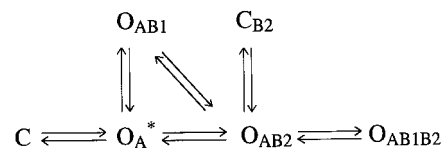


FIGURE 11 The fitting parameters of the kinetics of the NMDA open-channel blockade by MEM and MRZ 2/178 depending on the membrane potential ( $E_h$ ). The experimental scheme is shown in Fig. 10. The mean fitting parameters for the blocking and recovery phases of the current responses are shown in A, C, E and in B, D, F, respectively. Fast and slow time constants for the recovery from MRZ 2/178 decreased with membrane depolarization (B, D), whereas in the case of MEM,  $\tau_{fast}^{off}$  was practically voltage-independent (B). The amplitude of the fast component for the recovery from MRZ 2/178 had a nonmonotonous dependence on  $E_h$ , whereas  $A_{fast}^{off}$  for MEM was enhanced with a rise in  $E_h$  (F).

above. It is impossible, however, not to notice some quantitative discrepancies: 1) the slope of the  $A_{fast}^{off}$  dependence on the blocker concentration (Fig. 8 B) is much steeper than that observed in the experiment (Fig. 3 F); and 2) the Hill coefficient (Fig. 8 C) is much higher than that in the experiment. Furthermore, model 7 is unable to explain the nonmonotonous dependence of  $A_{fast}^{off}$  on the membrane potential for the channel recovery from the MRZ 2/178-induced blockade (cf. Figs. 11 F and 12 F). Evidently, the defects of model 7 are the strict succession, in which two blocking molecules can bind to their sites, and the failure to take into account the trapping block of NMDA channels by AAD. By analogy with Johnson et al. (1995), it is right to suppose that the channel cannot close with the blocker at the shallow site (1), but can do it with the blocker at the deeper

site (2). Thus, by adding the new states,  $O_{AB1}$  and  $C_{B2}$ , to model 7, we obtain the following model:



Model 8

which is the combination of models 3, 4, and 7. Unlike model 7, where the first blocking molecule reaches the deep blocking site 2 right from the external solution, model 8 gives this molecule another possibility to gain site 2 by way of sequential "jumps" from the extracellular medium to site 1 and from site 1 to site 2 (Fig. 14). For the sake of

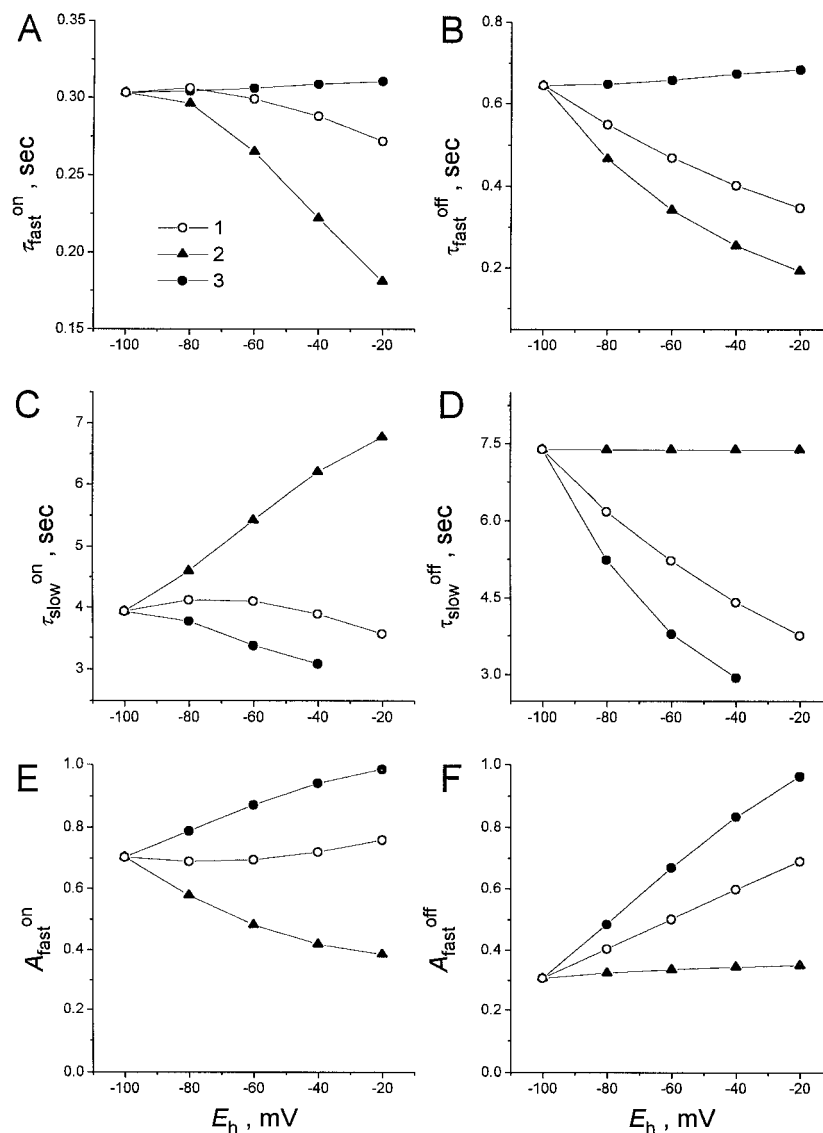


FIGURE 12 The fitting parameters of MRZ 2/178 kinetics depending on the membrane potential ( $E_h$ ) predicted by model 7. The experimental scheme is the same as that shown in Fig. 5 A. The mean fitting parameters for the blocking and recovery phases of modeling responses are shown in A, C, E and in B, D, F, respectively. The fast and slow time constants, and the amplitude of the fast component were plotted against  $E_h$  in three following cases when 1) both the first and second blocking transitions of model 7 depended on the membrane potential ( $\delta_1 = 0.45$ ,  $\delta_2 = 0.45$ ); 2) only the first ( $\delta_1 = 0.9$ ,  $\delta_2 = 0$ ) and 3) only the second transition ( $\delta_1 = 0$ ,  $\delta_2 = 0.9$ ) were voltage-dependent.  $\tau_{fast}^{off}$  for MRZ 2/178 did not decrease with  $E_h$  only in situations 3 (B), and  $\tau_{slow}^{off}$  did not decrease with  $E_h$  only in situation 2 (D).  $A_{fast}^{off}$  for MRZ 2/178 did not decrease with  $E_h$  in all three situations (F). The parameters for the blockade demonstrated qualitatively different voltage dependencies in the three cases considered (A, C, E).

simplicity, this model does not contain all possible desensitized and multiple open states of the channel. Nonetheless, model 8 can predict any slope of  $A_{fast}^{off}$  and any value of  $n_{Hill}$  intermediate between the values given by models 3, 4, and 7, i.e., it allows one to obtain the correspondence with the experimental values. This model, however, has many more degrees of freedom than the previous ones, and its constants cannot be defined unambiguously from the experimental data.

The potential dependence of the kinetics of AAD-induced responses allows one to understand why such high values of  $\delta$  were observed for the stationary block of NMDA channels (Table 2). Being some integral fraction of the electric field,  $\delta$  reflects the penetration of the membrane electric field by two charged blocking molecules up to their binding sites in the pore. Within the framework of model 7, we showed that both blocking sites for MEM and MRZ 2/178 were located in the depth of the membrane electric field. However, site 1 for MEM is located at a point much more shallower than

that for MRZ 2/178. Perhaps the long hydrophobic “tail” of MRZ 2/178 promotes the deeper binding of the blocker in the vicinity of site 1 by way of its interaction with the hydrophobic site in the channel pore (Subramaniam et al., 1994).

## APPENDIX A

The process of NMDA channel opening consists of two main events: its activation by means of agonists and coagonists binding to their sites and the opening of the gate, which proceeds with the probability  $P_0$ . The process of agonist binding was well described by a two-equivalent site model (Benveniste and Mayer, 1991b). Apparent microscopic association and dissociation rate constants for NMDA were determined to be  $2.1 \text{ s}^{-1} \mu\text{M}^{-1}$  and  $24 \text{ s}^{-1}$ , respectively. For the single binding site model 1(2), these constants were approximately two times as high. In our modeling experiments the values of dissociation ( $I_2$ ) and association ( $I_1$ ) rate constants were taken to be  $50 \text{ s}^{-1}$  and  $4 \text{ s}^{-1} \mu\text{M}^{-1}$ , respectively. The choice of the value of  $\alpha$  was based on investigations of single NMDA channels (Ascher et al., 1988; Cull-Candy and Usowich, 1989; Jahr and Stevens, 1990). As the mean open time in these works varied from 2.5 to 7 ms, we

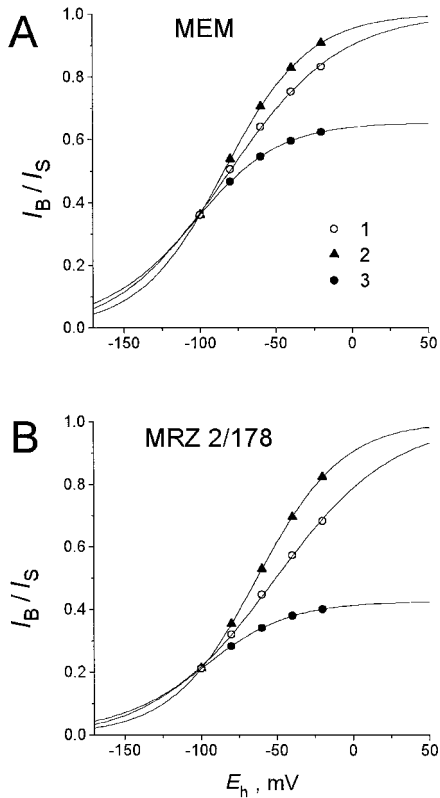


FIGURE 13 The voltage dependence of the stationary block by MEM and MRZ 2/178 predicted by model 7. The experimental scheme is the same as that shown in Fig. 5 A. The stationary values of the modeling responses in the presence of MEM and MRZ 2/178 ( $I_B$ ) divided by the corresponding control values ( $I_S$ ) were plotted against the membrane potential ( $E_h$ ) in A and B, respectively, in three different cases described in Fig. 12. The solid lines show the fitting of the modeling data with Eq. 3. The fitting parameter  $A$  is equal to 1 in the first and second situations for both MEM and MRZ 2/178. In the third situation,  $A = 0.65$  for MEM and  $A = 0.43$  for MRZ 2/178. The parameter  $\delta$  is equal to 0.70 and 0.66 for MEM and MRZ 2/178, respectively, in the first situation.  $A = 0.90$  in the second and third situations for both MEM and MRZ 2/178.

adopted the value of  $200 \text{ s}^{-1}$  for  $\alpha$ . The estimations of the opening probability of the activated channel in the majority of previous studies gave values between 0.2 and 0.5 (Jahr, 1992; Lester et al., 1993; Lin and Stevens, 1994; Benveniste and Mayer, 1995; Colquhoun and Hawkes, 1995), although Rosenmund et al. (1995) showed the low open probability for synaptic NMDA receptor channels. We adopted a value of 0.5. Thus the corresponding value for  $\beta$  proved to be  $200 \text{ s}^{-1}$ . Taking into account the rapidity of the agonist binding (we used the saturating concentration of ASP,  $100 \text{ }\mu\text{M}$ ) and channel opening, the time constant characterizing the process of desensitization is defined from the equation

$$\tau_D = 1/(\gamma + \epsilon) \quad (\text{A1})$$

where  $\gamma$  and  $\epsilon$  are the constants for the transition to and from the desensitized state, respectively. The ratio of  $\gamma$  and  $\epsilon$  can be obtained by using the value  $d = I_S/I_0$ . At the moment when the control current reaches its maximum value  $I_0$  (see Fig. 1, inset), the channels are distributed between states C,  $C_A$ , and  $O_A$  (model 2) in quasi-equilibrium. Assuming that the sum probability of occupying the states is equal to 1, the probability of occupying the open state will be defined as

$$[O_{A1}] = 1/(l_2\alpha/(l_1[A]\beta) + \alpha/\beta + 1) \quad (\text{A2})$$

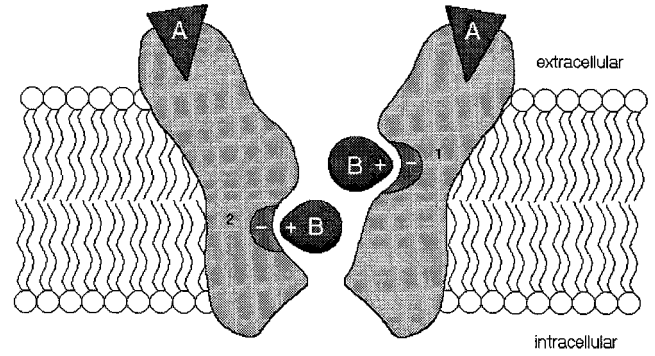


FIGURE 14 The two blocking sites of AADs in the open NMDA channel. The triangles (A) symbolize the molecules of the agonist bound to their sites. The shallow (1) and deep (2) blocking sites of amino-adamantanes are marked by a partial negative electric charge. Both sites are located in the depth of the membrane electric field. According to model 8, the blocker (B) can reach site 2 right from the external solution or by way of sequential “jumps” from the extracellular solution to site 1 and then to site 2. After that, another blocking molecule can occupy site 1. Thus two blocking sites in the open NMDA channel can be occupied simultaneously.

At the moment when the control current reaches its stationary value,  $I_S$ , we will obtain an equilibrium between states C,  $C_A$ ,  $O_A$ , and  $D_A$ . The probability of occupying of the open state will be defined as

$$[O_{A2}] = 1/(l_2\alpha/(l_1[A]\beta) + \alpha/\beta + 1 + \gamma\alpha/\epsilon\beta) \quad (\text{A3})$$

Substituting Eqs. A2 and A3 into the equation

$$I_S/I_0 = 1 - d = [O_{A2}]/[O_{A1}] \quad (\text{A4})$$

we obtain the equation for the ratio of  $\gamma$  and  $\epsilon$ :

$$\gamma/\epsilon = (1/(1 - d))(1 + \beta/\alpha + l_2/(l_1[A])) \quad (\text{A5})$$

Thus, from Eqs. A1 and A5 we define unambiguously the values of  $\gamma$  and  $\epsilon$ . In accordance with the experiment, the sum of  $\gamma$  and  $\epsilon$  was taken to be constant ( $2 \text{ s}^{-1}$ ), whereas their ratio varied in accordance with different values of  $d$  (Eq. A5).

Because of the rapidity ( $1/(\gamma + \epsilon) = 0.5 \text{ s}$ ) with respect to the slow component of the channel recovery from the AAD blockade ( $\tau_{\text{slow}}^{\text{off}} = 8 \text{ s}$  for MRZ 2/178 and  $\tau_{\text{slow}}^{\text{off}} = 18 \text{ s}$  for MEM), desensitization was proposed to explain the fast component of the AAD-induced kinetics. Then we had to consider the slow component as a result of one-site binding of the blocker to the channel. Thus the association rate constant  $k_1$  was defined from the results of the double-exponential fit (Fig. 3 C) by using the equation

$$1/\tau_{\text{slow}}^{\text{on}} = k_1[B] + k_2 \quad (\text{A6})$$

Mean values of  $1/\tau_{\text{slow}}^{\text{off}}$  for the channel recovery from the AAD-induced blockade (Fig. 3 D) gave values of the dissociation rate constant,  $k_2$ , according to the equation

$$1/\tau_{\text{slow}}^{\text{off}} = k_2 \quad (\text{A7})$$

The calculations gave the following values of association and dissociation rate constants:  $k_1 = 0.031 \text{ }\mu\text{M}^{-1} \text{ s}^{-1}$ ,  $k_2 = 0.056 \text{ s}^{-1}$  for MEM and  $k_1 = 0.058 \text{ }\mu\text{M}^{-1} \text{ s}^{-1}$ ,  $k_2 = 0.136 \text{ s}^{-1}$  for MRZ 2/178.

## APPENDIX B

To solve the linear system of differential equations

$$\frac{dX(t)}{dt} = \mathbf{A} X(t) \quad (\text{B1})$$



where  $X(t)$  is the vector of variables and  $\mathbf{A}$  is the matrix of constant coefficients, we have to find all of the eigenvalues of  $\mathbf{A}$  by solving the equation

$$|\mathbf{A} - \lambda \mathbf{E}| = 0 \quad (\text{B2})$$

where  $\lambda$  is variable and  $\mathbf{E}$  is the matrix with the diagonal elements equal to 1 and the nondiagonal elements equal to 0. As far as our models are concerned,  $X(t)$  represents the vector of probabilities of the channel occupying each of all possible states at time  $t$ .  $\mathbf{A}$ , the matrix of transitions between these states, has special properties (Colquhoun and Hawkes, 1977) that allow one to write the solution of Eq. B1 in the following form:

$$X(t) = X(0) \sum_{i=1}^n c_i e^{\lambda_i t} \quad (\text{B3})$$

where  $X(0)$  is the vector of initial probabilities of the channel state occupancies before the addition or removal of the blocker,  $\lambda_i$  is the  $i$ th solution of Eq. B2 or the  $i$ th eigenvalue of  $\mathbf{A}$ , and  $n$  is the number of states. Each of models 3, 4, and 7 has its own transition matrix with elements representing the sums of the kinetic constants multiplied, where necessary, by the agonist or blocker concentrations. The number of states is equal to 4, and the solution of Eq. B2 gives four values of  $\lambda$ :  $\lambda_1 = 0$  and  $\lambda_2, \lambda_3, \lambda_4 \neq 0$ . Fast channel opening is reflected on one in three nonzero eigenvalues,  $\lambda_2, \lambda_3$ , and  $\lambda_4$ . Let it be  $\lambda_2$ . Because of its high negative value with respect to the eigenvalues corresponding to the blockade, the second item of the sum in Eq. B3 can be omitted. The values of  $\lambda_3$  and  $\lambda_4$  correspond to the fast and slow components of the blocking kinetics at  $[B] = \text{const}$ . When  $[B] \neq 0$ , we deal with the onset of AAD, and the corresponding eigenvalues,  $\lambda_{3\text{ON}}$  and  $\lambda_{4\text{ON}}$ , are defined from the blocking kinetics:  $\lambda_{3\text{ON}} = -1/\tau_{\text{fast}}^{\text{on}}$  and  $\lambda_{4\text{ON}} = -1/\tau_{\text{slow}}^{\text{on}}$ . On the contrary, when  $[B] = 0$ , we deal with the offset of AAD, and the corresponding eigenvalues,  $\lambda_{3\text{OFF}}$  and  $\lambda_{4\text{OFF}}$ , are defined from the recovery kinetics:  $\lambda_{3\text{OFF}} = -1/\tau_{\text{fast}}^{\text{off}}$  and  $\lambda_{4\text{OFF}} = -1/\tau_{\text{slow}}^{\text{off}}$ . Thus four equations obtained after substitution of  $\lambda_{3\text{ON}}, \lambda_{4\text{ON}}, \lambda_{3\text{OFF}}$ , and  $\lambda_{4\text{OFF}}$  into Eq. B2 form a system with four variables:  $k_1, k_2, k_3$ , and  $k_4$ . The numerical solution of this system of equations gives the values of kinetic constants at every AAD concentration. In the modeling experiments we used the mean values of the constants over the whole range of the blocker concentrations (Table 3).

## APPENDIX C

To determine the probability of the channel to be in the open state (O) at equilibrium, the right part of Eq. B1 should be taken as being equal to zero. Thus we obtain the system of  $n$  linear equations,

$$\mathbf{A} X(t) = 0 \quad (\text{C1})$$

with  $n$  variables:  $x_1, \dots, x_n$ . However, because of the rank of  $\mathbf{A}$  equal to  $n - 1$ , only  $n - 1$  equations are independent. Adding the equation for the sum of probabilities of the channel occupying each of all possible states,

$$x_1 + x_2 + \dots + x_n = 1 \quad (\text{C2})$$

we obtain a system of  $n$  equations with  $n$  variables. The solutions for our models can be determined analytically. Thus the probabilities of the open state occupancy for models 2, 3, 4, and 7 are

$$[O] = 1/(1 + (\alpha/\beta)(1 + \gamma/\epsilon + l_2/(l_1 A)) + (k_1/k_2)[B]) \quad (\text{C3})$$

$$[O] = 1/(1 + l_2/(l_1 A) + (k_1/k_2)(1 + k_3/k_4)[B]) \quad (\text{C4})$$

$$[O] = 1/(1 + l_2/(l_1 A) + (k_1/k_2 + k_3/k_4)[B]) \quad (\text{C5})$$

$$[O] = 1/(1 + l_2/(l_1 A) + (k_1/k_2)[B] + (k_1 k_3/k_2 k_4)[B]^2) \quad (\text{C6})$$

respectively. The analytically determined values of  $[O]_{[B] \neq 0}/[O]_{[B] = 0}$  at different  $[B]$ , where  $[O]_{[B] \neq 0}$  is the probability of the open state occupancy at  $[B] \neq 0$  and  $[O]_{[B] = 0}$  is the probability of the open state occupancy at  $[B] = 0$ , respectively, give the dependence equivalent to the experimentally obtained concentration dependence of the stationary block ( $I_B/I_S$ ). The maximum power, to which  $[B]$  rises in items of denominators of Eqs. C3–C6, characterizes the Hill coefficient. If this power is equal to 1, the modeling  $n_{\text{Hill}}$  is equal to 1. Only the denominator of Eq. C6 contains the item with  $[B]$  to the second power. The expression for the probability of the open state occupancy for model 6 is too long to be presented here, but the maximum power of  $[B]$  is 1. Thus only model 7 can predict a Hill coefficient greater than 1.

The authors thank B. I. Khodorov for critical discussions and helpful comments on the earlier version of the manuscript. We are very grateful to our colleagues at Merz and Co., who kindly supplied us with amino-adamantanes.

This work has been supported by Russian Fund of Fundamental Investigations (no. 96-04-49228).

## REFERENCES

- Antonov, S. M., and J. W. Johnson. 1996. Voltage-dependent interaction of open channel blocking molecules with gating of NMDA receptors in rat cortical neurons. *J. Physiol. (Lond.)* 493:425–445.
- Araneda, R. C., R. S. Zukin, and M. V. L. Bennett. 1993. Effects of polyamines on NMDA-induced currents in rat hippocampal neurons: a whole-cell and single-channel study. *Neurosci. Lett.* 152:107–112.
- Ascher, P., P. Bregestovski, and L. Nowak. 1988. N-Methyl-D-aspartate-activated channels of mouse central neurones in magnesium-free solutions. *J. Physiol. (Lond.)* 399:207–226.
- Ascher, P., and L. Nowak. 1988. The role of divalent cations in the NMDA responses of mouse central neurones in culture. *J. Physiol. (Lond.)* 399:247–266.
- Benveniste, M., J. Clements, L. Vyklicky, and M. L. Mayer. 1990a. A kinetic analysis of the modulation of N-methyl-D-aspartic acid receptors by glycine in mouse cultured hippocampal neurones. *J. Physiol. (Lond.)* 428:333–357.
- Benveniste, M., and M. L. Mayer. 1991a. Structure-activity analysis of binding kinetics for NMDA receptor competitive antagonists: the influence of conformational restriction. *Br. J. Pharmacol.* 40:101–115.
- Benveniste, M., and M. L. Mayer. 1991b. Kinetic analysis of antagonist action at N-methyl-D-aspartic acid receptors. Two binding sites each for glutamate and glycine. *Biophys. J.* 59:560–573.
- Benveniste, M., and M. L. Mayer. 1993. Multiple effects of spermine on N-methyl-D-aspartic acid receptor responses of rat cultured hippocampal neurones. *J. Physiol. (Lond.)* 464:131–163.
- Benveniste, M., and M. L. Mayer. 1995. Trapping of glutamate and glycine during open channel block of rat hippocampal neuron NMDA receptors by 9-aminoacridine. *J. Physiol. (Lond.)* 483:367–384.
- Benveniste, M., J.-M. Mienville, E. Sernagor, and M. L. Mayer. 1990b. Concentration-jump experiments with NMDA antagonists in mouse cultured hippocampal neurons. *J. Neurophysiol.* 63:1373–1384.
- Blanpied, T. A., F. Boeckman, E. Aizenman, and J. W. Johnson. 1997. Trapping channel block of NMDA-activated responses by amantadine and memantine. *J. Neurophysiol.* 77:309–323.
- Chen, H.-S. V., and S. A. Lipton. 1997. Mechanism of memantine block of NMDA-activated channels in rat retinal ganglion cells: uncompetitive antagonism. *J. Physiol. (Lond.)* 499:1:27–46.
- Chen, H.-S. V., J. W. Pellegrini, S. K. Aggarwal, S. Z. Lei, S. Warach, F. E. Jensen, and S. A. Lipton. 1992. Open-channel block of NMDA responses by memantine: therapeutic advantage against NMDA receptor-mediated neurotoxicity. *J. Neurosci.* 12:4427–4436.
- Colquhoun, D., and A. G. Hawkes. 1977. Relaxation and fluctuations of membrane currents that flow through drug-operated channels. *Proc. R. Soc. Lond. B.* 199:231–262.

- Colquhoun, D., and A. G. Hawkes. 1995. Desensitization of *N*-methyl-D-aspartate receptors: a problem of interpretation. *Proc. Natl. Acad. Sci. USA*. 92:10327–10329.
- Cull-Candy, S. G., and M. M. Usowich. 1989. On the multiple-conductance single channels activated by excitatory amino acids in large cerebellar neurones of the rat. *J. Physiol. (Lond.)*. 415:555–582.
- Gibb, A. J., and D. Colquhoun. 1992. Activation of *N*-methyl-D-aspartate receptors by L-glutamate in cells dissociated from adult rat hippocampus. *J. Physiol. (Lond.)*. 456:143–179.
- Jahr, C. E. 1992. High probability opening of NMDA receptor channels by L-glutamate. *Science*. 255:470–472.
- Jahr, C. E., and C. F. Stevens. 1990. A quantitative description of NMDA receptor-channel kinetic behavior. *J. Neurosci.* 10:1830–1837.
- Johnson, J. W., S. M. Antonov, T. S. Blanpied, and Y. Li-Smerin. 1995. Channel block of NMDA receptor. In *Excitatory Amino Acids and Synaptic Transmission*. H. V. Wheal, editor. Academic Press, New York. 99–113.
- Johnson, J. W., and P. Ascher. 1990. Voltage-dependent block by intracellular  $Mg^{2+}$  of *N*-methyl-D-aspartate-activated channels. *Biophys. J.* 57:1085–1090.
- Koshelev, S. G., and B. I. Khodorov. 1992. Tetraethylammonium and tetrabutylammonium as tools to study NMDA channels of neuronal membrane. *Membr. Cell Biol.* 9:1365–1369.
- Koshelev, S., A. Sobolevsky, and B. Khodorov. 1997. Dual effect of memantine on NMDA channels in acutely isolated rat hippocampal neurones. *J. Physiol. (Lond.)*. 504P:52–53.
- Lester, R. A. J., G. Tong, and C. E. Jahr. 1993. Interactions between the glycine and glutamate binding sites of the NMDA receptor. *J. Neurosci.* 13:1088–1096.
- Lin, F., and C. F. Stevens. 1994. Both open and closed NMDA receptor channels desensitize. *J. Neurosci.* 14:2153–2160.
- MacBain, C. J., and M. L. Mayer. 1994. *N*-Methyl-D-aspartic acid receptor structure and function. *Physiol. Rev.* 74:723–760.
- Nowak, L. M., and J. M. Wright. 1992. Slow voltage-dependent changes in channel open-state probability underlie hysteresis of NMDA responses in  $Mg^{2+}$ -free solutions. *Neuron*. 8:181–187.
- Parsons, C. G., R. Gruner, J. Rozental, J. Millar, and D. Lodge. 1993. Patch clamp studies on the kinetics and selectivity of NMDA receptor antagonism by memantine. *Neuropharmacology*. 32:1337–1350.
- Parsons, C. G., G. Quack, I. Bresink, L. Baran, E. Przegalinski, W. Kostowski, P. Krzascik, S. Hartmann, and W. Danysz. 1995. Comparison of the potency, kinetics and voltage-dependency of a series of uncompetitive NMDA receptor antagonists in vitro with anticonvulsive and motor impairment activity in vivo. *Neuropharmacology*. 34:1239–1258.
- Rock, D. M., and R. L. MacDonald. 1992. The polyamine spermine has multiple actions on *N*-methyl-D-aspartate receptor single-channel currents in cultured cortical neurons. *Mol. Pharmacol.* 41:83–88.
- Rosenmund, C., A. Feltz, and G. L. Westbrook. 1995. Synaptic NMDA receptor channels have a low open probability. *J. Neurosci.* 15:2788–2795.
- Sobolevsky, A., S. Koshelev, and B. I. Khodorov. 1997. Bepridil-induced blockade of NMDA channels in rat hippocampal neurones. *Neuropharmacology*. 36:319–324.
- Subramaniam, S., S. D. Donevan, and M. A. Rogawski. 1994. Hydrophobic interactions of *n*-alkyl diamines with the *N*-methyl-D-aspartate receptor: voltage-dependent and -independent blocking sites. *Mol. Pharmacol.* 45:117–124.
- Vorobjev, V. S. 1991. Vibrodissociation of sliced mammalian nervous tissue. *J. Neurosci. Methods*. 38:145–150.
- Wyllie, D. J. A., P. Bene, R. S. Nassar, and D. Colquhoun. 1996. Single-channel currents from recombinant NMDA NR1a/NR2D receptors expressed in *Xenopus* oocytes. *Proc. R. Soc. Lond. (Biol.)*. 263:1079–1086.

# THE JOURNAL OF PHYSIOLOGY

## **Interaction of memantine and amantadine with agonist-unbound NMDA-receptor channels in acutely isolated rat hippocampal neurons**

Alexander I. Sobolevsky, Sergey G. Koshelev and Boris I. Khodorov

*J. Physiol.* 1998;512;47-60

**This information is current as of April 3, 2006**

This is the final published version of this article; it is available at:

<http://jp.physoc.org/cgi/content/full/512/1/47>

This version of the article may not be posted on a public website for 12 months after publication unless article is open access.

*The Journal of Physiology Online* is the official journal of The Physiological Society. It has been published continuously since 1878. To subscribe to *The Journal of Physiology Online* go to: <http://jp.physoc.org/subscriptions/>. *The Journal of Physiology Online* articles are free 12 months after publication. No part of this article may be reproduced without the permission of Blackwell Publishing: [JournalsRights@oxon.blackwellpublishing.com](mailto:JournalsRights@oxon.blackwellpublishing.com)

## Interaction of memantine and amantadine with agonist-unbound NMDA-receptor channels in acutely isolated rat hippocampal neurons

Alexander I. Sobolevsky, Sergey G. Koshelev and Boris I. Khodorov

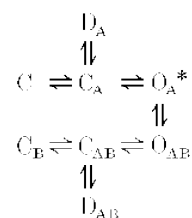
*Institute of General Pathology and Pathophysiology, Baltiyskaya 8, 125315, Moscow, Russia*

(Received 24 February 1998; accepted after revision 16 June 1998)

1. Using whole-cell patch-clamp techniques, the mechanisms of NMDA channel blockade by amino-adamantane derivatives (AADs) memantine (3,5-dimethyl-aminoadamantane, MEM) and amantadine (1-aminoadamantane, AM) have been studied in rat hippocampal neurons acutely isolated by the vibrodissociation method. A rapid concentration-jump technique was used to replace superfusing solutions.
2. The aspartate (Asp)-induced channel opening greatly accelerated but was not a prerequisite for the recovery from the block by MEM: it was able to leave the channel without agonist assistance. The co-agonist (glycine) as well as the competitive NMDA antagonist DL-2-amino-7-phosphonoheptanoic acid (APV), did not affect this recovery. Membrane depolarization accelerated it, strongly suggesting that this process proceeded via the hydrophilic pathway of the channel.
3. A comparison of the kinetics of the recovery from the block by AADs in the presence and absence of the agonist prompted a hypothesis that the blocker trapped in the channel increased the probability of its transition to the open state.
4. Both MEM and AM were able to block NMDA channels not only in the presence but also in the absence of Asp, although in the latter case the effective blocking concentrations were much higher and the rate of the block development was much smaller than in the former case. The extent of the block increased with the duration of the blocker application. Glycine enhanced this block, while APV attenuated it. The MEM-induced blockade of agonist-unbound channels was enhanced by membrane hyperpolarization and weakened by external  $Mg^{2+}$ . These findings strongly suggested that the blocker reached its binding sites via the same hydrophilic pathway both in the presence and absence of the agonist.
5. A comparative analysis of the channel unblocking kinetics in the presence of Asp after their blockade with or without the agonist assistance led us to conclude that in the two cases AADs were bound to the same blocking sites in the channel.

Recently it has been established that the amino-adamantane derivatives (AADs), memantine (MEM) and amantadine (AM) belong to the class of blockers manifesting the so-called 'trapping block' of NMDA channels (Johnson *et al.* 1995). Other representatives of this group are the well-known non-competitive NMDA-receptor antagonists MK-801, phencyclidine and ketamine (Huettner & Bean, 1987; Kemp *et al.* 1987; MacDonald *et al.* 1991). When applied externally, these drugs can enter into an open NMDA channel and bind to its 'blocking site' located deep in the pore. This binding, however, does not prevent the subsequent channel closure after the fast removal of the agonist from the medium. Therefore the blocking molecules can remain in the pore for a relatively long time being trapped 'behind the closed activation gate'. Agonist reapplication opens the gate and

thus allows the blocker to leave the channel. The simplified kinetic model of this block appears as follows:



**Model 1**

where C, D and O represent the channel in closed, desensitized and open states, respectively; the subscripts A

and B indicate the binding of all agonists and blockers to every possible site, respectively; and the asterisk indicates the conducting state. Proceeding from this assumption, one could expect that in the absence of the agonist both MEM and AM will be unable to block NMDA channels. However, this is not the case.

The data presented in this work show that in acutely isolated rat hippocampal neurons the aspartate (Asp)-induced opening of NMDA channels is not a prerequisite for their blockade by MEM and AM. These cationic compounds have proved to be able, although much more slowly, to enter and leave the NMDA channel via the 'hydrophilic route' without the assistance of the agonist. Moreover, the externally applied blocker reaches the same blocking site to which it binds in open channels. Some preliminary results from this study have been published in abstract form (Sobolevsky *et al.* 1996).

## METHODS

Two- to four-week-old Wistar rats were killed by cervical dislocation. Hippocampal slices were prepared according to the procedure described by Vorobiev (1991). Pyramidal neurons were mechanically isolated from the CA-1 region of the slice by vibrodissociation (Vorobiev, 1991). The experiments were started no earlier than 3 h after incubation of the hippocampal slices in a medium containing (mM): NaCl, 124; KCl, 3; CaCl<sub>2</sub>, 1.4; MgCl<sub>2</sub>, 2; glucose, 10; NaHCO<sub>3</sub>, 26. The solution was bubbled with carbogen and maintained at 32 °C. During the whole period of isolation and current recording, nerve cells were washed with a Mg<sup>2+</sup>-free solution (mM): NaCl, 140; KCl, 5; CaCl<sub>2</sub>, 2; glucose, 15; Hepes, 10; pH 7.3. All the drugs were dissolved in water. Concentrated drug stock solutions were prepared and kept frozen until use. Fast replacement of the superfusing solutions ( $\tau < 30$  ms) was achieved by using the concentration-jump technique (Benveniste *et al.* 1990; Vorobiev, 1991). The currents were recorded at 18 °C in the whole-cell configuration by using micropipettes made from Pyrex tubes and filled with an 'intracellular' solution (mM): CsF, 140; NaCl, 4;

Hepes, 10; pH 7.2. Electrical resistance of the filled micropipettes was 3–7 M $\Omega$ . The analog current signals were digitized at 1 kHz frequency.

Statistical analysis was performed with the aid of Origin 3.5 (Microcal Software Inc., MA, USA) software. All the data are presented as means  $\pm$  s.e.m. and comparisons were made using Student's paired *t* test except as noted. To distinguish between one- and two-exponential fits, Fischer's test was used.

Amino-adamantane derivatives were synthesized at MERZ (Eckenheimer Landstr. 100–104, 60318 Frankfurt-am-Main, Germany). The p*K*<sub>a</sub> value for MEM is 10.27. Under our experimental conditions (pH 7.3) MEM and the more hydrophilic AM were almost completely dissociated and carried the charge of +1.

## RESULTS

### Blockade of open NMDA channels by MEM and AM

In agreement with previous reports (Chen *et al.* 1992; Parsons *et al.* 1993, 1995; Bresink *et al.* 1996; Blanpied *et al.* 1997; Chen & Lipton, 1997), MEM and AM produced a concentration-, time- and voltage-dependent blockade of open NMDA channels.

Ionic currents through NMDA channels were elicited by fast application of 100  $\mu$ M aspartate (Asp) in a Mg<sup>2+</sup>-free, 3  $\mu$ M glycine-containing solution. In all experiments except for those studying the voltage dependencies, the membrane potential was held at  $-100$  mV. Asp induced an inward current which, after an initial fast rise ( $\tau < 30$  ms) up to the value  $I_C$ , indicating the opening of NMDA channels, decreased gradually ( $\tau_D = 374 \pm 26$  ms) down to a certain plateau level  $I_0$  (Fig. 1*A*, first trace). Such a current decay under continued action of the agonist is a result of desensitization of the receptor–channel complex. The rate of recovery from desensitization was fast (Fig. 1*A*). The time constant of this process measured in six cells with a fraction of desensitized channels,  $d = 1 - I_0/I_C = 0.50 \pm 0.03$ , was  $1.17 \pm 0.05$  s (Fig. 1*B*).

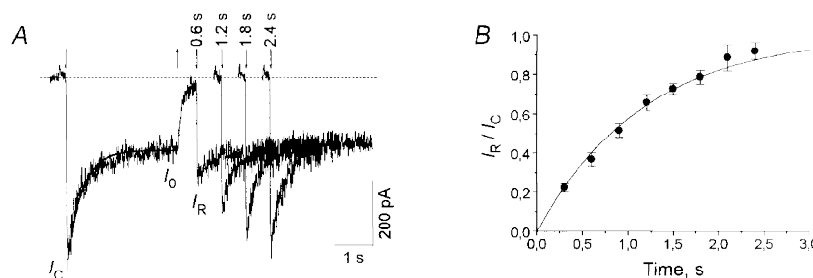


**Figure 1. Desensitization of NMDA channels**

*A*, inward current through NMDA channels was elicited by a 3 s application of 100  $\mu$ M Asp at the membrane potential of  $-100$  mV. The dotted line indicates zero current level. The desensitization-induced current decay during the Asp pulse was fitted with the single exponential function with the time constant  $\tau_D = 374 \pm 26$  ms (continuous line). The second to the fifth traces are the currents elicited by the test Asp application 0.6–2.4 s after the termination of the first (conditioning) Asp application. The initial current ( $I_R$ ) recovered with an increase in the time interval between the Asp applications. The downward and upward arrows indicate the beginning and termination of the Asp applications, respectively. *B*, time course of the recovery from desensitization. The continuous line is the single exponential fitting of  $I_R/I_C$  with the time constant  $\tau = 1.17 \pm 0.05$  s.



MEM was applied at different concentrations in the continuous presence of Asp ( $100\ \mu\text{M}$ ). The two-exponential fitting of the current traces (Fig. 2*A*) made it possible to reveal the existence of two (fast and slow) kinetic components in both blocking and recovery processes. The average values of the fast and slow time constants ( $\tau_{\text{fast}}$  and  $\tau_{\text{slow}}$ , respectively) and the amplitude of the fast component ( $A_{\text{fast}}$ ) for the recovery from the MEM block are presented in Table 1.  $A_{\text{fast}}$  decreased with a rise in the blocker concentration (the values of  $A_{\text{fast}}$  at any two different concentrations were significantly different,  $P < 0.0002$ ). This decrease is the evidence for two distinct blocking sites of MEM in open NMDA channels which can be simultaneously occupied by two blocker molecules (Sobolevsky & Koshelev, 1998). For the sake of simplicity, this point is not reflected in Model 1.

The kinetics of AM were much faster than those of MEM and were well fitted with monoexponential functions. The value of the time constant for the recovery from the AM

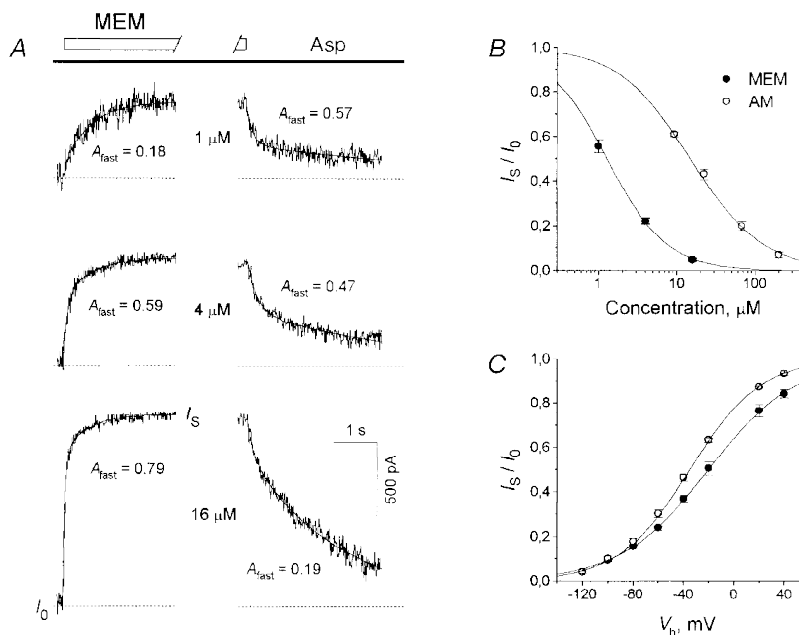
block did not depend on the AM concentration, being on average  $0.25 \pm 0.04\ \text{s}$  ( $n = 8$ ).

Figure 2*B* shows the concentration dependencies of the stationary block of open NMDA channels by MEM and AM measured according to the experimental protocol shown in Fig. 2*A*. The fitting was performed in accordance with a two-parameter logistic equation:

$$I_s/I_o = 1/(1 + ([C]/IC_{50})^{n_H}), \quad (1)$$

where  $I_o$  is the stationary current amplitude in the absence of the blocker,  $[C]$  is the blocker concentration,  $IC_{50}$  is the concentration resulting in 50% block and  $n_H$  is the Hill coefficient. The respective  $IC_{50}$  values and the Hill coefficient were:  $1.28 \pm 0.10\ \mu\text{M}$  and  $1.15 \pm 0.07$  ( $n = 6$ ) for MEM and  $14.9 \pm 0.3\ \mu\text{M}$  and  $0.94 \pm 0.04$  ( $n = 9$ ) for AM.

The extent of the block increased with membrane hyperpolarization. Figure 2*C* demonstrates the voltage dependence of the stationary blockade by MEM ( $10\ \mu\text{M}$ ) and AM ( $200\ \mu\text{M}$ ) examined using the experimental protocol shown



**Figure 2. Kinetics, concentration and voltage dependencies of the amino-adamantane derivative-induced blockade of open NMDA channels**

*A*, kinetics of the open NMDA channel interaction with MEM. Asp ( $100\ \mu\text{M}$ ) was applied continuously. MEM was co-administered at different concentrations for 5 s with Asp. Original NMDA responses were recorded at MEM concentrations of 1–16  $\mu\text{M}$ . The current traces presented in the left and right panels show the onset and offset kinetics of MEM, respectively. The continuous lines show the fitting of these traces with two-exponential functions.  $A_{\text{fast}}$ , the fraction of the fast component, rose with the MEM concentration at the onset and diminished at the offset. *B*, concentration dependence of the stationary blockade by MEM and AM. AADs were applied at different concentrations in the continuous presence of Asp, as shown in *A*. Plateau current responses ( $I_s$ ) divided by the control plateau value ( $I_o$ ) were plotted against the concentration of the blockers. The continuous lines show the fittings of the data with the logistic equation (eqn (1)). The fit parameters are:  $IC_{50} = 1.28\ \mu\text{M}$ ,  $n_H = 1.15$  for MEM and  $IC_{50} = 14.9\ \mu\text{M}$ ,  $n_H = 0.94$  for AM. *C*, voltage dependence of the open-channel blockade by AADs. MEM ( $10\ \mu\text{M}$ ) or AM ( $200\ \mu\text{M}$ ) at different membrane potentials were applied in the continuous presence of Asp, as shown in Fig. 2*A*. The  $I_s/I_o$  values were plotted against the membrane potential. The continuous lines show the fitting of the experimental data with eqn (2). The fit parameters are:  $K_{d(0)} = 17.9\ \mu\text{M}$ ,  $\delta = 0.73$  for MEM and  $K_{d(0)} = 694\ \mu\text{M}$ ,  $\delta = 0.90$  for AM.

in Fig. 2A. The fitting was performed according to the equation:

$$I_s = I_0 / ((1 + [C]/K_{d(0)}) \exp(\delta F V_h / RT)), \quad (2)$$

where  $I_0$  is the stationary current amplitude in the absence of the blocker,  $[C]$  is the blocker concentration,  $V_h$  is the holding membrane potential,  $K_{d(0)}$  is the equilibrium dissociation constant at  $V_h = 0$  mV, and  $\delta$  is the fraction of the membrane electric field seen by the blocker bound to a single blocking site.  $F$ ,  $R$  and  $T$  have their usual physical meanings. The voltage dependence had the following parameters:  $K_{d(0)} = 17.9 \pm 1.0 \mu\text{M}$  and  $\delta = 0.73 \pm 0.02$  ( $n = 5$ ) for MEM;  $K_{d(0)} = 694 \pm 17 \mu\text{M}$  and  $\delta = 0.90 \pm 0.01$  ( $n = 4$ ) for AM.

### Recovery of NMDA channels from the block without agonist assistance

Model 1 predicts that the blocker can leave the closed blocked state of the channel,  $C_B$ , only after the binding of the

agonist to the receptor. However, the data presented below show that the channel unblocking may also proceed without agonist assistance, the agonist greatly accelerating this process. The time course of this unblocking was monitored using the experimental protocol shown in Fig. 3A. The specific blocker of the NMDA receptor, APV ( $100 \mu\text{M}$ ), was added to the washout solution in order to avoid possible activation of the channels by putative traces of the agonist in the medium. At the beginning of the experiment, Asp ( $100 \mu\text{M}$ ) and MEM ( $25 \mu\text{M}$ ) were co-applied once or several times up to a practically complete inhibition of the stationary current ( $I_F$ ). At this point, the value of  $I_F/I_C$  was  $0.026 \pm 0.002$  ( $n = 19$ ). At the end of Asp and MEM co-application, the majority of channels were in states  $O_{AB}$ ,  $C_{AB}$  and  $D_{AB}$  and only a small number of them were in states  $O_A^*$ ,  $C_A$  and  $D_A$  (see Model 1). After washout during the time interval  $t$  (from 10 to 300 s), the cell was stimulated with an Asp ( $100 \mu\text{M}$ ) test pulse. The latter elicited a fast current increase ( $I_B$ ) followed by its gradual elevation. The

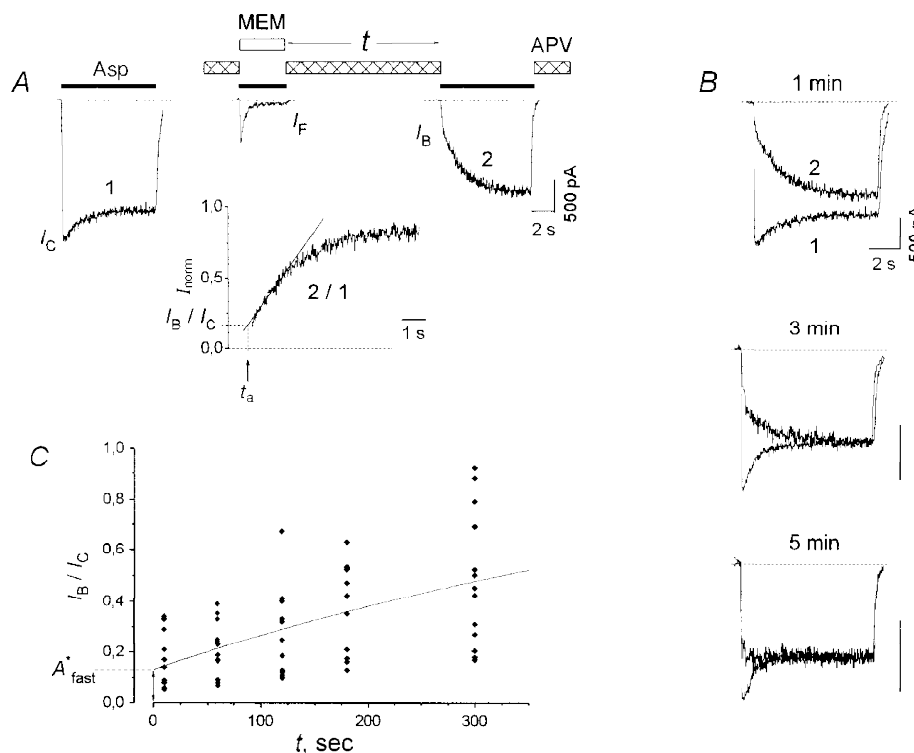


**Figure 3. NMDA channel recovery from AAD blockade without agonist assistance**

A, the experimental protocol was used to study the unblocking kinetics of the channels in the absence of the agonist. After MEM ( $25 \mu\text{M}$ ) and Asp ( $100 \mu\text{M}$ ) co-application, the cell was washed with an agonist-free control solution for 1 min. To ensure the absence of the agonist contamination, APV ( $100 \mu\text{M}$ ) was added to the washout solution. The inset shows the ratio of test (2) and control (1) current traces. The linear part of the slow gradual increase of this ratio from the moment when APV dissociated from the channel was fitted with the linear equation  $I_{\text{norm}} = a + b(t - t_a)$  (continuous line). The value 'a' on this line corresponding to the beginning of the test Asp application ( $t = t_a$ ) is  $I_B/I_C$ . B, the superposition of control and test current traces obtained by using the experimental protocol shown in A at different (1, 3 and 5 min) washout time intervals. The dissociation of APV was fast; therefore the distortion of the initial current increase is not seen on this time scale. Note that the slow component of the current recovery decreases, while the fast component rises with an increase in  $t$ . C, the time course of the  $I_B/I_C$  recovery in the absence of the agonist. The continuous line shows the fitting of the time dependence of mean  $I_B/I_C$  values with eqn (3). The fit parameters are:  $A = 1$ ,  $A^*_{\text{fast}} = 0.13$  and  $\tau^*_{\text{slow}} = 592$  s.

**Table 1. Asp-induced dissociation kinetics of MEM under different conditions**

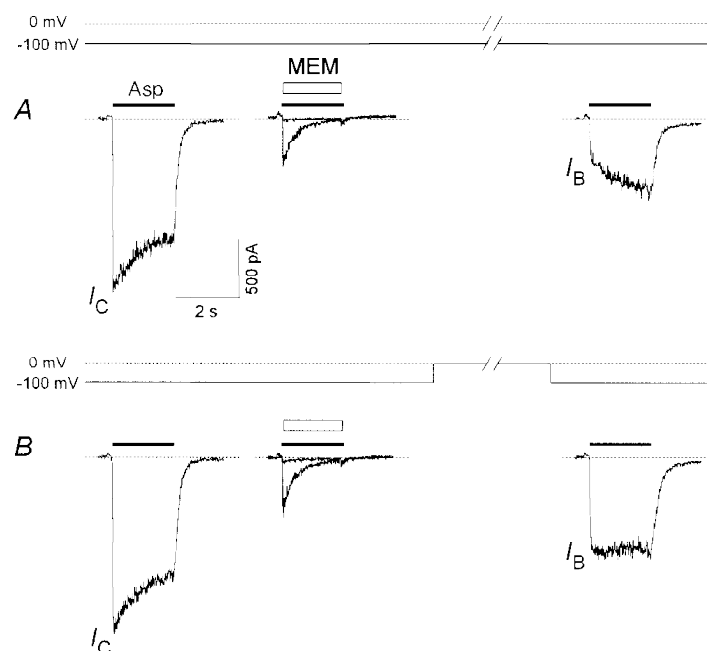
[MEM] ( $\mu\text{M}$ )	$A_{\text{fast}}$	$\tau_{\text{fast}}$ (s)	$\tau_{\text{slow}}$ (s)
In the continuous presence of agonist			
1	$0.55 \pm 0.05$	$1.5 \pm 0.3$	$20.4 \pm 4.3$
4	$0.42 \pm 0.03$	$1.3 \pm 0.5$	$18.8 \pm 1.1$
16	$0.19 \pm 0.01$	$1.3 \pm 0.3$	$17.0 \pm 1.9$
After blockade, without agonist assistance			
50	$0.24 \pm 0.02$	$1.7 \pm 0.5$	$21.3 \pm 4.4$

slow current increase up to its control stationary level ( $I_0$ ) evidently reflected the process of Asp-induced recovery from the block (the transitions from states  $C_B$ ,  $C_{AB}$ ,  $D_{AB}$  and  $O_{AB}$  to  $O_A^*$  in Model 1). The value of the  $I_B$  time constant,  $\tau_{\text{ini}}$ , was equal to  $118 \pm 6$  ms ( $n = 18$ ), which exceeded that measured in the absence of APV in the washout solution ( $\tau = 70 \pm 10$  ms,  $n = 11$ ). This slow-down of the initial fast component of the current recovery was evidently determined from the dissociation kinetics of APV. As  $\tau_{\text{ini}}$  was much smaller than  $\tau_{\text{fast}}$  of the current recovery kinetics in the presence of Asp (Fig. 2A, Table 1),  $I_B$  may be considered as a current through those NMDA channels which had already reached the closed state C by the beginning of the Asp test

pulse (see Model 1) and were ready to open right after APV dissociation. To estimate the value of  $I_B$ , the following procedure was used. To exclude the influence of desensitization of non-blocked channels (transitions to state D) on the Asp-induced current recovery from the blocked states ( $C_B$ ,  $C_{AB}$ ,  $D_{AB}$  and  $O_{AB}$ ), the test current trace (2) was divided by the control current trace (1). The  $I_B/I_C$  value was estimated via linear approximation of the initial phase of this quotient to the beginning of the Asp application after complete APV dissociation (Fig. 3A, inset). The fast component,  $I_B$ , increased with the lengthening of the washout time interval  $t$  (Fig. 3B). The values of  $I_B/I_C$  at  $t = 0$  s and 5 min were significantly different ( $P < 0.00025$ ,  $n = 10$ ); their difference was on average  $0.32$  (s.d. =  $0.17$ ). Figure 3C shows the time dependence of the  $I_B/I_C$  values. The time dependence of the mean  $I_B/I_C$  values included two components: (1) the fast component with a time constant smaller than 10 s and (2) the slow component with a time constant,  $\tau_{\text{slow}}^*$ , greater than 100 s. To estimate the amplitude of the fast component,  $A_{\text{fast}}^*$ , and the time constant of the slow component, the data were fitted with the following equation:

$$I_B/I_C = A - (A - A_{\text{fast}}^*) \exp(-t/\tau_{\text{slow}}^*), \quad (3)$$

where  $A$  is 1,  $A_{\text{fast}}^*$  is  $0.13 \pm 0.03$  and  $\tau_{\text{slow}}^*$  is  $592 \pm 129$  s ( $n = 18$ ). The parameter  $A$  was taken as unity because the fitting of the mean data and the individual fittings in the majority of cells ( $n = 11/15$ ) with free  $A$  gave the value

**Figure 4. Voltage dependence of the recovery of the NMDA channels from the MEM block in the absence of the agonist**

**A**, washout of the cell for 1 min at  $-100$  mV after a practically complete blockade by MEM ( $25 \mu\text{M}$ ) led to the clearing of a relatively small fraction of the channels ( $I_B/I_C = 0.19 \pm 0.03$ ,  $n = 9$ ). **B**, many more channels ( $I_B/I_C = 0.30 \pm 0.05$ ,  $n = 9$ ) were recovered when the membrane potential was switched to  $0$  mV during the same washout interval.



The following experiments were carried out without addition of APV to the washout solution. This did not affect the rate of the NMDA channel recovery from the MEM-induced blockade in the absence of the agonist. Thus, the values of  $I_B/I_C$  at  $t = 1$  min were  $0.20 \pm 0.03$  and  $0.20 \pm 0.02$  in the presence and absence of APV ( $100 \mu\text{M}$ ), respectively (these values were not significantly different,  $P > 0.92$ ,  $n = 10$ ). This observation provided strong evidence that our solutions were not contaminated with traces of NMDA receptor agonists.

The recovery from the MEM block without agonist assistance was found to be voltage dependent (Fig. 4). Membrane depolarization accelerated this process. Thus, after a 1 min washout at  $-100$  mV,  $I_B/I_C$  was  $0.19 \pm 0.03$ , whereas in the case when the membrane potential was switched to  $0$  mV during the washout time interval,  $I_B/I_C$  was  $0.30 \pm 0.05$  (these values were significantly different,  $P < 0.01$ ,  $n = 9$ ). The switch-over of  $V_h$  to  $0$  mV was performed  $10$  s after the Asp plus MEM co-application and the reversal switch-over to  $-100$  mV was performed  $2$  s before the test Asp pulse.

Non-addition of glycine to the washout solution did not affect the rate of the unblocking of the agonist-independent channels. Thus, after  $3$  min washout of the cell with a glycine ( $3 \mu\text{M}$ )-containing solution and in the case when during the washout time interval this solution was switched to a nominally glycine-free solution, the values of  $I_B/I_C$  were  $0.32 \pm 0.04$  and  $0.31 \pm 0.03$ , respectively (these values were not significantly different,  $P > 0.5$ ,  $n = 9$ ). The switching of the solutions was performed  $10$  s after the Asp plus MEM co-application and  $20$  s before the test Asp pulse.

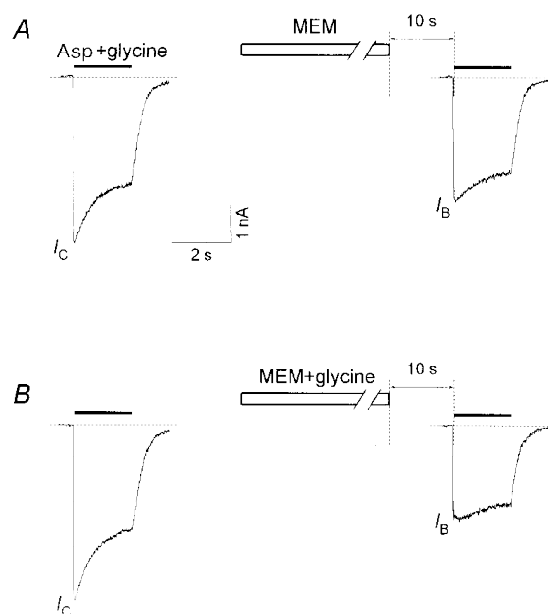
The recovery of the Asp-induced current after a practically complete inhibition by Asp and AM ( $250 \mu\text{M}$ ) co-application ( $I_F/I_C = 0.029 \pm 0.006$ ,  $n = 8$ ) proceeded much faster than after the Asp plus MEM co-application. Thus, already after  $10$  s washout of the cell, the value of  $I_B/I_C$  was  $0.63 \pm 0.02$  ( $n = 8$ ).

### AAD-induced blockade of NMDA channels in the absence of the agonist

As MEM is able to leave the NMDA channel without agonist assistance, it may be supposed that it can enter the channel in the absence of the agonist. Indeed, prolonged MEM application in the absence of Asp in the superfusing solution caused a pronounced blockade of NMDA channels. The experimental protocol used in this study is shown in Fig. 5B. At first, the control current was elicited by an  $8$  s  $100 \mu\text{M}$  Asp pulse. Not earlier than  $20$  s after this pulse, the cell was exposed to MEM ( $50 \mu\text{M}$ ) for  $1$  min, then washed for  $10$  s with the control solution to remove all possible traces of MEM in the medium and, finally, once again stimulated with the Asp test pulse. Glycine ( $3 \mu\text{M}$ ) was present in all these solutions. In control experiments, glycine failed to induce even a weak current through NMDA channels (Fig. 5A). Moreover, addition of APV ( $100 \mu\text{M}$ ) to the glycine-containing solution did not cause any change in the zero-level current (the mean and s.d. values were not significantly different at  $P > 0.26$ ,  $n = 15$ ). These observations provide strong evidence that the glycine-containing control solution was not contaminated with traces of NMDA receptor agonists. The current responses to the test Asp application following MEM washout were similar to those observed in studies of recovery of unliganded channels. When the inhibition of the initial current was considerable and desensitization was not very strong, the initial fast current increase was followed by the slow current elevation resulting from Asp-induced channels unblocking. However, when the inhibition of the Asp-induced current by MEM in the absence of the agonist was modest, desensitization caused a slow current decrease masking the slow current recovery (see Figs 6B, 9 and 10B). The latter became evident with more prolonged test Asp applications (not shown). As the initial fast current increase ( $I_B$ ) reflects the opening of unblocked channels, the value  $I_C - I_B$  may be considered as a measure for the fraction of NMDA

**Figure 6. Effect of glycine on the MEM-induced blockade of NMDA channels in the absence of Asp**

A, a  $1$  min application of MEM ( $50 \mu\text{M}$ ) in the absence of glycine produced only a modest decrease in the initial current response caused by the test application of Asp ( $100 \mu\text{M}$ ) plus glycine ( $3 \mu\text{M}$ ) ( $I_B/I_C = 0.78 \pm 0.14$ ,  $n = 6$ ). B, a much more profound block was produced by the same MEM application in the continuous presence of glycine ( $I_B/I_C = 0.51 \pm 0.12$ ,  $n = 6$ ).





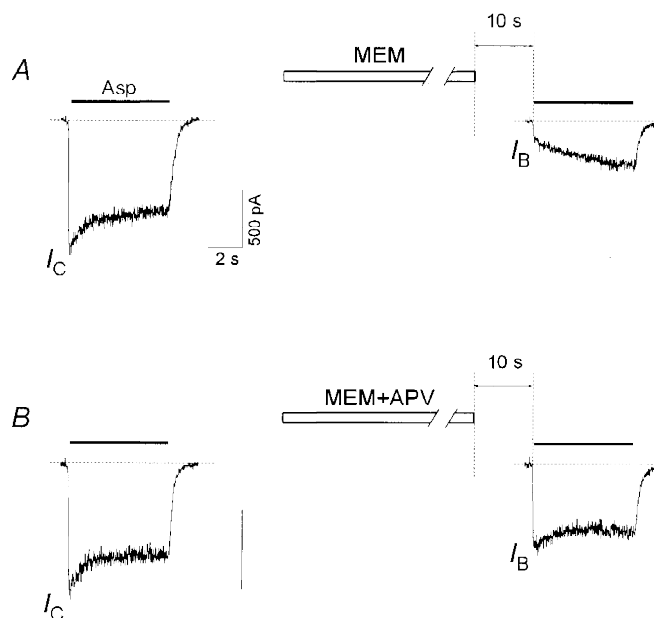


**Figure 7.** Effect of APV on the MEM-induced blockade of NMDA channels in the absence of Asp

*A*, a 1 min application of MEM (50  $\mu\text{M}$ ) caused significant inhibition of the initial current in response to the test Asp (100  $\mu\text{M}$ ) application ( $I_B/I_C = 0.32 \pm 0.04$ ,  $n = 16$ ). *B*, addition of APV (100  $\mu\text{M}$ ) to a MEM-containing solution greatly decreased the inhibition of the initial current response ( $I_B/I_C = 0.79 \pm 0.05$ ,  $n = 16$ ).

channels which trapped the blocker without agonist assistance (the number of channels in state  $C_B$  of Model 1). A more thorough analysis of the Asp-induced slow current recovery revealed two kinetic components: one fast and one slow. As in the case of recovery of the NMDA channels in the absence of the agonist we fitted not the original current trace but the result of its division by the control trace,  $I_{\text{norm}}$  (Fig. 5*B*, inset). The parameters of the two-exponential fitting equation:

$$I_{\text{norm}} = 1 - (1 - I_B/I_C) \{ A_{\text{fast}} \exp(-t/\tau_{\text{fast}}) + (1 - A_{\text{fast}}) \exp(-t/\tau_{\text{slow}}) \} \quad (4)$$

proved to be:  $A_{\text{fast}} = 0.24 \pm 0.02$ ;  $\tau_{\text{fast}} = 1.7 \pm 0.5$  s; and

$\tau_{\text{slow}} = 21.3 \pm 4.4$  s ( $n = 7$ ). A comparison of these fitting parameters with the corresponding kinetic parameters for the open-channel blockade is given in Table 1. As in the case of the recovery of the channels in the absence of the agonist (see above), the value of  $I_B/I_C$  and, correspondingly, the rate of blockade of the NMDA channels by MEM in the absence of the agonist varied greatly in different cells. Thus, the mean value of  $I_B/I_C$  for all our experiments, in which MEM was applied for 1 min in the absence of the agonist, was  $0.35$  (s.d. =  $0.19$ ,  $n = 33$ ).

Addition of 3  $\mu\text{M}$  glycine to the MEM-containing solution enhanced the blocking effect of MEM (Fig. 6). Thus a 1 min application of MEM (50  $\mu\text{M}$ ) in the presence of glycine

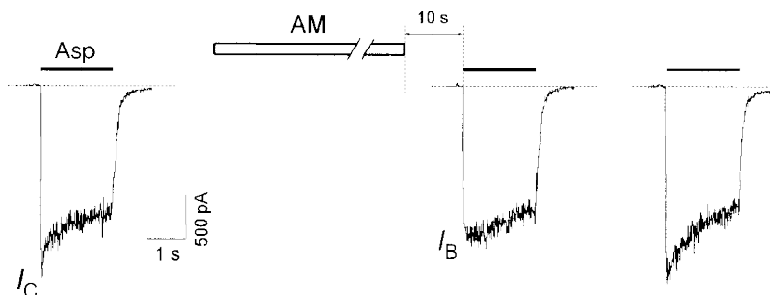


**Figure 8.** AM-induced blockade of NMDA channels in the absence of Asp

A 1 min application of AM (1 mM) in the absence of the agonist produced only a modest reduction of the initial current ( $I_B/I_C = 0.8$ ) in response to the test application of Asp (100  $\mu\text{M}$ ). The next test application of Asp 4 s after the first one induced a current response identical to the control.

induced a stronger blockade of the channels without agonist assistance ( $I_B/I_C = 0.51 \pm 0.12$ ,  $n = 6$ ) than in the nominally glycine-free solution ( $I_B/I_C = 0.78 \pm 0.14$ ,  $n = 6$ ). These values were significantly different ( $P < 0.003$ ,  $n = 6$ ).

Addition of APV ( $100 \mu\text{M}$ ) to the MEM-containing solution considerably diminished the inhibition of the initial current elicited by test application of Asp (Fig. 7). The  $I_B/I_C$  values after a 1 min application of MEM in the presence ( $0.79 \pm 0.05$ ) and absence of APV ( $0.32 \pm 0.04$ ) were significantly different ( $P < 10^{-6}$ ,  $n = 16$ ).

AM also proved to be able to block the channels in the absence of the agonist (Fig. 8). In this case, however, most of the channels became cleared during a 10 s washout interval (see above). Therefore, the AM-induced blockade of the agonist-unbound channels was manifested only as a reduction of the initial current value ( $I_B/I_C < 1$ ) in response to the test application of Asp. Because of the fast recovery from the block by AM, the Asp application 4 s after the test one induced a current response identical to that of the control (Fig. 8, last trace).

The blockade of NMDA channels by MEM in an Asp-free medium increased with the duration of the blocker application (Fig. 9). In Fig. 9 the desensitization of the channels during the control Asp pulse increased slowly over the time course of the experiment (cf. control responses in A

and C). In this case we increased the duration of MEM application from A to C. However, we also conducted another experiment in which the longest MEM application was used at first and then its duration was decreased. The result was the same: the fraction of blocked channels increased with the lengthening of the MEM application. Thus, the fact that the agonist-induced desensitization increased with time did not affect the results of our experiments. The single-exponential fit of the  $I_B/I_C$  time dependence gave the value of the time constant of  $84 \pm 6$  s ( $n = 5$ ). Neglecting the small fast component of recovery of the channels from the MEM-induced block in the absence of the agonist (13%, see Fig. 3C), the unblocking of the channels can be also considered as a single-exponential process. Thus, within the frame of a bimolecular reaction process, the association and dissociation rate constants for MEM binding and unbinding in the absence of the agonist can be estimated as  $2.04 (\pm 0.44) \times 10^2 \text{ M}^{-1} \text{ s}^{-1}$  and  $1.68 (\pm 0.129) \times 10^{-3} \text{ s}^{-1}$ , respectively. The apparent  $K_d$  value ( $8.3 \mu\text{M}$ ) proved to be six times higher than the  $\text{IC}_{50}$  for the MEM-induced blockade of open channels ( $1.3 \mu\text{M}$ ). Therefore, the affinity of NMDA channels to MEM in the absence of the agonist is about six times smaller than in its presence.

Membrane depolarization attenuated this block (Fig. 10). Thus, at  $-100$  mV a 1 min MEM ( $50 \mu\text{M}$ ) treatment induced a profound blockade ( $I_B/I_C = 0.21 \pm 0.03$ ). Membrane

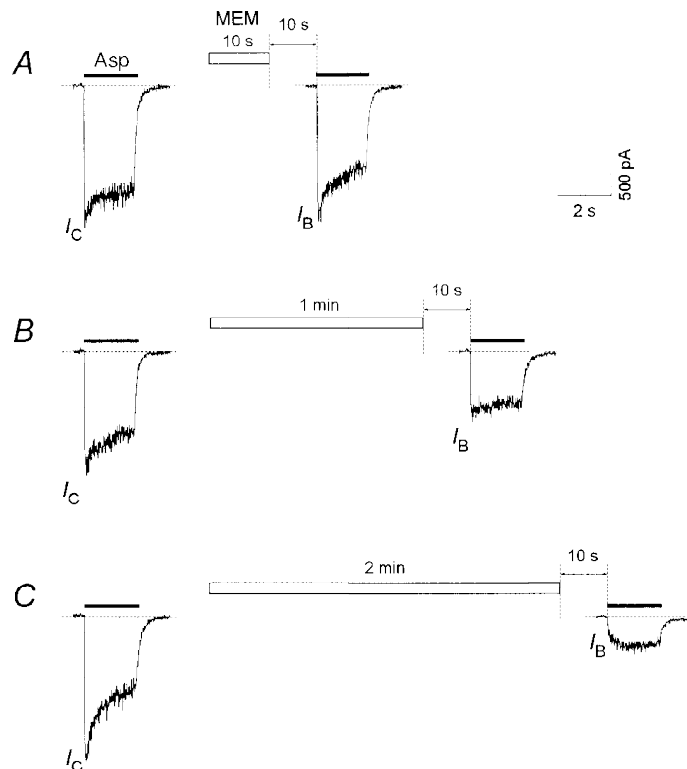


**Figure 9.** Kinetics of the MEM-induced blockade of NMDA channels in the absence of Asp

Applications of MEM ( $50 \mu\text{M}$ ) for 10 s (A), 1 min (B) and 2 min (C) produced an increasing inhibition of the initial current ( $I_B/I_C = 0.95$ ,  $0.58$  and  $0.14$ , respectively) in response to the test Asp ( $100 \mu\text{M}$ ) application. All recordings were made from the same cell.

depolarization to 0 mV during the period of MEM application diminished this block ( $I_B/I_C = 0.39 \pm 0.07$ ; these values were significantly different,  $P < 0.03$ ,  $n = 4$ ). The switching of the membrane potential was performed 2 s after the beginning and 2 s before the termination of the MEM application.

### Magnesium antagonized the MEM-induced blockade of NMDA channels in both the presence and the absence of Asp

In a  $Mg^{2+}$ -free Asp ( $100 \mu M$ )-containing solution, a 5 s application of MEM ( $15 \mu M$ ) caused a practically complete blockade of open NMDA channels. In this case, only a small fast component ( $17 \pm 3\%$ ,  $n = 5$ ) was observed in the offset kinetics of the MEM block (Fig. 11A, first trace). Addition of  $Mg^{2+}$  ( $2.5 \text{ mM}$ ) to the MEM-containing solution (Fig. 11A, third trace) greatly increased this fast component ( $48 \pm 1\%$ ,  $n = 5$ ). The offset kinetics of  $Mg^{2+}$  (Fig. 11A, second trace) is known to be very fast (Ascher & Nowak, 1988). Therefore, the difference between the above-mentioned fast component values (they were significantly different,  $P < 0.001$ ) reflects the minimal hindrance of  $Mg^{2+}$  to the blockade of open channels by MEM ( $31 \pm 3\%$ ,  $n = 5$ ).

In the second series of our experiments, we examined the effect of  $Mg^{2+}$  on the MEM-induced blockade of NMDA channels in the absence of Asp (Fig. 11B). MEM ( $50 \mu M$ ) and  $Mg^{2+}$  ( $2.5 \text{ mM}$ ) co-application induced a less profound blockade ( $I_B/I_C = 0.67 \pm 0.04$ ) of NMDA channels than

MEM itself ( $I_B/I_C = 0.33 \pm 0.05$ ). These values were significantly different ( $P < 0.03$ ,  $n = 6$ ). Thus  $Mg^{2+}$  prevented the MEM-induced blockade of NMDA channels not only in the presence but also in the absence of the agonist.

## DISCUSSION

Blockade of NMDA channels by AAD does not prevent the subsequent closure of the channel after removal of the agonist from the medium (Johnson *et al.* 1995; Chen & Lipton, 1997). The finding that Asp reapplication readily cleared the channels was considered as an indication that the blocking molecule had been trapped in the channel by the closed activation gate. Our experiments showed, however, that agonist-induced channel openings greatly accelerated but were not a prerequisite for the recovery from the AAD blockade (Fig. 3). What is the pathway whereby the blocker leaves the channel without agonist assistance? The finding that membrane depolarization accelerates recovery of the channels from AADs not only in the presence (Fig. 2C) but also in the absence of Asp (Fig. 4) allows us to conclude that in the two cases the blocker exits the channel via the same route (the 'hydrophilic' pathway in Hille's (1977) terminology). If so, provided that the blocker cannot leave the closed channel, we have to assume that in addition to the agonist-induced openings of NMDA channels there exist some infrequent agonist-independent transitions between the closed and open states of the channel. Therefore, in the

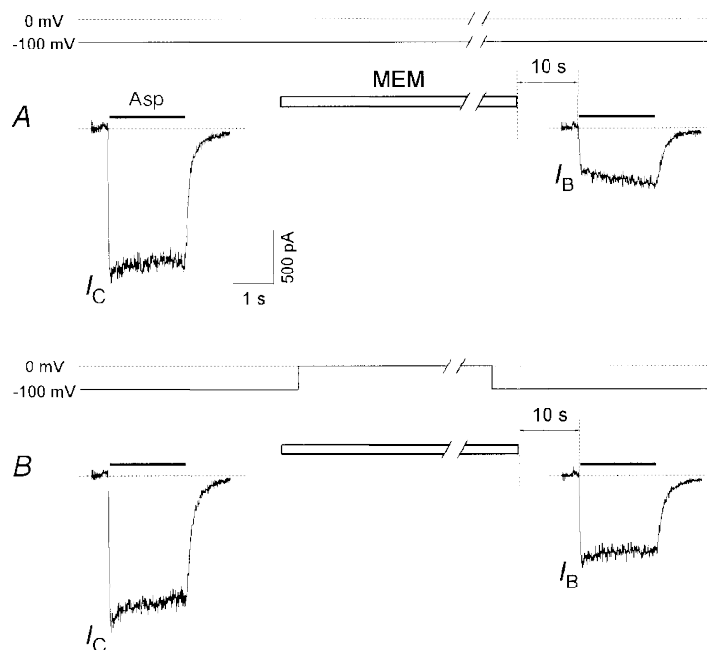


**Figure 10.** Voltage dependence of the MEM-induced blockade of NMDA channels in the absence of Asp

A, a 1 min application of MEM ( $50 \mu M$ ) at  $-100 \text{ mV}$  caused significant inhibition of the initial current in response to the test application of Asp ( $100 \mu M$ ) ( $I_B/I_C = 0.21 \pm 0.03$ ,  $n = 4$ ). B, a less profound MEM block ( $I_B/I_C = 0.39 \pm 0.07$ ,  $n = 4$ ) was produced when the membrane potential was switched to 0 mV during MEM application.

absence of the agonist the unblocking of the channels is thought to be as follows:  $C_B \rightarrow O_B \rightarrow O \rightarrow C$ , where all the transitions are agonist independent and the transition from  $O_B \rightarrow O$  is voltage dependent. The  $C_B \rightarrow O_B$  transition provides a much slower recovery from the AAD-induced block in the absence of the agonist than the transition  $C_{AB} \rightarrow O_{AB}$  (see Model 1) in its presence. Thus, for MEM the slow recovery time constant in the absence of the agonist (Fig. 3C) was approximately thirty times greater than that for the unblocking of open channels (Table 1). If the unblocking of the channels in the absence of Asp resulted from spontaneous transitions of channels from the closed to the open states, these openings would generate a permanent inward current of only 30 times smaller magnitude than that elicited by  $100 \mu\text{M}$  Asp. However, this is not the case (Fig. 5A). To our knowledge, up to now there is still no evidence for the existence of spontaneous NMDA channel openings (i.e.  $C \rightarrow O$  transitions), although such openings are well known for acetylcholine-activated ligand-gated channels (Jackson, 1986). Glycine alone was shown to

activate recombinant heteromeric NMDA channels (Meguro *et al.* 1992; Monyer *et al.* 1992). In our experiments, glycine alone did not induce a current through the NMDA channels (Fig. 5A). Moreover, the glycine independence of recovery of the NMDA channels from the MEM block in the absence of the agonist strongly indicates that glycine alone does not induce channel opening. Therefore, we have to assume that the blocking molecule trapped in the channel promotes in some way random channel openings. This supposition is in good agreement with the recent finding that MEM binding inside the channel pore shifts the open–closed equilibrium towards the channel opening by  $\sim 4.81 \text{ kJ mol}^{-1}$  (Chen & Lipton, 1997).

The ability of AADs to leave the unliganded NMDA channel led us to examine their capability of blocking the channels without agonist assistance. It has been found that MEM and AM are able to block the agonist-unbound channels, although this process is much slower (Fig. 9) and requires much higher concentrations than the open channel blockade.

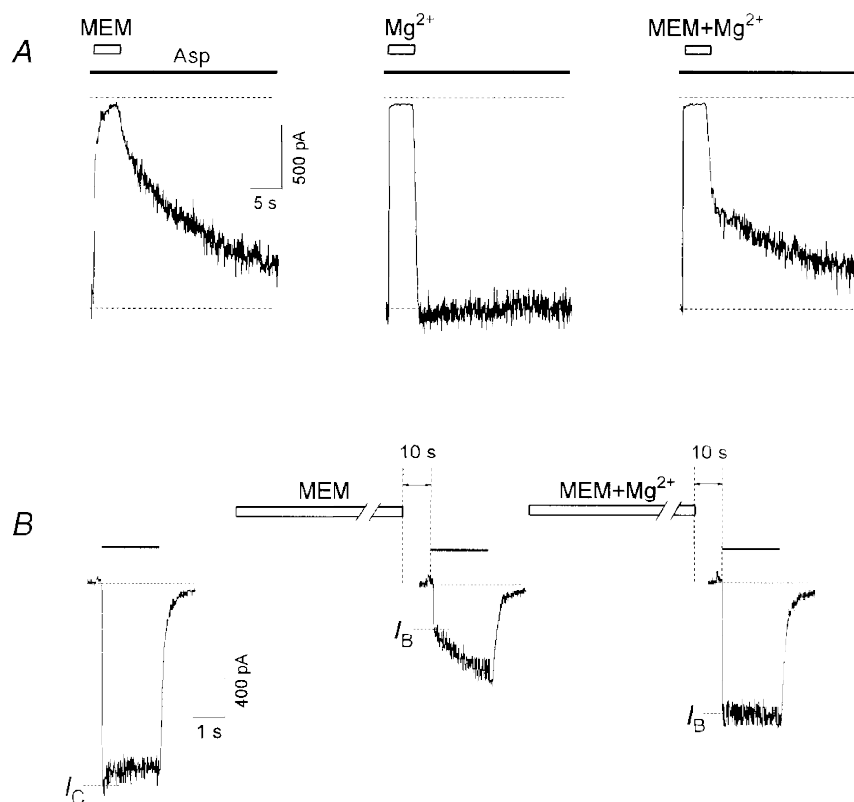
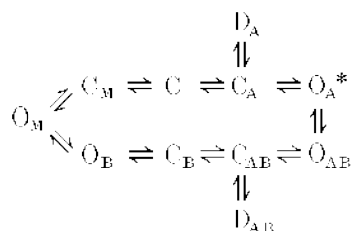


**Figure 11. Effect of  $\text{Mg}^{2+}$  on the MEM-induced blockade of NMDA channels**

A, effect of  $\text{Mg}^{2+}$  on the MEM-induced open-channel blockade. Asp ( $100 \mu\text{M}$ ) was applied continuously. MEM ( $15 \mu\text{M}$ ) applied for 5 s manifested mainly slow, while  $\text{Mg}^{2+}$  ( $2.5 \text{ mM}$ ) manifested very fast open-channel kinetics. After MEM and  $\text{Mg}^{2+}$  co-application, the double-exponential unblocking kinetics (intermediate between those mentioned above) reflects the minimal hindrance of  $\text{Mg}^{2+}$  to the MEM-induced open-channel blockade. B, effect of  $\text{Mg}^{2+}$  on the MEM-induced blockade in the absence of Asp. A 1 min application of MEM ( $50 \mu\text{M}$ ) caused significant inhibition of the initial current in response to the test application of Asp ( $100 \mu\text{M}$ ) ( $I_B/I_C = 0.33 \pm 0.05$ ,  $n = 6$ ). Addition of  $\text{Mg}^{2+}$  ( $2.5 \text{ mM}$ ) to a MEM-containing solution caused a less profound inhibition of the initial current response ( $I_B/I_C = 0.67 \pm 0.04$ ,  $n = 6$ ).

Membrane hyperpolarization enhanced the MEM-induced blockade of agonist-unbound NMDA channels (Fig. 10) as well as the open-channel blockade (Fig. 2C). External  $Mg^{2+}$  effectively antagonized the MEM block development in both the presence (Fig. 11A) and the absence (Fig. 11B) of Asp. These findings strongly support the hypothesis that the blocker reaches its binding site in the agonist-unbound channel via the same 'hydrophilic pathway' as in the presence of the agonist.

By drawing an analogy with recovery from the AAD block for unliganded channels, we may assume that the blocker alone is able to promote agonist-independent channel transitions to the open state which provides a subsequent channel blockade. A possible mechanism of blockade of the channels and, correspondingly, the unblocking in the absence of the agonist is shown in Fig. 12. AAD binding to the modulatory site (M-site) promotes the agonist-independent channel openings. During these openings, AAD 'jumps' to the blocking site (B-site) and becomes trapped behind the closed activation gate. The  $O_M$  state can be the non-conducting or short-living (comparing with state  $O_A^*$  in Model 1) conducting state of the NMDA channel which cannot be detected at our time resolution. It is therefore not surprising that no openings were observed in our experiments with the AAD-induced blockade and recovery from it in the absence of the agonist. Thus, the new states ( $C_M$ ,  $O_M$  and  $O_B$ ) should be added to Model 1, resulting in the simplified Model 2.



Model 2

The fact that APV effects in the absence of the agonist were not symmetrical (APV hindered the MEM-induced blockade but did not influence unblocking of the channels) can be easily explained in terms of Model 2. APV can prevent the

MEM binding to the M-site but does not affect its binding to the blocking site.

There are at least two other possible answers to the question 'How can externally applied AAD reach its binding site located deep in the channel pore via the hydrophilic pathway without agonist assistance?'. (1) MEM and AM block NMDA channels during their infrequent spontaneous openings. (2) The NMDA receptor co-agonist glycine induces random channel openings. As discussed above, the involvement of spontaneous and glycine-induced openings in the recovery of unliganded channels from the AAD-induced blockade seems to be doubtful. As far as the blockade of the agonist-unbound channels is concerned, our data do not allow us to make a choice between spontaneous, glycine-induced or blocker-induced openings.

The kinetics of recovery of the channels from the MEM block in the presence of the agonist deserve special attention. In our experiments, NMDA channels were blocked by MEM in the presence (see Fig. 2A) or absence of Asp (see Fig. 5B). In the two cases, the agonist-induced current recovery appeared to be identical (Table 1). A good coincidence of the corresponding time constants for single- or two-exponential fittings allowed us to conclude that the blocking sites for MEM in the channel did not depend on whether the channels were blocked in the presence or absence of the agonist. The fact that the 10 s washout interval did not change either of the components of the Asp-induced unblocking kinetics (Table 1) suggests that these binding sites are located 'behind the activation gate' of the channel and that MEM being bound to these sites did not prevent the channel closure after removal of the agonist from the medium.

Our interpretation of the interaction of MEM with the majority of NMDA channels differs from that of Blanpied *et al.* (1997) who proposed two different mechanisms for MEM action. According to their opinion, MEM is able to produce (1) a trapping block where the blocker cannot leave without the agonist assistance and (2) non-competitive inhibition of NMDA channels where the blocker reaches its site via the hydrophobic pathway. In our opinion, MEM blocks and leaves the agonist-unbound channel via the same hydrophilic

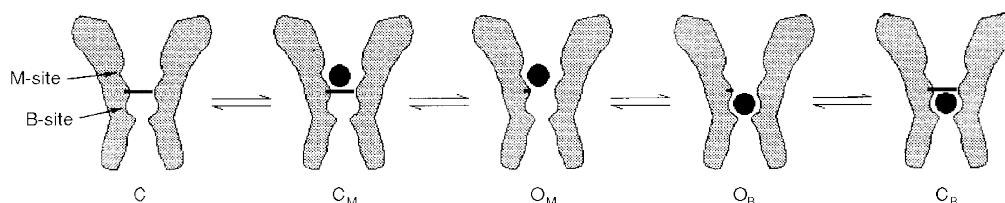


Figure 12. Schematic presentation of a possible mechanism of AAD interaction with the NMDA channel in the absence of the agonist

AAD binding to the modulatory site (M-site) or the blocking site (B-site) promotes the agonist-independent channel openings. During these openings, AAD 'jumps' from the M-site to the B-site or back, and either becomes trapped by the closed activation gate or leaves the channel.  $O_M$  can be the non-conducting or short-lived conducting state of the NMDA channel.



pathway as it does in the open channel. Even the binding sites remain the same and only the rate of the MEM interaction with the channels in the absence of the agonist is slowed down. However, in our experiments the recovery from the MEM block in the absence of the agonist was not complete in some cells (4/15). In these cases, the mechanism of MEM action can probably be described as in Blanpied *et al.* (1997). The existence of different mechanisms of MEM action can be explained by the heterogeneity of NMDA channels in the neuronal membrane.

It is also necessary to discuss the major methodological differences between our study and that of Blanpied *et al.* (1997). We used a saturating agonist concentration (100  $\mu\text{M}$  Asp), while Blanpied *et al.* (1997) used a very low agonist concentration (5  $\mu\text{M}$  NMDA). Therefore, in the latter study the blockade reached its steady-state level very slowly: after 1 min agonist and blocker co-application even at a high MEM concentration (50  $\mu\text{M}$ ). In contrast, in our experiments 2–5 s co-application appeared to be quite sufficient to induce an almost complete block.

As MEM affinity for the NMDA channel in the absence of the agonist is only about six times smaller than in its presence, the wide therapeutic application of memantine (Danysz *et al.* 1995) can be partly due to its slow interaction with NMDA channels during the intervals between glutamate releases.

A more profound analysis is required to explain the difference in the mechanisms of MEM interaction with the gating machinery of closed NMDA channels in two cases: when the blocker trapped in the channel 'attempts' to leave it and when the blocker is present in the external medium and 'knocks' at the closed channel gate. Different effects of APV point to different mechanisms of MEM action in these two cases.

- ASCHER, P. & NOWAK, L. (1988). The role of divalent cations in the N-methyl-D-aspartate responses of mouse central neurones in culture. *Journal of Physiology* **399**, 247–266.
- BENVENISTE, M., CLEMENTS, J., VYKICKY, J. & MAYER, M. L. (1990). A kinetic analysis of the modulation of NMDA receptors by glycine in mouse cultured hippocampal neurones. *Journal of Physiology* **428**, 333–357.
- BLANPIED, T. A., BOECKMAN, F., AIZENMAN, E. & JOHNSON, J. W. (1997). Trapping channel block of NMDA-activated responses by amantadine and memantine. *Journal of Neurophysiology* **77**, 309–323.
- BRESINK, I., BENKE, T. A., COLLETT, V. J., SEAL, A. J., PARSONS, C. G., HENLEY, J. M. & COLLINGRIDGE, G. L. (1996). Effects of memantine on recombinant rat NMDA receptors expressed in HEK 293 cells. *British Journal of Pharmacology* **119**, 195–204.
- CHEN, H.-S. V. & LIPTON, S. A. (1997). Mechanism of memantine block of NMDA-activated channels in rat retinal ganglion cells: uncompetitive antagonism. *Journal of Physiology* **499**, 27–46.
- CHEN, H.-S. V., PELLEGRINI, J. W., AGGARWAL, S. K., LEI, S. Z., WARACH, S., JENSEN, F. E. & LIPTON, S. A. (1992). Open-channel block of NMDA responses by memantine: therapeutic advantage against NMDA receptor-mediated neurotoxicity. *Journal of Neuroscience* **12**, 4427–4436.
- DANYSZ, W., PARSONS, C. G., BRESINK, I. & QUACK, G. (1995). Glutamate in CNS disorders. *Drug News and Perspectives* **8**, 261–277.
- HILLE, B. (1977). Local anesthetics: hydrophilic and hydrophobic pathways for the drug–receptor reaction. *Journal of General Physiology* **69**, 497–515.
- HUETTNER, J. E. & BEAN, B. P. (1987). Block of N-methyl-D-aspartate-activated current by the anticonvulsant MK-801: selective binding to open channels. *Proceedings of the National Academy of Sciences of the USA* **85**, 1307–1311.
- JACKSON, M. B. (1986). Kinetics of unliganded acetylcholine receptor channel gating. *Biophysical Journal* **49**, 663–672.
- JOHNSON, J. W., ANTONOV, S. M., BLANPIED, T. S. & LI-SMERIN, Y. (1995). Channel block of NMDA receptor. In *Excitatory Amino Acids and Synaptic Transmission*, ed. WHEAL, H. V., pp. 99–113. Academic Press, Inc., London.
- KEMP, J. A., FOSTER, A. C. & WONG, E. H. F. (1987). Non-competitive antagonists of excitatory amino acid receptors. *Trends in Neurosciences* **10**, 294–298.
- MCBAIN, C. J. & MAYER, M. L. (1994). N-methyl-D-aspartic acid receptor structure and function. *Physiological Reviews* **74**, 723–760.
- MACDONALD, J. F., BARTLETT, M. C., MODY, I., PAHAPILL, P., REYNOLDS, J. N., SALTER, M. W., SCHNEIDERMAN, J. H. & PENNEFATHER, P. S. (1991). Actions of ketamine, phencyclidine and MK-801 on NMDA receptor currents in cultured mouse hippocampal neurones. *Journal of Physiology* **432**, 483–508.
- MEGURO, H., MORI, H., ARAKI, K., KUSHINA, E., KUTSUWADA, T., YAMAZAKI, M., KUMANISHI, T., ARAKAWA, M., SAKIMURA, K. & MISHINA, M. (1992). Functional characterization of a heteromeric NMDA receptor channel expressed from cloned cDNAs. *Nature* **357**, 70–74.
- MONYER, H., SPRENGEL, R., SCHOEPFER, R., HERB, A., HIGUCHI, M., LOMELI, H., BURNASHEV, N., SAKMANN, B. & SEEBURG, P. H. (1992). Heteromeric NMDA receptors: molecular and functional distinction of subtypes. *Science* **256**, 1217–1221.
- PARSONS, C. G., GRUNER, R., ROZENTAL, J., MILLAR, J. & LODGE, D. (1993). Patch clamp studies on the kinetics and selectivity of NMDA receptor antagonism by memantine. *Neuropharmacology* **32**, 1337–1350.
- PARSONS, C. G., QUACK, G., BRESINK, I., BARAN, L., PRZEGALINSKI, E., KOSTOWSKI, W., KRZASCIK, P., HARTMANN, S. & DANYSZ, W. (1995). Comparison of the potency, kinetics and voltage-dependency of a series of uncompetitive NMDA receptor antagonists *in vitro* with anticonvulsive and motor impairment activity *in vivo*. *Neuropharmacology* **34**, 1239–1258.
- SOBOLEVSKY, A. & KOSHELEV, S. G. (1998). Two blocking sites of amino-adamantane derivatives in open N-methyl-D-aspartate channels. *Biophysical Journal* **74**, 1305–1319.
- SOBOLEVSKY, A., KOSHELEV, S. G. & KHODOROV, B. I. (1996). Memantine-induced blockade of NMDA channels without agonist assistance. *Journal of Physiology* **495**, P. 49P.
- VOROBIEV, V. (1991). Vibrodissociation of sliced mammalian nervous tissue. *Journal of Neuroscience Methods* **38**, 145–150.

**Acknowledgements**

The authors thank Dr P. Behe (Department of Pharmacology, University College London, UK) for critical discussion and helpful comments on an earlier version of this manuscript. We are very grateful to our colleagues at MERZ & Co. who have kindly provided us with amino-adamantanes. This work was supported by the Russian Fund of Fundamental Research (Nos 960449227 and 960449228) and an ISSEP grant to A.I.S. (No. a98-2018). The financial help of Dr Vadim Bogomolov is also highly appreciated.

**Corresponding author**

A. Sobolevsky: Institute of General Pathology and Pathophysiology, Baltiyskaya 8, 125315, Moscow, Russia.

Email: rans@rans.msk.ru

**Interaction of memantine and amantadine with agonist-unbound NMDA-receptor channels in acutely isolated rat hippocampal neurons**

Alexander I. Sobolevsky, Sergey G. Koshelev and Boris I. Khodorov

*J. Physiol.* 1998;512;47-60

**This information is current as of April 3, 2006**

**Updated Information  
& Services**

including high-resolution figures, can be found at:  
<http://jp.physoc.org/cgi/content/full/512/1/47>

**Permissions & Licensing**

Information about reproducing this article in parts (figures, tables) or in its entirety can be found online at:  
<http://jp.physoc.org/misc/Permissions.shtml>

**Reprints**

Information about ordering reprints can be found online:  
<http://jp.physoc.org/misc/reprints.shtml>

## Two-component blocking kinetics of open NMDA channels by organic cations

Alexander I. Sobolevsky \*

*Institute of General Pathology and Pathophysiology, Baltiyskaya 8, 125315 Moscow, Russia*

Received 20 July 1998; received in revised form 27 October 1998; accepted 30 October 1998

---

### Abstract

NMDA receptor channel responses were recorded from acutely isolated rat hippocampal neurons, using whole-cell patch-clamp techniques. In the continuous presence of aspartate, tetraethylammonium, tetrabutylammonium, 1-amino-3-propyl-adamantane and 9-aminoacridine caused changes in the current through NMDA channels, which were described by two-exponential functions. It was established that depending on the behavior of the amplitude of the fast component for the recovery kinetics, the blocker action can be assigned to one of five types described by the simplest models. The effects of tetraethylammonium, tetrabutylammonium and 1-amino-3-propyl-adamantane were well described by these models. Using 9-aminoacridine as an example, it was shown that the simplest models cannot describe all possible types of the blocker-channel interaction. In such cases, the method of the simplest models combination can be used. The application of the simplest kinetic models analysis allowed to make the following conclusions: at least two molecules of 1-amino-3-propyl-adamantane or 9-aminoacridine can simultaneously bind to the open channel and block it; the occupation of 9-aminoacridine blocking sites in the channel can proceed in at least two different ways; the binding of tetrabutylammonium and 9-aminoacridine prevented the closure of the activation and/or desensitization gates of the channel, while that of tetraethylammonium did not. © 1999 Elsevier Science B.V. All rights reserved.

**Keywords:** *N*-Methyl-D-aspartate channel; Hippocampal neuron; Patch clamp; Kinetics; Blockade

---

### 1. Introduction

The two-component kinetics of *N*-methyl-D-aspartate (NMDA)-mediated current changes induced by different blockers were described earlier. Thus, in the continuous presence of the NMDA channel agonists the existence of two kinetic components was shown for memantine [1–3] and other aminoadamantanes [4], long-chain adamantanes [5,6]; tetraalkylammonium compounds [7,8]; 1,2,3,4-tetrahydro-9-aminoacridine and 9-aminoacridine [9,8]. As NMDA chan-

nels play an important role in the processes of learning and memory, it is important to gain insight into the origin of multi-component kinetics manifested by NMDA channel blockers, especially when it is considered that some of them can be used as drugs in the treatment of a wide variety of neurodegenerative diseases [10].

The present study provides a simple method of a two-component kinetic analysis of changes induced in the stationary NMDA-mediated current by the blocker application. The analysis consists in the consideration of the amplitude of the fast component for the kinetics of recovery from the blockade ( $A_{\text{fast}}$ ) depending on the blocker concentration. The study

---

\* Fax: +7-095-151-0421; E-mail: rans@rans.msk.ru

of the  $A_{\text{fast}}$ -dependence on the blocker concentration allows one to describe the blocker action by one of the five simplest kinetic models or by their combination. The NMDA channel blockers: tetraethylammonium (TEA), tetrabutylammonium (TBA), 1-amino-3-propyl-adamantane or MRZ 2/178 (MRZ) and 9-aminoacridine (9-AA) were analyzed according to the  $A_{\text{fast}}$ -criterion. The kinetic models obtained for these blockers have made it possible to make conclusions about the number of blocking sites and the ways, by which the blockers reached these sites as well as about the blocker interaction with the gating machinery of the NMDA channel.

## 2. Materials and methods

Pyramidal neurons were acutely isolated from the CA1 region of rat hippocampus using 'vibrodissociation techniques' [11]. The experiments were begun not earlier than after 3 h incubation of the hippocampal slices in a solution containing (mM): NaCl, 124; KCl, 3; CaCl<sub>2</sub>, 1.4; MgCl<sub>2</sub>, 2; glucose, 10; NaHCO<sub>3</sub>, 26. The solution was bubbled with carbogen at 32°C. During the whole period of isolation and current recording, nerve cells were washed with a Mg<sup>2+</sup>-free solution (mM): NaCl, 140; KCl, 5; CaCl<sub>2</sub>, 2; glucose, 15; Hepes, 10; pH 7.3. Fast replacement of the superfusion solutions was achieved by using the concentration-jump technique [11,12]. The currents were recorded at 18°C in the whole-cell configuration using micropipettes made from pyrex tubes and filled with an 'intracellular' solution (mM): CsF, 140; NaCl, 4; Hepes, 10; pH 7.2. Electric resistance of the filled micropipettes was 3–7 MΩ. Analog current signals were digitized at 1 kHz frequency.

Statistical analysis was performed using the scientific and technical graphics computer program Microcal Origin (version 3.5 for Windows). The data presented are mean ± S.D. except as noted; comparison of means was done by ANOVA, with  $P < 0.05$  taken as significant.

The kinetic models used to simulate the blockers action were based on the conventional rate theory and used independent forward and reverse rate constants to simultaneously solve first-order differential equations representing the transitions between all

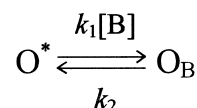
possible states of the channel. The rate constants were calculated by the method described in Appendix A with the help of Mathcad (version 5.0). Differential equations were solved numerically using the algorithm analogous to that described previously [13].

MRZ 2/178 was synthesized by MERZ (Eckenhaim, Frankfurt-am-Main, Germany); tetraethylammonium and tetrabutylammonium were purchased from Aldrich (USA); 9-aminoacridine from Sigma (USA). The three-dimensional structures of these compounds were obtained with the help of the Molecular Modeling System HyperChem (Release 3 for Windows).

## 3. Results

Application of aspartate (ASP) in the saturating concentration of 100 μM at the membrane potential of −100 mV in a Mg<sup>2+</sup>-free, 3 μM glycine-containing solution elicited an inward current through NMDA channels. After the initial fast rise ( $\tau < 30$  ms) this current decreased down to the value,  $I_0$ , with the time constant varying from 250 to 750 ms. Such a current decay in the continuous presence of the agonist is a result of desensitization of the receptor-channel complex. Only after the current reached its stationary level,  $I_S$ , various NMDA channel blockers were applied in the continuous presence of ASP.

Magnesium (1 mM) caused a practically complete blockade of the ASP-induced current. The onset and the offset kinetics of Mg<sup>2+</sup> were well fitted with single exponential functions (Fig. 1). The onset and offset time constants were:  $\tau_{\text{ON}} = 9.24 \pm 2.84$  ms and  $\tau_{\text{OFF}} = 137 \pm 71$  ms ( $n = 11$ ), respectively. If these constants were defined by the association and dissociation of the blocker molecules, the mechanism of Mg<sup>2+</sup> action can be described by the following simplest model:



Model 1

where O and O<sub>B</sub> represent the channel in the open and the open blocked states, respectively. The aster-



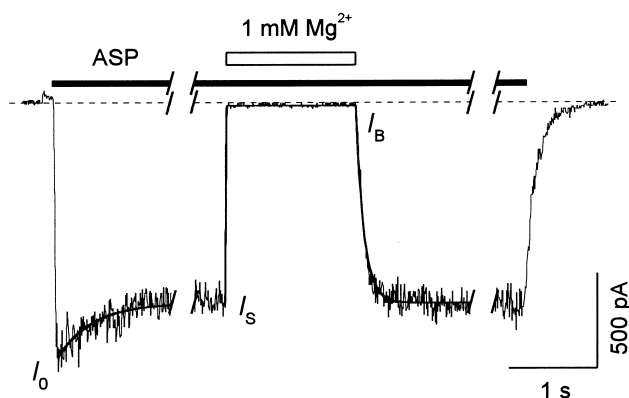


Fig. 1. The kinetics of  $\text{Mg}^{2+}$ -induced changes in the NMDA-mediated current. The current elicited by ASP (100  $\mu\text{M}$ ) gained its stationary level ( $I_S$ ) decreasing from the maximal value ( $I_0$ ) with the time constant of 482 ms (the fitting is shown by a solid line).  $\text{Mg}^{2+}$  (1 mM) was applied 20 s after the beginning of ASP application and induced a practically complete inhibition of the current. The time constant of the current decrease,  $\tau_{\text{ON}} = 4.8$  ms. After the termination of  $\text{Mg}^{2+}$  application the current recovered with the time constant,  $\tau_{\text{OFF}} = 112$  ms.

isk indicates the conducting state;  $k_1$  and  $k_2$  are the kinetic constants.  $[B]$  is the blocker concentration. As the experiments were carried out in the continuous presence of high concentrations of ASP and glycine; here and further it is suggested that all the agonist and co-agonist sites are completely occupied and, correspondingly, all the states of the channel represented in the models are the agonist and the coagonist bound ones. The association ( $k_1$ ) and dissociation ( $k_2$ ) constants for model 1 are defined from the following equations:

$$\tau_{\text{ON}} = 1/(k_1[B] + k_2) \quad (1)$$

and

$$\tau_{\text{OFF}} = 1/k_2 \quad (2)$$

The values of the association and dissociation rate constants defined from Eqs. 1 and 2 were the following:  $k_1 = 1.01 \pm 0.36 \times 10^5 \text{ M}^{-1} \text{ s}^{-1}$  and  $k_2 = 7.3 \pm 1.1 \text{ s}^{-1}$ . These values were much smaller than those defined in single-channel recording experiments [14]:  $k_1 = 2.2 \times 10^8 \text{ M}^{-1} \text{ s}^{-1}$  and  $k_2 = 640 \text{ s}^{-1}$ . Therefore, the association and dissociation kinetics of  $\text{Mg}^{2+}$  are really much faster than those predicted by our measurements and the time constants of the current increase at the beginning,  $\tau_{\text{ON}}$ , and the current decrease at the end of  $\text{Mg}^{2+}$  application,  $\tau_{\text{OFF}}$ , depend

crucially on the onset and offset rates of the solution exchange system, respectively.

Many well-known blockers manifest multicomponent blocking kinetics of liganded NMDA channels. The changes in the ASP-induced current in response to the beginning and termination of TEA (5 mM), TBA (2 mM), 9-AA (40  $\mu\text{M}$ ) and MRZ (150  $\mu\text{M}$ ) applications after the plateau current had reached its stationary level ( $I_S$ ) were fitted with the sum of the two exponents (Fig. 2A,B,C,D, respectively). The recovery kinetics will be studied in order to elucidate the mechanisms of the blockers action. These kinetics are easier to analyze than the blocking kinetics due to the conjectural independence of the recovery time constants on the blocker concentration. The current recovery after termination of the blocker action was fitted by the following equation (Fig. 2E):

$$I(t) = I_S + (I_B - I_S) \times \{A_{\text{fast}} \times \exp(-t/\tau_{\text{fast}}) + (1 - A_{\text{fast}}) \times \exp(-t/\tau_{\text{slow}})\} \quad (3)$$

where  $A_{\text{fast}}$  is the amplitude of the fast component,  $\tau_{\text{fast}}$  and  $\tau_{\text{slow}}$  are the fast and the slow time constants, respectively. The values of the parameters proved to be as follows:  $A_{\text{fast}} = 0.63 \pm 0.02$ ,  $\tau_{\text{fast}} = 198 \pm 14$  ms, and  $\tau_{\text{slow}} = 2.43 \pm 0.17$  s for TEA;  $A_{\text{fast}} = 2.12 \pm 0.24$ ,  $\tau_{\text{fast}} = 105 \pm 8$  ms, and  $\tau_{\text{slow}} = 289 \pm 29$  ms for TBA;  $A_{\text{fast}} = 1.83 \pm 0.07$ ,  $\tau_{\text{fast}} = 727 \pm 24$  ms, and  $\tau_{\text{slow}} = 1.54 \pm 0.53$  s for 9-AA;  $A_{\text{fast}} = -0.36 \pm 0.07$ ,  $\tau_{\text{fast}} = 1.35 \pm 0.28$  s, and  $\tau_{\text{slow}} = 5.48 \pm 0.20$  s for MRZ. The slow changes in the unblocking kinetics do not probably result from the action of other ion exchangers/transporters because no such slow kinetics was observed on the recovery from the  $\text{Mg}^{2+}$  block. It is evident that the value of  $A_{\text{fast}}$  did not obviously lie between 0 and 1 (TEA) but can be greater than 1 (TBA and 9-AA) and lower than 0 (MRZ). The proximity of  $\tau_{\text{fast}}$  for TEA and TBA and the time constant of the current recovery after termination of  $\text{Mg}^{2+}$  application ( $\tau_{\text{OFF}} = 137 \pm 71$  ms) may imply that the fast component of their unblocking is masked by the rate of the solution replacement. This can explain the apparent inadequacy of the double exponential fit of the recovery kinetics in the case of TBA (Fig. 2E).

To elucidate the mechanism of the blocker action,

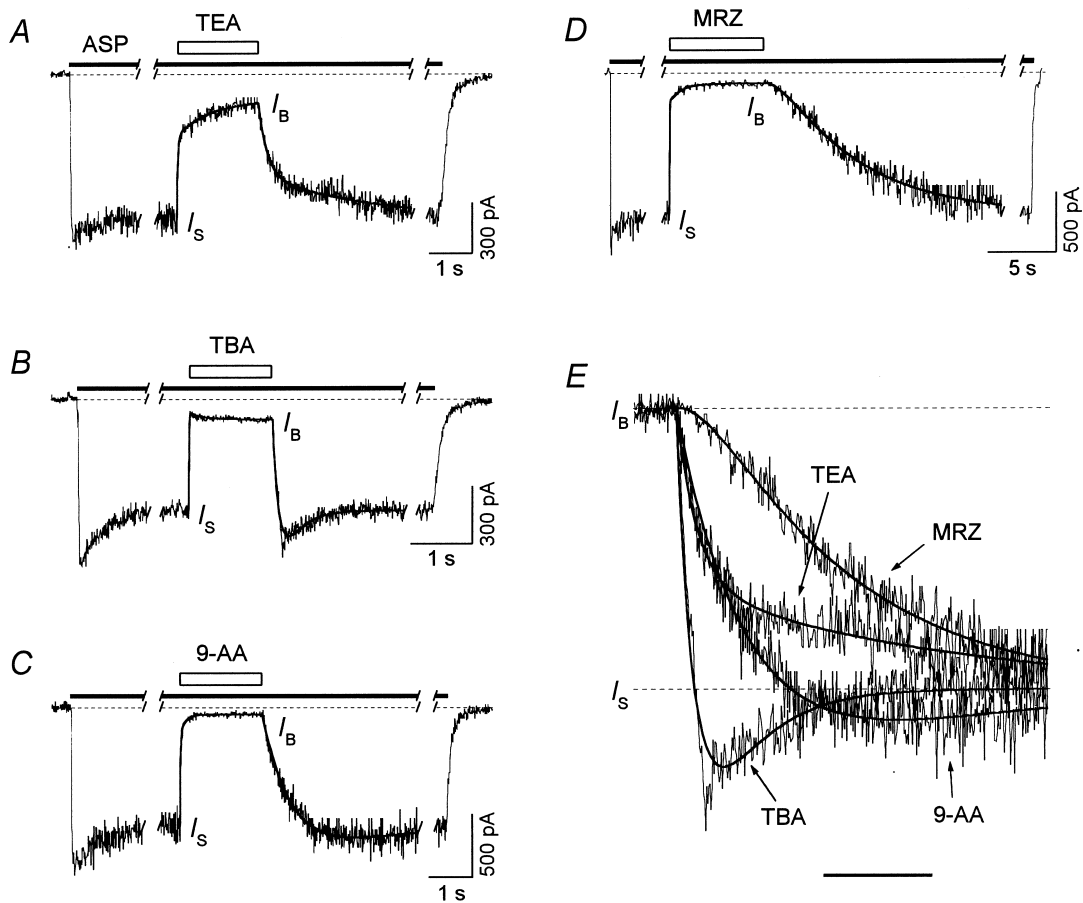
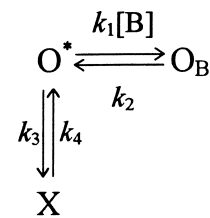


Fig. 2. The two-component kinetics of the NMDA channels blockade. The experimental protocol is the same as shown in Fig. 1. 5 mM TEA (A), 2 mM TBA (B), 40  $\mu$ M 9-AA (C) and 150  $\mu$ M MRZ (D) were applied against the background of ASP (100  $\mu$ M). The current changes induced by the beginning and termination of the blocker application were fitted with double exponential functions (solid lines). (E) The recovery kinetics from A–D are presented on an expanded time scale. The fittings were made with Eq. 3 (solid lines). Note that the value of  $A_{\text{fast}}$  was equal to 0.63 for TEA, 2.12 for TBA, 1.83 for 9-AA and  $-0.36$  for MRZ. The bar is equal to 1 s for TEA and 9-AA, 0.6 s for TBA and 4 s for MRZ.

all possible models with three states of the channel were considered. These models are the simplest which can simulate the two-component blocking kinetics. As in the previous study [4], the behavior of the amplitude of the fast component ( $A_{\text{fast}}$ ) depending on the blocker concentration was taken as a criterion of discrimination between these models. There are only five simplest models with three states which describe the blocker and the channel interaction in the continuous presence of the saturating concentration of the agonist. Two of them are parallel. The first one is the following:



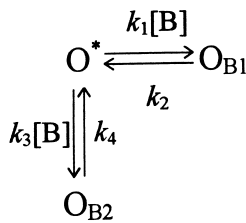
Model 2

where X can represent the closed (C) or the desensitized (D) state of the channel or their combination, which provides the kinetics with the rate-limiting

transitions from the open state with the constant,  $k_3$ , and to the open state with the constant,  $k_4$ . The amplitude of the fast component does not depend on the blocker concentration and, if  $k_2 > k_3 + k_4$ , is defined by the following equation (see Appendix A):

$$A_{\text{fast}} = 1 - \frac{k_2 \cdot k_3}{k_4 \cdot (k_3 + k_4 - k_2)} \quad (4)$$

In the case when  $k_2 < k_3 + k_4$ , the amplitude of the fast component will be equal to  $1 - A_{\text{fast}}$ , where  $A_{\text{fast}}$  is defined from Eq. 4. The second parallel model is:

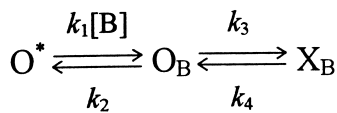


### Model 3

where  $\text{O}_{\text{B1}}$  and  $\text{O}_{\text{B2}}$  represent the two open blocked states of the channel corresponding to two different blocker binding sites. The amplitude of the fast component does not depend on the blocker concentration and, if  $k_2 > k_4$ , is defined by the following equation (see Appendix A):

$$A_{\text{fast}} = \frac{1}{1 + \frac{k_2 \cdot k_3}{k_1 \cdot k_4}} \quad (5)$$

The values of  $A_{\text{fast}}$  defined by Eq. 5 are within the interval between 0 and 1. There are three sequential kinetic models. The first one is as follows:



### Model 4

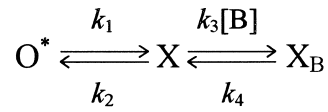
where  $\text{X}_{\text{B}}$  may represent other open ( $\text{O}_{\text{B2}}$ ) or closed ( $\text{C}_{\text{B}}$ ) or desensitized ( $\text{D}_{\text{B}}$ ) blocked states of the channel. The amplitude of the fast component does not depend on the blocker concentration and, if  $k_2 + k_3 > k_4$ , is defined by the following equation (see Appendix A):

$$A_{\text{fast}} = \frac{1}{1 - \frac{\lambda_1^2 \cdot (k_4 + \lambda_2)}{\lambda_2^2 \cdot (k_4 + \lambda_1)}} \quad (6)$$

where

$$\lambda_{1,2} = -0.5 \cdot \{ (k_2 + k_3 + k_4) \pm [(k_2 + k_3 + k_4)^2 - 4 \cdot k_2 \cdot k_4]^{0.5} \}.$$

In the case when  $k_2 + k_3 < k_4$ , the amplitude of the fast component will be equal to  $1 - A_{\text{fast}}$ , where  $A_{\text{fast}}$  is defined from Eq. 6. It is easy to demonstrate that the values of  $A_{\text{fast}}$  defined by Eq. 6 lie within the interval between 0 and 1. The second sequential kinetic model is as follows:

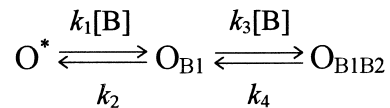


### Model 5

where X can represent the closed (C) or the desensitized (D) and  $\text{X}_{\text{B}}$ , the closed blocked ( $\text{C}_{\text{B}}$ ) or the desensitized blocked ( $\text{D}_{\text{B}}$ ) states of the channel, respectively. The amplitude of the fast component does not depend on the blocker concentration either and, when  $k_1 + k_2 > k_4$ , is defined by the following equation (see Appendix A):

$$A_{\text{fast}} = \frac{k_4}{k_4 - k_1 - k_2} \quad (7)$$

In the case when  $k_1 + k_2 < k_4$ , the amplitude of the fast component will be equal to  $1 - A_{\text{fast}}$ , where  $A_{\text{fast}}$  is defined from Eq. 7. In both cases, however, the value of the amplitude of the fast component is negative (and equal to zero when  $k_1 + k_2 = k_4$ ). Finally, the third sequential model is as follows:



### Model 6

where  $\text{O}_{\text{B1B2}}$  represents the open blocked state, in which two blocker molecules simultaneously bind to the channel. The amplitude of the fast component decreases with the blocker concentration and, when  $k_2 > k_4$ , is defined by the following equation (see Appendix A):

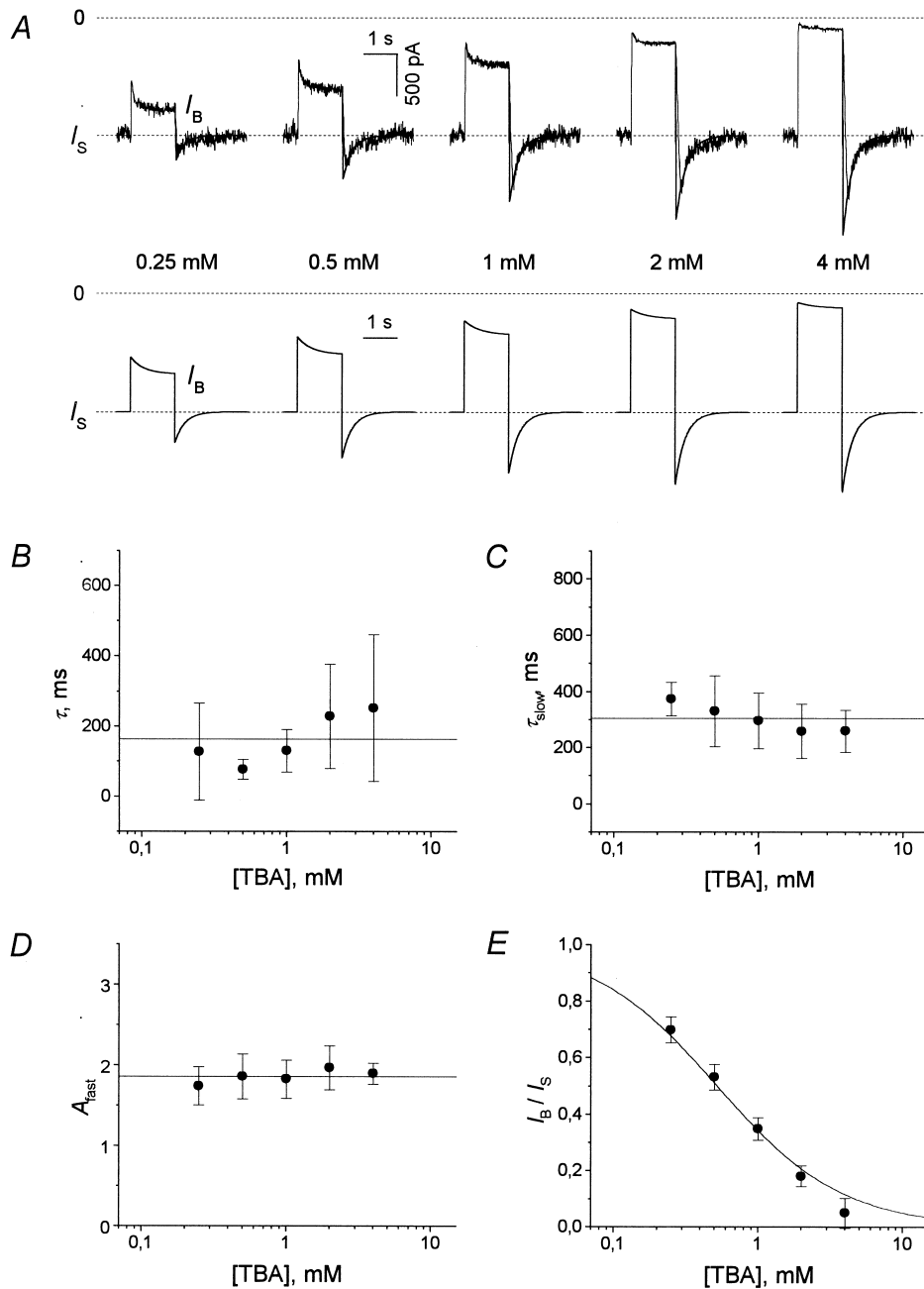


Fig. 3. The kinetics of TBA. (A) The experimental (first row) and modeling (second row) current traces in response to the application of different concentrations of TBA (0.25–4 mM) in the continuous presence of ASP (100  $\mu$ M). The recovery kinetics of the experimental currents were fitted with Eq. 3 at fixed  $\tau_{\text{fast}} = 1$  ms (solid lines). (B) The time constant,  $\tau$ , obtained by the monoexponential fitting of the fast descending phase of the current recovery after termination of TBA application.  $\tau$  was essentially independent of the blocker concentration and was equal, on average, to  $163 \pm 142$  ms,  $n = 7$  (horizontal line). (C,D) The slow time constant and the amplitude of the fast component obtained by the fitting of the current recovery after termination of TBA application with Eq. 3 at fixed  $\tau_{\text{fast}} = 1$  ms. Their values were essentially independent of TBA concentration and were, on average,  $\tau_{\text{slow}} = 304 \pm 99$  ms and  $A_{\text{fast}} = 1.86 \pm 0.24$ ,  $n = 7$  (horizontal lines). (E) The concentration dependence of the stationary block ( $I_B/I_S$ ) which was fitted with Eq. A9 (solid line). The value of the parameter  $K$  is equal to  $1.91 \pm 0.18 \times 10^3 \text{ M}^{-1}$ ,  $n = 7$ .

$$A_{\text{fast}} = \frac{1 - \frac{k_3}{k_2 - k_4} [\text{B}]}{1 + \frac{k_3}{k_4} [\text{B}]} \quad (8)$$

In the case when  $k_2 < k_4$ , the amplitude of the fast component will be equal to  $1 - A_{\text{fast}}$  where  $A_{\text{fast}}$  is defined from Eq. 8. Eq. 8 predicts that  $A_{\text{fast}}$  becomes negative at the values of the blocker concentration,  $[\text{B}]$ , greater than  $(k_2 - k_4)/k_3$ .

### 3.1. The kinetics of TBA

Fig. 3A (first row) gives an example of application of different concentrations of TBA (0.25–4 mM) in the continuous presence of ASP (100  $\mu\text{M}$ ). The fitting of the descending phase of the current response to the termination of TBA application by the single exponential function yielded the fast time constant,  $\tau$ , which was essentially independent ( $P > 0.05$ ) of TBA concentration (Fig. 3B). The mean value of  $\tau$  proved to be  $163 \pm 142$  ms ( $n = 7$ ) and was not significantly different from the time constant of the current recovery after termination of  $\text{Mg}^{2+}$  application ( $\tau_{\text{OFF}} = 137 \pm 71$  ms). Thus, one may suppose that the real fast component of the channels recovery from the TBA block is very fast and is masked by the process of the solution exchange. Indeed, in the study of the interaction of TBA with the gating machinery of NMDA channels using the kinetic models [8], the value of the fast time constant of TBA unblocking was  $1000 \text{ s}^{-1}$  stipulating the fast time constant,  $\tau_{\text{fast}} = 1$  ms. Thus, it is clear that the fitting shown in Fig. 2E for TBA is inadequate. The fitting of the current recovery by Eq. 3 after termination of TBA application was carried out with fixed  $\tau_{\text{fast}} = 1$  ms in the interval excluding the fast current decrease, which reflected the process of solution exchange (Fig. 3A, first row, solid lines). The value of  $\tau_{\text{fast}}$  was taken

to be low enough and its decrease did not lead to the variations in other parameters ( $\tau_{\text{slow}}$  and  $A_{\text{fast}}$ ) of Eq. 3. In Fig. 3C,D, respectively, the values of  $\tau_{\text{slow}}$  and  $A_{\text{fast}}$  are plotted as a function of TBA concentration. Neither of these parameters depended on the blocker concentration ( $P > 0.05$ ); their mean values were as follows:  $\tau_{\text{slow}} = 304 \pm 99$  ms and  $A_{\text{fast}} = 1.86 \pm 0.24$  ( $n = 7$ ).

It is important to emphasize that fixation of the parameter  $\tau_{\text{fast}}$  did not affect the behavior of the parameters  $\tau_{\text{slow}}$  and  $A_{\text{fast}}$  depending on TBA concentration. Thus, the fitting of TBA recovery kinetics with non-fixed  $\tau_{\text{fast}}$  (see Fig. 2E) gave the same result: neither  $\tau_{\text{slow}}$  nor  $A_{\text{fast}}$  depended on the blocker concentration ( $P > 0.05$ ), although the mean value of  $\tau_{\text{slow}}$  ( $273 \pm 94$  ms) was slightly lower and the mean value of  $A_{\text{fast}}$  ( $2.29 \pm 0.62$ ) was slightly higher than the corresponding values obtained with  $\tau_{\text{fast}} = 1$  ms. The cases when  $\tau_{\text{fast}} = 1$  ms and with non-fixed  $\tau_{\text{fast}}$  limited the range of  $\tau_{\text{fast}}$  values, which affected  $\tau_{\text{slow}}$  and  $A_{\text{fast}}$  (in the case of  $\tau_{\text{fast}} < 1$  ms the values of  $\tau_{\text{slow}}$  and  $A_{\text{fast}}$  were practically the same as in the case of  $\tau_{\text{fast}} = 1$  ms, i.e., the value  $\tau_{\text{fast}} = 1$  ms can be considered as minimal; in the case of non-fixed  $\tau_{\text{fast}}$  the value of  $\tau_{\text{fast}}$  was maximal). At any value of this range  $\tau_{\text{slow}}$  and  $A_{\text{fast}}$  ( $> 1$ ) did not vary with the blocker concentration.

Therefore, the arbitrary choice of the value of  $\tau_{\text{fast}}$  for fitting did not affect the choice of the kinetic model because as the value of  $A_{\text{fast}}$  did not depend on the blocker concentration and was greater than unity, the only simplest model which can describe the kinetics of the TBA action is model 2. The degree of the stationary blockade predicted by this model is defined by Eq. A9 (see Appendix A). The value of the parameter  $K$  for this equation was equal to  $1.91 \pm 0.18 \times 10^3 \text{ M}^{-1}$ ,  $n = 7$  (Fig. 3E). The system of equations which was obtained by the substitution of the mean values of the parameters  $\tau_{\text{slow}}$ ,  $A_{\text{fast}}$  and

Table 1  
The kinetic constants for TEA, TBA and MRZ

Compound	Model	$k_1, 10^6 \text{ M}^{-1} \text{ s}^{-1}$	$k_2, \text{ s}^{-1}$	$k_3$	$k_4, \text{ s}^{-1}$
TBA	2	3.5	$10^3$	$1.52 \text{ s}^{-1}$	1.77
TEA	3	0.523	$10^3$	$118 \text{ M}^{-1} \text{ s}^{-1}$	0.47
	4	0.516	$10^3$	$0.24 \text{ s}^{-1}$	0.47
MRZ	6	0.088	1.14	$1.4 \times 10^4 \text{ M}^{-1} \text{ s}^{-1}$	0.13



$K$ , and  $\tau_{\text{fast}} = 1$  ms into Eq. A4, Eq. A5, Eq. 4 and Eq. A9 made it possible to estimate the values of all kinetic constants. The values of  $k_1$ ,  $k_2$ ,  $k_3$  and  $k_4$  for TBA are presented in Table 1. Fig. 3A (second row) shows the currents predicted by model 2 at these values of the kinetic constants.

As the choice of the kinetic model describing TBA action depended on the behavior of the fitting parameters  $\tau_{\text{slow}}$  and  $A_{\text{fast}}$ , it is important to establish the effect of the solution exchange time,  $\tau_{\text{wash}}$ , on the values of these parameters (assuming that the solution exchange is a single-exponential process, [13]). Fig. 4A shows the recovery of the currents predicted by model 2 at different values of  $\tau_{\text{wash}}$ . The typical example of the experimental current recovery is shown in Fig. 4B. This curve was fitted with Eq. 3 as was described above (Fig. 4B, thin smooth line).

In this case the solution exchange is instantaneous. If we compare Fig. 4A and B, it becomes clear that always at  $\tau_{\text{wash}}$  values of the range of  $\tau_{\text{fast}}$  value (1 ms) the recovery looks like those when the solution exchange is instantaneous. In reality,  $\tau_{\text{wash}}$  is much greater than  $\tau_{\text{fast}}$ . This is why the real experimental curve is better approximated by the modeling curve with  $\tau_{\text{wash}} = 30$  ms (Fig. 4B, thick smooth line). The modeling curves at  $\tau_{\text{wash}} = 1, 30$  and 100 ms and different blocker concentrations were fitted in the same way as the experimental curves (with  $\tau_{\text{fast}} = 1$  ms). The values of the parameters  $\tau_{\text{slow}}$  and  $A_{\text{fast}}$  depending on the blocker concentration are shown in Fig. 4C,D, respectively. It can be seen that  $\tau_{\text{slow}}$  rose with an increase in  $\tau_{\text{wash}}$  remaining practically concentration-independent. An essential increase in  $A_{\text{fast}}$  with concentration was observed only at high values of

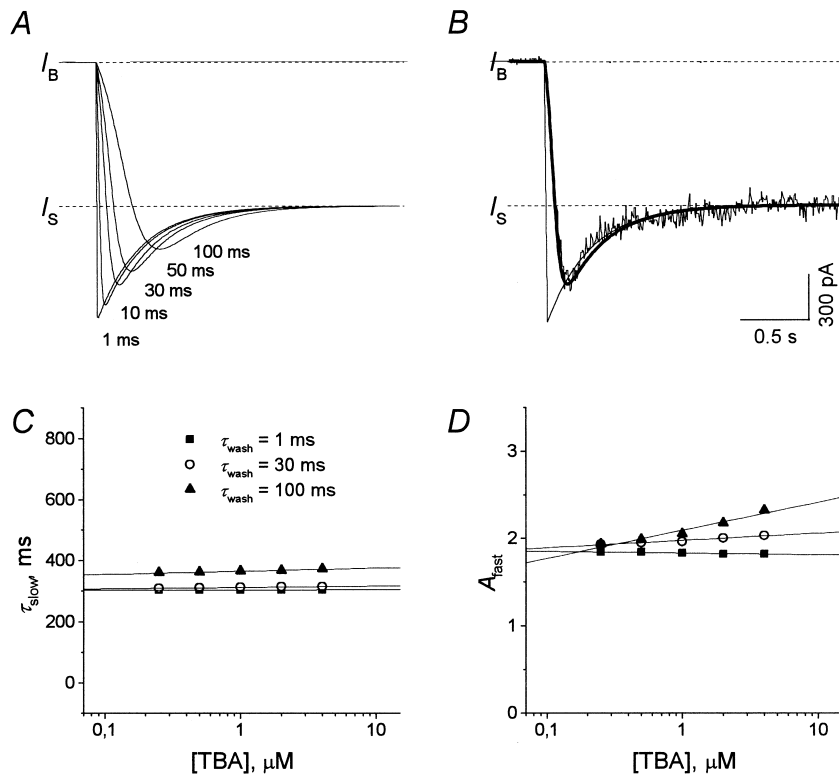


Fig. 4. The dependence of the recovery kinetics predicted by model 2 for TBA on the solution exchange time. (A) The current recovery predicted by model 2 at different values of the solution exchange time,  $\tau_{\text{wash}}$  (1, 10, 30, 50, and 100 ms). TBA concentration is 2 mM. (B) An example of an experimental current recovery. TBA concentration is 2 mM. The thin smooth line shows the fitting of the current with Eq. 3 at fixed  $\tau_{\text{fast}} = 1$  ms. The thick smooth line is the normalized modeling current at  $\tau_{\text{wash}} = 30$  ms. (C,D) The slow time constant and the amplitude of the fast component obtained by the fitting of the modeling current recovery with Eq. 3 at fixed  $\tau_{\text{fast}} = 1$  ms at different values of  $\tau_{\text{wash}}$  (1, 30, and 100 ms) depending on the blocker concentration. Solid lines show the apparent linear fit.

$\tau_{\text{wash}}$  (100 ms). In experiments with TBA the mean value of  $\tau_{\text{wash}}$  was approximately 30 ms (the corresponding value of  $\tau = 163$  ms). At this value of  $\tau_{\text{wash}}$  the parameters  $\tau_{\text{slow}}$  and  $A_{\text{fast}}$  did not practically depend on the blocker concentration (open circles in Fig. 4C,D) and the small vertical shift of the  $\tau_{\text{slow}}$  and  $A_{\text{fast}}$  concentration dependencies was smaller than the value of the experimental error (cf. Fig. 4C with Fig. 3C and Fig. 4D with Fig. 3D). Therefore, the non-instantaneous solution exchange did not significantly affect the values and behavior of the fitting parameters and, correspondingly, did not affect the choice of the simplest model, which describes the kinetics of TBA action. Possible minor changes in the values of the kinetic constants due to the non-instantaneous solution exchange are not a matter of principle.

### 3.2. The kinetics of TEA

Fig. 5A (first row) shows an example of application of different concentrations of TEA (0.625–10 mM) in the continuous presence of ASP (100  $\mu\text{M}$ ). The fitting of the recovery kinetics with Eq. 3 by analogy with the fitting presented in Fig. 2E yielded the value of the fast time constant, which was essentially independent ( $P > 0.05$ ) of TEA concentration (Fig. 5B). The mean value of  $\tau_{\text{fast}}$  proved to be  $218 \pm 52$  ms ( $n = 4$ ) and was not significantly different from the time constant of the current recovery after termination of  $\text{Mg}^{2+}$  application ( $\tau_{\text{OFF}} = 137 \pm 71$  ms). This finding prompts an idea that, as in the case of TBA, the fast component of the channels recovery from the TEA block is masked by the process of the solution exchange. Indeed, in the single-channel study [15], the dissociation of TEA from the NMDA channel was considered to be too fast to be measured at the sampling frequency of 4 kHz. Thus, the value of  $\tau_{\text{fast}}$  should be less than 1 ms. It is clear that the fitting shown in Fig. 2E for TEA is inadequate. The fitting by Eq. 3 of the current recovery after termination of TEA application was carried out with fixed  $\tau_{\text{fast}} = 1$  ms in the interval excluding the fast current decrease reflected the process of the solution exchange (Fig. 5A, first row, solid lines). The value of  $\tau_{\text{fast}}$  was taken small enough and its decrease caused no variations in other parameters ( $\tau_{\text{slow}}$  and  $A_{\text{fast}}$ ) of Eq. 3. The values of  $\tau_{\text{slow}}$  and  $A_{\text{fast}}$  as a

function of TEA concentration are presented in Fig. 5C and D, respectively. None of these parameters depended on the blocker concentration ( $P > 0.05$ ) and their mean values proved to be as follows:  $\tau_{\text{slow}} = 2.14 \pm 0.61$  s and  $A_{\text{fast}} = 0.67 \pm 0.09$  ( $n = 4$ ).

As in the case of TBA, fixation of the parameter  $\tau_{\text{fast}}$  did not affect the behavior of the parameters  $\tau_{\text{slow}}$  and  $A_{\text{fast}}$  depending on TEA concentration. The fitting of TEA recovery kinetics with non-fixed  $\tau_{\text{fast}}$  (see Fig. 2E) gave the same result: neither  $\tau_{\text{slow}}$ , nor  $A_{\text{fast}}$  depended on the blocker concentration ( $P > 0.05$ ), although the mean values of  $\tau_{\text{slow}}$  ( $2.75 \pm 0.88$  s) and  $A_{\text{fast}}$  ( $0.72 \pm 0.03$ ) were slightly higher than the corresponding values obtained with  $\tau_{\text{fast}} = 1$  ms. Therefore, as in the case of TBA, the arbitrary choice of the value of  $\tau_{\text{fast}}$  for fitting will not affect the choice of the kinetic models describing the TEA action.

As the value of  $A_{\text{fast}}$  did not depend on the blocker concentration and was greater than 0, the three simplest models which can describe the kinetics of TEA action are models 2, 3 and 4. The degree of the stationary blockade predicted by these models is defined by Eq. A9 (see Appendix A). The value of the parameter  $K$  for this equation was equal to  $777 \pm 82$   $\text{M}^{-1}$ ,  $n = 4$  (Fig. 5E). The systems of equations obtained by the substitution of the mean values of the parameters  $\tau_{\text{slow}}$ ,  $A_{\text{fast}}$ , and  $K$  and  $\tau_{\text{fast}} = 1$  ms into Eq. A4, Eq. A5, Eq. 4 and Eq. A9 for model 2, Eq. A4, Eq. A5, Eq. 5 and Eq. A9 for model 3 and Eq. A4, Eq. A5, Eq. 6 and Eq. A9 for model 4 allowed to estimate the values of the kinetic constants. The values of the kinetic constants for model 2 proved to be the following:  $k_1 = 0.52 \times 10^6$   $\text{M}^{-1} \text{s}^{-1}$ ;  $k_2 = 0.47$   $\text{s}^{-1}$ ;  $k_3 = 999$   $\text{s}^{-1}$  and  $k_4 = 0.69$   $\text{s}^{-1}$ . The state X cannot be the desensitized state in this case because the value of  $k_3$  is three order of magnitude smaller than the kinetic constant of the transition from the open to the desensitized state [16]. Alternatively, if state X is the closed state, then the open probability,  $P_0$  is equal to  $k_4/(k_3 + k_4) < 10^{-3}$ . However, the value of  $P_0$  for NMDA channels was found to vary from 0.04 to 0.5 [16–21]. Therefore, X in model 2 cannot be either the closed or desensitized state of the channel. Thus, model 2 cannot describe the real mechanism of the TEA interaction with NMDA channels.

The values of  $k_1$ ,  $k_2$ ,  $k_3$  and  $k_4$  for models 3 and 4

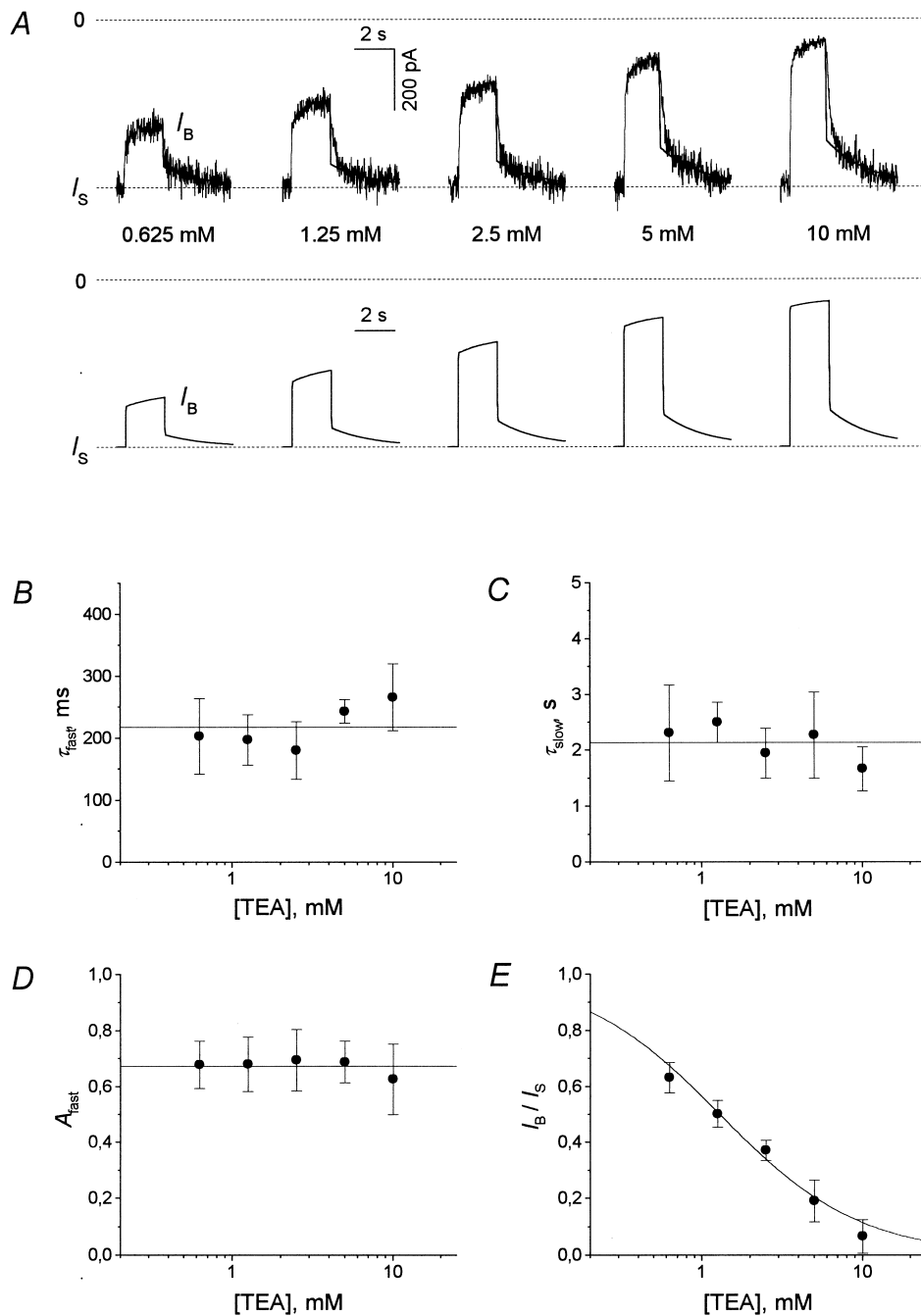


Fig. 5. The kinetics of TEA. (A) The experimental (first row) and modeling (second row) current traces in response to the application of different concentrations of TEA (0.625–10 mM) in the continuous presence of ASP (100  $\mu$ M). The recovery kinetics of the experimental currents were fitted with Eq. 3 with fixed  $\tau_{fast} = 1$  ms (solid lines). (B) The fast time constant obtained from the fitting of the current recovery after termination of TEA application with Eq. 3.  $\tau_{fast}$  was essentially independent of the blocker concentration and was equal, on the average, to  $218 \pm 52$  ms,  $n = 4$  (horizontal line). (C,D) The slow time constant and the amplitude of the fast component obtained from the fitting of the current recovery after termination of TEA application with Eq. 3 at fixed  $\tau_{fast} = 1$  ms. Their values were essentially independent of TEA concentration and were, on average,  $\tau_{slow} = 2.14 \pm 0.61$  s and  $A_{fast} = 0.67 \pm 0.09$ ,  $n = 4$  (horizontal lines). (E) The concentration dependence of the stationary block ( $I_B/I_S$ ), which was fitted with Eq. A9 (solid line). The value of the parameter  $K$  is equal to  $777 \pm 82$  M $^{-1}$ ,  $n = 4$ .

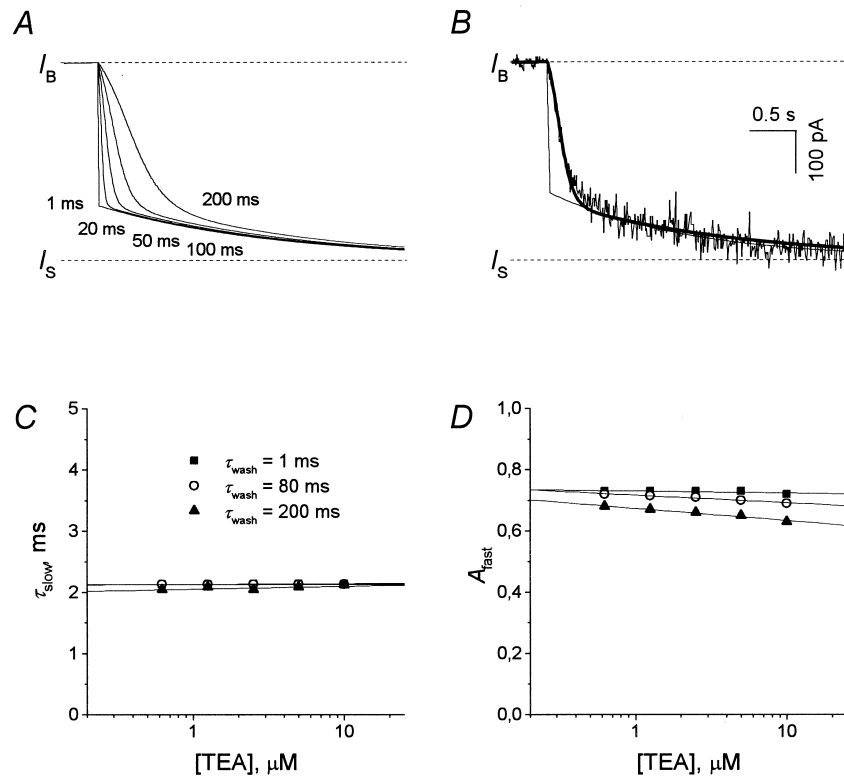


Fig. 6. The dependence of the recovery kinetics predicted by model 4 for TEA on the solution exchange time. (A) The current recovery predicted by model 4 at different values of the solution exchange time,  $\tau_{\text{wash}}$  (1, 20, 50, 100, and 200 ms). TEA concentration is 10 mM. (B) An example of an experimental current recovery. TEA concentration is 10 mM. The thin smooth line shows the fitting of the current with Eq. 3 at fixed  $\tau_{\text{fast}} = 1$  ms. The thick smooth line is the normalized modeling current at  $\tau_{\text{wash}} = 80$  ms. (C,D) The slow time constant and the amplitude of the fast component obtained by the fitting of the modeling current recovery with Eq. 3 at fixed  $\tau_{\text{fast}} = 1$  ms at different values of  $\tau_{\text{wash}}$  (1, 80, and 200 ms) depending on the blocker concentration. The solid lines show the apparent linear fit.

are presented in Table 1. Fig. 5A (second row) shows the currents predicted by model 4. The currents predicted by model 3 are exactly the same.

The dependence of the recovery kinetics predicted by model 4 for TEA on the solution exchange time is shown in Fig. 6A. The typical experimental curve (Fig. 6B) was well approximated by modeling curve with  $\tau_{\text{wash}} = 80$  ms (Fig. 6B, thick smooth line). The values of the parameters  $\tau_{\text{slow}}$  and  $A_{\text{fast}}$  depending on the blocker concentration are shown in Fig. 6C,D, respectively. It can be seen that  $\tau_{\text{slow}}$  did not practically depend on  $\tau_{\text{wash}}$  and TEA concentration. An essential decrease in  $A_{\text{fast}}$  with concentration was observed only at high values of  $\tau_{\text{wash}}$  (200 ms). In experiments with TEA the mean value of  $\tau_{\text{wash}}$  was approximately equal to 80 ms (the corresponding

value of  $\tau_{\text{fast}}$  is 218 ms). At this value of  $\tau_{\text{wash}}$ , the parameters  $\tau_{\text{slow}}$  and  $A_{\text{fast}}$  did not practically depend on the blocker concentration (open circles in Fig. 6C,D) and the small vertical shift of the  $\tau_{\text{slow}}$  and  $A_{\text{fast}}$  concentration dependencies was much smaller than the value of the experimental error (cf. Fig. 6C with Fig. 5C and Fig. 6D with Fig. 5D). The results for model 3 were quite the same. Therefore, the non-instantaneous solution exchange did not significantly affect the values and behavior of the fitting parameters and, correspondingly, did not affect the choice of the simplest model, which describes the kinetics of TEA action. As in the case of TBA, possible small changes in the values of the kinetic constants due to the non-instantaneous solution exchange are not a matter of principle.

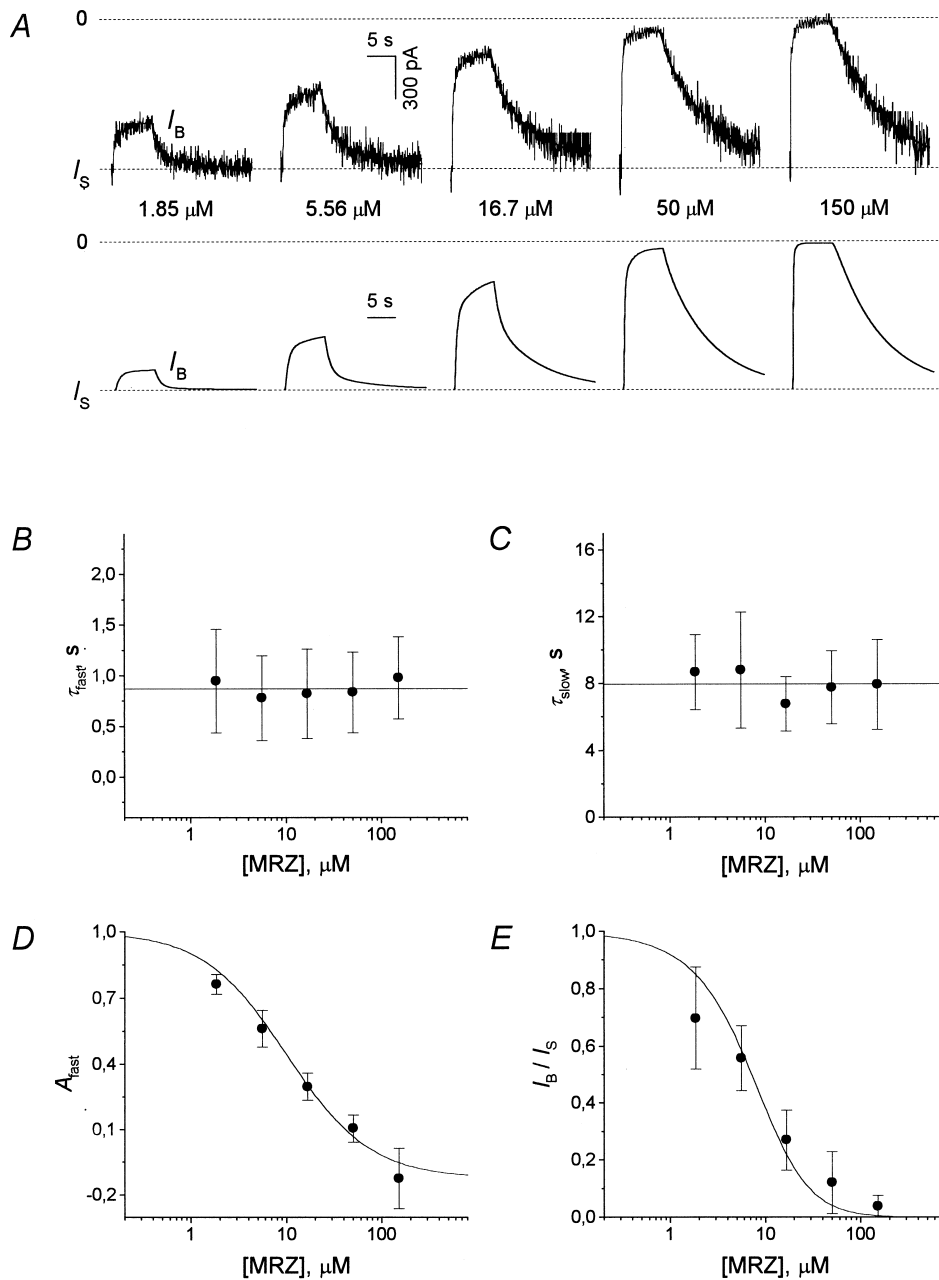


Fig. 7. The kinetics of MRZ. (A) The experimental (first row) and modeling (second row) current traces in response to application of different concentrations of MRZ (1.85–150 μM) in the continuous presence of ASP (100 μM). The recovery kinetics of the experimental currents were fitted with Eq. 3 (solid lines). (B–D) The fast and the slow time constants and the amplitude of the fast component of the current recovery. The values of  $\tau_{fast}$  and  $\tau_{slow}$  were essentially independent of MRZ concentration and were equal to  $0.87 \pm 0.41$  s and  $8.0 \pm 2.6$  s ( $n = 12$ ), respectively (horizontal lines).  $A_{fast}$  decreased with MRZ concentration. The  $A_{fast}$  dependence on the blocker concentration was fitted with Eq. 8 at fixed  $k_2 = 1.14$  s $^{-1}$  and  $k_4 = 0.13$  s $^{-1}$  (solid line). The value of  $k_3$  proved to be  $1.4 \pm 0.2 \times 10^4$  M $^{-1}$  s $^{-1}$  ( $n = 12$ ). (E) The concentration dependence of the stationary block.  $I_B/I_S$  dependence on MRZ concentration was fitted with Eq. A10 (solid line). The value of the unknown parameter,  $k_1$ , proved to be of  $8.8 \pm 3.2 \times 10^4$  M $^{-1}$  s $^{-1}$  ( $n = 12$ ).



### 3.3. The kinetics of MRZ

Fig. 7A (first row) gives an example of application of different concentrations of MRZ (1.85–150  $\mu\text{M}$ ) in the continuous presence of ASP (100  $\mu\text{M}$ ). The fitting of the recovery kinetics with Eq. 3 (solid lines) showed that neither the fast, nor the slow time constants depended ( $P > 0.05$ ) on MRZ concentration (Fig. 7B,C). The mean values of  $\tau_{\text{fast}}$  and  $\tau_{\text{slow}}$  were  $0.87 \pm 0.41$  s and  $8.0 \pm 2.6$  s ( $n = 12$ ), respectively. In contrast with tetraalkylammonium compounds, the amplitude of the fast component decreased with a rise in the blocker concentration (Fig. 7D). The values of  $A_{\text{fast}}$  at different concentrations were significantly different ( $P < 0.05$ ). model 6 is the only simplest model predicted the changes in  $A_{\text{fast}}$  with the blocker concentration. The Eq. A4 and Eq. A5 of Appendix A for model 6 are as follows:  $k_2 = 1/\tau_{\text{fast}}$  and  $k_4 = 1/\tau_{\text{slow}}$ . The values of the dissociation constants defined from them allowed to fit the  $A_{\text{fast}}$  dependence on MRZ concentration by Eq. 8 with only one unknown parameter,  $k_3$  (Fig. 7D). The value of  $k_3$  proved to be  $1.4 \pm 0.2 \times 10^4 \text{ M}^{-1} \text{ s}^{-1}$ . The approximated value of  $A_{\text{fast}}$  at infinitely high MRZ concentrations is equal to  $-k_4/(k_2 - k_4)$  and is negative ( $-0.123$ ). The decrease in the fraction of the stationary block with a rise in MRZ concentration fitted by Eq. A10 with  $k_2$ ,  $k_3$  and  $k_4$  equal to their mean values found above (Fig. 7E) allowed to estimate the value of  $k_1 = 8.8 \pm 3.2 \times 10^4 \text{ M}^{-1} \text{ s}^{-1}$ . It should be noted that the fitting of the concentration dependence of the stationary block with the logistic equation gave the values of the half-blocking concentration,  $\text{IC}_{50} = 10.3 \pm 3.3 \text{ } \mu\text{M}$  and the Hill coefficient,  $n_{\text{Hill}} = 1.34 \pm 0.26$  ( $n = 12$ ). The high value of  $n_{\text{Hill}}$  supports the idea that not only one but two molecules of MRZ can bind to the NMDA channel. The values of all kinetic constants for MRZ are given in Table 1. The corresponding current traces predicted by model 6 are shown in Fig. 7A (second row). The inadequacy of model 6 for the description of the MRZ interaction with NMDA channels can be seen from the more steeper dependence of the stationary block fraction predicted by model 6 than that obtained in the experiment. Thus, the changes in the stationary current produced by the blocker application at low concentrations are considerably smaller for the model than for the experiment (cf. Fig. 7A, first and

second rows). Correspondingly, the mean values of  $I_{\text{B}}/I_{\text{S}}$  at low MRZ concentrations lay below the fitting curve in Fig. 7E. This fact can be explained by the existence of a NMDA channel population with a high affinity for MRZ and, in contrast with model 6, by the existence of a non-strict succession, in which two blocking molecules can bind to their specific sites [4].

In contrast to TBA and TEA, the value of the fast time constant for MRZ was much higher than the value of the solution exchange time. Therefore in the case of MRZ the solution exchange was fast enough not to affect the definition of time and, correspondingly, kinetic constants.

### 3.4. The kinetics of 9-AA

Fig. 8A (first row) gives an example of application of different concentrations of 9-AA (2.5–40  $\mu\text{M}$ ) in the continuous presence of ASP (100  $\mu\text{M}$ ). The fitting of the recovery kinetics with Eq. 3 (solid lines) showed that the fast time constant increased exponentially with 9-AA concentration (Fig. 8B) - from  $180 \pm 56$  ms (S.E.,  $n = 7$ ) at 2.5  $\mu\text{M}$  up to the stationary level of  $648 \pm 56$  ms (S.E.,  $n = 7$ ), the concentration constant being  $6.8 \pm 1.5 \text{ } \mu\text{M}$  ( $n = 7$ ). The values of  $\tau_{\text{fast}}$  at different concentrations were significantly different ( $P < 0.05$ ). The slow time constant was essentially independent ( $P > 0.05$ ) of 9-AA concentration (Fig. 8C). The mean value of  $\tau_{\text{slow}}$  proved to be  $2.13 \pm 1.11$  s ( $n = 7$ ). The amplitude of the fast component increased with a rise in the blocker concentration (Fig. 8D). The values of  $A_{\text{fast}}$  at different concentrations were significantly different ( $P < 0.05$ ). The increase in the amplitude of the fast component with the blocker concentration is not predicted by any simplest models. What combination of the simplest models can simulate the experimentally observed 9-AA kinetics? Firstly, the resulting model should contain model 6, for which  $A_{\text{fast}}$  changes with the blocker concentration. Otherwise, any combination of models with  $A_{\text{fast}}$  independent on the blocker concentration will manifest the kinetics with the amplitudes of components that are also independent on the blocker concentration. model 6 is also the only simplest model, which suggests that not one but two blocker molecules can bind to the NMDA channel. This suggestion is supported by the steepness of the

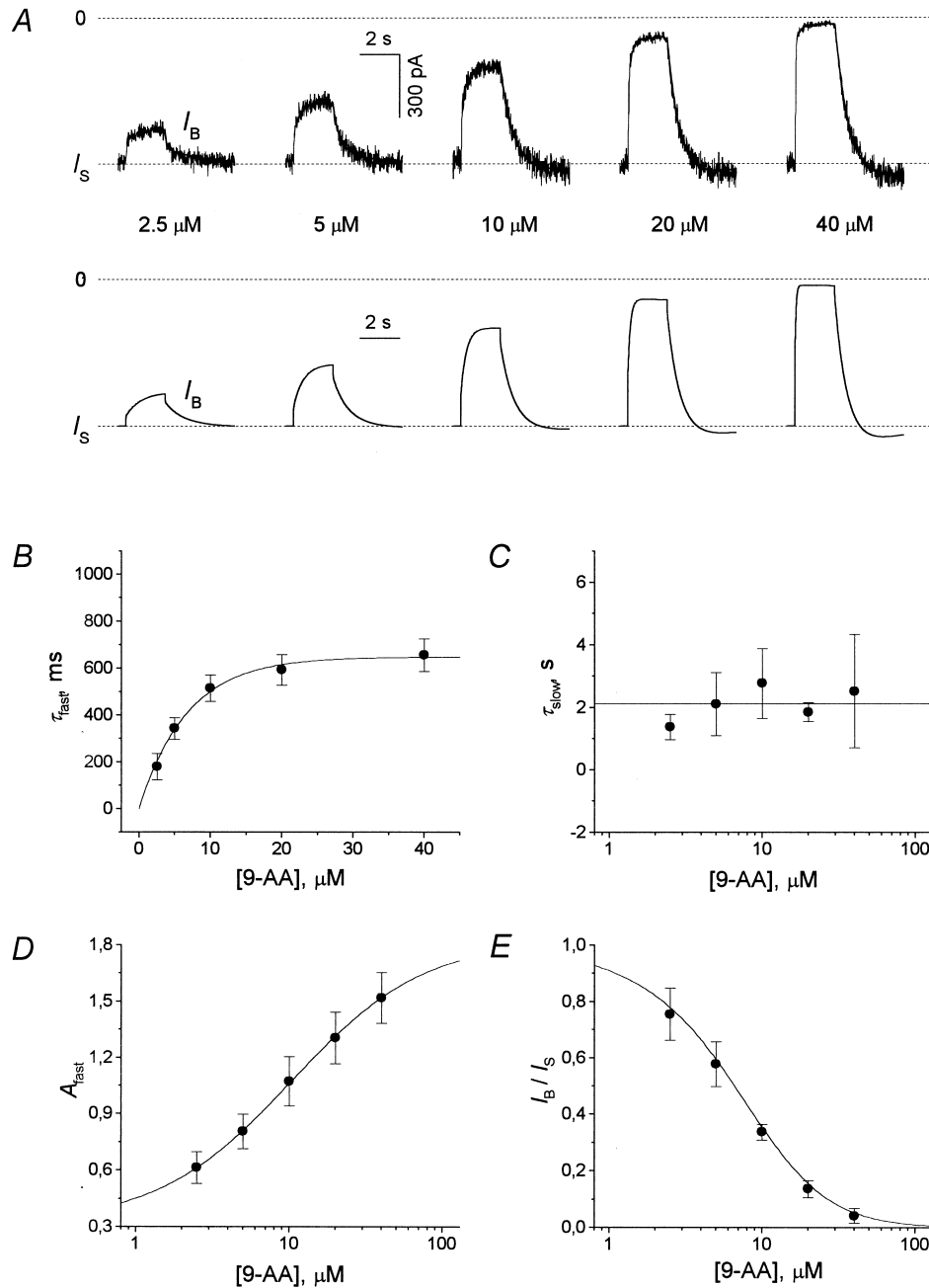
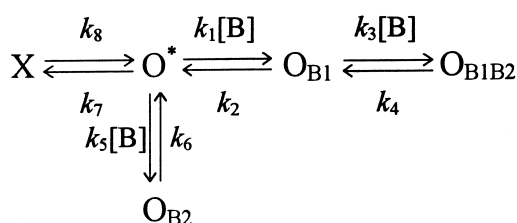


Fig. 8. The kinetics of 9-AA. (A) The experimental (first row) and modeling (second row) current traces in response to the application of different concentrations of 9-AA (2.5–40 μM) in the continuous presence of ASP (100 μM). The recovery kinetics of the experimental currents were fitted with Eq. 3 (solid lines). (B) The  $\tau_{fast}$  (mean  $\pm$  S.E.) dependence on 9-AA concentration. The fast time constant of the recovery increased exponentially with the concentration constant of  $6.8 \pm 1.5$  μM,  $n=7$  (solid line). (C) The slow time constant of the current recovery. The value of  $\tau_{slow}$  was essentially independent of 9-AA concentration and was equal, on the average, to  $2.13 \pm 1.11$  s,  $n=7$  (horizontal line). (D) The amplitude of the fast component of the current recovery.  $A_{fast}$  increased with 9-AA concentration. The fitting of the  $A_{fast}$  dependence on the blocker concentration with Eq. 9 gave the following values of parameters:  $a=0.56 \pm 0.33$ ,  $b=3.14 \pm 1.00$  and  $c=0.30 \pm 0.20$  ( $n=7$ ). (E) The concentration dependence of the stationary block. The  $I_B/I_S$  dependence on the 9-AA concentration was fitted with Eq. A13 (solid line). The values of parameters are as follows:  $a=0.091 \pm 0.045$  and  $b=0.0109 \pm 0.0045$  ( $n=7$ ).

9-AA dose–response relationship shown in Fig. 8E. Thus, the fitting of the  $I_B/I_S$  dependence with the logistic equation gave the value of  $IC_{50} = 6.3 \pm 0.6$   $\mu$ M and a high value of  $n_{Hill} = 1.56 \pm 0.20$  ( $n = 7$ ). Secondly, the experimentally observed dependence of  $A_{fast}$  on 9-AA concentration contains the values greater than 1. model 6 predicts the values of  $A_{fast}$  smaller than 1 and the only model, which can simulate  $A_{fast} > 1$ , is model 2. It is model 2 that should also be contained in the resulting model. The simplest appropriate combination of models 2 and 6 is as follows:



Model 7

Without the state designated as  $O_{B2}$ , this model, similarly to model 6, is able to simulate only the decrease in  $A_{fast}$  with the blocker concentration. For this reason, the existence of  $O_{B2}$  is necessary. The state designated as  $O_{B2}$  can be designated on equal terms as  $O_{B3}$  but an increase in the number of the blocker binding sites is not necessary here. Thus, model 7 can be interpreted in the following way. The blocker molecule can bind to sites 1 or 2 when the channel is in the open state ( $O^*$ ). The binding of one blocker molecule to the shallow site 2 prevents the other molecule to reach the vacant site 1 located deep in the channel pore. The binding of

the blocker directly to site 2 allows the other blocker to bind to site 1.

The increase in  $A_{fast}$  with 9-AA concentration can be explained in the following way. Let the transitions from  $O_{B1}$  to  $O$  and from  $O_{B1B2}$  to  $O_{B1}$  be faster than those from  $X$  to  $O$  and from  $O_{B2}$  to  $O$ . Then the amplitude of the fast component is defined as a ratio of the total number of channels in states  $O_{B1}$  and  $O_{B1B2}$  and in states  $X$ ,  $O_{B1}$ ,  $O_{B2}$  and  $O_{B1B2}$  at the moment of termination of the blocker application. At low blocker concentrations, the occupation of the  $O_{B2}$  state is comparable with those of the  $O_{B1}$  and  $O_{B1B2}$  states. The number of channels in the latter two states with respect to the total number of channels in  $X$ ,  $O_{B1}$ ,  $O_{B2}$  and  $O_{B1B2}$  states is small and, consequently,  $A_{fast}$  is also small. After the increasing of the blocker concentration more and more channels accumulate in the double-blocked  $O_{B1B2}$  state. The contribution of  $O_{B1}$  and  $O_{B1B2}$  states increases and  $A_{fast}$  rises with it.

The kinetic constants for model 7 can be estimated as follows. The theory predicts (see Appendix A) that the process of the current recovery after termination of the blocker application is described by a sum of four exponents with the following time constants:  $\tau_1 = 1/(k_7 - k_8)$ ;  $\tau_2 = 1/k_2$ ;  $\tau_3 = 1/k_4$ ;  $\tau_4 = 1/k_6$ . As the value of  $\tau_{fast}$  at 2.5  $\mu$ M 9-AA ( $180 \pm 147$  ms) did not differ significantly from the switching solution time ( $\tau_{OFF} = 137 \pm 71$  ms), it seemed correct to suggest the existence of a very fast component of the channels recovery from the 9-AA block, which was masked by the process of the solution exchange as it was suggested in the cases of TBA and TEA. Therefore, the value of the dissociation constant of the fastest transition,  $k_2$ , was adopted as  $1000 \text{ s}^{-1}$ . The increase in the  $\tau_{fast}$  value with 9-AA concentration and its attainment of the stationary level ( $649 \pm 147$  ms) at 40  $\mu$ M (Fig. 8B) may be considered as evidence of enhancement and saturation in the occupation of the  $O_{B1B2}$  state of the channel. Therefore, the value of the dissociation constant of the rate-limiting fast transition,  $k_4$ , was adopted as  $1/0.649 \text{ s} = 1.54 \text{ s}^{-1}$ . The slow dissociation constant,  $k_6$ , was estimated from the value of the slow time constant, which did not depend on 9-AA concentration (Fig. 8C):  $k_6 = 1/\tau_{slow} = 0.47 \text{ s}^{-1}$ . Eq. A12 (see Appendix A) defines the amplitude of the fast component for model

Table 2  
The kinetic constants for 9-AA

Kinetic constant	Value
$k_1$	$2.9 \times 10^7 \text{ M}^{-1} \text{ s}^{-1}$
$k_2$	$10^3 \text{ s}^{-1}$
$k_3$	$0.74 \times 10^6 \text{ M}^{-1} \text{ s}^{-1}$
$k_4$	$1.54 \text{ s}^{-1}$
$k_5$	$0.54 \times 10^5 \text{ M}^{-1} \text{ s}^{-1}$
$k_6$	$0.47 \text{ s}^{-1}$
$k_7$	$0.17 \text{ s}^{-1}$
$k_8$	$0.3 \text{ s}^{-1}$

7 as:

$$A_{\text{fast}} = \frac{1 + a \cdot [\text{B}]}{b + c \cdot [\text{B}]} \quad (9)$$

where

$$a = \frac{k_2 \cdot k_3 \cdot (k_2 - k_7 - k_8)}{(k_2 - k_4) \cdot (k_2 - k_8)}$$

$$\left\{ \frac{k_4 - k_8}{k_4 \cdot (k_4 - k_7 - k_8)} - \frac{k_2 - k_8}{k_2 \cdot (k_2 - k_7 - k_8)} \right\}$$

$$b = \frac{k_2 \cdot k_8 \cdot (k_2 - k_7 - k_8)}{k_1 \cdot (k_7 + k_8) \cdot (k_2 - k_8)} \left\{ \frac{k_1}{k_2} + \frac{k_5}{k_6} \right\}$$

$$c = \frac{k_3 \cdot k_8 \cdot (k_2 - k_7 - k_8)}{k_4 \cdot (k_7 + k_8) \cdot (k_2 - k_8)}$$

The  $A_{\text{fast}}$  defined by Eq. 9 increases with the blocker concentration when  $a \cdot b > c$ , decreases when  $a \cdot b < c$ , and is constant (equal to  $1/b$ ) when  $a \cdot b = c$ . The fitting of the  $A_{\text{fast}}$  dependence on 9-AA concentration by Eq. 9 (Fig. 8D) and of the  $I_{\text{B}}/I_{\text{S}}$  dependence on 9-AA concentration by Eq. A13 (Fig. 8E) gave only four independent equations for determination of the kinetic constants  $k_1$ ,  $k_3$ ,  $k_5$ ,  $k_7$  and  $k_8$ . The solutions of this system of equations were found at different values of  $k_8$ , which varied from 0 to  $1.5 \text{ s}^{-1}$  (at  $k_8 > 1.5 \text{ s}^{-1}$   $A_{\text{fast}}$  did not increase but decreased with a rise in 9-AA concentration). At  $k_8 = 0.3 \text{ s}^{-1}$  the current curves predicted by model 7 (Fig. 8A, second row) looked like those in the experiment. The corresponding values of the kinetic constants for model 7 in this case are presented in Table 2.

#### 4. Discussion

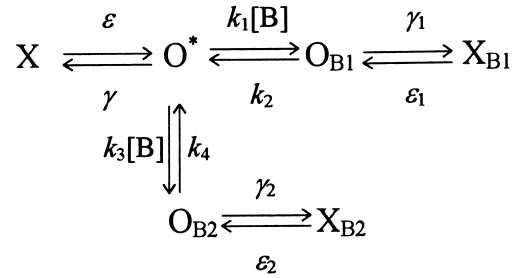
The present study offers a method for determining the simplest kinetic model for the blocker interaction with a ligand-gated channel proceeding from the manifested two-component kinetics. The use of this method supplemented, wherever possible, by other experimental data yields valuable information about the origin of the kinetic components and the information for constructing a physical model of the channel–blocker interaction. It provides the answers to the following questions: How does the blocker interact with the gating machinery of the channel?

How many blocker binding sites in the channel, what is the sequence and scheme of their occupation? The criterion of finding the best model is the behavior of the amplitude of the fast component ( $A_{\text{fast}}$ ) as a function of the blocker concentration. Depending on the value and constancy or a decrease in  $A_{\text{fast}}$  with the blocker concentration, the blocker action can be described by one of the five simplest kinetic models (models 2–6). Models 2–5 predict the blocking kinetics when  $A_{\text{fast}}$  does not depend on the blocker concentration (Eqs. 4–7). These models differ by the predicted range of  $A_{\text{fast}}$  value: for model 2 this parameter can be of any value, for model 3 and 4 is greater than 0 but smaller than 1, while for model 5 it is always negative. Model 6 predicts the blocking kinetics when  $A_{\text{fast}}$  decreases with the blocker concentration (Eq. 8). The examples of the blockers, the action of which can be described by the simplest kinetic models, are provided by the NMDA open channel blockers: TBA, TEA and MRZ.

The value of  $A_{\text{fast}}$  for TBA did not depend on the blocker concentration and was greater than 1. Therefore, within the framework of the simplest kinetic models the effect of TBA can be described only by model 2. The X state of this model can be the closed or the desensitized or some combination of the closed and the desensitized states of the channel. However, the time constants of the transitions from the closed to the open state of the NMDA channel and reverse are much faster than those defined by the kinetic constants,  $k_3$  and  $k_4$ , for model 2 (Table 1). Thus, the smallest value of the kinetic constant for the transition from the open to the closed state ( $140 \text{ s}^{-1}$ ) is estimated from the mean open time varying in single NMDA channel experiments from 2.5 to 7 ms [22–24]. Knowing this constant and the open probability of NMDA channels,  $P_0$ , it is easy to estimate the kinetic constant of the transition from the closed to the open state. As it has been mentioned above, in the majority of studies the value of  $P_0$  was estimated as being rather great (0.2–0.5). But even if we adopt the smallest value of 0.04 [21], the kinetic constant of the transition from the closed to the open state ( $6 \text{ s}^{-1}$ ) will prove to be 3–4-times higher than  $k_3$  and  $k_4$  for TBA. Therefore, the X state in model 2 is more probably the desensitized one or represents a combination of the closed and the desensitized states of the channel. Thus, model 2 shows that the NMDA chan-

nel can close and/or desensitize in the open conducting state, while this channel cannot do it when blocked by TBA. Such asymmetry of model 2 points to the interaction of the blocker with the gating machinery of the NMDA channel. TBA bound to its blocking site prevents the closure of the activation and/or desensitization gates of the NMDA channel. This fact has been established in the experiments where the ASP and TBA coapplication was followed by the transient current increase (the so-called ‘hook’ current), which exceeded the control current level [8].

With respect to the interaction with the gating machinery of the NMDA channel, it is interesting to compare TBA with another tetraalkylammonium compound, TEA. Its action can be described by models 3 and 4. Model 3 does not contain either closed or desensitized states of the channel and, correspondingly, is symmetric with respect to the ability of the open and the open-blocked state of the channel to close and/or desensitize. The more realistic representation of this model is as follows:



Model 8

where  $X$ ,  $X_{B1}$  and  $X_{B2}$  represent the states analogous to those in models 2, 4, 5 and 7. If we suppose for simplicity that TEA does not affect the processes of the channel closure and/or desensitization and, correspondingly,  $\gamma = \gamma_1 = \gamma_2$  and  $\varepsilon = \varepsilon_1 = \varepsilon_2$ , the kinetics predicted by model 8 (Fig. 9A) is qualitatively the same ( $A_{\text{fast}}$  is within [0,1] interval and does not depend on the blocker concentration) as the kinetics predicted by model 3 (Fig. 5A, second row). The

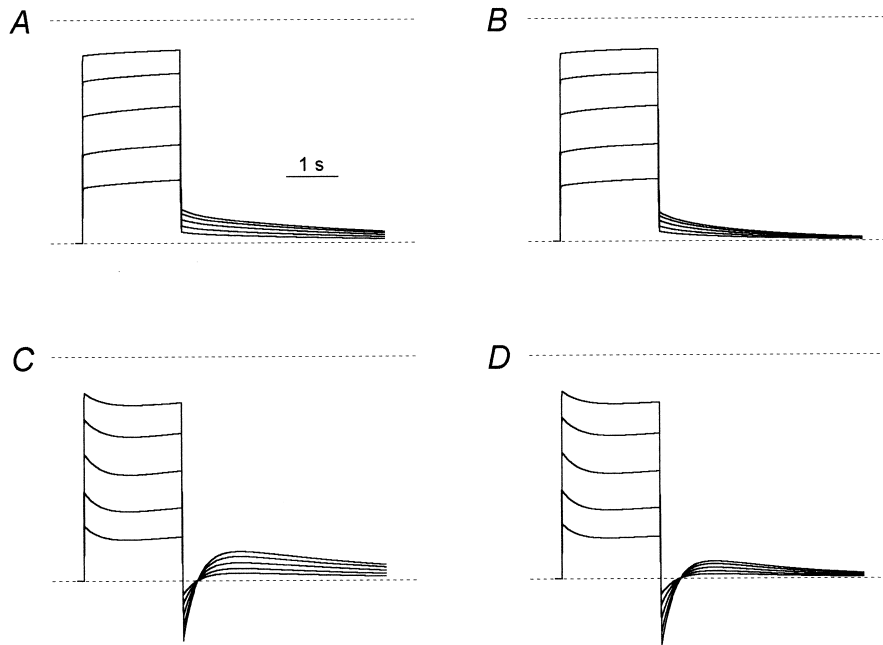
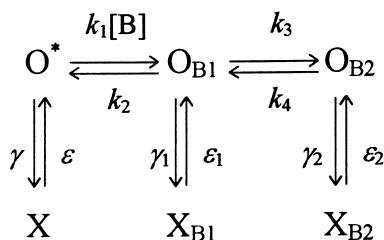


Fig. 9. The kinetics for TEA predicted by model 8. The values of the kinetic constants,  $k_1$ ,  $k_2$ ,  $k_3$ , and  $k_4$ , are the same as in model 3 (see Table 1). The kinetic constants for the transitions  $O \rightarrow X$ ,  $O_{B1} \rightarrow X_{B1}$ , and  $O_{B2} \rightarrow X_{B2}$  are the same as for the transition  $O \rightarrow X$  in model 2 for TBA:  $\gamma = \gamma_1 = \gamma_2 = 1.52 \text{ s}^{-1}$  and  $\varepsilon = \varepsilon_1 = \varepsilon_2 = 1.77 \text{ s}^{-1}$ . TEA concentrations are: 0.625, 1.25, 2.5, 5 and 10 mM. The curves presented are the modeling currents predicted by (A) model 8;  $A_{\text{fast}} = 0.84$  and does not depend on the blocker concentration; (B) model 8 without the  $X_{B2}$  state;  $A_{\text{fast}} = 0.86$  and does not depend on the blocker concentration; (C) model 8 without the  $X_{B1}$  state; (D) model 8 without the  $X_{B1}$  and  $X_{B2}$  states. In C and D the overshoot of the modeling current ( $A_{\text{fast}} > 1$ ) is observed.



removal of the  $X_{B2}$  state next to the slow blocked state,  $O_{B2}$ , from model 8 does not change this kinetics significantly (Fig. 9B). However, removal of the  $X_{B1}$  state next to the fast blocked state,  $O_{B1}$ , from model 8 leads to the appearance of the current overshoot ( $A_{\text{fast}} > 1$ ), which resembles that observed in the kinetics of TBA (Fig. 9C,D). Therefore, TEA binding to the channel in the fast blocked state,  $O_{B1}$ , does not prevent the closure of the activation and/or desensitization gate. Whether this is true for TEA binding to the channel in the slow blocked state,  $O_{B2}$ , remains unclear because the  $O_{B2}-X_{B2}$  transition is faster than the transition from  $O_{B2}$  to  $O$ .

The  $X_B$  state in model 4 can be interpreted as: (1) the second open blocked ( $O_{B2}$ ) and (2) closed blocked ( $C_B$ ) or desensitized blocked ( $D_B$ ), or a combination of the closed and the desensitized blocked states of the channel. In the first case, the transition from  $O_{B1}$  to  $O_{B2}$  means a 'jump' of the blocker from one blocking site to another. The succession of binding of the blocker molecule to the sites is strict: at first site 1 becomes occupied and then site 2 follows it. In this case, models 3 and 4 can represent the parts of a more complex model with the transitions  $O_{B1}-O_{B2}$ ,  $O-O_{B1}$  and  $O-O_{B2}$  (a combination of models 3 and 4). Such a model describes the situation when the only blocker molecule can bind to any of the two blocking sites in the channel in any succession and can 'jump' from one blocking site to another. Thus, in the first case model 4 is symmetric with respect to the ability of the open and the open-blocked state of the channel to close and/or desensitize. The more realistic representation of this model is as follows:

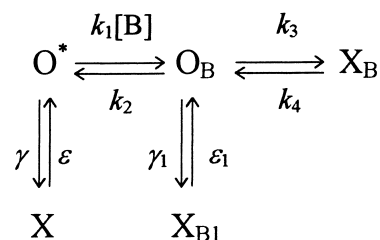


#### Model 9

As in the case of model 8, the kinetics predicted by model 9 is qualitatively the same as the kinetics predicted by model 3 (Fig. 5A, second row). The remov-

al of  $X_{B2}$  state does not significantly change the recovery kinetics, while the removal of  $X_{B1}$  state leads to the appearance of the current overshoot ( $A_{\text{fast}} > 1$ ), which resembles that observed in the kinetics of TBA. Therefore, TEA binding to the channel in state  $O_{B1}$  does not prevent the closure of the activation and/or desensitization gate of the channel. Whether this is true for TEA binding to the channel in state  $O_{B2}$  remains unclear because the  $O_{B2}-X_{B2}$  transition is faster than the  $O_{B2}-O_{B1}$  transition.

In the second case, the existence of the closed or desensitized (or their combination) states of the blocked channel and their absence in the non-blocked channel may imply: (a) the ability of the blocker to increase the number of closed blocked and/or desensitized blocked states when the more realistic representation of model 4 is as follows:



#### Model 10

and (b) the channel closes and/or desensitizes more readily with the blocker inside (the state  $X_{B1}$  is absent in model 10 but the  $O_B-X_B$  equilibrium is shifted to  $X_B$  with respect to model 4). Both (a) (Fig. 10A) and (b) (Fig. 10B) possibilities demonstrate the kinetics, which are qualitatively similar ( $A_{\text{fast}}$  is within the [0,1] interval and does not depend on the blocker concentration) to that predicted by model 4 (Fig. 5A, second row), but quite different from that which is predicted by model 4 with addition of only the  $X$  state similar to model 2 for TBA (or by model 10 without the  $X_{B1}$  state) (Fig. 10C).

Thus, all the simplest models (3 and 4) describing the mechanism of TEA action predict that this blocker does not prevent the closure of the activation and/or desensitization gates of the NMDA channel when bound to at least one site and even possibly promotes this process.

The difference in the interaction of tetraalkylammonium compounds with the gating machinery of

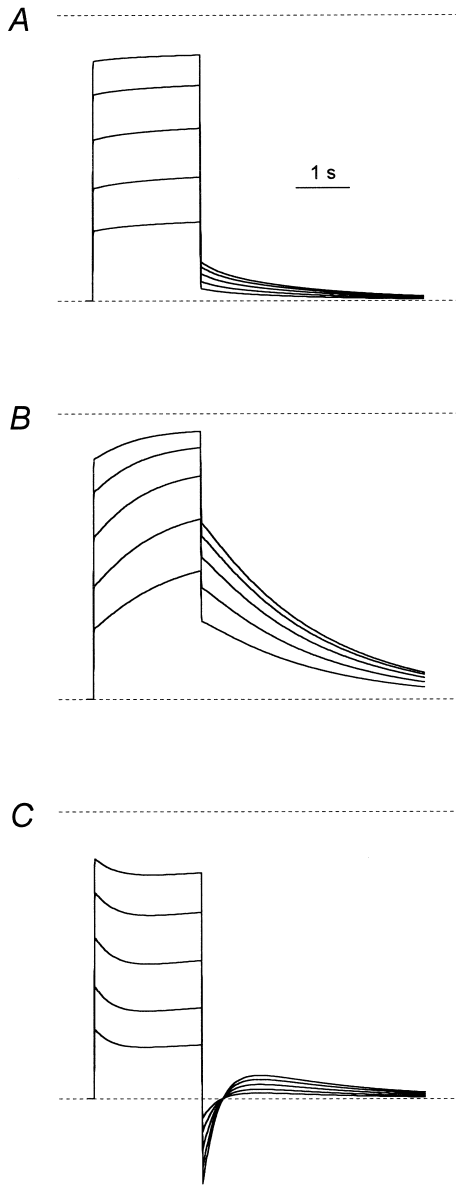
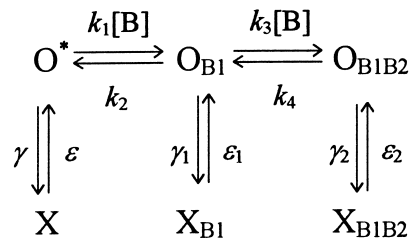


Fig. 10. The kinetics predicted by model 10 for TEA. The values of the kinetic constants,  $k_1$ ,  $k_2$  and  $k_4$ , are the same as in model 4 (see Table 1). The kinetic constants for the transitions  $O \rightarrow X$  and  $O_B \rightarrow X_{B1}$  are the same as for the transition  $O \rightarrow X$  in model 2 for TBA:  $\gamma = \gamma_1 = 1.52 \text{ s}^{-1}$  and  $\varepsilon = \varepsilon_1 = 1.77 \text{ s}^{-1}$ . TEA concentrations are 0.625, 1.25, 2.5, 5 and 10 mM. The curves presented are the modeling currents predicted by (A) model 10; the value of  $k_3 = 118 \text{ M}^{-1} \text{ s}^{-1}$  is the same as in model 4;  $A_{\text{fast}} = 0.86$  and does not depend on the blocker concentration; (B) model 10 without the  $X_{B1}$  state; the value of  $k_3 = 1180 \text{ M}^{-1} \text{ s}^{-1}$  is ten times higher than that in model 4;  $A_{\text{fast}} = 0.33$  and does not depend on the blocker concentration; (C) model 10 without the  $X_{B1}$  state; the value of  $k_3 = 118 \text{ M}^{-1} \text{ s}^{-1}$  is the same as in model 4. In C the overshoot of the modeling current ( $A_{\text{fast}} > 1$ ) is observed.

the NMDA channel can be explained by different size of the blocking molecules [25]. Thus, the larger blocker, TBA, prevents the closure of activation and/or desensitization gates, while the smaller one, TEA, which enters deep into the channel pore allows the gates to close after it.

The value of  $A_{\text{fast}}$  decreased with MRZ concentration. The only simplest model describing qualitatively such  $A_{\text{fast}}$  behavior is model 6. This model suggested the existence of two non-overlapping blocking sites of MRZ in the open NMDA channel. These two sites can be occupied simultaneously by different blocker molecules and the succession is strict: site 1 is occupied at first, and site 2 is occupied secondly. In reality, the situation may be more complex. It is correct to suppose that the blocker can reach site 1 not only directly from the external solution but also by way of sequential 'jumps' from the external solution to site 2 and then to site 1 [4]. Thus, the transition  $O^* \rightarrow O_{B1}$  of model 6 can imply two sequential transitions:  $O^* \rightarrow O_{B2}$  and  $O_{B2} \rightarrow O_{B1}$ . Contrary to TBA and TEA, the kinetics of the MRZ-induced blockade is much slower than the kinetics of NMDA channel closure and desensitization. Therefore, the more realistic version of model 6:



### Model 11

demonstrates practically the same recovery kinetics as model 6 (Fig. 7A, second row) in all possible cases when: (1)  $X_{B1}$ , or (2)  $X_{B1B2}$ , or (3)  $X_{B1}$  and  $X_{B1B2}$  states are removed, or (4) all states of model 11 are present. The fact is that the method used in the present study cannot answer the question 'Does the blocker prevent the closure of the activation and/or desensitization gate of NMDA channel?' concerning the blockers with such slow kinetics as that of MRZ because this method is applicable only for fast blockers [8]. However, other experiments do provide an answer to this question. Thus, the ability of another

aminoadamantane derivative, memantine, differing from MRZ by two methyl groups and hydrogen instead of one propyl and two hydrogen attached to three equivalent sites of 1-adamantanamine, to produce the trapping block of NMDA channels has been reported previously [5,26]. (1) The existence of two components in the kinetics of agonist-induced channels recovery after MEM-induced open-channel block and subsequent washout of the cell in an agonist-free solution [3], and (2) the fact that two similar components in the recovery kinetics of MEM in the continuous presence of agonist were explained by simultaneous occupation by MEM of two different blocking sites in the NMDA channel [4] strongly suggest that both MEM blocking sites are located below the activation gate and two MEM molecules bound to them can be closed within the NMDA channel. The data obtained in our laboratory (unpublished observation) indicate that in all probability this is also true for MRZ.

The only simplest model which remained without an example of a blocker is model 5. This model predicts the blocker association not with the open but mainly with the closed and/or desensitized states of the channel. In my opinion, up to now nobody has studied the NMDA channel blocker with the kinetics

predicted by model 5 ( $A_{\text{fast}} < 0$  and does not depend on the blocker concentration). Probably, such a blocker will be found in future.

In the case when the blocker-induced kinetics cannot be described by any of the simplest models the method of the simplest models combination can be used. Thus, not every simplest model describes the increase in  $A_{\text{fast}}$  with the blocker concentration. Such behavior of  $A_{\text{fast}}$  can be obtained by combination of model 6, the only simplest model predicting a change in  $A_{\text{fast}}$  with the blocker concentration, with one or several from models 2–5. 9-AA is an example of an NMDA open-channel blocker, the amplitude of the fast component for which increased with concentration.

As  $A_{\text{fast}}$  was greater than unity at high 9-AA concentrations, the simplest model simulating 9-AA kinetics (except for model 6) should contain model 2. The resulting model 8 predicts the existence of at least two non-overlapping 9-AA blocking sites, which can be simultaneously occupied by two different blocker molecules in two different successions. model 7 is asymmetric with respect to the ability of the channel to close and/or desensitize in the blocked and the non-blocked states. It predicts that 9-AA bound to the channel prevents the closure of the

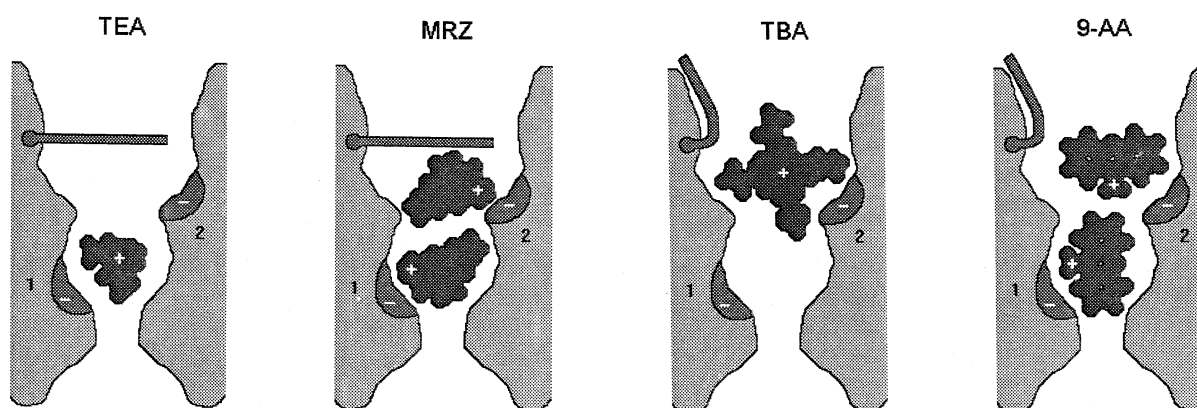


Fig. 11. Possible interpretation of the NMDA open-channel block by organic cations. The smallest cation, TEA, can bind either to the deep blocking site 1 or the shallow blocking site 2 and does not prevent the closure of the gate. Strong electrical repulsion of two TEA molecules prevents their simultaneous occupation of the sites. On the contrary, two molecules of MRZ being electrical dipoles can bind to the two blocking sites simultaneously and do not prevent the closure of the gate. Due to its large size, the TBA molecule can bind only to the shallow site 2 and thus prevents the closure of the gate. When oriented along the channel pore, the 9-AA molecule can quickly reach the deep site 1 (right from the external solution or by way of sequential 'jumps' from the external solution to site 2 and then to site 1 as is in the case with MRZ) and allow another 9-AA molecule to bind to site 2 in the orientation across the channel pore. When site 1 is vacant and the binding of the 9-AA molecule to the shallow site 2 proceeds in orientation across the channel pore, the channel constriction between sites 1 and 2 prevents the 9-AA molecule binding to site 2 to 'jump' to site 1.

activation and/or desensitization gates. The ability of 9-AA to prevent the closure of the NMDA channel was reported previously [9,19,8].

Previous studies on the open-channel structure allow to represent the NMDA channel as a pore with large extracellular and small cytoplasmic mouths. The narrow part of the pore (selectivity filter) is short and has a cross-sectional area of 22–26 Å<sup>2</sup> [27,28]. Based on the results of kinetic analysis presented for TBA, TEA, MRZ and 9-AA, the simplest physical models of the open NMDA channel interaction with organic cations can be suggested (Fig. 11).

The simplest kinetic models describing the effects of NMDA open-channel blockers with the constants collected in Tables 1 and 2 have significance in principle but do not pretend to describe completely all the possible states and substates of the NMDA channel. Simplification of the models presented above can be seen in the following facts. The value of  $k_2$  (10<sup>3</sup> s<sup>-1</sup>) for TBA, TEA and 9-AA was chosen arbitrarily. This value can be much higher. An increase in the value of  $k_2$  may cause a considerable change in the value of  $k_1$ , although other kinetic constants will not vary significantly. The values of  $k_3$  and  $k_7$  as well as the values of  $k_4$  and  $k_8$  in model 2 for TBA and in model 7 for 9-AA, respectively (see Tables 1 and 2), were different, although the physical meaning of these constants was the same. The concentration dependence of the fraction of the stationary block by MRZ predicted by model 6 was steeper than that obtained in the experiment (see Fig. 7E). Depending on the problem, each of the simplest models can be complicated by addition of multiple closed, desensitized and open states of the channel. The existence of different populations of the channels can also be taken into account. However, all these changes will not concern such questions of principle as the minimal number of simultaneously occupied blocking sites in the channel and the minimal number of the ways, by which the blocker can reach these sites [4] and the ability of the blocker being bound to the channel to prevent or not prevent the closure of the activation and/or the desensitization gates.

## Acknowledgements

The author thanks B.I. Khodorov and S.G.

Koshelev for critical discussions, and R.L. Birnova for help in preparation of the manuscript. I am also very grateful to the colleagues at MERZ and Co. for the generous supply of 1-amino-3-propyl-adamantane (MRZ 2/178). This work has been supported by the RFBR (N 96 04 49228), and ISSEP (N a98-2018).

## Appendix A

Let  $X(t)$  be the vector of probabilities of the channel occupying each of all possible states at the time,  $t$ . The behavior of  $X(t)$  is defined by the linear system of differential equations:

$$\frac{dX(t)}{dt} \mathbf{A}X(t) \quad (\text{A1})$$

where  $\mathbf{A}$  is the matrix of transitions between the states of the channel. To solve system A1, it is necessary to find all the eigenvalues of  $\mathbf{A}$  by solving the following equation:

$$|\mathbf{A} - \lambda \mathbf{E}| = 0 \quad (\text{A2})$$

where  $\lambda$  is variable and  $\mathbf{E}$  is the matrix with the diagonal elements equal to 1 and the nondiagonal elements equal to 0. In the case of the simplest models presented in this study, Eq. A2 has no multiple roots and the solution of Eq. A1 can be written in the following form:

$$X(t) = \sum_{i=1}^n C_i v_i e^{\lambda_i t} \quad (\text{A3})$$

where  $C_i$  is the  $i$ th constant;  $v_i$  is the  $i$ th eigenvector of  $\mathbf{A}$  corresponding to the  $i$ th eigenvalue,  $\lambda_i$ ;  $n$  is the number of states. The constants  $C_i$  ( $i = 1, \dots, n$ ) can be estimated from the probabilities of the channel to be in all possible states at equilibrium by posing  $t = 0$  in Eq. A3. Each of models 2–6 has its own transition matrix with elements representing the sums of the kinetic constants multiplied, where necessary, by the blocker concentration. The number of states is equal to 3, and the solution of Eq. A2 gives three values of  $\lambda$ :  $\lambda_1 = 0$  and  $\lambda_2, \lambda_3 \neq 0$ . Let  $\lambda_2$  correspond to the fast and  $\lambda_3$  to the slow component of the kinetics. When  $[B] = 0$ , there is a case of the channels recovery after the block. The fast and the slow time

constants of the channels recovery,  $\tau_{\text{fast}}$  and  $\tau_{\text{slow}}$ , respectively, are given by the following equations:

$$\lambda_2(k_1, k_2, k_3, k_4) = -1/\tau_{\text{fast}} \quad (\text{A4})$$

$$\lambda_3(k_1, k_2, k_3, k_4) = -1/\tau_{\text{slow}} \quad (\text{A5})$$

where  $\lambda_2(k_1, k_2, k_3, k_4)$  and  $\lambda_3(k_1, k_2, k_3, k_4)$  are defined from the solution of Eq. A2 relative to  $\lambda_2$  and  $\lambda_3$ .

To determine the probabilities of the channel to be in all possible states at equilibrium ( $t=0$ ), the right part of Eq. A1 should be taken as being equal to zero. Thus, we obtain a system of  $n$  linear equations:

$$\mathbf{A} \cdot \mathbf{X}(0) = 0 \quad (\text{A6})$$

with  $n$  variables:  $x_1(0), \dots, x_n(0)$ . As the rank of  $\mathbf{A}$  is equal to  $n-1$ , only  $n-1$  equations are independent. Adding the equation of the sum of probabilities of the channel occupying each of all possible states:

$$x_1(0) + x_2(0) + \dots + x_n(0) = 1 \quad (\text{A7})$$

we obtain a system of  $n$  equations with  $n$  variables which allows to determine the probabilities of the channel occupying each of all possible states at equilibrium in terms of kinetic constants. The fraction of non-blocked channels at equilibrium at the  $[\mathbf{B}]$  blocker concentration is defined via the probabilities of the open ( $j$ th) state occupancy in the absence,  $[\mathbf{O}]_{[\mathbf{B}]=0} = x_j(0)_{[\mathbf{B}]=0}$ , and the presence,  $[\mathbf{O}]_{[\mathbf{B}] \neq 0} = x_j(0)_{[\mathbf{B}] \neq 0}$ , of the blocker, respectively:

$$d = [\mathbf{O}]_{[\mathbf{B}] \neq 0} / [\mathbf{O}]_{[\mathbf{B}]=0} \quad (\text{A8})$$

The calculation of  $d$  for models 2–5 leads to the following equation:

$$d = \frac{1}{1 + K \cdot [\mathbf{B}]} \quad (\text{A9})$$

where  $K$  is equal to  $k_1 \cdot k_4 / k_2 / (k_3 + k_4)$  for model 2,  $k_1 / k_2 + k_3 / k_4$  for model 3,  $k_1 \cdot (1 + k_3 / k_4) / k_2$  for model 4 and  $k_1 \cdot k_3 / k_4 / (k_1 + k_2)$  for model 5. Only the denominator of the equation for model 6 contains the item with  $[\mathbf{B}]$  rose to the second power:

$$d = \frac{1}{1 + (k_1 / k_2) \cdot [\mathbf{B}] + (k_1 \cdot k_3 / k_2 / k_4) \cdot [\mathbf{B}]^2} \quad (\text{A10})$$

The amplitude of the fast component,  $A_{\text{fast}}$ , for

models 2–6 is determined from Eq. A3 for the probability of the open ( $j$ th) state occupancy:

$$A_{\text{fast}}(k_1, k_2, k_3, k_4, [\mathbf{B}]) = \frac{C_2 \cdot v_{2j}}{C_2 \cdot v_{2j} + C_3 \cdot v_{3j}} \quad (\text{A11})$$

The substitution of the mean experimental values of the fast and slow time constants into Eq. A4 and Eq. A5, the estimation of the parameters of Eq. A9 or Eq. A10 due to the fitting of the experimental  $I_B / I_S$  dependence on the blocker concentration and the parameters of Eq. A11 due to the fitting of the experimental  $A_{\text{fast}}$  dependence on the blocker concentration give a system of equations which allows to determine all the kinetic constants:  $k_1, k_2, k_3$  and  $k_4$ . The values of the kinetic constants for TBA, TEA and MRZ are presented in Table 1.

Model 7 contains five states of the channel. The eigenvalues for the recovery process defined from Eq. A2 are the following:  $\lambda_1 = 0$ ;  $\lambda_2 = -k_7 - k_8$ ;  $\lambda_3 = -k_2$ ;  $\lambda_4 = -k_4$ ;  $\lambda_5 = -k_6$ . If the amplitude of the fast component is defined as the ratio of changes in the total number of channels in  $\mathbf{O}_{B1}$  and  $\mathbf{O}_{B1B2}$  states and in the total number of channels in  $\mathbf{C}$ ,  $\mathbf{O}_{B1}$ ,  $\mathbf{O}_{B2}$  and  $\mathbf{O}_{B1B2}$  states induced by a removal of the blocker, then  $A_{\text{fast}}$  will be defined from Eq. A3 as follows:

$$A_{\text{fast}} = \frac{C_3 \cdot v_{3j} + C_4 \cdot v_{4j}}{C_2 \cdot v_{2j} + C_3 \cdot v_{3j} + C_4 \cdot v_{4j} + C_5 \cdot v_{5j}} \quad (\text{A12})$$

Eq. A8 for the fraction of non-blocked channels at equilibrium for model 7 is defined by the following way:

$$d = \frac{1}{1 + a \cdot [\mathbf{B}] + b \cdot [\mathbf{B}]^2} \quad (\text{A13})$$

where

$$a = \frac{k_8 \cdot (k_1 / k_2 + k_5 / k_6)}{k_7 + k_8}, \quad b = \frac{k_1 \cdot k_3 \cdot k_8}{k_2 \cdot k_4 \cdot (k_7 + k_8)}$$

## References

- [1] T. Frankiewicz, B. Potier, Z.I. Bashir, G.L. Collingridge, C.G. Parsons, Effects of memantine and MK-801 on NMDA-induced currents in cultured neurones and on synaptic transmission and LTP in area CA1 of rat hippocampal slices, *Br. J. Pharmacol.* 117 (1996) 689–697.
- [2] I. Bresink, T.A. Benke, V.J. Collett, A.J. Seal, C.G. Parsons,

- J.M. Henley, G.L. Collingridge, Effects of memantine on recombinant rat NMDA receptors expressed in HEK 293 cells, *Br. J. Pharmacol.* 119 (1996) 195–204.
- [3] T.A. Blanpied, F. Boeckman, E. Aizenman, J.W. Johnson, Trapping channel block of NMDA-activated responses by amantadine and memantine, *J. Neurophysiol.* 77 (1997) 309–323.
- [4] A. Sobolevsky, S. Koshelev, Two blocking sites of amino-adamantane derivatives in open *N*-methyl-D-aspartate channels, *Biophys. J.* 74 (1998) 1305–1319.
- [5] J.W. Johnson, S.M. Antonov, T.S. Blanpied, Y. Li-Smerin, Channel block of NMDA receptor, in: H.V. Wheal (Ed.), *Excitatory Amino Acids and Synaptic Transmission*, Academic Press, London, 1995, pp. 99–113.
- [6] S.M. Antonov, J.W. Johnson, N.Y. Lukomsкая, N.N. Potapyeva, V.E. Gmiro, L.G. Magazanik, Novel adamantane derivatives act as blockers of open ligand-gated channels and as anticonvulsants, *Mol. Pharmacol.* 47 (1995) 558–567.
- [7] S.G. Koshelev, B.I. Khodorov, Tetraethylammonium and tetrabutylammonium as tools to study NMDA channels of the neuronal membrane, *Biologicheskie Membrany* 9 (1992) 1365–1369.
- [8] S.G. Koshelev, B.I. Khodorov, Blockade of open NMDA channel by tetrabutylammonium, 9-aminoacridine and taurine prevents channels closing and desensitization, *Membr. Cell Biol.* 9 (1995) 93–109.
- [9] A.C.S. Costa, E.X. Albuquerque, Dynamics of the actions of tetrahydro-9-aminoacridine and 9-aminoacridine on glutamatergic currents: Concentration-jump studies in cultured rat hippocampal neurons, *J. Pharmacol. Exp. Ther.* 268 (1994) 503–514.
- [10] W. Danysz, C.G. Parsons, I. Bresink, G. Quack, Glutamate in CNS disorders, *DN and P* 8 (1995) 261–277.
- [11] V.S. Vorobjev, Vibrodissociation of sliced mammalian nervous tissue, *J. Neurosci. Methods* 38 (1991) 145–150.
- [12] M. Benveniste, J.-M. Mienville, E. Sernagor, M.L. Mayer, Concentration-jump experiments with NMDA antagonists in mouse cultured hippocampal neurons, *J. Neurophysiol.* 63 (1990) 1373–1384.
- [13] M. Benveniste, J. Clements, L. Vyklicky, M.L. Mayer, A kinetic analysis of the modulation of *N*-methyl-D-aspartic acid receptors by glycine in mouse cultured hippocampal neurones, *J. Physiol.* 428 (1990) 333–357.
- [14] P. Ascher, L. Nowak, The role of divalent cations in the *N*-methyl-D-aspartate responses of mouse central neurones in culture, *J. Physiol.* 399 (1988) 247–266.
- [15] J.M. Wright, P.A. Kline, L.M. Nowak, Multiple effects of tetraethylammonium on *N*-methyl-D-aspartate receptor-channels in mouse brain neurons in cell culture, *J. Physiol.* 439 (1991) 579–604.
- [16] F. Lin, C.F. Stevens, Both open and closed NMDA receptor channels desensitize, *J. Neurosci.* 14 (1994) 2153–2160.
- [17] C.E. Jahr, High probability opening of NMDA receptor channels by L-glutamate, *Science* 255 (1992) 470–472.
- [18] R.A.J. Lester, G. Tong, C.E. Jahr, Interactions between the glycine and glutamate binding sites of the NMDA receptor, *J. Neurosci.* 13 (1993) 1088–1096.
- [19] M. Benveniste, M.L. Mayer, Trapping of glutamate and glycine during open channel block of rat hippocampal neuron NMDA receptors by 9-aminoacridine, *J. Physiol.* 483 (1995) 367–384.
- [20] D. Colquhoun, A.G. Hawkes, Desensitization of *N*-methyl-D-aspartate receptors: a problem of interpretation, *Proc. Natl. Acad. Sci. U.S.A.* 92 (1995) 10327–10329.
- [21] C. Rosenmund, A. Feltz, G.L. Westbrook, Synaptic NMDA receptor channels have a low open probability, *J. Neurosci.* 15 (1995) 2788–2795.
- [22] P. Ascher, P. Bregestovski, L. Nowak, *N*-Methyl-D-aspartate-activated channels of mouse central neurones in magnesium-free solutions, *J. Physiol.* 399 (1988) 207–226.
- [23] S.G. Cull-Candy, M.M. Usowich, On the multiple-conductance single channels activated by excitatory amino acids in large cerebellar neurones of the rat, *J. Physiol.* 415 (1989) 555–582.
- [24] C.E. Jahr, C.F. Stevens, A quantitative description of NMDA receptor-channel kinetic behavior, *J. Neurosci.* 10 (1990) 1830–1837.
- [25] S. Koshelev, B. Khodorov, Probing of NMDA receptor channels by organic cations. Location of activation and inactivation gates, in: J. Lerma, P.H. Seeburg (Eds.), *Workshop on Molecular Mechanisms of Synaptic Function*, Madrid, 1994, p. 64.
- [26] H.-S.V. Chen, S.A. Lipton, Mechanism of memantine block of NMDA-activated channels in rat retinal ganglion cells: uncompetitive antagonism, *J. Physiol.* 499 (1997) 27–46.
- [27] M.M. Zarei, J.A. Dani, Structural basis for explaining open-channel blockade of the NMDA receptor, *J. Neurosci.* 15 (1995) 1446–1454.
- [28] A. Villarroel, N. Burnashev, B. Sakmann, Dimensions of the narrow portion of a recombinant NMDA receptor channel, *Biophys. J.* 68 (1995) 866–875.



# Probing of NMDA Channels with Fast Blockers

Alexander I. Sobolevsky, Sergey G. Koshelev, and Boris I. Khodorov

*Institute of General Pathology and Pathophysiology, 125315 Moscow, Russia*

Using whole-cell patch-clamp techniques, we studied the interaction of open NMDA channels with tetraalkylammonium compounds: tetraethylammonium (TEA), tetrapropylammonium (TPA), tetrabutylammonium (TBA), and tetrapentylammonium (TPentA). Analysis of the blocking kinetics, concentration, and agonist dependencies using a set of kinetic models allowed us to create the criteria distinguishing the effects of these blockers on the channel closure, desensitization, and agonist dissociation. Thus, it was found that TPentA prohibited, TBA partly prevented, and TPA and TEA did not prevent either the channel closure or the agonist dissociation. TPentA and TBA prohibited, TPA slightly prevented, and TEA did not affect the channel desensitization. These data along with the voltage dependence of the stationary current inhibition led us to hypothesize that: (1) there are activation and desensitization gates in the NMDA

channel; (2) these gates are distinct structures located in the external channel vestibule, the desensitization gate being located deeper than the activation gate. The size of the blocker plays a key role in its interaction with the NMDA channel gating machinery: small blockers (TEA and TPA) bind in the depth of the channel pore and permit the closure of both gates, whereas larger blockers (TBA) allow the closure of the activation gate but prohibit the closure of the desensitization gate; finally, the largest blockers (TPentA) prohibit the closure of both activation and desensitization gates. The mean diameter of the NMDA channel pore in the region of the activation gate localization was estimated to be  $\sim 11$  Å.

**Key words:** NMDA; gating machinery; tetraalkylammonium compounds; blockade; desensitization; kinetics; patch-clamp; whole-cell; hippocampal neurons

Considerable progress has been achieved over the last few years in studies of the molecular structure of the NMDA subtype of glutamate receptors (for review, see McBain and Mayer, 1994; Dingledine et al., 1999) (Kuryatov et al., 1994; Kuner et al., 1996; Krupp et al., 1996, 1998; Laube et al., 1997, 1998; Villarroel et al., 1998; Anson et al., 1998; Beck et al., 1999). However, some fundamental questions concerning their gross architecture and gating have not yet been finally settled. Present-day views on the functional architecture of voltage-sensitive  $\text{Na}^+$  and  $\text{K}^+$  channels are primarily based on the data obtained in studies of the mechanism of their direct blockade by various quaternary ammonium cations (for review, see Hille, 1992; Armstrong and Hille, 1998).

Probing with blocking compounds has also been used in studies of the functional architecture of some ligand-gated channels, in particular nicotinic acetylcholine channels and NMDA receptor channels. The use of this method clearly demonstrated that the activation gate of these channels is located in the external vestibule (Neher and Steinbach, 1978). Then, by analogy with voltage-sensitive channels (Armstrong, 1971; Strichartz, 1973; Yeh and Narahashi, 1977; Cahalan, 1978; Armstrong and Croop, 1982), it was found that, depending on the type of interaction with the gating machinery, most of the blockers of open receptor-operated channels can be subdivided into at least two groups, namely, those that do not prevent the channel closure, yielding the so-called trapping block (Neely and Lingle, 1986; Huetter and Bean, 1988; MacDonald et al., 1991; Johnson et al., 1995; Blanpied et

al., 1997; Chen and Lipton, 1997; Sobolevsky et al., 1998) and those that prohibit the channel closure (Koshelev and Khodorov, 1992, 1995; Costa and Albuquerque, 1994; Vorobjev and Sharonova, 1994; Benveniste and Mayer, 1995; Johnson et al., 1995; Antonov and Johnson, 1996).

A comparative analysis of blocking effects of a series of organic cations on NMDA channels led Koshelev and Khodorov (1992, 1995) to suggest that, along with the activation gate, the NMDA channel, like the voltage-sensitive  $\text{Na}^+$  channel, is equipped with a desensitization gate; the closure of the latter was assumed to underlie the channel desensitization.

In the present study we investigated the interaction of tetraalkylammonium compounds (TAA) with open NMDA channels using a set of kinetic models. We found the criteria for distinguishing the blockers with a kinetics faster than the channel closure (fast blockers), which prohibited or did not prohibit the channel closure, desensitization, and agonist dissociation. According to these criteria, we analyzed the action of tetraethylammonium (TEA), tetrapropylammonium (TPA), tetrabutylammonium (TBA), and tetrapentylammonium (TPentA). The results of this analysis provide new evidence in favor of the hypothesis on the existence of functionally and spatially distinct activation and desensitization gates in the NMDA channel and offer a radically new approach to the study of their reciprocal position. Thus, TAA proved to be useful tools to study NMDA channel gating.

## MATERIALS AND METHODS

Pyramidal neurons were acutely isolated from the CA-1 region of rat hippocampus using "vibrodissociation techniques" (Vorobjev, 1991). The experiments were begun after 3 hr of incubation of the hippocampal slices in a solution containing (in mM): NaCl, 124; KCl, 3;  $\text{CaCl}_2$ , 1.4;  $\text{MgCl}_2$ , 2; glucose, 10; and  $\text{NaHCO}_3$ , 26. The solution was bubbled with carbogen at 32°C. During the whole period of isolation and current recording, nerve cells were washed with an  $\text{Mg}^{2+}$ -free 3  $\mu\text{M}$  glycine-containing solution (in mM: NaCl, 140; KCl, 5;  $\text{CaCl}_2$ , 2; glucose, 15; and

Received July 27, 1999; revised Sept. 27, 1999; accepted Sept. 29, 1999.

This work was supported by the Russian Foundation for Basic Research Grants N 96-15-97866 and N 99-04-48770 and International Soros Science Education Program Grant N a99-1650 to A.I.S. We thank R. L. Birnova and M. V. Yelshansky for help in preparation and Dr. R. Schoepfer for reading this manuscript.

Correspondence should be addressed to Alexander I. Sobolevsky, Institute of General Pathology and Pathophysiology, Baltiyskaya 8, 125315 Moscow, Russia. E-mail: rans@rans.msk.ru.

Copyright © 1999 Society for Neuroscience 0270-6474/99/1910611-16\$05.00/0

HEPES, 10, pH 7.3). Fast replacement of superfusion solutions was achieved by using the concentration jump technique (Benveniste et al., 1990a; Vorobjev, 1991) with one application tube. This technique allows substitution of the tubular for the flowing solution with a time constant <30 msec but backward with the time constant of 30–100 msec (Sobolevsky, 1999). Therefore, except where noted, the rate of the solution exchange was fast at the beginning of any application and slightly slower at its termination. The currents were recorded at 18°C in the whole-cell configuration using micropipettes made from Pyrex tubes and filled with an “intracellular” solution (in mM: CsF, 140; NaCl, 4; and HEPES, 10; pH 7.2). Electric resistance of the filled micropipettes was 3–7 MΩ. Analog current signals were digitized at 1 kHz frequency.

Statistical analysis was performed using the scientific and technical graphics computer program Microcal Origin (version 4.1 for Windows). The data presented are mean  $\pm$  SE; comparison of the means was done by ANOVA, with  $p < 0.05$  taken as significant.

The kinetic models used to simulate the action of the blockers (Fig. 1) were based on the conventional rate theory and used independent forward and reverse rate constants to simultaneously solve first-order differential equations representing the transitions between all possible states of the channel. These models were obtained from a completely symmetric model for the open-channel blockade (model 5) by means of consecutive reduction of the blocked states. The processes of NMDA channel activation, opening, and desensitization were described in accordance with a kinetic model proposed by Lester and Jahr (1992). The choice of values of the kinetic constants was made as described previously (Sobolevsky and Koshelev, 1998). Thus, the values of the kinetic constants for the agonist binding and unbinding were  $k_1 = 2 \mu\text{M}^{-1} \cdot \text{sec}^{-1}$  and  $k_2 = 25 \text{ sec}^{-1}$ , respectively; the entrance and recovery from desensitization were  $\gamma = 1.2$  and  $\epsilon = 0.8 \text{ sec}^{-1}$ , respectively, and the kinetic constant of the channel closure was  $\alpha = 200 \text{ sec}^{-1}$ . The value of the rate constant of the channel opening,  $\beta$ , was chosen according to the value of the open probability,  $P_0 = \beta/(\alpha + \beta)$ , which was previously defined in a wide range of 0.04–0.5 (Jahr, 1992; Lester et al., 1993; Lin and Stevens, 1994; Benveniste and Mayer, 1995; Colquhoun and Hawkes, 1995; Rosenmund et al., 1995; Lu et al., 1998). In the majority of computer experiments, except where noted, the value of  $P_0$  was taken to be rather low (0.09) by the reason clarified in Results. The values of the blocking and unblocking kinetic constants,  $k_1$  and  $k_2$ , respectively, were too fast to be estimated. The value of the unblocking kinetic constant was taken to be sufficiently high,  $k_2 = 1000 \text{ sec}^{-1}$ . The value of  $k_1$  was taken arbitrarily ( $3.5 \mu\text{M}^{-1} \cdot \text{sec}^{-1}$ , as for TBA in the previous study by Sobolevsky, 1999) but the blocker concentration was measured in the values of the microscopic  $K_d = k_2/k_1$ . As it will be shown below from variation of the values of  $k_2$  and  $k_1$ , their arbitrary choice does not affect the major conclusions of this paper.

Differential equations were solved numerically using the algorithm analogous to that described previously (Benveniste et al., 1990b).

Tetraalkylammonium compounds were purchased from Aldrich (Milwaukee, WI). The three-dimensional structures of the blockers were obtained with the help of Molecular Modeling System HyperChem (release 3 for Windows).

## RESULTS

### Concentration and voltage dependence of the TAA-induced blockade

At the holding potential of  $-100 \text{ mV}$ , aspartate (ASP) ( $100 \mu\text{M}$ ) elicited an inward current through the NMDA channels, which after the initial fast rise ( $\tau < 30 \text{ msec}$ ) up to the value,  $I_{C0}$ , decreased gradually ( $\tau = 250\text{--}750 \text{ msec}$ ) to the stationary level,  $I_{CS}$ . This current decay under the continuing action of the agonist is interpreted as a result of NMDA receptor channel desensitization. When coapplied with ASP, TAA suppressed both initial,  $I_{B0}$  (measured at the termination of the initial fast current increase), and stationary,  $I_{BS}$ , currents. Representative superpositions of the currents elicited by ASP alone (control) or by ASP coapplied with TEA, TPA, TBA, and TPentA used at different concentrations are shown in Figure 2. Termination of ASP coapplication with each of these blockers was followed by a transient increase in the inward current (“hooked” tail current), which was absent in the control. In all the experiments with TEA and TPA,

the maximal value of the hooked current,  $I_P$ , was smaller than  $I_{CS}$  at any blocker concentration. In contrast, for TBA at high concentrations  $I_P$  was greater than  $I_{CS}$  in 60% of the cells ( $n = 32$  of 53), and even greater than  $I_{C0}$  in three cells ( $n = 3$  of 53). The maximal value of the hooked current for TPentA used at high concentrations was always greater than  $I_{CS}$  ( $n = 22$ ), and in six cells ( $n = 6$  of 22) it was larger than  $I_{C0}$ . The amplitude of the hooked tail current,  $I_P - I_{BS}$ , increased with the blocker concentration for all TAA. However, this increase was considerably greater for TBA and TPentA than for TEA and TPA. Another important difference between the hooked tail currents concerns their time course. In the case of ASP coapplication with TEA or TPA, the hooked tail current always lay below the control tail current. In contrast, for TBA and TPentA the hooked tail current and the control tail current intersected.

The blockade of NMDA channels by TAA was voltage-dependent. The current responses to ASP application and to ASP coapplication with TBA ( $2 \text{ mM}$ ) at the holding potential,  $E_h$ , which varied from  $-100$  to  $40 \text{ mV}$  (with the step of  $20 \text{ mV}$ ), are shown in Figure 3A. The control and blocked stationary  $I$ - $V$  curves are shown in the *inset*. The degree of the stationary block,  $1 - I_{BS}/I_{CS}$ , (as well as the amplitude of the hooked tail current; Fig. 3A) diminished with membrane depolarization (Fig. 3B). According to the model of Woodhull (1973), the voltage dependence can be fitted with the following equation:

$$1 - I_{BS}/I_{CS} = 1 - 1/(1 + [B]/K_{0.5}(0) \times \exp(\delta FE_h/RT)), \quad (1)$$

where  $K_{0.5}(0) = 5.34 \pm 0.27 \text{ mM}$  is the equilibrium dissociation constant at  $E_h = 0$ , and  $\delta = 0.60 \pm 0.02$  ( $n = 7$ ) is the fraction of the electric field that contributed to the energy of the blocker at the blocking site.  $F$ ,  $R$ , and  $T$  have their usual meanings. The values of  $\delta$  and  $K_{0.5}(0)$  estimated for other compounds are presented in Table 1. The value of  $\delta$  increased for TAA with a decrease in the alkyl chain length from  $0.29 \pm 0.03$  (TPentA) to  $0.90 \pm 0.04$  (TEA). This means that according to the Woodhull model the smaller TAA penetrate deeper into the membrane electric field. All the experiments described below were performed at the holding potential of  $-100 \text{ mV}$ .

To study the effect of the TAA on NMDA channel closure, desensitization, and agonist dissociation, we considered five kinetic models (Fig. 1; see Materials and Methods). The first model implies that the blocker prohibits both the channel closure and desensitization. In the second model, the blocker can be trapped in the closed channel but does not allow the channel to desensitize and the agonist to dissociate from the channel. The third model implies that the blocker only prohibits the agonist dissociation from the blocked channel. Model 4 describes the situation when the blocker prohibits the channel desensitization but does not prohibit the channel closure and the agonist dissociation from the blocked channel. The fifth model is completely symmetric and implies that the blocker prohibits neither the channel closure and desensitization nor the agonist dissociation.

We tried to classify the action of the fast NMDA channel blockers according to models 1–5 assuming, for simplicity sake, that the rate constants for the transitions between the blocked states of the channel ( $\alpha'$ ,  $\beta'$ ,  $\gamma'$ ,  $\epsilon'$ ,  $l_2'$ , and  $l_1'$ ) are equal to the corresponding rate constants for the nonblocked channels ( $\alpha$ ,  $\beta$ ,  $\gamma$ ,  $\epsilon$ ,  $l_2$ , and  $l_1$ ). Multiple experimental and modeling protocols will be used to associate each blocker with a model.

On the condition that the blocking kinetics is rather fast, all five models predict the appearance of the hooked tail current immedi-

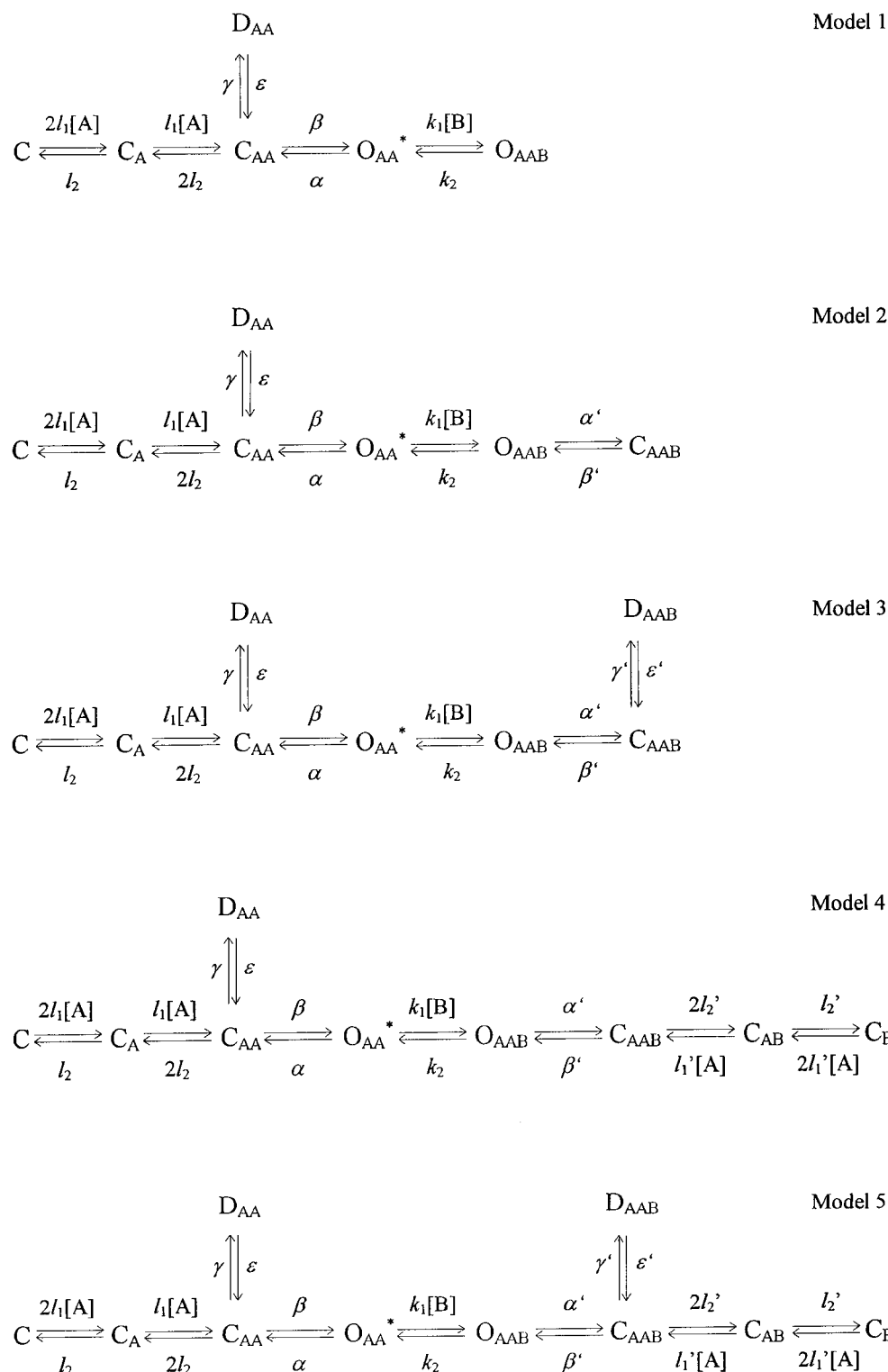


**Figure 1.** Kinetic models used to simulate the open-channel blocker action. *C*, *D*, *O*, Channel in closed, desensitized, and open states, respectively; *subscripts A, AA, B*, binding of one agonist and two and one blocker molecules to the channel, respectively; *asterisk*, conducting state, *[A]*, *[B]*, agonist and blocker concentrations, respectively.

ately after the termination of the agonist and the blocker coapplication (Fig. 4A). The kinetic analysis showed that the ascending phase of the hooked current reflects the blocker dissociation from the channel (transition from  $O_{AAB}$  to  $O_{AA}^*$  state), whereas the falling phase reflects the processes of the channel closure, desen-

sitization and the agonist dissociation. In Figure 4A the degree of the stationary current inhibition,  $1 - I_{BS}/I_{CS}$ , is the same for all models (0.86). To achieve this degree of stationary current inhibition, the blocker concentration was taken equal to 175, 16, 7, 13, and 6.5  $K_d$  for models 1, 2, 3, 4, and 5, respectively. The significant

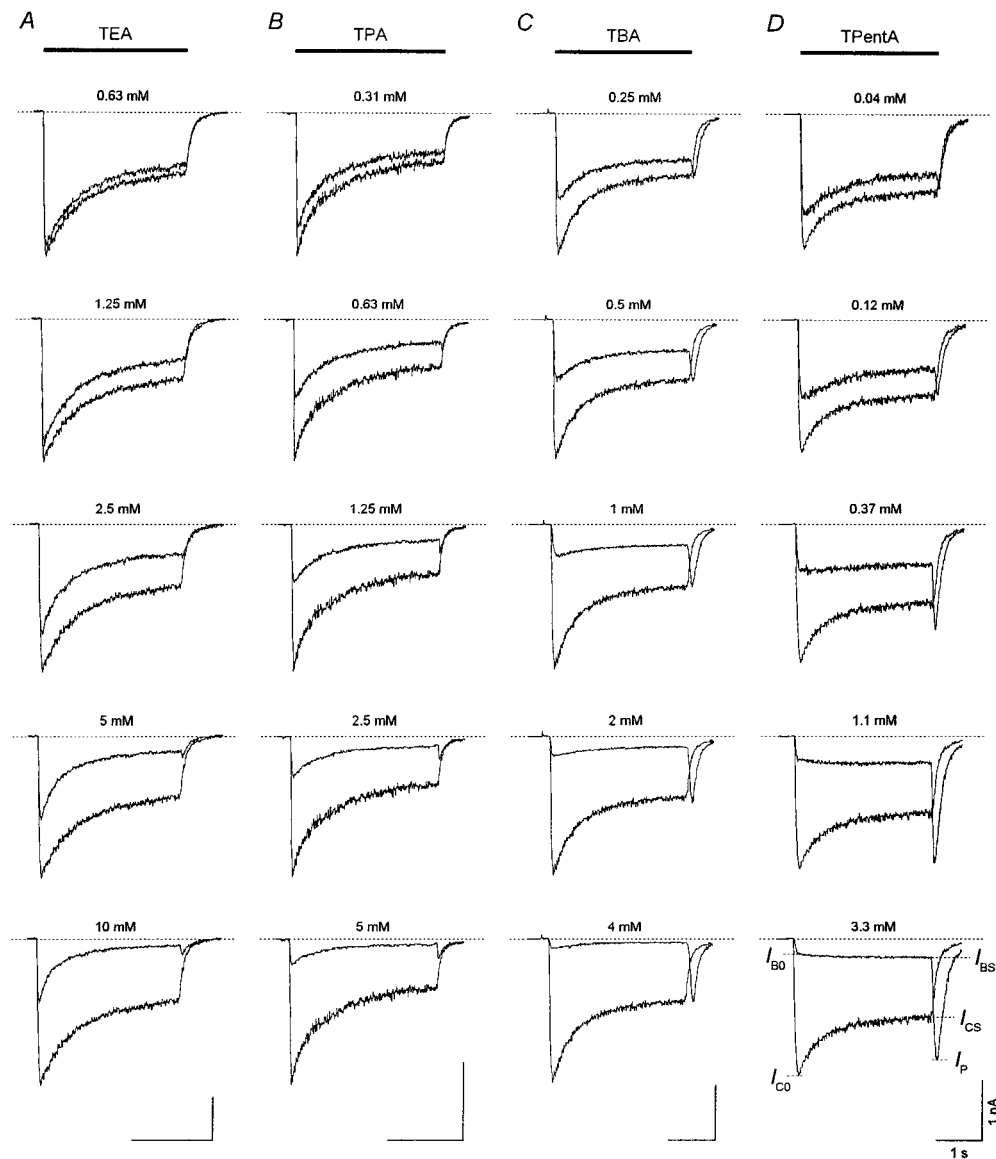


**Figure 2.** Coapplications of TAA with ASP. The control current elicited by ASP ( $100 \mu\text{M}$ ) application is superimposed with the current induced by ASP coapplication with TEA, TPA, TBA, or TPentA at different concentrations. A transient increase in the inward current (the hooked-tail current) appears after termination of the agonist and the blocker coapplication and is more pronounced at high TAA concentrations. The same labels apply to all calibrations.

difference in blocker concentration ( $[B]$ ) for different models clearly demonstrates that the apparent affinity of the blocker ( $1/IC_{50}$ ) is defined not only by its association–dissociation kinetics (the association and dissociation rate constants for different models were the same) but, to a considerable extent, by the blocker effect on the channel closure, desensitization, and agonist dissociation.

The amplitude of the hooked current,  $I_P - I_{BS}$ , is different for different models (Fig. 4*A*, inset). It would be tempting to choose this amplitude as a criterion by which the action of the blocker can be attributed to one of models 1–5. However, we found that a number of factors affect the amplitude of the hooked current. We illustrated this with the simplest model (model 1) as an example.

The first factor is the value of the open probability,  $P_0$ . A rise in  $P_0$  increases the magnitude of the simulated control current and enhances the simulated current stationary inhibition at a given blocker concentration. Thus, to achieve the same degree of the stationary current inhibition, we took smaller  $[B]$  at higher  $P_0$ ; the relative amplitude of the hooked current,  $(I_P - I_{BS})/I_{CS}$ ,

decreased with increasing  $P_0$ . This can be clearly seen in Figure 4*B*, where the stationary levels of the control simulated current at different  $P_0$  were normalized.

The time constant of the solution exchange (assuming that the solution exchange is a single-exponential process; Benveniste et al., 1990b),  $\tau_{\text{wash}}$ , is the next factor that crucially affects the amplitude of the hooked current (Fig. 4*C*). The hooked current becomes higher and thinner with diminishing  $\tau_{\text{wash}}$ .

A qualitatively inverse dependence of the amplitude of the hooked current on the value of the unblocking rate constant,  $k_2$ , is observed (Fig. 4*D*). The hooked current becomes smaller and wider with the slowing of the blocking kinetics, and at  $k_2 = 0.3\text{--}0.5 \text{ sec}^{-1}$  it disappears completely.

The next factor is the blocker concentration,  $[B]$  (Fig. 5*A*). The higher the  $[B]$ , the deeper is the block and the greater is the amplitude of the hooked current. Such an experimental dependence is clearly seen in Figure 2.

The nature of the dependencies of the hooked current ampli-

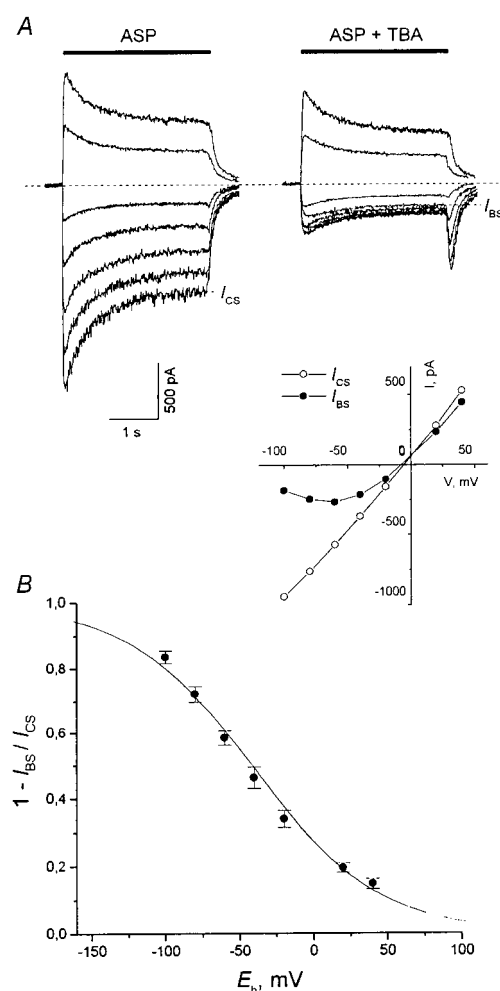


**Figure 3.** Voltage dependence of the stationary current inhibition. The voltage dependence is illustrated with 2 mM TBA as an example. *A*, Experimental curves. ASP (100 μM) was applied alone (*left traces*) or was coapplied with 2 mM TBA (*right traces*) for 3 sec at different holding membrane potentials,  $E_h = -100, -80, -60, -40, -20, 20,$  and  $40$  mV. The degree of the stationary current inhibition,  $1 - I_{BS}/I_{CS}$ , diminished with membrane depolarization. *Inset*, Control and blocked stationary  $I-V$  curves. *B*, The mean  $1 - I_{BS}/I_{CS}$  values were plotted against  $E_h$ . The fitting with Equation 1 (*solid line*) gave the following values of parameters:  $K_{0.5}(0) = 5.34 \pm 0.27$  mM and  $\delta = 0.60 \pm 0.02$  ( $n = 7$ ).

**Table 1. Voltage dependence parameters**

Compound	$\delta$	$K_{0.5}(0)$ (mM)	$n$
TEA	$0.90 \pm 0.04$	$62.2 \pm 6.0$	6
TPA	$0.72 \pm 0.05$	$10.0 \pm 1.5$	4
TBA	$0.60 \pm 0.02$	$5.34 \pm 0.27$	7
TPentA	$0.29 \pm 0.03$	$1.84 \pm 0.11$	5

tude on  $P_0$ ,  $\tau_{wash}$ ,  $k_2$ , and  $[B]$  will be considered elsewhere. However, the variety of parameters that affect the amplitude of the hooked current (as well as its latency) makes it doubtful to consider this value as a criterion of choice among models 1–5. Apparently, it would be much better to find a qualitative criterion. For example, the intersection of the hooked tail current and the control tail current (Fig. 4*A*, *inset*) is predicted by models 1–4

(but not by model 5) at any  $P_0$ ,  $\tau_{wash}$ ,  $k_2$ , and  $[B]$  values considered. Thus, we have obtained the first criterion, which allows us to select a model for describing the action of a blocker. This criterion permits one to distinguish the blockers whose action can be described by model 5 from those whose action can be described by models 1–4. According to this criterion, the TEA and TPA action can be described by model 5, whereas the TBA and TPentA action can be described by one of models 1–4. Other qualitative criteria should be found to make a choice between models 1–4. The first of these criteria is the plateau/peak ratio.

### Plateau/peak ratio

As can be seen from Figure 2, the plateau/peak ratio for the block,  $I_{BS}/I_{B0}$ , may differ significantly from that for the control,  $I_{CS}/I_{C0}$ . To compare the plateau/peak ratio for the block and the control, we calculated it at different blocker concentrations. The mean values of the normalized plateau/peak ratio,  $(I_{BS}/I_{B0})/(I_{CS}/I_{C0})$ , for different NMDA open-channel blockers were plotted against the degree of the stationary current inhibition,  $1 - I_{BS}/I_{CS}$  (Fig. 5*B*), which increased monotonically with  $[B]$  (Fig. 2). The mean  $(I_{BS}/I_{B0})/(I_{CS}/I_{C0})$  values for TPentA ( $n = 7$ ) and TBA ( $n = 10$ ) were greater than unity; those for TPA ( $n = 5$ ) were slightly lower than unity. However, individual measurements for TPA revealed three cells in which the normalized plateau/peak ratio was lower than unity and two cells in which the normalized plateau/peak ratio was slightly higher than unity. The  $(I_{BS}/I_{B0})/(I_{CS}/I_{C0})$  values for TEA ( $n = 5$ ) were considerably lower than unity.

Models 1–5 also demonstrate different plateau/peak ratios for the block with respect to the control (Fig. 4*A*). For example, the simulated currents at different blocker concentrations (Fig. 5*A*) indicate that for model 1 the gradual current decay during the agonist application diminishes with an increase in  $[B]$ . The values of the normalized plateau/peak ratio calculated for all models are plotted in Figure 5*C*. Evidently, these values are higher than unity for the models that imply that the blocker prohibits the channel desensitization (models 1, 2, and 4) and slightly lower than unity for the models that predict that the blocker does not prohibit this process (models 3 and 5). Therefore, the reason, why  $I_{BS}/I_{B0} > I_{CS}/I_{C0}$  for models 1, 2, and 4, is the absence of the  $D_{AAB}$  state in which the blocked channels can be gradually accumulated during the agonist and the blocker coapplication. Thus, the greater the gradual decrease in the simulated currents during the agonist and the blocker coapplication for models 3 and 5 in comparison with that of models 1, 2, and 4 (Fig. 4*A*) indicates that in the first case both blocked and nonblocked channels desensitize, whereas in the second case it is only the nonblocked channels that desensitize.

According to the plateau/peak ratio criterion, TPentA and TBA prohibited channel desensitization, whereas TPA did not. In the case of TBA, the reason by which the  $(I_{BS}/I_{B0})/(I_{CS}/I_{C0})$  curve is bent down at high values of  $1 - I_{BS}/I_{CS}$  (Fig. 5*B*) is not clear. Presumably, it can be explained by nonspecific TBA-induced inhibition of NMDA receptors or a comparatively slow TBA-induced blockade of the residual nonselective cation current (Xiong et al., 1997). The fact that in some cells the normalized plateau/peak ratio for TPA is slightly higher than unity indicates that under certain conditions TPA can decrease the probability of NMDA channel desensitization. The plateau/peak ratio criterion is valid at any  $P_0$  (from 0.04 to 0.5) and  $\tau_{wash}$  (from 0 to 300 msec) but only for fast blockers ( $k_2 > 10 \text{ sec}^{-1}$ ), because a high value of



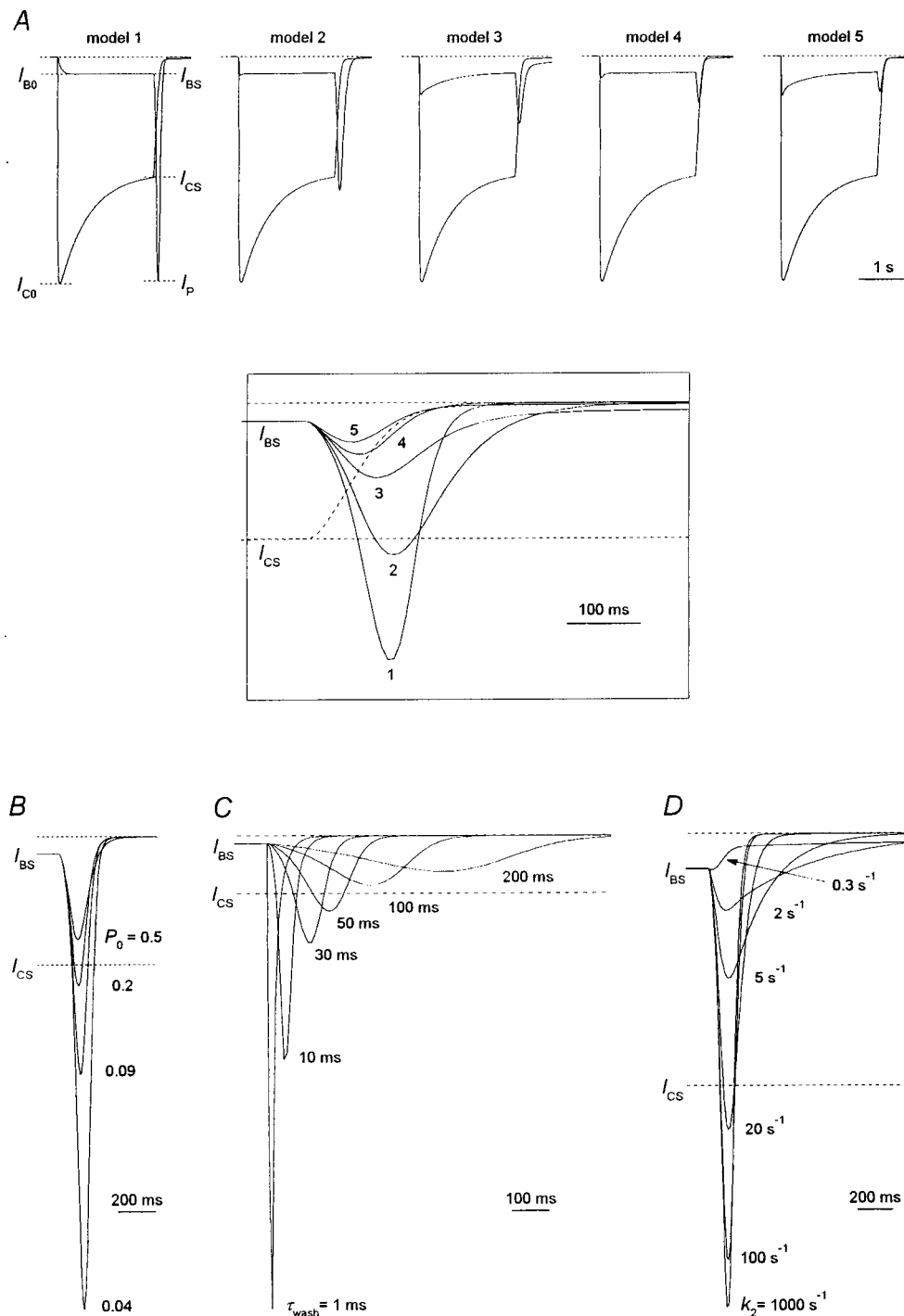


**Figure 4.** Simulated hooked tail currents. *A*, The simulated currents in response to the agonist application are superimposed with simulated currents in response to the agonist coapplication with the blocker. All models 1–5 predict the appearance of the hooked current after termination of the agonist and the blocker coapplication. To obtain the same degree of the stationary current inhibition,  $I_{BS}/I_{CS}$ , we used the blocker concentrations  $[B] = 175$ , 16, 7, 13, and  $6.5 K_d$  for models 1, 2, 3, 4, and 5, respectively. Hereafter (except as noted) the time constant of the solution exchange,  $\tau_{wash} = 30$  msec, the open probability,  $P_0 = 0.09$ , and the kinetic constant of the blocker dissociation,  $k_2 = 1000 \text{ sec}^{-1}$ . *Inset*, The control tail current (*dashed line*) and the hooked tail currents predicted by models 1–5 (*solid lines*) are superimposed. All the models except for model 5 predict the intersection of the control and hooked tail currents. *B*, Hooked tail currents predicted by model 1 at different  $P_0$  values. The hooked currents at  $P_0 = 0.04$ , 0.09, 0.2, and 0.5 were plotted after the stationary levels of the control simulated current at different  $P_0$  values were normalized. The value of  $P_0$  was varied by means of change in the value of the rate constant of the channel opening,  $\beta$ . The degree of the stationary block is the same at different  $P_0$  values.  $\beta = 8.33$ , 20, 50, and  $200 \text{ sec}^{-1}$ ;  $[B] = 413$ , 175, 77, and  $23.5 K_d$  for  $P_0 = 0.04$ , 0.09, 0.2, and 0.5, respectively. *C*, Hooked tail currents predicted by model 1 at different  $\tau_{wash}$  values. The hooked currents at  $\tau_{wash} = 1$ , 10, 30, 50, 100, and 200 msec are presented.  $[B] = 175 K_d$ . *D*, Hooked tail currents predicted by model 1 at different  $k_2$  values. The hooked currents at  $k_2 = 0.3$ , 2, 5, 20, 100, and  $1000 \text{ sec}^{-1}$  ( $k_1 = 1.05$ , 7, 17.5, 70, 350, and  $3500 \text{ mM}^{-1} \cdot \text{sec}^{-1}$ , respectively) are presented.  $[B] = 175 K_d$ .



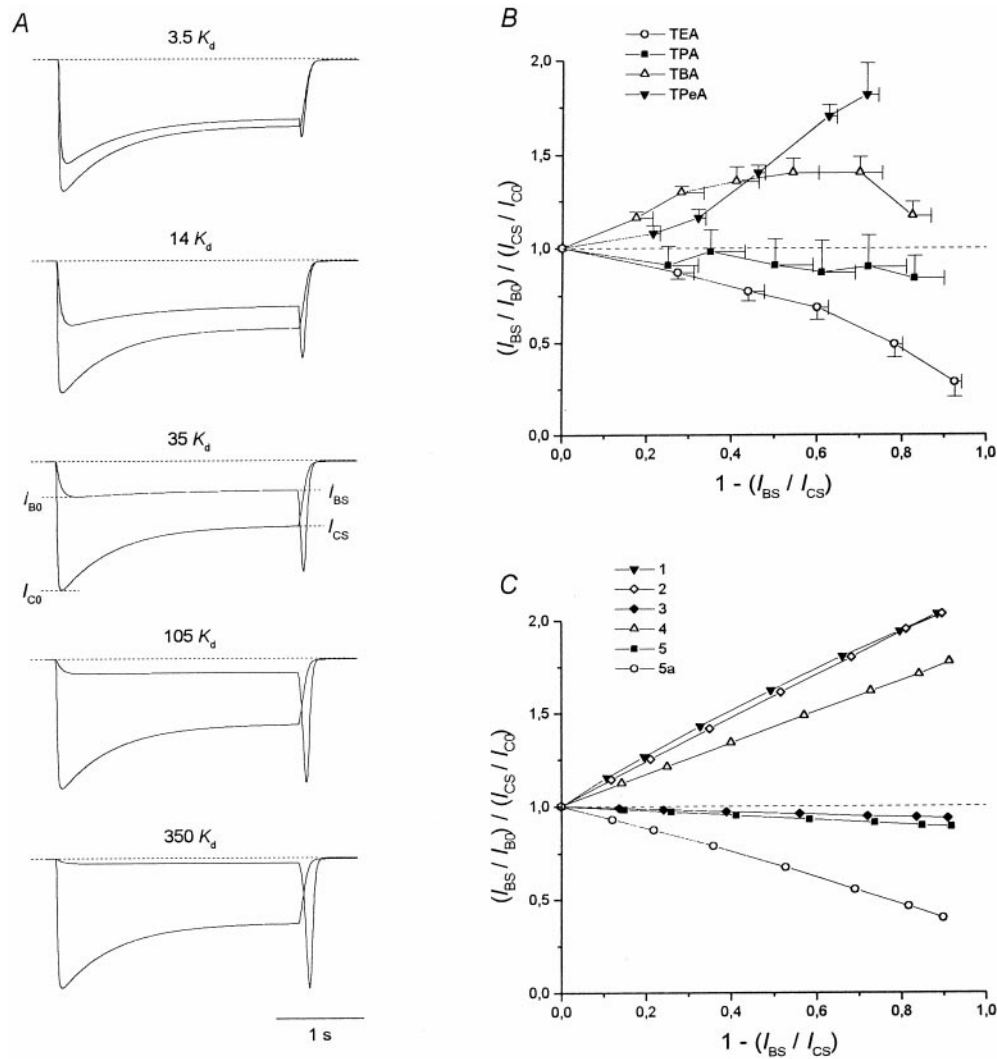
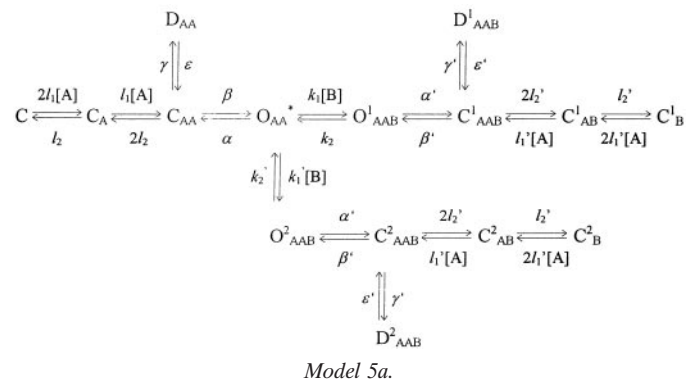


**Figure 5.** Plateau/peak ratio. *A*, The current responses to the agonist application and its coapplication with the blocker at different concentrations ( $[B] = 3.5, 14, 35, 105$ , and  $350 K_d$ ) predicted by model 1 are superimposed. *B*, The experimental values of the plateau/peak ratio normalized to the control,  $(I_{BS}/I_{B0})/(I_{CS}/I_{C0})$ , are plotted against the degree of the stationary current inhibition,  $1 - I_{BS}/I_{CS}$ , for different TAA. *C*,  $(I_{BS}/I_{B0})/(I_{CS}/I_{C0})$  curves predicted by models 1–5 and 5a. Values of parameters for *A* and *C*:  $P_0 = 0.09$ ,  $\tau_{wash} = 30$  msec, and  $k_2 = 1000 \text{ sec}^{-1}$ .

$I_{B0}/I_{BS}$  can be a consequence of the noncomplete initial blockade of the channels because of a slow development of the block.

The  $(I_{BS}/I_{B0})/(I_{CS}/I_{C0})$  curve for TEA proved to be much lower than even those predicted by models 3 and 5 (Fig. 5*B*). This fact can imply (Sobolevsky, 1999) either (1) the existence of a slow blocking kinetics component, or (2) that TEA promotes the channel desensitization by increasing the number of desensitized states or because of a shift of the  $C_{AAB} - D_{AAB}$  equilibrium toward the  $D_{AAB}$  state. To examine the first possibility, model 5 was modified by addition of a new blocking site, site 2 (Model 5a).

Model 5a does not contain any additional assumptions. In this sense, this model is the simplest one. Thus, the properties of site 2 are qualitatively similar to those of site 1. The blocker can bind to site 2 during the channel opening and does not prohibit the subsequent channel closure, desensitization, and agonist dissociation. Sites 1 and 2 cannot be occupied simultaneously, because the amplitude of the fast component in the recovery kinetics for TEA in the continuous presence of ASP does not depend on the blocker concentration (Sobolevsky, 1999, his Fig. 5). The main difference between these two sites is in their respective rates of



blocker association and dissociation. Thus, the value of the dissociation rate constant from the new site 2 was taken to be 250 times lower than  $k_2$ :  $k_2' = 4 \text{ sec}^{-1}$ . The value of the association rate constant was lowered proportionally ( $k_1' = k_1/250 = 0.014 \mu\text{M}^{-1} \cdot \text{sec}^{-1}$ ), so that the value of the microscopic  $K_d = k_2/k_1$  remained the same (0.29 mM). The  $(I_{BS}/I_{B0})/(I_{CS}/I_{C0})$  curve pre-

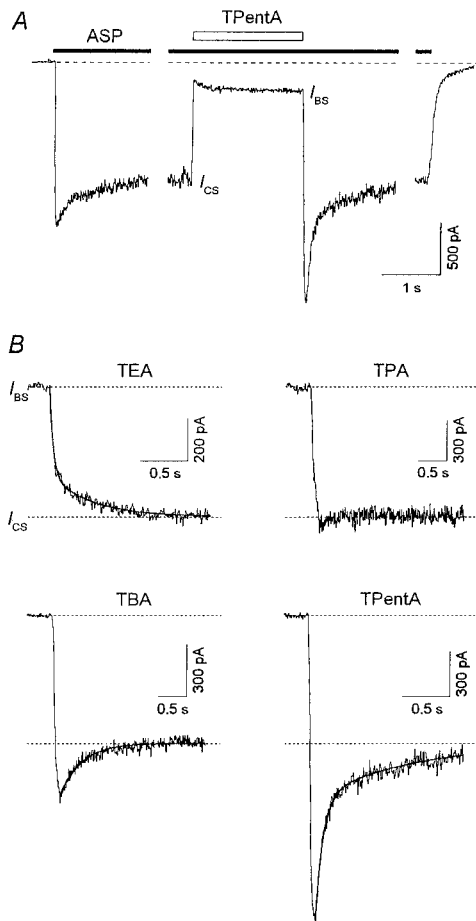


**Figure 6.** The TAA recovery kinetics in the continuous presence of ASP. *A*, The experimental protocol. TPentA (2 mM) was applied for 2 sec in the continuous presence of ASP (100  $\mu$ M) when the inward current gained its stationary level,  $I_{CS}$ . The solution exchange at the termination of TPentA application was fast. *B*, Representative examples of the current recovery after termination of TEA (5 mM), TPA (2 mM), TBA (2 mM), and TPentA (2 mM) application in the continuous presence of ASP. The solid lines are double-exponential fittings of the recovery kinetics in the cases of TEA and TPentA ( $\tau_{fast} = 40$  msec,  $\tau_{slow} = 440$  msec, and  $A_{fast} = 0.68$  for TEA;  $\tau_{fast} = 74$  msec,  $\tau_{slow} = 987$  msec, and  $A_{fast} = 0.68$  for TPentA) and a single-exponential fitting in the case of TBA ( $\tau = 368$  msec).

dicted by model 5a is shown in Figure 5C. At high blocker concentrations, the plateau/peak value becomes much lower than unity in compliance with that observed in the TEA experiment (Fig. 5B). The modifications of model 5 implying that the blocker favored channel desensitization predicted a similar change in  $(I_{BS}/I_{B0})/(I_{CS}/I_{C0})$  curve (data not shown). The criterion that allows one to distinguish these modifications of model 5 from model 5a will be considered below.

### Blocking kinetics in the continuous presence of the agonist

Investigation of the blocking kinetics in the continuous presence of the agonist provides valuable information about the mechanism of the blocker–channel interaction (Sobolevsky and Koshelev, 1998; Sobolevsky, 1999). The experimental protocol is shown in Figure 6A with TPentA as an example. The blocker was applied when the ASP-induced current already reached its stationary level,  $I_{CS}$ . Examples of the recovery kinetics are shown in Figure 6B. The recovery kinetics for all TAA contained a fast

ascending component, which reflected the rapid dissociation of the blocker from the channel (the transition from  $O_{AAB}$  to  $O_{AA}^*$ ); the time constant of this component is mainly determined by the process of the solution exchange (Sobolevsky, 1999).

Along with a fast component ( $\tau_{fast} = 155 \pm 27$  msec;  $n = 8$ ), the recovery kinetics for TEA also contained a slow component with the time constant  $\tau_{slow} = 2.04 \pm 0.34$  sec ( $n = 8$ ). The amplitude of the fast component,  $A_{fast}$ , measured as a relative weight of the fast exponent in the sum of the fast and slow components, was  $0.69 \pm 0.04$  ( $n = 8$ ).

In the case of TPA, the slow component, if existed, was small. The value of  $A_{fast}$  for TPA was either slightly lower ( $n = 4$ ) or slightly higher ( $n = 4$ ; see the example in Fig. 6B) but, on the average, was equal to unity.

In the case of TBA, the fast component was so large that after a rapid increase the current reached a value exceeding considerably the stationary current level. As in the previous study (Koshelev and Khodorov, 1995), the recovery current exceeding the stationary level,  $I_{CS}$ , will be referred to as an “overshoot.” In the majority of experiments with TBA, the fast ascending phase of the overshoot was followed by a slow ( $\tau_{slow} = 389 \pm 38$  msec;  $n = 10$ ) current decrease back to  $I_{CS}$ . However, in three cells for which the solution exchange was comparatively fast ( $\tau_{wash} \leq 10$  msec), the descending phase of the current contained, along with the slow component, also a fast component.

Such a fast component was present in the recovery kinetics for TPentA, which also exhibited an overshoot. Double-exponential fitting of the overshoot descending phase allowed us to determine the time constants of the fast and slow components,  $\tau_{fast} = 54 \pm 7$  msec and  $\tau_{slow} = 596 \pm 85$  msec ( $n = 7$ ), respectively; the amplitude of the fast component,  $A_{fast}$ , is  $0.63 \pm 0.04$  ( $n = 7$ ).

Computer simulation showed (Fig. 7A) that the overshoot in the recovery kinetics is predicted by models 1, 2, and 4 but is not predicted by models 3 and 5. Thus, the recovery kinetics predicted by model 5 contains only a fast component (the involvement of the second component is not justified statistically, Fischer’s test; Korn and Korn, 1974). There is a small slow component in the recovery kinetics predicted by model 3. The fitting of the recovery curve predicted by model 3 gave the values of the time constants,  $\tau_{fast} = 80$  msec and  $\tau_{slow} = 1.2$  sec, and the amplitude of the fast component,  $A_{fast} = 0.93$ . Therefore, the existence of an overshoot is the criterion distinguishing fast NMDA channel blockers that prohibit channel desensitization from those that do not. This criterion is valid at any blocker concentration in the range of the  $P_0$ ,  $\tau_{wash}$ , and  $k_2$  values identified in the legend to Figure 4. According to this criterion, TEA and TPA do not prohibit channel desensitization, whereas TBA and TPentA do. The above-mentioned cases for TPA, when  $A_{fast}$  was somewhat larger than unity can be interpreted as cases when TPA slightly hinders channel desensitization.

Another important conclusion, which clearly follows from the consideration of the recovery kinetics, concerns the effect of the blocker on the NMDA channel closure. Model 1, which is the only one implying that the blocker prohibits the channel closure, predicts the existence of a fast component in the falling phase of an overshoot. Thus, the falling phase of the overshoot predicted by models 2 and 4 contains only a slow component with the time constant,  $\tau_{slow} = 600$  msec. In contrast, the falling phase of the recovery kinetics for model 1, along with a slow component, contains also a fast component. The double-exponential fit of the recovery kinetics illustrated in Figure 7A revealed the time constant and the amplitude of this component:  $\tau_{fast} = 35$  msec;  $A_{fast}$

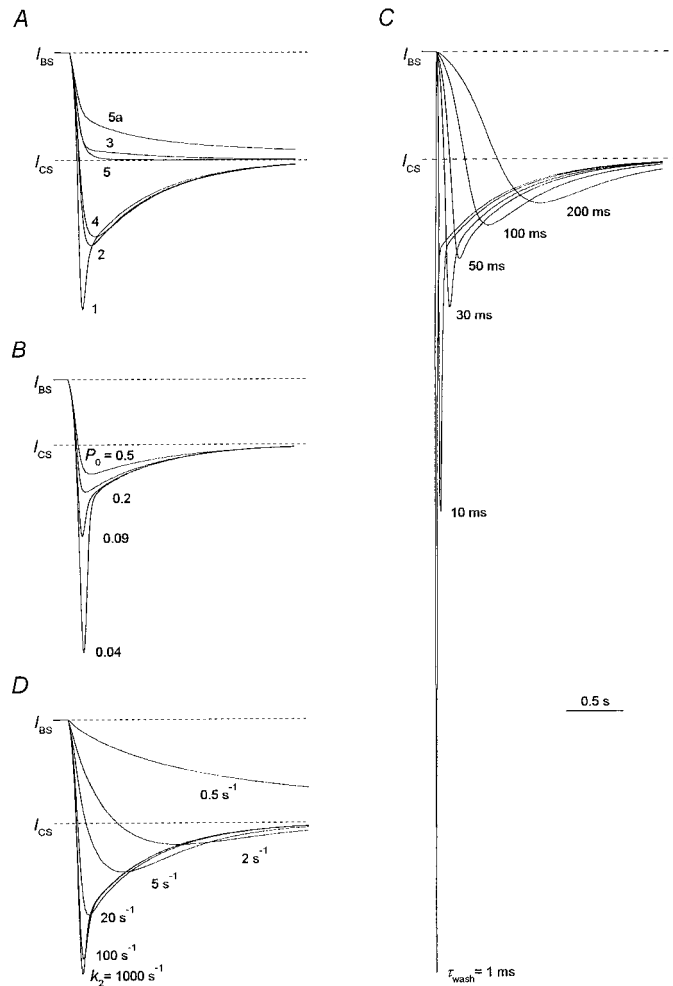


**Figure 7.** Modeling of the recovery kinetics in the continuous presence of the agonist. The values of parameters are the same as listed in the legend to Figure 4. *A*, Recovery kinetics predicted by models 1–5 and 5a. *B*, Recovery kinetics predicted by model 1 at different open probabilities,  $P_0$ . The simulated currents at  $P_0 = 0.04, 0.09, 0.2$ , and  $0.5$  are presented. *C*, Recovery kinetics predicted by model 1 at different time constants of the solution exchange,  $\tau_{\text{wash}}$ . The simulated currents at  $\tau_{\text{wash}} = 1, 10, 30, 50, 100$ , and  $200$  msec are presented. *D*, Recovery kinetics predicted by model 1 at different kinetic constants of the blocker dissociation,  $k_2$ . The simulated currents at  $k_2 = 0.3, 2, 5, 20, 100$ , and  $1000 \text{ sec}^{-1}$  are presented.

$= 0.4$ . Our simulations showed that the slow component of the falling phase reflects channel desensitization (the slow transition from  $C_{AA}$  to  $D_{AA}$ ) and does not depend on the agonist association–dissociation kinetics. The latter conclusion was confirmed by the observation that the time constant of the slow component for the falling phase of the overshoot did not depend on the agonist type. Thus, this time constant was  $394 \pm 65$  msec for ASP and  $377 \pm 32$  msec for NMDA (these values were not significantly different ( $p > 0.7$ ;  $n = 6$ )). The fast component of the falling phase of the overshoot reflects the closure of the unblocked channels (the transition from  $O_{AA}^*$  to  $C_{AA}$ ). The fast component for model 1 appears if the channel closure is slower than the blocker dissociation and is not masked by a more slow solution exchange, i.e.,  $\beta < k_2$  and  $\beta < 1/\tau_{\text{wash}}$ , respectively. These conditions are fulfilled at any blocker concentrations if the channel has a low open probability ( $P_0 < 0.1$ ; Fig. 7*B*), the solution exchange is not very slow ( $\tau_{\text{wash}} < 50$  msec; Fig. 7*C*), and the blocker dissociation

constant is fast enough ( $k_2 > 20 \text{ sec}^{-1}$ ; Fig. 7*D*) (for models 2 and 4 the fast component in the falling phase of an overshoot does not appear at any values of  $P_0$ ,  $\tau_{\text{wash}}$ , and  $k_2$ ).

Therefore, we have considered TPentA as a blocker that prohibits the NMDA channel closure. Our experiments with TBA, in which the value of  $\tau_{\text{wash}}$  was comparatively low ( $\leq 10$  msec), and the falling phase of the recovery kinetics contained the fast component may imply that TBA at least hampers the channel closure if not prohibits it. The appearance of the fast component in the falling phase of the recovery kinetics for TPentA and TBA was that reason, which forced us to adopt the value of the open probability,  $P_0$ , to be rather low (0.09).

The experimental value of  $A_{\text{fast}}$  for TEA ( $0.69 \pm 0.04$ ) was noticeably lower than the values predicted by models 3 (0.93) and 5 (1.00). The recovery kinetics predicted by model 5a is shown in Figure 7*A*. The value of  $A_{\text{fast}}$  (0.67) is close to that observed in the experiment with TEA. As in the case of the plateau/peak criterion, we also examined the modifications of model 5, implying that the blocker promotes channel desensitization (see above). These modifications provide similar changes in the recovery kinetics as those predicted by model 5a (data not shown). Only the following criterion allows one to restrict the choice of model 5 modification, satisfactorily describing the blocking effect of TEA.

#### Dependence of the stationary current inhibition on the agonist concentration

Tetraalkylammonium compounds demonstrated different dependencies for the degree of the stationary current inhibition,  $1 - I_{\text{BS}}/I_{\text{CS}}$ , on the agonist concentration. The superposition of the currents elicited by ASP application and its coapplication with TPentA (1 mM) at different ASP concentrations is shown in Figure 8*A*. As seen, the degree of TPentA-induced stationary current inhibition increases with ASP concentration. The mean values of  $1 - I_{\text{BS}}/I_{\text{CS}}$  for TEA (2 mM), TPA (1 mM), TBA (0.15 mM), and TPentA (1 mM) depending on ASP concentration are shown in Figure 8*B*. The degree of the stationary current inhibition did not depend on the agonist concentration for TEA (the mean values were not significantly different,  $p > 0.9$ ;  $n = 7$ ) and TPA (the mean values were not significantly different,  $p > 0.3$ ;  $n = 6$ ). In the case of TBA,  $1 - I_{\text{BS}}/I_{\text{CS}}$  decreased (the mean  $1 - I_{\text{BS}}/I_{\text{CS}}$  values were significantly different,  $p < 0.003$ ;  $n = 5$ ), whereas in the case of TPentA it rose with the agonist concentration (the mean  $1 - I_{\text{BS}}/I_{\text{CS}}$  values were significantly different,  $p < 10^{-6}$ ;  $n = 6$ ).

Models 1–5 also predicted qualitatively different agonist dependencies (Fig. 9).  $1 - I_{\text{BS}}/I_{\text{CS}}$  for models 1–3 increased with the agonist concentration. The corresponding agonist dependencies coincided at the blocker concentration,  $[B] = 28, 2.6$ , and  $1.1 K_d$  for models 1, 2, and 3, respectively, and were well fitted with the following logistic equation:

$$1 - \frac{I_{\text{BS}}}{I_{\text{CS}}} = \frac{A_1 - A_2}{1 + ([A]/[A]_0)^{n_{\text{Hill}}}} + A_2. \quad (2)$$

The values of parameters were as follows:  $A_1 = 0$ ,  $A_2 = 0.515 \pm 0.002$ ,  $[A]_0 = 8.18 \pm 0.15 \mu\text{M}$ , and  $n_{\text{Hill}} = 1.39 \pm 0.04$ . On the contrary, the  $1 - I_{\text{BS}}/I_{\text{CS}}$  value for model 4 decreased with the agonist concentration. The corresponding agonist dependence at  $[B] = 2.5 K_d$  was well fitted with Equation 2 at  $A_1 = 0.733 \pm 0.003$ ,  $A_2 = 0.515 \pm 0.001$ ,  $[A]_0 = 17.9 \pm 0.6 \mu\text{M}$ , and  $n_{\text{Hill}} = 1.13 \pm 0.03$ . The degree of the stationary current inhibition for model 5 did not depend on the agonist concentration and was equal to 0.515

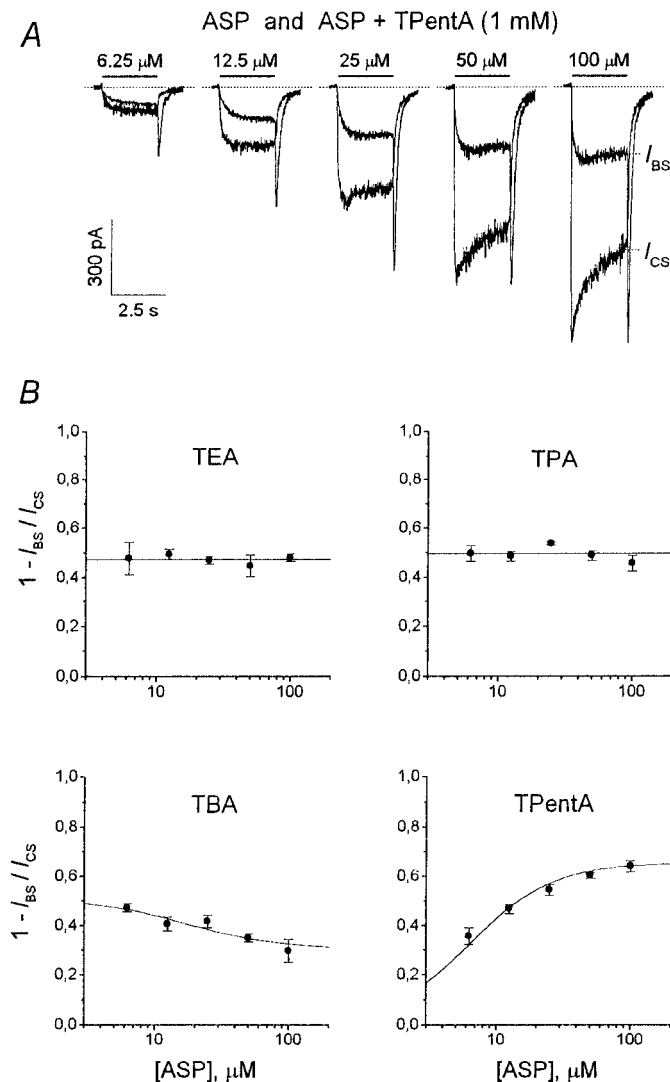


**Figure 8.** Experimental dependence of the stationary current inhibition on the agonist concentration. *A*, Example of experimental curves. ASP alone and together with 1 mM TPentA was applied for 2.5 sec at concentrations of 6.25, 12.5, 25, 50, and 100  $\mu\text{M}$ . The superposition of the control and blocked currents at each ASP concentration is shown. *B*, The mean values of the degree of the stationary current inhibition,  $1 - I_{BS}/I_{CS}$ , for tetraalkylammonium compounds were plotted against the ASP concentration. The  $1 - I_{BS}/I_{CS}$  values for TEA (2 mM) and TPA (1 mM) were not significantly different at different ASP concentrations. The mean  $1 - I_{BS}/I_{CS}$  values for TEA ( $0.47 \pm 0.02$ ;  $n = 7$ ) and TPA ( $0.50 \pm 0.01$ ;  $n = 4$ ) are represented by horizontal lines and correspond to the agonist dependence predicted by model 5 at  $[B] = 0.91$  and  $0.98 K_d$ , respectively. The  $1 - I_{BS}/I_{CS}$  values for TBA (0.15 mM) and TPentA (1 mM) were significantly different at different ASP concentrations. The degree of the stationary current inhibition decreased with the ASP concentration for TBA ( $n = 8$ ) and increased for TPentA ( $n = 6$ ). The solid lines are the predictions of model 4 at  $[B] = 1.02 K_d$  for TBA and model 1 at  $[B] = 51 K_d$  for TPentA (see Results).

at  $[B] = 1.1 K_d$ . Therefore, the models that imply that the agonist cannot dissociate from the blocked channel (models 1–3) predict an increasing degree of block with increasing agonist concentration, whereas the models that imply that the blocker does not prevent the agonist dissociation predict a decreasing degree of block with increasing agonist concentration (model 4) or no dependence of the degree of block on agonist concentration at all (model 5). The agonist dependence criterion is valid at any values

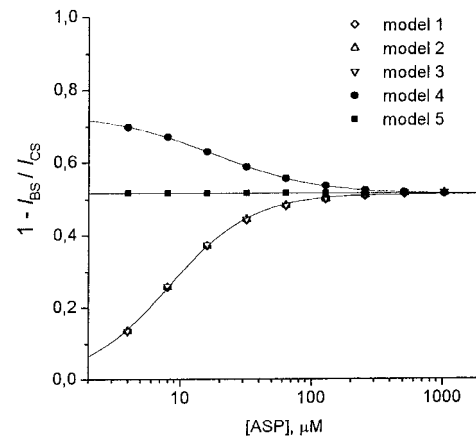


**Figure 9.** Agonist dependencies of the stationary current inhibition predicted by models 1–5. The degree of the stationary current inhibition,  $1 - I_{BS}/I_{CS}$ , rises with the agonist concentration for models 1–3, decreases for model 4, and is constant for model 5. The agonist dependencies predicted by models 1, 2, and 3 coincided at  $[B] = 28$ , 2.6, and  $1.1 K_d$ , respectively, and were well fitted with Equation 2 (solid line). The values of the fitting parameters were as follows:  $A_1 = 0$ ,  $A_2 = 0.515 \pm 0.002$ ,  $[A]_0 = 8.18 \pm 0.15 \mu\text{M}$ , and  $n_{Hill} = 1.39 \pm 0.04$ . The fitting of the agonist dependence predicted by model 4 at  $[B] = 2.5 K_d$  (solid line) gave the following values of the fitting parameters:  $A_1 = 0.733 \pm 0.003$ ,  $A_2 = 0.515 \pm 0.001$ ,  $[A]_0 = 17.9 \pm 0.6 \mu\text{M}$ , and  $n_{Hill} = 1.13 \pm 0.03$ . The degree of the stationary current inhibition for model 5 did not depend on the agonist concentration and was equal to 0.515 at  $[B] = 1.1 K_d$ . The values of parameters were as follows:  $P_0 = 0.09$ ,  $\tau_{wash} = 30$  msec, and  $k_2 = 1000 \text{ sec}^{-1}$ .

of  $[B]$  in the range of the  $P_0$ ,  $\tau_{wash}$ , and  $k_2$  values identified in the Figure 4 legend. By this criterion, the action of TAA must be described by one of models 1–3 in the case of TPentA, by model 4 in the case of TBA, and by model 5 in the cases of TPA and TEA. The corresponding simulated agonist dependencies for TEA, TPA, TBA, and TPentA are shown in Figure 8*B* by solid lines at  $[B] = 0.91 K_d$  (model 5),  $0.98 K_d$  (model 5),  $1.02 K_d$  (model 4), and  $51 K_d$  (model 1), respectively. The fitting parameters for TBA (model 4) and TPentA (model 1) were as follows:  $A_1 = 0.518 \pm 0.002$ ,  $A_2 = 0.304 \pm 0.001$ ,  $[A]_0 = 15.9 \pm 0.3 \mu\text{M}$ , and  $n_{Hill} = 1.18 \pm 0.02$  for TBA and  $A_1 = 0$ ,  $A_2 = 0.655 \pm 0.003$ ,  $[A]_0 = 6.46 \pm 0.10 \mu\text{M}$ , and  $n_{Hill} = 1.42 \pm 0.04$  for TPentA. The agonist dependence criterion is sensitive to the blocker effect on desensitization. Thus, model 5, implying that the blocker does not affect channel desensitization, demonstrates the absence of the agonist dependence, although the same model without a desensitized blocked state (model 4), implying that the blocker prohibits the channel desensitization, predicts that the degree of the stationary current inhibition diminishes with the agonist concentration. Correspondingly, all the modifications of model 5, implying that the blocker promotes channel desensitization predict an increasing agonist dependence (data not shown). In contrast, model 5a, implying the existence of two blocking sites, demonstrates the absence of the agonist dependence as in the case of the nonmodified symmetric model 5. Therefore, modifications of model 5, implying that the blocker promotes channel desensitization, cannot describe the TEA action, for which the fraction of the stationary current inhibition did not depend on ASP concentration (Fig. 8*B*). However, it can be well described by model 5a with two binding sites that cannot be occupied simultaneously by two different TEA molecules and differing by the rates of the blocker binding to and dissociation from them. A variety of two-site model modifications could be also offered to describe the



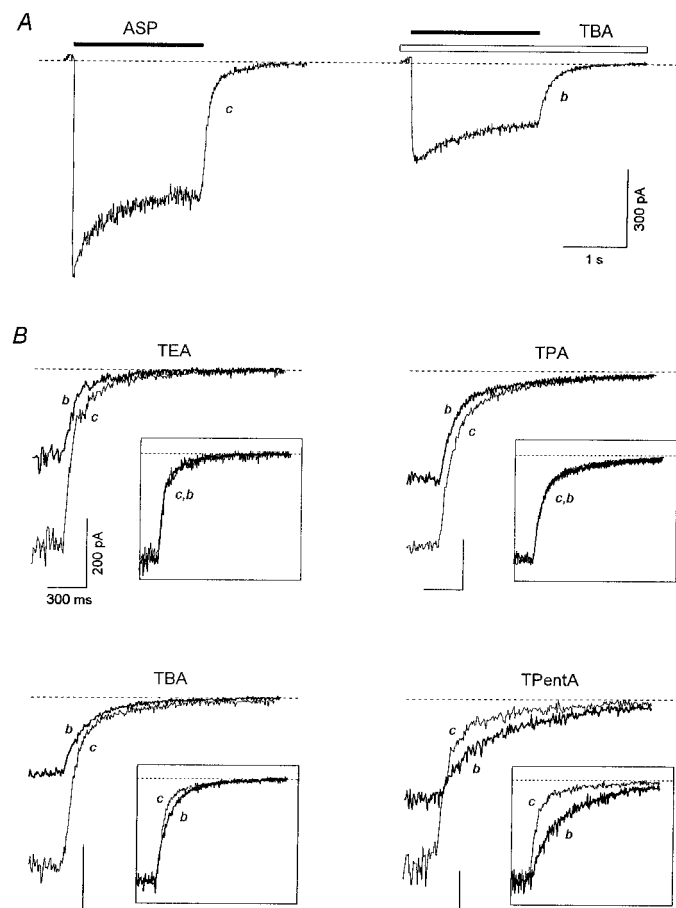


**Figure 10.** Effects of the continuous presence of the blocker on tail currents. *A*, Experimental protocol with TBA as an example. ASP (100  $\mu$ M) was applied for 2 sec in the control external solution or in the continuous presence of 1 mM TBA. *B*, The control tail currents (*c*) are superimposed with the tail currents in the continuous presence of TEA (2 mM), TPA (0.6 mM), TBA (1 mM), and TPentA (0.5 mM) (*b*). The same labels apply to all calibrations. *Insets*, Superposition of the normalized curves *c* and *b*.

effects of TEA. Thus, the consequence of occupation of the sites could be different (Sobolevsky, 1999): (1) any site can be available from the external media, but the blocking molecule bound to one of them cannot “jump” to the other; (2) only one site can be available from the external medium, and the second site can be occupied via a sequential jump of the blocker molecule from the first site; and (3) both sites are available from the external medium, and the blocker bound to one of them can jump to the other. A much greater number of two binding site models could be obtained by possible variations of the kinetic constants. Analysis of such a huge variety of two binding site models was not the aim of the present study, and here we will not develop this topic any more. The only clear conclusion that can be made from the consideration of model 5a is the existence of a fast-occupied TEA blocking site in the NMDA channel, the blocker molecule binding to which does not prevent the channel closure, desensitization, and agonist dissociation.

Another important criterion for the effect of the blocker on agonist dissociation is the kinetics of tail currents after termination of the agonist application in the continuous presence of the blocker. This criterion is not sensitive to the effect of the blocker on channel desensitization.

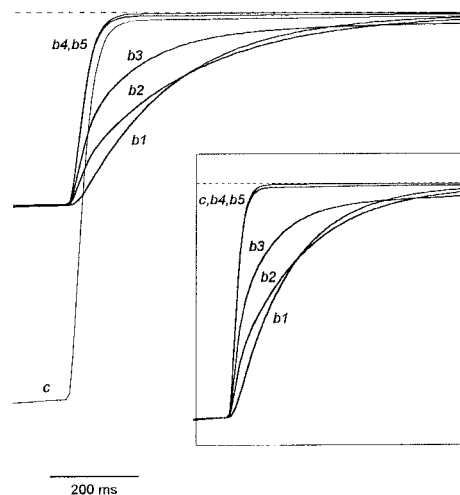


**Figure 11.** Tail currents in the continuous presence of the blocker predicted by models 1–5. The experimental protocol is the same as shown in Figure 10*A*. The control tail current (*c*) is superimposed with the tail currents in the continuous presence of the blocker for models 1–5 (curves *b1*–*b5*, respectively). Curves *b1*–*b3* intersect with curve *c*, whereas curves *b4* and *b5* do not. To achieve the same degree of the stationary current inhibition, the blocker concentration was different for different models:  $[B] = 28, 2.55, 1.09, 2.07$ , and  $0.98 K_d$  for models 1, 2, 3, 4, and 5, respectively. The values of the parameters are as follows:  $P_0 = 0.09$ ,  $\tau_{wash} = 30$  msec, and  $k_2 = 1000$  sec $^{-1}$ . *Inset*, Normalized curves *c* and *b1*–*b5*. The control tail current (curve *c*) and the normalized tail currents in the continuous presence of the blocker predicted by models 4 and 5 (curves *b4* and *b5*) practically coincide.

### Tail currents in the continuous presence of the blocker

In contrast to the agonist and the blocker coapplication (Fig. 2), the application of ASP in the continuous presence of the blocker was not followed by the hooked current, as illustrated in Figure 10*A* with TBA (1 mM). The kinetics of the tail current after ASP application in the continuous presence of the blocker (*b*) was different in comparison with that of the control (*c*) for different blockers (Fig. 10*B*). Such blockers as TEA and TPA did not affect the tail current kinetics: the *b* decay was practically identical to the *c* decay. This fact is clearly illustrated in the *insets*, where the normalized *c* and *b* curves are superimposed. In contrast, TPentA caused a pronounced delay in the current recovery kinetics, which is manifested in the intersection of curves *c* and *b*. Such an intersection was never observed in the case of TBA: curves *c* and *b* were tangent, or curve *b* was clearly below curve *c* (Fig. 10*B*). However, there was a small delay in the recovery kinetics, which can be revealed only after superposition of the normalized tail currents (Fig. 10*B*, *inset*). In the majority of cells ( $n = 14$  of 16), the normalized curve *c* was below the normalized curve *b*, but in 2 of 16 cells these curves coincided.

Computer simulation clarified the origin of all these effects. Figure 11 shows that the time course of the tail current in the continuous presence of the blocker predicted by models 4 and 5 is very similar to the control tail current: the nonnormalized curves *b4* and *b5* do not intersect with the control curve *c*, whereas the normalized curves *b4* and *b5* coincide with curve *c* (see *inset*). In contrast, intersection of curves *b1*, *b2*, and *b3* with curve *c* points to a considerable blocker-induced delay in the tail current kinetics predicted by models 1, 2, and 3, respectively. The common feature of these three different models (1–3) is that they exclude the agonist dissociation from the blocked channel. Thus, it is just the trapping of the agonist in the blocked channel that is responsible

**Table 2. Criteria attributing the blocker effect to one of the kinetic models**

Model	Intersection of the control tail current and the tail current after the agonist and the blocker co-application (Fig. 4A, inset)	Channel desensitization criteria			Agonist dissociation criteria		
		The normalized plateau/peak ratio ( $I_{BS}/I_{B0}$ )/( $I_{CS}/I_{C0}$ ) > 1 (Fig. 5C)	The recovery current overshoot in the continuous presence of the agonist (Fig. 7A)	Channel closure criterion, fast component in the falling phase of the overshoot (Fig. 7A)	Agonist dependence (Fig. 9)	Intersection of the control tail current with the tail current in the continuous presence of the blocker (Fig. 11)	Examples of the blockers
1	+	+	+	+	Increasing	+	TPentA
2	+	+	+	–	Increasing	+	–
3	+	–	–	–	Increasing	+	–
4	+	+	+	–	Decreasing	–	TBA
5	–	–	–	–	Constant	–	TPA
5a	–	–	–	–	Constant	–	TEA

for the delay in the final channel closure in the presence of the blocker in the washout solution. The criterion of the tail currents in the continuous presence of the blocker is valid at any values of  $P_0$  (from 0.04 to 0.5),  $\tau_{wash}$  (from 0 to 300 msec), and  $[B]$  and  $k_2 > 0.3 \mu\text{M}/\text{sec}$ . According to this criterion, TEA, TPA, and TBA, do not prohibit the agonist dissociation, whereas TPentA does.

The criterion under consideration can also be named as a criterion of the blocker-induced prolongation of NMDA channel activation. Thus, the blocker prohibiting the agonist dissociation induces prolongation of NMDA channel activation. If during such prolongation we accelerate the channel transition from the blocked state,  $O_{AAB}$ , to the nonblocked state,  $O_{AA}^*$  (models 1–3), a large-amplitude tail current will be generated. Such acceleration was achieved in the experiments with 9-aminoacridine by termination of the blocker application (Benveniste and Mayer, 1995; Koshelev, 1995) or membrane depolarization (Benveniste and Mayer, 1995). In the latter case, the large-amplitude tail current had an outward direction. Our computer experiments showed that the amplitude of such tail currents increases with the blocker concentration (when the occupation of the blocked states increases) and a decrease in the time between the termination of the agonist application and the accelerating stimulus, whereas their kinetics is mainly defined by the rate constant of the blocker dissociation,  $k_2$  (data not shown).

### Consideration of TAA action according to a set of criteria

Based on consideration of models 1–5, the present study reveals a set of criteria that allow one to determine the effect of fast blockers on the channel closure, desensitization, and agonist binding (dissociation). These criteria are listed in Table 2.

According to criteria listed in Table 2 and taking into account everything mentioned above, TEA action can be described by model 5a with two blocking sites, to which two blocker molecules cannot bind simultaneously. To explain the inability of the simultaneous occupancy, these sites can be supposed to overlap or to be located so close that electrostatic repulsion does not allow two TEA molecules to bind to them simultaneously (Sobolevsky, 1999). The binding of the TEA molecule to the fast occupied site (the main site, because  $A_{fast} = 0.67$ ) does not prohibit the channel closure, desensitization, and agonist dissociation from the blocked channel. Elucidation of the properties of the second, slowly occupied TEA blocking site requires further experiment.

The effect of TPA can be best described by model 5. Therefore,

we may conclude that TPA does not prohibit the channel closure, desensitization, and agonist dissociation from the blocked channel. The cases when the  $A_{fast}$  and  $(I_{BS}/I_{B0})/(I_{CS}/I_{C0})$  values were slightly higher than unity gave us the reason to suppose that TPA can slightly prevent NMDA channel desensitization.

TPentA action can be well described by model 1. According to this model, TPentA prohibits both the channel closure and desensitization and the agonist dissociation from the blocked channel.

According to the set of criteria listed in Table 2, TBA action should rather be described by model 4. However, some observations point to the necessity of its modification. These observations are as follows: (1) in contrast with the prediction of model 4 with  $\alpha' = \alpha$ ,  $\beta' = \beta$ ,  $l_2' = l_2$ , and  $l_1' = l_1$  (see Fig. 4A), in the majority of experiments the hooked current exceeded the value of the stationary control current,  $I_{CS}$  (see Fig. 2); (2) at low values of the time constant of the solution exchange,  $\tau_{wash} \leq 10$  msec, the fast component appeared in the falling phase of the recovery kinetics of TBA in the continuous presence of ASP; (3) in accordance with modeling prediction (Fig. 11), the control tail current and the nonnormalized blocked tail current in the continuous presence of TBA did not intersect (Fig. 10B). However, in the majority of experiments the normalized blocked tail current lay above the control tail current (Fig. 10B, inset); this circumstance is in obvious contradiction with model 4, which predicted their coincidence (Fig. 11, inset).

In principle, modification of model 4 can be fulfilled by means of changes in the closure–opening transition ( $O_{AAB}$ – $C_{AAB}$ ) or the agonist binding–dissociation transitions ( $C_{AAB}$ – $C_{AB}$ – $C_B$ ). When we modified model 4 via changes in the agonist binding–dissociation transitions, in compliance with the three facts listed above, we were forced to predict that the blocker hampered the agonist dissociation from the closed blocked channel. Such a modification did not predict the fast component in the falling phase of the recovery kinetics in the continuous presence of the agonist (similar to model 2) and considerably changed the agonist dependence of the stationary block by transforming it from the “descending type” predicted by the nonmodified model 4 (Fig. 9) to the “ascending” one similar to the agonist dependencies predicted by models 1–3. However, in the cases when the solution exchange was comparatively fast, the descending phase of the TBA recovery kinetics contained the fast component (see above), and the agonist dependence observed experimentally was de-



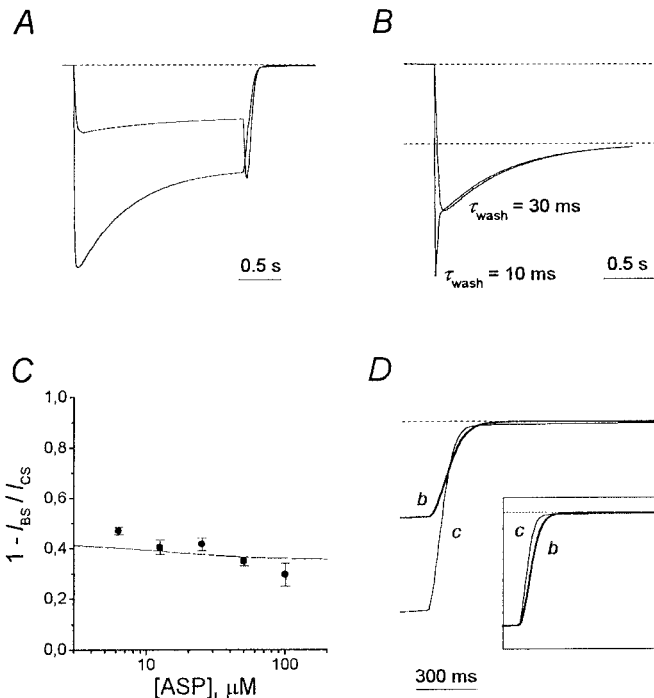


**Figure 12.** Predictions of model 4, implying that the blocker slows the channel closure. The open probability for the nonblocked channel (the  $C_{AA}-O_{AA}$  transition),  $P_{0,} = \beta/(\alpha + \beta) = 0.09$ , whereas the open probability for the blocked channel (the  $C_{AAB}-O_{AAB}$  transition),  $P_{0'} = \beta/(\alpha' + \beta) = 0.5$ . The blocker concentration for *A*, *B*, and *D*,  $[B]_0 = 12.3 K_d$ . The values of parameters, except as noted specially, are as follows:  $P_0 = 0.09$ ,  $\tau_{wash} = 30$  msec, and  $k_2 = 1000 \text{ sec}^{-1}$ . *A*, The hooked current exceeds the level of the stationary control current,  $I_{CS}$ . *B*, The falling phase of the recovery kinetics in the continuous presence of the agonist contains only one visible component when  $\tau_{wash} = 30$  msec and two components when  $\tau_{wash} = 10$  msec. *C*, Agonist dependence. The value of the stationary current inhibition,  $1 - I_{BS}/I_{CS}$  (solid line), decreased with the agonist concentration. This curve is the fitting of the modeling data ( $[B] = 7.18 K_d$ ) with Equation 2. The values of the fitting parameters are as follows:  $A_1 = 0.423 \pm 0.001$ ,  $A_2 = 0.357 \pm 0.001$ ,  $[A]_0 = 13.0 \pm 0.6 \mu\text{M}$ , and  $n_{Hill} = 1.19 \pm 0.04$ . The solid circles are the experimental data for TBA. *D*, The tail current in the continuous presence of the blocker (*b*) does not lie below the control tail current (*c*), as was the case with the nonmodified model 4 (see Fig. 11), but slightly intersects it. The blocker-induced delay in the tail current kinetics becomes clear when curves *c* and *b* are normalized (*inset*).

scending (Fig. 8*B*). Therefore, the only possibility to modify model 4 to simulate the experimental observations was to correct the  $O_{AAB}-C_{AAB}$  transition, implying that the blocker increased the open probability of the blocked channel. There are two ways to increase the open probability. The first one is to increase the kinetic constant of the channel opening,  $\beta'$ . In this case, the blocker promotes the channel opening. The second one consists in reducing the rate constant of the channel closure,  $\alpha'$ . In this case, the blocker slows the channel closure. This case is especially natural because the larger tetraalkylammonium compound, TPentA, was found to prohibit the channel closure. Both cases stipulate similar changes in the modeling kinetics. An example of predictions of model 4, implying that the blocker slows the channel closure, is shown in Figure 12. The kinetic constant of the channel opening,  $\beta$ , was assumed to be the same ( $20 \text{ sec}^{-1}$ ) for a blocked and a nonblocked channel. In contrast, the value of the closure rate constant for the blocked channel was assumed to be 10 times lower ( $\alpha' = 20 \text{ sec}^{-1}$ ) than that for the nonblocked

channel ( $\alpha = 200 \text{ sec}^{-1}$ ). Thus, the open probability of the blocked channel (0.5) proved to be greater than the open probability of the nonblocked channel (0.09). Such a modified model 4 predicts the appearance of the hooked current exceeding the stationary level of the control current (Fig. 12*A*), as well as the appearance of the fast component in the falling phase of the recovery kinetics in the continuous presence of the agonist at high values of  $\tau_{wash}$  and in its absence at low values of  $\tau_{wash}$  (Fig. 12*B*). The agonist dependence of this modified model 4 remained descending as for the nonmodified model 4 (Fig. 12*C*). Such a descending agonist dependence is the main reason why TBA action cannot be described, for example, by modified model 5, because any modification of model 5 assuming that the blocker increases the open probability for the blocked channel predicts the ascending agonist dependence (which is intermediate between those predicted by models 1 and 5). The tail current in the continuous presence of the blocker was delayed so that it even slightly intersected the control tail current (Fig. 12*D*). The fact that the normalized tail current in the continuous presence of the blocker for the modified model 4 lies below the control tail current is obvious from Figure 12*D*, *inset*. Therefore, the modified model 4 is able to simulate all the major features of the TBA-induced kinetics and the stationary parameter behavior. From this we may conclude that TBA allows the agonist dissociation from the blocked channel but prohibits the channel desensitization and partly inhibits the channel closure.

Therefore, the blocking action of TAA can be described by models 1, 4, and 5 (modified when necessary). This finding raises the question, are models 2 and 3 realistic, or can the blocker permit channel closure but not the agonist dissociation? Thus, Benveniste and Mayer (1995) supposed that the open state should manifest increased affinity for agonist. The best answer to this question would be to give an example of the blocker that would satisfy the criteria for models 2 and 3. However, we did not find such an example. The positive answer to this question would mean the existence of additional allosteric interaction between the blocker binding site and the agonist receptor. In our opinion, the existence of such a complex additional mechanism in the NMDA channel is doubtful.

## DISCUSSION

Summarizing the results of the comparative analysis of interaction of different TAA with open NMDA channels, we may conclude that (1) there are blockers that prohibit (TPentA), partly prevent (TBA), or do not prevent (TPA and TEA) either the channel closure or the agonist dissociation; and (2) there are blockers that prohibit (TPentA and TBA), slightly prevent (TPA), or do not prevent (TEA) the channel desensitization. The first conclusion confirms the existence of an NMDA channel activation gate postulated previously. The second conclusion speaks well for the earlier hypothesis about the existence of a desensitization gate in the NMDA channel (Koshelev and Khodorov, 1992). The existence of a blocker that prohibits channel desensitization but does not prohibit the channel closure (TBA) provides clear evidence that there are two functionally and spatially different NMDA channel structures responsible for the activation and desensitization processes.

The mechanism of the blocker action affects its apparent affinity to NMDA channels. The apparent affinity can be measured by the values of  $1/IC_{50}$  or  $1/K_{0.5}(0)$  at 0 mV (Table 1). A decrease in  $K_{0.5}(0)$  with the lengthening of the alkyl chains can be explained by a gain in the energy of hydrophobic interactions of

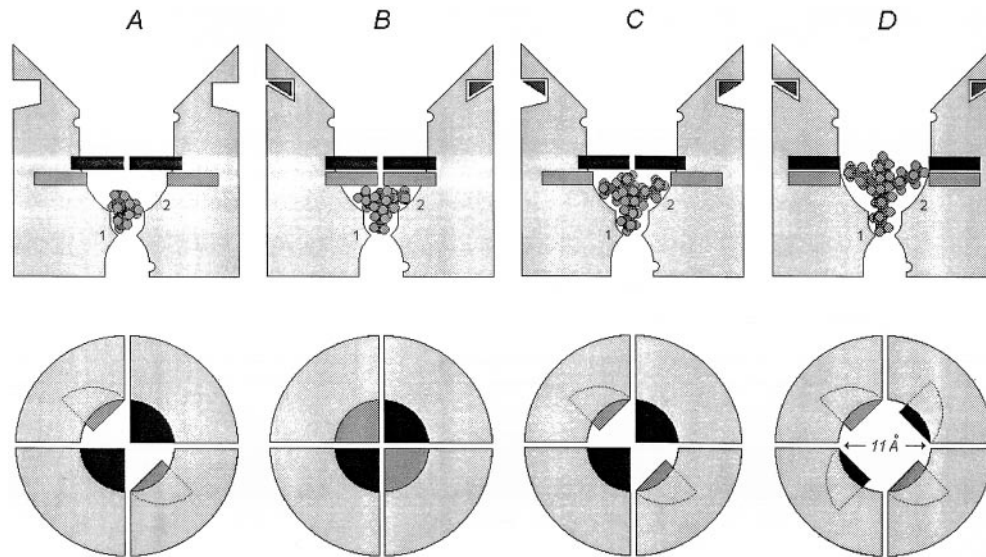


**Figure 13.** Hypothetical schematic representation of the NMDA channel pore region illustrating the interaction of TAA with the gating machinery. *First line*, Side view. The narrowest part of the pore is the selectivity filter. The blocking sites are indicated by 1 and 2. The binding sites for permeant ions (one in the intracellular vestibule and two in the extracellular vestibule) are indicated by open semicircles. The activation gate is black, whereas the desensitization gate is gray. TEA and TPA permit the closure of both activation and desensitization gates; TBA prohibits the closure of the desensitization gate but permits the closure of the activation gate; and TPentA prohibits the closure of both activation and desensitization gates. Different blocked states of the NMDA channel are illustrated with different TAA. *A*, TEA is bound to the channel in the closed, agonist-unbound state ( $C_B$ ). *B*, TPA is bound to the channel in the desensitized state ( $D_{AAB}$ ). *C*, TBA is bound to the channel in the closed, agonist-bound state ( $C_{AAB}$ ). *D*, TPentA is bound to the channel in the open state ( $O_{AAB}$ ). *Second line*, The above view illustrates the positions of the activation (black) and desensitization (gray) gates in different states of the channel. The four segments symbolize the four NMDA receptor channel-forming subunits.

TAA with the NMDA channel, which affects the microscopic  $K_d = k_2/k_1$ . However, the difference between the  $K_d$  values for some blockers is considerably greater than that between the corresponding  $IC_{50}$  [ $K_{0.5}(0)$ ] values, because the latter depends on the mechanism of the blocker action, and  $IC_{50}/K_d$  increases from TEA to TPentA. Thus, although models 5a for TEA and 5 for TPA predict  $IC_{50}/K_d = 1$ , the modified model 4 for TBA predicts  $IC_{50}/K_d = 12.7$ , and model 1 for TPentA predicts  $IC_{50}/K_d = 29.1$ .

The size of the blocking molecules that prohibit the closure or desensitization is larger than the size of the blockers that only partly prevent these processes and considerably larger than the size of the blockers that do not prevent the closure or desensitization. This fact supports the earlier proposed hypothesis (Koshlev and Khodorov, 1994) that the size of the blocker plays a critical role in its interaction with the gating machinery of the NMDA channel and provides evidence that the gating is local and cannot be, for example, the whole pore pinch or a twist (Hille, 1992). Based on the present notion that NMDA channel is a pore with a small cytoplasmic vestibule and a large extracellular vestibule that contains a narrow region extending  $\sim 6$  Å outward from the selectivity filter with a cross-sectional area of  $22\text{--}26$  Å<sup>2</sup> (Villarroel et al., 1995; Zarei and Dani, 1995), we tried to represent schematically the pore region with two blocking sites (Sobolevsky and Koshlev, 1998; Sobolevsky, 1999) and binding sites for permeant ions (Antonov et al., 1998) (Fig. 13).

In Figure 13 the positively charged nitrogens of TAA at the blocking positions are shown to be located slightly deeper for small TAA than for large ones. Nevertheless, the difference in the measured  $\delta$  for TAA is great (0.90 for TEA and 0.29 for TPentA; see Table 1). Although the Woodhull model can be too rough for the description of the NMDA open-channel block because of possible excessive "ionic pressure" in the narrow part of the pore (Ruppersberg et al., 1994), the effect of permeant cations (An-

tonov et al., 1998), or possible surface charge effects of TAA on the local electric field (Zarei and Dani, 1994), such a great difference in  $\delta$  not only supports the notion represented in Figure 13 when the smaller blocker can penetrate deeper into the NMDA channel pore than the larger blocker but also confirms the suggestion that the electric field in NMDA channel is far from being uniform and is concentrated near the blocking sites and the selectivity filter (Subramaniam et al., 1994; Antonov et al., 1998).

In Figure 13 the two different structures responsible for channel activation and desensitization are represented as activation and desensitization gates located in the external vestibule of the NMDA channel pore. This representation is in obvious contradiction with the conclusion made by Beck et al. (1999), who stated that the extracellular vestibule does not contain any channel gate. However, these authors stated that their experimental paradigm cannot resolve possible subtle conformational changes of pre-M1, M3<sub>C</sub>, and M4<sub>N</sub> segments that may be associated with channel gating. Additionally, two of the mutants studied (S535C and Y629C) failed to generate detectable glutamate-activated currents, thus indicating that the corresponding residues may participate in the formation of the channel gate.

Taking into account that only one TAA blocking molecule can bind to the open NMDA channel (Zarei and Dani, 1995; Sobolevsky, 1999), the representation in Figure 13 provides a clear illustration of the results of the present study: TEA and TPA permit the closure of both activation and desensitization gates; TBA prohibits the closure of the desensitization gate but does not exclude the closure of the activation gate; and TPentA prohibits the closure of both activation and desensitization gates. According to models 1–5, the agonist can bind to or dissociate from the channel only when the activation gate is closed but the desensitization gate is open. Additionally, the desensitization gate can close only when the activation gate is already closed.

There are several types of NMDA channel desensitization (McBain and Mayer, 1994). Under our experimental conditions (3  $\mu$ M glycine), glycine-dependent desensitization (Mayer et al., 1989) was hardly probable. Calcium-dependent inactivation manifested at low agonist concentrations (Legendre et al., 1993) was not observed in our experiments either (see Fig. 8A). Thus, practically we dealt only with glycine-independent desensitization (Sather et al., 1990).

The small difference in the sizes of TBA and TPentA molecules requires close location of the activation and desensitization gates deep in the channel pore. It is doubtful that both gates consist of consecutive segments of the same pore-forming amino acid chain but, rather, of fragments of different transmembrane domains, most probably belonging to different NMDA subunits (Fig. 13). The latter observation is in good agreement with the recent findings on the molecular determinants of the NMDA channel structure and function. Thus, the NR1 (but not NR2) subunit proved to be necessary and enough to form functional NMDA receptors (Moriyoshi et al., 1991; Yamazaki et al., 1992; Nakanishi et al., 1992). On the other hand, the fragments of the NR2 subunit are responsible for NMDA receptor glycine-independent desensitization (Krupp et al., 1998; Villarreal et al., 1998).

One could suppose alternative structures of the NMDA channel gating machinery. For example, the structure responsible for channel desensitization may not be obviously the gate within the channel pore but some entity within the pore-forming walls that is able to fix the completely closed activation gate (thus transposing the channel into the nonconducting desensitized state). Within the frame of this hypothesis, TPentA holds the activation gate fully open, prohibiting both desensitization and the agonist dissociation. TBA does not allow the activation gate to close completely, as TEA and TPA do, but only partly, and in this "half-open" state desensitization does not occur either, but the agonist can dissociate. However, this alternative hypothesis demands the involvement of new half-open states of the channel into the kinetic models, whereas the hypothesis illustrated in Figure 13 is in good agreement with a simple activation kinetic model used in the present study (Lester and Jahr, 1992).

Irrespective of the structure of the desensitization mechanism, the diameter of the open NMDA channel pore at the level of the activation gates is approximately equal to the size of TPentA (11.1 Å), calculated as the mean of the two smallest dimensions of the smallest size box containing space-filling models of the TPentA molecule (HyperChem). The distance from the activation gate to the deep blocking site 1 should not be larger than the length of 1-ammonio-5-(1-adamantanemethylammonio)pentane dibzomide (16.7 Å), the stretched molecule that at holding potentials more positive than  $-90$  mV is thought to bind to site 1 by its ammonium end group and that prevents the closure of the activation gate by its adamantane head (Antonov et al., 1995; Johnson et al., 1995; Antonov and Johnson, 1996).

In experiments with 9-aminoacridine (Costa and Albuquerque, 1994; Koshelev and Khodorov, 1994, 1995; Benveniste and Mayer, 1995) it was hypothesized that this blocker prohibits NMDA channel closure. Our study of 9-aminoacridine-induced kinetics (Sobolevsky, 1999) revealed the existence of two non-overlapping 9-aminoacridine blocking sites in the open NMDA channel, which can be occupied by two 9-aminoacridine molecules simultaneously. It was suggested that 9-aminoacridine binding to the shallow site (Fig. 13, site 2) in the orientation across the channel pore prevented the closure of the activation and/or

desensitization gates. Taking into account the cross-cut size of the 9-aminoacridine molecule (11.1 Å), we may conclude that this suggestion is in good coincidence with the hypothesis represented in Figure 13.

In conclusion, TAA have proved to be useful tools in studies of the gross architecture of the NMDA channel, and one could thus expect that a combination of this experimental approach with molecular biology methods may ensure considerable progress in the deciphering of molecular mechanisms of channel gating.

## REFERENCES

- Anson LC, Chen PE, Wyllie DJA, Colquhoun D, Schoepfer R (1998) Identification of amino acid residues of the NR2A subunit that control glutamate potency in recombinant NR1/NR2A NMDA receptors. *J Neurosci* 18:581–589.
- Antonov SM, Johnson JW (1996) Voltage-dependent interaction of open-channel blocking molecules with gating of NMDA receptors in rat cortical neurons. *J Physiol (Lond)* 493:425–445.
- Antonov SM, Johnson JW, Lukomskaya NY, Potapyeva NN, Gmiro VE, Magazanik LG (1995) Novel adamantane derivatives act as blockers of open ligand-gated channels and as anticonvulsants. *Mol Pharmacol* 47:558–567.
- Antonov SM, Gmiro VE, Johnson JW (1998) Binding sites for permeant ions in the channel of NMDA receptors and their effects on channel block. *Nat Neurosci* 1:451–461.
- Armstrong CM (1971) Interaction of tetraethylammonium ion derivatives with the potassium channels of giant axons. *J Gen Physiol* 58:413–437.
- Armstrong CM, Croop RS (1982) Simulation of Na channel inactivation by thiazin dyes. *J Gen Physiol* 80:641–662.
- Armstrong CM, Hille B (1998) Voltage-gated ion channels and electrical excitability. *Neuron* 20:371–380.
- Beck C, Wollmuth LP, Seeburg PH, Sakmann B, Kuner T (1999) NMDAR channel segments forming the extracellular vestibule inferred from the accessibility of substituted cysteines. *Neuron* 22:559–570.
- Benveniste M, Mayer ML (1995) Trapping of glutamate and glycine during open channel block of rat hippocampal neuron NMDA receptors by 9-aminoacridine. *J Physiol (Lond)* 483:367–384.
- Benveniste M, Mienville J-M, Sernagor E, Mayer ML (1990a) Concentration-jump experiments with NMDA antagonists in mouse cultured hippocampal neurons. *J Neurophysiol* 63:1373–1384.
- Benveniste M, Clements J, Vyklicky Jr L, Mayer ML (1990b) A kinetic analysis of the modulation of *N*-methyl-D-aspartic acid receptors by glycine in mouse cultured hippocampal neurones. *J Physiol (Lond)* 428:333–357.
- Blanpied TA, Boeckman F, Aizenman E, Johnson JW (1997) Trapping channel block of NMDA-activated responses by amantadine and memantine. *J Neurophysiol* 77:309–323.
- Cahalan MD (1978) Local anesthetic block of sodium channels in normal and pronase-treated squid giant axons. *Biophys J* 23:285–311.
- Chen H-SV, Lipton SA (1997) Mechanism of memantine block of NMDA-activated channels in rat retinal ganglion cells: uncompetitive antagonism. *J Physiol (Lond)* 499:27–46.
- Colquhoun D, Hawkes AG (1995) Desensitization of *N*-methyl-D-aspartate receptors: a problem of interpretation. *Proc Natl Acad Sci USA* 92:10327–10329.
- Costa ACS, Albuquerque EX (1994) Dynamics of the actions of tetrahydro-9-aminoacridine and 9-aminoacridine on glutamatergic currents: concentration-jump studies in cultured rat hippocampal neurons. *J Pharmacol Exp Ther* 268:503–514.
- Dingledine R, Borges K, Bowie D, Traynelis SF (1999) The glutamate receptor ion channels. *Pharmacol Rev* 51:7–61.
- Hille B (1992) Ionic channels of excitable membranes. Sunderland, MA: Sinauer.
- Huetter JE, Bean BP (1988) Block of *N*-methyl-D-aspartate-activated current by the anticonvulsant MK-801: selective binding to open channels. *Proc Natl Acad Sci USA* 85:1307–1311.
- Jahr CE (1992) High probability opening of NMDA receptor channels by L-glutamate. *Science* 255:470–472.
- Johnson JW, Antonov SM, Blanpied TS, Li-Smerin Y (1995) Channel block of NMDA receptor. In: *Excitatory amino acids and synaptic transmission* (Wheal HV, ed), pp 99–113. New York: Academic.



- Korn GA, Korn TM (1974) Mathematical handbook for scientist and engineers. Definitions, theorems, formulas. Moscow: Science.
- Koshelev SG (1995) The block of NMDA channels in rat hippocampal neurones by organic cations. PhD thesis, Institute of General Pathology and Pathophysiology, Russian Academy of Medical Sciences, Moscow.
- Koshelev SG, Khodorov BI (1992) Tetraethylammonium and tetrabutylammonium as tools to study NMDA channels of the neuronal membrane. *Biol Membr* 9:1365–1369.
- Koshelev S, Khodorov B (1994) Probing of NMDA receptor channels by organic cations. Location of activation and inactivation gates. Presented at the Workshop on Molecular Mechanisms of Synaptic Function (Lerma J, Seeburg PH, organizers), Madrid, March.
- Koshelev SG, Khodorov BI (1995) Blockade of open NMDA channel by tetrabutylammonium, 9-aminoacridine and tacrine prevents channels closing and desensitization. *Membr Cell Biol* 9:93–109.
- Krupp JJ, Vissel B, Heinemann SF, Westbrook GL (1996) Calcium-dependent inactivation of recombinant *N*-methyl-D-aspartate receptors is NR2 subunit specific. *Mol Pharmacol* 50:1680–1688.
- Krupp JJ, Vissel B, Heinemann SF, Westbrook GL (1998) N-terminal domains in the NR2 subunit control desensitization of NMDA receptors. *Neuron* 20:317–327.
- Kuner T, Wollmuth LP, Karlin A, Seeburg PH, Sakmann B (1996) Structure of the NMDA receptor channel M2 segment inferred from the accessibility of substituted cysteines. *Neuron* 17:343–352.
- Kuryatov A, Laube B, Betz H, Kushe J (1994) Mutational analysis of the glycine-binding site of the NMDA receptor: structural similarity with bacterial amino acid-binding proteins. *Neuron* 12:1291–1300.
- Laube B, Hirai H, Sturgess M, Betz H, Kuhse J (1997) Molecular determinants of agonist discrimination by NMDA receptor subunits: analysis of the glutamate binding site on the NR2B subunit. *Neuron* 18:493–503.
- Laube B, Kuhse J, Betz H (1998) Evidence for tetrameric structure of recombinant NMDA receptors. *J Neurosci* 18:2954–2961.
- Legendre P, Rosenmund C, Westbrook GL (1993) Inactivation of NMDA channels in cultured hippocampal neurons by intracellular calcium. *J Neurosci* 13:674–684.
- Lester RAJ, Jahr CE (1992) NMDA channel behavior depends on agonist affinity. *J Neurosci* 12:635–643.
- Lester RAJ, Tong G, Jahr CE (1993) Interactions between the glycine and glutamate binding sites of the NMDA receptor. *J Neurosci* 13:1088–1096.
- Lin F, Stevens CF (1994) Both open and closed NMDA receptor channels desensitize. *J Neurosci* 14:2153–2160.
- Lu W-Y, Xiong Z-G, Orser BA, MacDonald JF (1998) Multiple sites of action of neomycin,  $Mg^{2+}$  and spermine on the NMDA receptors of rat hippocampal CA1 pyramidal neurones. *J Physiol (Lond)* 512:29–46.
- MacDonald JF, Bartlett MC, Mody I, Pahapill P, Reynolds JN, Salter MW, Schneiderman JH, Pennefather PS (1991) Actions of ketamine, phencyclidine and MK-801 on NMDA receptor currents in cultured mouse hippocampal neurones. *J Physiol (Lond)* 432:483–508.
- Mayer ML, Vyklicky Jr L, Clements J (1989) Regulation of NMDA receptor desensitization in mouse hippocampal neurons by glycine. *Nature* 338:425–427.
- Moriyoshi K, Masu M, Ishii T, Shigemoto R, Mizuno N, Nakanishi S (1991) Molecular cloning and characterization of the rat NMDA receptor. *Nature* 354:31–37.
- McBain CJ, Mayer ML (1994) NMDA receptor structure and function. *Physiol Rev* 74:723–760.
- Nakanishi N, Axel R, Shneider NA (1992) Alternative splicing generates functionally distinct *N*-methyl-D-aspartate receptors. *Proc Natl Acad Sci USA* 89:8552–8556.
- Neely A, Lingle J (1986) Trapping of an open-channel blocker at the frog neuromuscular acetylcholine channel. *Biophys J* 50:981–986.
- Neher E, Steinbach JH (1978) Local anesthetics transiently block currents through single acetylcholine-receptor channels. *J Physiol (Lond)* 277:153–176.
- Rosenmund C, Feltz A, Westbrook GL (1995) Synaptic NMDA receptor channels have a low open probability. *J Neurosci* 15:2788–2795.
- Ruppersberg JP, Kitzing EV, Schoepfer R (1994) The mechanism of magnesium block of NMDA receptors. *Semin Neurosci* 6:87–96.
- Sather W, Johnson JW, Henderson G, Ascher P (1990) Glycine-insensitive desensitization of NMDA responses in cultured mouse embryonic neurons. *Neuron* 4:725–731.
- Sobolevsky AI (1999) Two-component blocking kinetics of open NMDA channels by organic cations. *Biochim Biophys Acta* 1416:69–91.
- Sobolevsky A, Koshelev S (1998) Two blocking sites of amino-adamantane derivatives in open *N*-methyl-D-aspartate channels. *Biophys J* 74:1305–1319.
- Sobolevsky AI, Koshelev SG, Khodorov BI (1998) Interaction of mephentidine and amantadine with agonist-unbound NMDA-receptor channels in acutely isolated rat hippocampal neurons. *J Physiol (Lond)* 512:47–60.
- Strichartz GR (1973) The inhibition of sodium currents in myelinated nerve by quaternary derivatives of lidocaine. *J Gen Physiol* 62:37–57.
- Subramaniam S, Donevan SD, Rogawski MA (1994) Hydrophobic interactions of *n*-alkyl diamines with the *N*-methyl-D-aspartate receptor: voltage-dependent and -independent blocking sites. *Mol Pharmacol* 45:117–124.
- Villarroel A, Burnashev N, Sakmann B (1995) Dimensions of the narrow portion of a recombinant NMDA receptor channel. *Biophys J* 68:866–875.
- Villarroel A, Paz Regalado M, Lerma J (1998) Glycine-independent NMDA receptor desensitization: localization of structural determinants. *Neuron* 20:329–339.
- Vorobjev VS (1991) Vibrodissociation of sliced mammalian nervous tissue. *J Neurosci Methods* 38:145–150.
- Vorobjev VS, Sharonova IN (1994) Tetrahydroaminoacridine blocks and prolongs NMDA receptor-mediated responses in a voltage-dependent manner. *Eur J Pharmacol* 253:1–8.
- Woodhull AM (1973) Ionic blockage of sodium channels in nerve. *J Gen Physiol* 61:687–708.
- Xiong Z, Lu W, MacDonald JF (1997) Extracellular calcium sensed by a novel cation channel in hippocampal neurons. *Proc Natl Acad Sci USA* 94:7012–7017.
- Yamazaki M, Mori H, Araki K, Mori KJ, Mishina M (1992) Cloning, expression and modulation of a mouse NMDA receptor subunit. *FEBS Lett* 300:39–45.
- Yeh JZ, Narahashi T (1977) Kinetic analysis of pancuronium interaction with sodium channels in squid axon membranes. *J Gen Physiol* 69:293–323.
- Zarei MM, Dani JA (1994) Ionic permeability characteristics of the *N*-methyl-D-aspartate receptor channel. *J Gen Physiol* 103:231–248.
- Zarei MM, Dani JA (1995) Structural basis for explaining open-channel blockade of the NMDA receptor. *J Neurosci* 15:1446–1454.

# Blocker Studies of the Functional Architecture of the NMDA Receptor Channel

A. I. Sobolevskii and B. I. Khodorov

*Translated from Rossiiskii Fiziologicheskii Zhurnal imeni I. M. Sechenova, Vol. 86, No. 9, pp. 1118–1137, September, 2000. Original article submitted March 7, 2000.*

Blockade of ion channels passing through the NMDA receptors of isolated rat hippocampus pyramidal neurons with tetraalkylammonium compounds, 9-aminoacridine, and  $Mg^{2+}$  was studied using patch-clamp methods in the whole-cell configuration. Currents through NMDA channels were evoked by application of 100  $\mu M$  aspartate in magnesium-free medium containing glycine (3  $\mu M$ ) to neurons. Analysis of the kinetics, charge transfer, and relationships between the extent of suppression of stationary currents on the one hand and membrane potential, agonist concentration, and blocker concentration on the other showed that blockers had different effects on the closing, desensitization, and agonist dissociation of NMDA channels. The size of the blocker was found to be the decisive factor determining its action on the gating functions of NMDA channels: larger blockers prevented closure and/or desensitization of the channel; smaller blockers only had partial effects on these processes, while the smallest blockers had no effect at all. These experiments showed that the apparent affinity of the blocker for the channel ( $1/IC_{50}$ ) depended not only on the microscopic equilibrium dissociation constant ( $K_d$ ), but also on the number of blocker binding sites, their mutual influences, and, of particular importance, the interaction of the blocker with the gating structures of the channel. These data led us to propose hypotheses relating to the geometry of the NMDA channel and the structure of its gating mechanism. The channel diameter at the level of activated gates was estimated to be 11 Å.

**KEY WORDS:** NMDA channels, gating structures, blockade, kinetic modeling, hippocampal neurons, patch-clamping.

The properties of the NMDA (N-methyl-D-aspartate) subtype of glutamate channels, such as the high permeability for calcium ions [28], potential-dependent magnesium blockade [30], and slow activation kinetics [22, 25] determine their major contribution to physiological processes.

According to current concepts, NMDA channels play a key role in learning and memory processes [8, 12, 29]. Their involvement in generating rhythmic movement activity has been demonstrated [36], along with their role in the development of the nervous system at the embryo stage [13, 14, 24]. Many neurodegenerative processes are associated with hyperactivity of NMDA channels. On this principle, NMDA channel blockers such as memantine (1-amino-3,5-dimethyladamantane) and amantadine (1-adamantanamine) are used in the treatment of Alzheimer's disease, Parkin-

son's disease, Huntingdon's chorea, dyskinesia, sclerosis, allergic encephalomyelitis, epilepsy, depression, ischemia, schizophrenia, hemiplegia, the chronic pains involved in all types of dementia, including AIDS-associated dementia, and paralysis [17, 18, 27, 31, 32].

Recent years have seen significant progress in studies of the molecular structures, subunit composition, and selectivity of NMDA channels [19], though the question of the mechanisms of NMDA channel activation and desensitization has still not been elucidated completely.

The present article summarizes the results of studies conducted by our group in recent years with the aim of identifying the functional architecture of NMDA channels and their gating mechanism. The tools for these studies were organic cations (9-aminoacridine and tetraalkylammonium compounds) and magnesium ions, which can enter open channels and interact in different ways with the structural elements of the channels responsible for activation and desensitization processes [1, 2, 33, 35].

Institute of General Pathology and Pathophysiology, Russian Academy of Medical Sciences, 8 Baltiiskaya Street, 125315 Moscow, Russia.

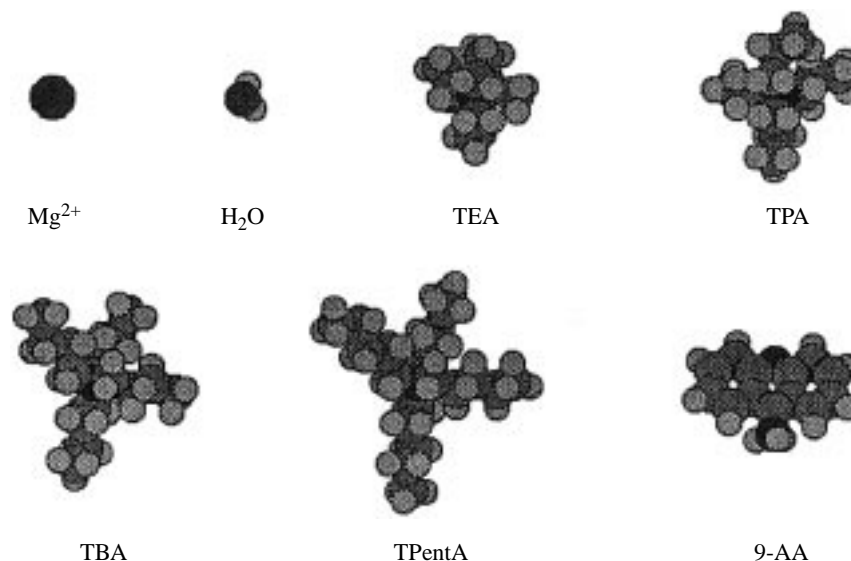


Fig. 1. NMDA channel blockers:  $\text{Mg}^{2+}$ , water ( $\text{H}_2\text{O}$ ), tetraethylammonium (TEA), tetrapropylammonium (TPA), tetrabutylammonium (TBA), tetrapentylammonium (TPentA), and 9-aminoacridine (9-AA). Black circles show nitrogen and magnesium atoms, dark gray circles show carbon and oxygen atoms, and light gray circles show hydrogen atoms.

## METHODS

Experiments were performed on pyramidal neurons from field CA1 of the rat hippocampus. Sections were made of brains from Wistar rats aged 2–4 weeks, as described previously [38]. Neurons were extracted from sections using a vibrodissociation method [38]. Experiments were started after at least 3 h of incubation in medium containing 124 mM NaCl, 3 mM KCl, 1.4 mM  $\text{CaCl}_2$ , 2 mM  $\text{MgCl}_2$ , 10 mM glucose, and 26 mM  $\text{NaHCO}_3$ . Incubation was conducted with the solution continuously saturated with gas mix (96%  $\text{O}_2$ , 4%  $\text{CO}_2$ ), at a temperature of 32°C. During removal from sections and recording of currents, neurons were kept in magnesium-free medium containing 140 mM NaCl, 5 mM KCl, 2 mM  $\text{CaCl}_2$ , 15 mM glucose, and 10 mM HEPES, pH 7.3. All blockers were dissolved in water; solutions were stored in a freezer and were thawed immediately before experiments. A rapid flow control system was used for exchanging solutions [11, 38]. Transmembrane currents in whole cells were recorded by a patch-clamping method at room temperature using micropipettes made of hard borosilicate glass (Pyrex), filled with “intracellular” solution containing 140 mM CsF, 4 mM NaCl, and 10 mM HEPES, pH 7.2. The resistance of filled micropipettes was 3–7 M $\Omega$ . Currents were digitized at a frequency of 1 kHz and recorded in a computer memory.

Data were analyzed statistically using Microcal Origin version 3.5 for Windows. Data are presented as means  $\pm$  standard errors.

Kinetic modeling was based on the solution of linear systems of first-order differential equations with constant coefficients by numerical methods, as described previously [11].

Three-dimensional models of blocker molecules were calculated using the molecular modeling program HyperChem version 3 for Windows.

## RESULTS AND DISCUSSION

**Kinetics and Stationary Characteristics of Open NMDA Channel Blockade.** Figure 1 shows the NMDA channel blockers used here:  $\text{Mg}^{2+}$ , tetraethylammonium, tetrapropylammonium, tetrapentylammonium, and 9-aminoacridine, whose effects were studied in the present experiments.

Currents through NMDA channels arose in response to the application of 100  $\mu\text{M}$  aspartate in magnesium-free medium containing glycine (3  $\mu\text{M}$ ). At a membrane potential  $E_h = -100$  mV, the current was an influx current; after a rapid ( $\tau < 30$  msec) increase to a peak value ( $I_{\text{CO}}$ ), it started to decay slowly ( $\tau = 570 \pm 25$  msec,  $n = 7$ ) until it reached a certain stationary value ( $I_{\text{CS}}$ ) (Fig. 2, A). This decay in the current in the constant presence of agonist is interpreted as desensitization of NMDA channels. The extent of desensitization ( $1 - (I_{\text{CS}}/I_{\text{CO}})$ ) varied from cell to cell over a wide range, from 0.08 to 0.75.

Used simultaneously with agonist, blockers decreased both the peak ( $I_{\text{BO}}$ ) and stationary ( $I_{\text{BS}}$ ) currents (Fig. 2, A). After coapplication ended, an influx aftercurrent appeared (a “hook”), which quickly reached a peak ( $I_{\text{P}}$ ) and then decayed to zero. The relative amplitude of the hook  $[(I_{\text{P}} - I_{\text{BS}})/I_{\text{CS}}]$  increased with increasing blocker concentrations and, correspondingly, with increases in the degree of suppression of the

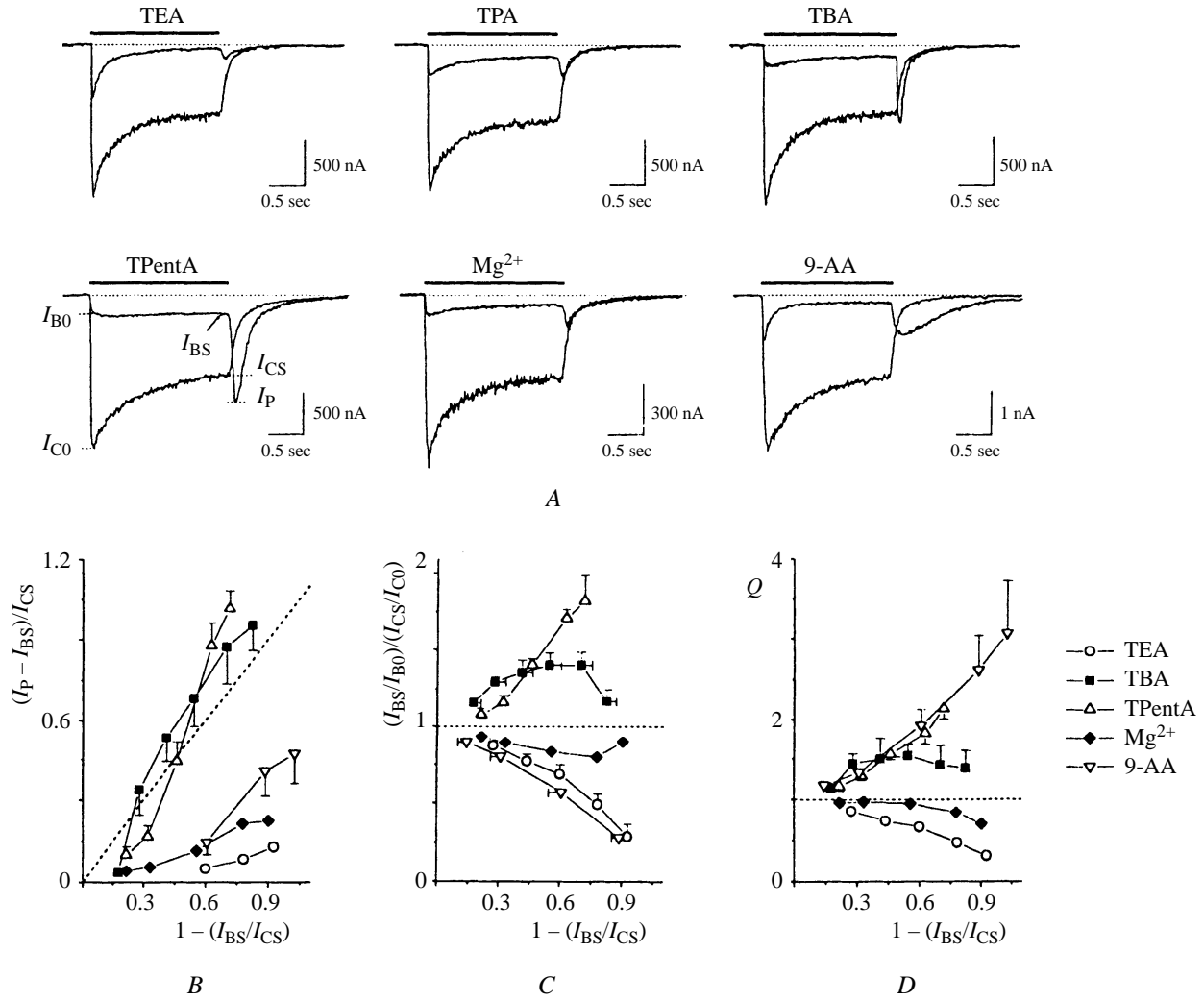


Fig. 2. The effects of simultaneous exposure to blockers and agonist. A) Superimposition of control current in response to application of aspartate (100  $\mu$ M) and the blocked current in response to simultaneous application of aspartate and tetraethylammonium (TEA, 10 mM), tetrapropylammonium (TPA, 2 mM), tetrabutylammonium (TBA, 2 mM), tetrapentylammonium (TPentA, 3 mM),  $Mg^{2+}$  (100  $\mu$ M), and 9-aminoacridine (9-AA, 10  $\mu$ M); B, C, D) relationships of the maximum hook amplitude  $(I_P - I_{BS})/I_{CS}$  (B), the control-normalized ratio of stationary current to peak current  $[(I_{BS}/I_{B0})/(I_{CS}/I_{C0})]$  (C), and the control-normalized charge transfer during the aftercurrent ( $Q$ ) (D) with the extent of suppression of the stationary current  $(1 - (I_{BS}/I_{CS}))$ .

TABLE 1. Parameters of Potential Dependence (from [35] with additional data)

Substance	$\delta$	$K_{0.5}(0)$ , mm	$n$
Tetraethylammonium	$0.90 \pm 0.04$	$62.2 \pm 6.0$	6
Tetrapropylammonium	$0.72 \pm 0.05$	$10.0 \pm 1.5$	4
Tetrabutylammonium	$0.60 \pm 0.02$	$5.34 \pm 0.27$	7
Tetrapentylammonium	$0.29 \pm 0.03$	$1.84 \pm 0.11$	5
$Mg^{2+}$	$0.93 \pm 0.19$	$6.57 \pm 2.95$	11
9-Aminoacridine	$0.65 \pm 0.05$	$0.162 \pm 0.070$	4



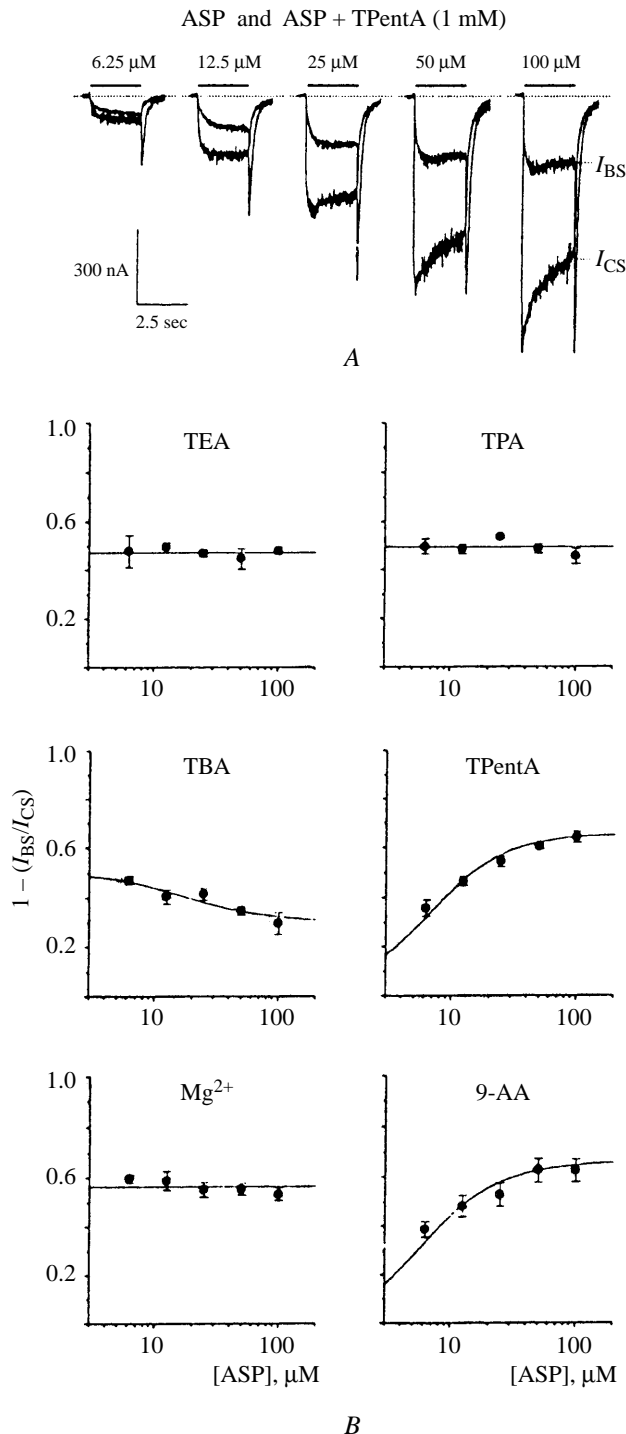


Fig. 3. Agonist-dependent blockade. A) Currents in response to simultaneous use of tetrapentylammonium (TPentA, 1 mM) and aspartate (ASP) at different concentrations superimposed on control traces; B) relationships between mean extents of suppression of the stationary current ( $1 - (I_{BS}/I_{CS})$ ) and the ASP concentration (from [35] with additional data).

stationary current ( $1 - (I_{BS}/I_{CS})$ ) (Fig. 2, B). For  $Mg^{2+}$ , tetraethylammonium, tetrapropylammonium, and 9-aminoacridine,  $(I_P - I_{BS})/I_{CS}$  was less than  $1 - I_{BS}/I_{CS}$ , while in the cases of tetrabutylammonium and tetrapentylammonium, especially at high blocker concentrations,  $(I_P - I_{BS})/I_{CS}$  was greater than  $1 - I_{BS}/I_{CS}$  (in Fig. 2, B, the points lie above the dotted line corresponding to  $(I_P - I_{BS})/I_{CS} = 1 - (I_{BS}/I_{CS})$ ).

Changes in the kinetics of aftercurrents in the presence of different blockers were different. The decay phase of the hook was delayed as compared with decay in the control current when tetrabutylammonium, tetrapentylammonium, and 9-aminoacridine were used (intercepts of aftercurrents in Fig. 2, A); these coincided in the case of  $Mg^{2+}$  and tetrapropylammonium, while decay in controls was slightly delayed compared with decay of currents blocked by tetraethylammonium.

The "desensitization" decay in the current during coapplication of aspartate and blockers ( $I_{BO}/I_{BS}$ ) was smaller than in controls ( $I_{CO}/I_{CS}$ ) in the presence of tetrabutylammonium and tetrapentylammonium, essentially the same in the presence of tetrapropylammonium and  $Mg^{2+}$ , and greater than in controls in the presence of tetraethylammonium and 9-aminoacridine (Fig. 2, A). This is well illustrated by the integral curves of  $(I_{BS}/I_{BO})/(I_{CS}/I_{CO})$ , which for these blockers were greater than 1, around 1, and less than 1 respectively (Fig. 2, C).

Transfer of charge through NMDA channels, measured by integration of current curves after the end of coapplication of aspartate and blockers, for tetrabutylammonium, tetrapentylammonium, and 9-aminoacridine was greater than charge transfer after the end of exposure to aspartate alone. The ratios of these charges ( $Q$ ) were greater than 1 and increased with increasing blocker concentration (Fig. 2, D). In the case of  $Mg^{2+}$ , tetraethylammonium, and tetrapropylammonium,  $Q$  was less than unity and decreased with increasing blocker concentrations (Fig. 2, D).

All blockers decreased the level of suppression of the stationary current ( $1 - (I_{BS}/I_{CS})$ ) with increases in the level of cell membrane depolarization. The relationship between  $1 - (I_{BS}/I_{CS})$  and membrane potential ( $E_h$ ) fit the model [39] described by the following equation:

$$1 - I_{BS}/I_{CS} = 1 - 1/(1 + [B]/K_{0.5}(0) \cdot \exp(\delta FE_h/RT)),$$

where  $K_{0.5}(0)$  is the equilibrium dissociation constant at  $E_h = 0$  and  $\delta$  is the proportion of the membrane potential obtaining at the blocker binding site in the channel pore. Smaller blockers penetrated deeper into the channel across the transmembrane field than larger blockers. This is clearly illustrated in Table 1, which give values for  $\delta$  and  $K_{0.5}(0)$  for all blockers.

The degrees of suppression of the stationary current ( $1 - (I_{BS}/I_{CS})$ ) for different blockers showed different relationships with agonist concentration. Figure 3, A shows,

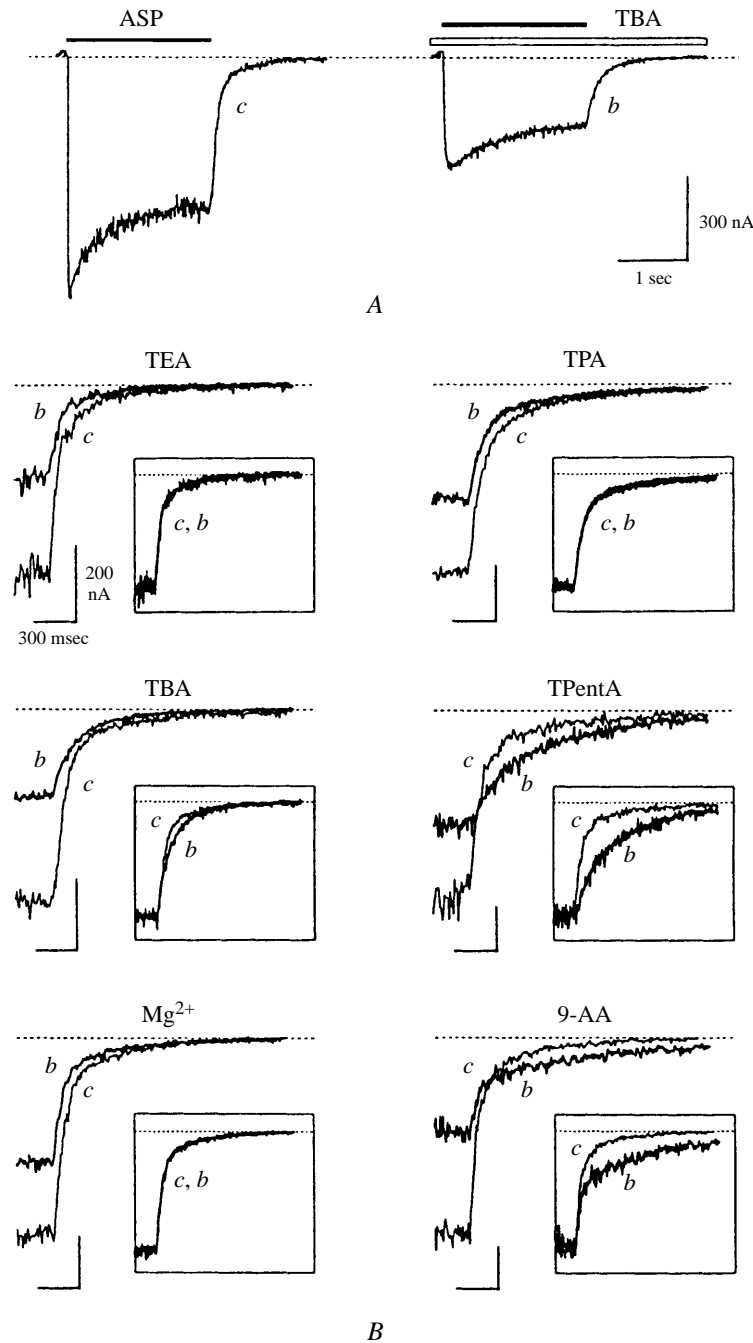


Fig. 4. The effect of exposure to agonist in the continuous presence of blocker (from [35] with additional data). A) Experimental scheme based on the example of 100  $\mu$ M aspartate (ASP) and 1 mM tetrabutylammonium (TBA); B) aftercurrents after the end of exposure to agonist in the continuous presence of tetraethylammonium (TEA, 2 mM), tetrapropylammonium (TPA, 0.6 mM), tetrabutylammonium (TBA, 1 mM), tetrapentylammonium (TPentA, 0.5 mM),  $Mg^{2+}$  (10  $\mu$ M), and 9-aminoacridine (9-AA, 10  $\mu$ M) (b) superimposed on control traces (c). Inserts show current curves for b and c with normalized stationary levels.

using tetrapentylammonium as an example, that  $1 - (I_{BS}/I_{CS})$  increased with increases in the aspartate concentration. Apart from tetrapentylammonium, a positive agonist relationship was seen for 9-aminoacridine. In the cases of

tetraethylammonium, tetrapropylammonium, and  $Mg^{2+}$ , the degree of suppression of the stationary current was independent of the aspartate concentration, while for tetrabutylammonium the agonist relationship was negative (Fig. 3, B).

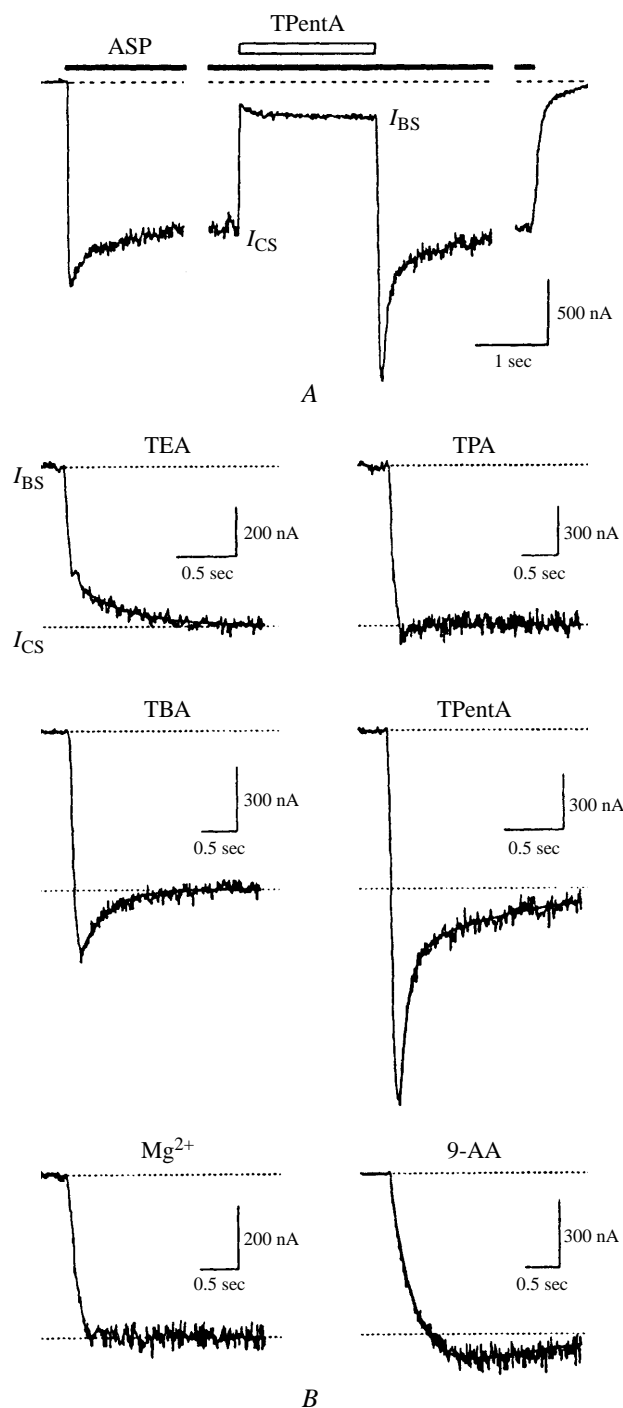


Fig. 5. Exposure to blockers in the continuous presence of agonist (from [35] with additional data). A) Experimental scheme based on the example of 2 mM tetrapentylammonium (TPentA) and 100  $\mu$ M aspartate (ASP); B) aftercurrents after the end of exposure to tetraethylammonium (TEA, 5 mM), tetrapropylammonium (TPA, 2 mM), tetrabutylammonium (TBA, 2 mM), tetrapentylammonium (TPentA, 2 mM),  $Mg^{2+}$  (100  $\mu$ M), and 9-aminoacridine (9-AA, 40  $\mu$ M) in the continuous presence of ASP (100  $\mu$ M).

When the blocker was constantly present in the solution washing the cell, there was no hook after the end of agonist exposure. The experiment is illustrated in Fig. 4, A, using 100  $\mu$ M aspartate and 1 mM tetrabutylammonium as an example. The aftercurrent kinetics after the end of aspartate exposure were very interesting. Superimpositions of aftercurrents in controls (*c*) and evoked by application of agonist in the constant presence of blocker (*b*) are shown in Fig. 4, B for different blockers. Curves *b* and *c* intersected in the cases of tetrapentylammonium and 9-aminoacridine, but not for the other blockers. The inserts in Fig. 4, B, where the stationary levels of current curves *c* and *b* are normalized, show that tetrapentylammonium and 9-aminoacridine produced strong delays in *b* as compared with *c*, this being very slight for tetrabutylammonium; normalized *c* and *b* curves coincided for  $Mg^{2+}$ , tetraethylammonium, and tetrapropylammonium.

Figure 5, A explains the experiment using blocker on a background of constant exposure to agonist solution, using tetrapentylammonium (2 mM) as an example. Blocker was used only after the aspartate-induced current had reached its stationary level ( $I_{CS}$ ). After the end of tetrapentylammonium application, the current increased sharply to levels exceeding the stationary level of the control current ( $I_{CS}$ ) and then gradually decayed to this level. The aftercurrent, which was greater than the stationary level in the control, subsequently demonstrated "overshoot." The overshoot decay in the case of tetrapentylammonium (Fig. 5, B) was well described by two exponents with time characteristics for the fast and slow components of  $\tau_{fast} = 54 \pm 7$  msec and  $\tau_{slow} = 596 \pm 85$  msec respectively ( $n = 7$ ). Overshoot was also seen with tetrabutylammonium; when solution exchange was slow ( $\tau_{wash} > 50$  msec), the descending phase of the overshoot contained one slow component ( $\tau = 389 \pm 38$  msec,  $n = 10$ ), while rapid solution exchange ( $\tau_{wash} = 5\text{--}30$  msec) gave an overshoot decay which, as in the case of tetrapentylammonium, was well described by two exponents. In the cases of tetrapropylammonium and  $Mg^{2+}$ , overshoot, although present, was hardly detectable (Fig. 5, B). On average, the kinetics of current recovery after exposure to tetrapropylammonium and  $Mg^{2+}$ , in the continuous presence of aspartate, consisted of single rapid components reflecting the rate of solution exchange. Overshoot with 9-aminoacridine was only seen at high blocker concentrations, and its ascending phase was much slower ( $\tau = 656 \pm 69$  msec at 40  $\mu$ M,  $n = 7$ ) than in the cases of tetrabutylammonium and tetrapentylammonium. Overshoot did not develop at all with tetraethylammonium. In fact, the kinetics of recovery always contained a slow component, and the current was well described by two exponents with rapid- and slow-component time characteristics of  $\tau_{fast} = 155 \pm 27$  msec and  $\tau_{slow} = 2.04 \pm 0.34$  sec respectively; the amplitude of the fast component was  $A_{fast} = 0.69 \pm 0.04$  ( $n = 8$ ).

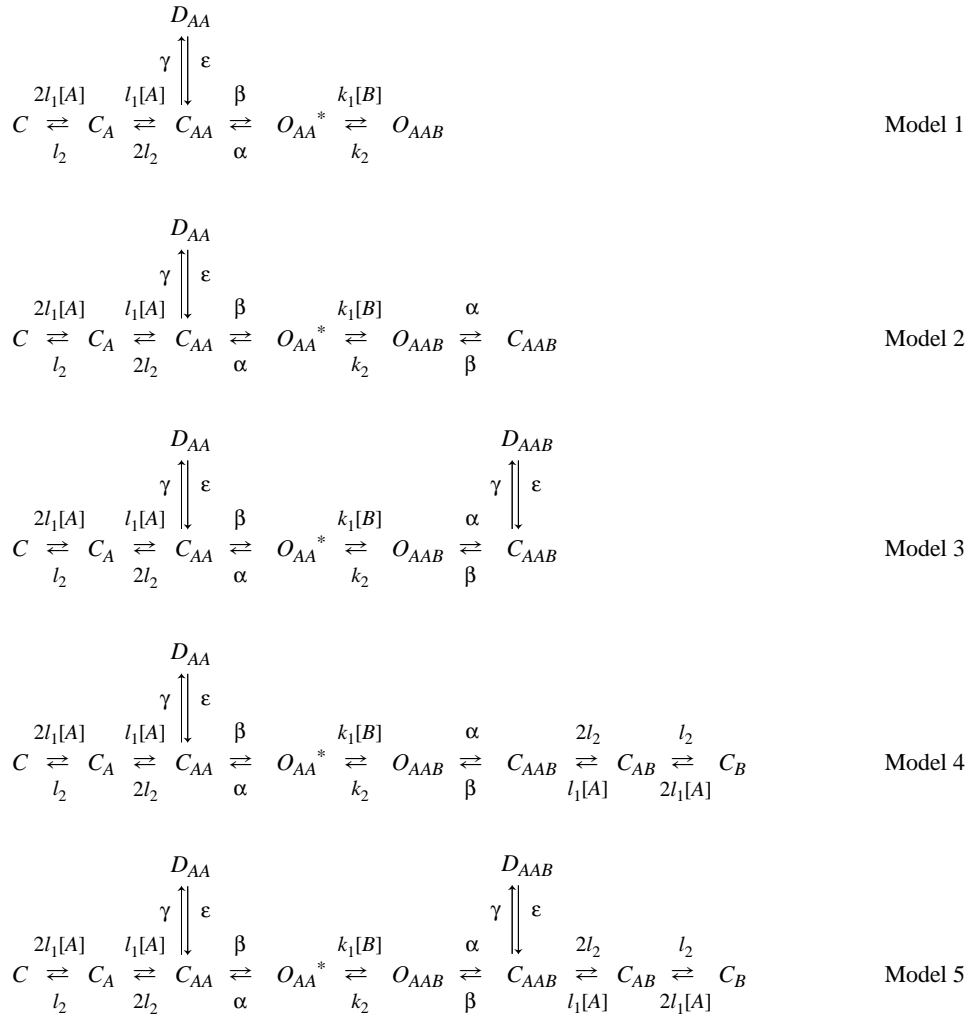


Fig. 6. Kinetic models describing different types of interaction between blocker and the NMDA channel (from [35]).  $C$ ,  $D$ , and  $O$  indicate the channel in the closed, desensitized, and open states respectively. Indexes  $A$ ,  $AA$ , and  $B$  designate the attachment of one molecule of agonist, two molecules of agonist, and one molecule of blocker respectively. Asterisks indicate the conducting state of the channel.  $[A]$  and  $[B]$  are the agonist and blocker concentrations respectively.

**Kinetic Modeling.** The effects of blockers on open channels were described by adding the blocked state to the standard kinetic model for activation of NMDA channels. Figure 6 shows five possible models obtained by sequential addition to the scheme of activation suggested by Lester and Jahr [26], the open blocked state ( $O_{AAB}$ ), the closed blocked, agonist-non-bound ( $C_{AAB}$ ), the desensitized blocked ( $D_{AAB}$ ), and closed blocked states, in which agonist had already vacated the channel ( $C_{AB}$ ,  $C_B$ ).

The five models presented in Fig. 6 can be regarded as sequentially reduced models from the completely symmetrical model 5. The advantage of this set of models is that they are simple and allow the interactions of the blocker with the gating mechanism of the NMDA channel to be predicted. Model 1 describes the situation in which the blocker channel opening and, consequently, desensiti-

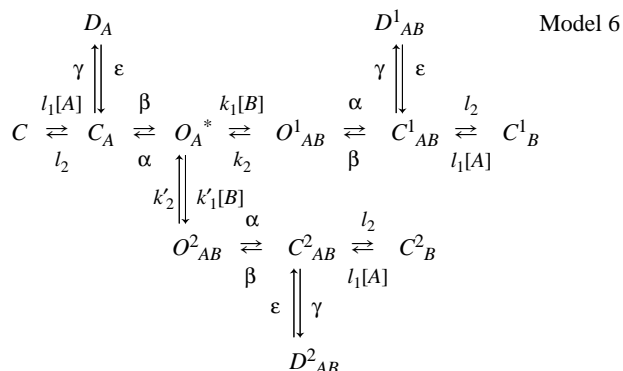
zation and agonist dissociation. The second model is based on the supposition that the channel can close with the blocker inside, but cannot undergo desensitization and the agonist-receptor complex cannot dissociate to such a stage that the channel is in the blocked state. The third model forbids only dissociation of the agonist, while the fourth only forbids desensitization. The last, fifth, model is symmetrical and forbids neither closure of the blocked channel, nor its desensitization, nor agonist dissociation. The values of kinetic constants, selected from our results and published data [7, 10, 16, 20, 33–35], were as follows:  $l_1 = 2 \mu\text{M}^{-1}\text{sec}^{-1}$ ,  $l_2 = 25 \text{ sec}^{-1}$ ,  $\alpha = 200 \text{ sec}^{-1}$ ,  $\beta = 10 \text{ sec}^{-1}$ ,  $\gamma = 1.2 \text{ sec}^{-1}$ ,  $\xi = 0.8 \text{ sec}^{-1}$ ,  $k_1 = 3.5 \mu\text{M}^{-1}\text{sec}^{-1}$ , and  $k_2 = 1000 \text{ sec}^{-1}$ . Testing of models 1–5 over wide ranges of parameters led to construction of the table of predictions (Table 2).

Comparison of the experimental data (Figs. 2–5) with the predictions of models 1–5 (Table 2) showed that the interaction of tetrapentylammonium with open NMDA channels was satisfactorily described by model 1.

The experimental data with  $Mg^{2+}$  and tetrapropylammonium were well described by symmetrical model 5. This model suggests that the blocker binds to the channel without preventing it from closing or undergoing desensitization or dissociation of agonist. The small deviations of the experimental data from the results of model experiments can be explained by the fact that  $Mg^{2+}$  and tetrapropylammonium can nonetheless have some effect on the desensitization of NMDA channels.

Comparison of the predictions of models 1–5 (Table 2) with the experimental data for tetraethylammonium suggests that the best model for describing its interaction is model 5. Two facts, however, indicate that model 5 cannot provide a complete description of the effects of tetraethylammonium: 1) the depth of the experimentally observed desensitization decay is significantly greater than predicted by the model [values of  $(I_{BS}/I_{BO})/(I_{BS}/I_{CO})$  were significantly lower than predicted by model 5; compare Fig. 7, B and Fig. 2, C]; 2) the kinetics of recovery of the current after tetraethylammonium application ended, with aspartate present throughout, contained a slow component (Fig. 5, B), which is not predicted by model 5 (Fig. 7, E).

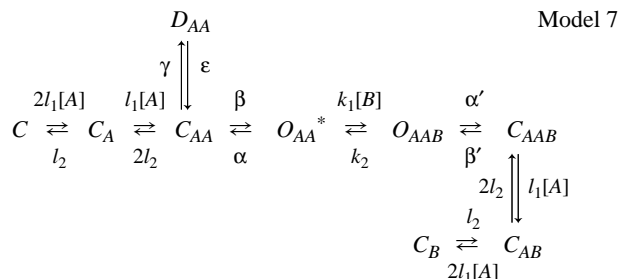
The simplest kinetic model providing a satisfactory description of the experimental data obtained with tetraethylammonium is the model with two binding sites for blocker, i.e., a fast site (1) and a slow site (2).



The binding and dissociation constants for site 2 were taken to be 250 times smaller than the corresponding constants for site 1:  $k_2' = k_2/250 = 4 \text{ sec}^{-1}$  and  $k_1' = k_1/250 = 0.014 \mu\text{M}^{-1}\text{sec}^{-1}$ . Analysis of the results of modeling may indicate that the NMDA channel contains two blocking sites for the binding of tetraethylammonium, which cannot be occupied simultaneously by two blocker molecules, and that binding with site 1, which has rapid binding and dissociation kinetics, does not prevent binding and desensitization of the NMDA channel and dissociation of agonist.

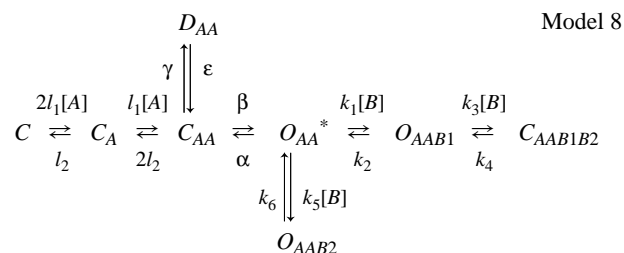
Returning to Table 2, it seems that the best model for describing the effects of tetraethylammonium is model 4.

The following points, however, suggest that model 4 cannot describe all its effects: 1) the hook exceeds the stationary level of the control current (Fig. 2, A); 2) there is a delay in aftercurrent decay kinetics in the continuous presence of blocker in solution, as compared with controls (Fig. 4, B); and 3) there is a rapid phase in the overshoot decay on rapid exchange of solutions. The simplest model satisfactorily describing the experimental data is model 4 with an alteration in the  $O_{AAB}-C_{AAB}$  transition.



Kinetic analysis showed that correspondence with the experimental data needed tetraethylammonium to increase the maximum probability of opening of blocked channels [ $P_0' = \beta' / (\alpha' + \beta')$ ] as compared with the corresponding value for the unblocked channel [ $P_0 = \beta / (\alpha + \beta)$ ]. There are two possible ways to do this: to alter the closing constant ( $\alpha'$ ) or to alter the opening constant ( $\beta'$ ). Decreases in  $\alpha'$  would suggest that the blocker prevents closure of channels, while increases in  $\beta'$  would suggest that the blocker, having entered the channel, facilitates its opening. Both possibilities produce qualitatively identical results. Figure 7 shows the results of model experiments addressing the possibility that the blocker hinders channel closure by a factor of 20 ( $\alpha' = \alpha/20 = 10 \text{ sec}^{-1}$ ,  $\beta' = \beta$ ).

The simplest kinetic model describing the effects of 9-aminoacridine supposes that the blocker prevents closure of the channel and thus prevents desensitization and dissociation of agonist [10, 15, 33], and also assumes two binding sites for 9-aminoacridine in the NMDA channel and the possibility that these can simultaneously be occupied by two different blocker molecules [33].



This model supposes that the blocker bound with either of the sites prevents both closure of the channel and its desensitization and dissociation of agonist. Figure 7 shows the predictions of model 8 with the following values of the

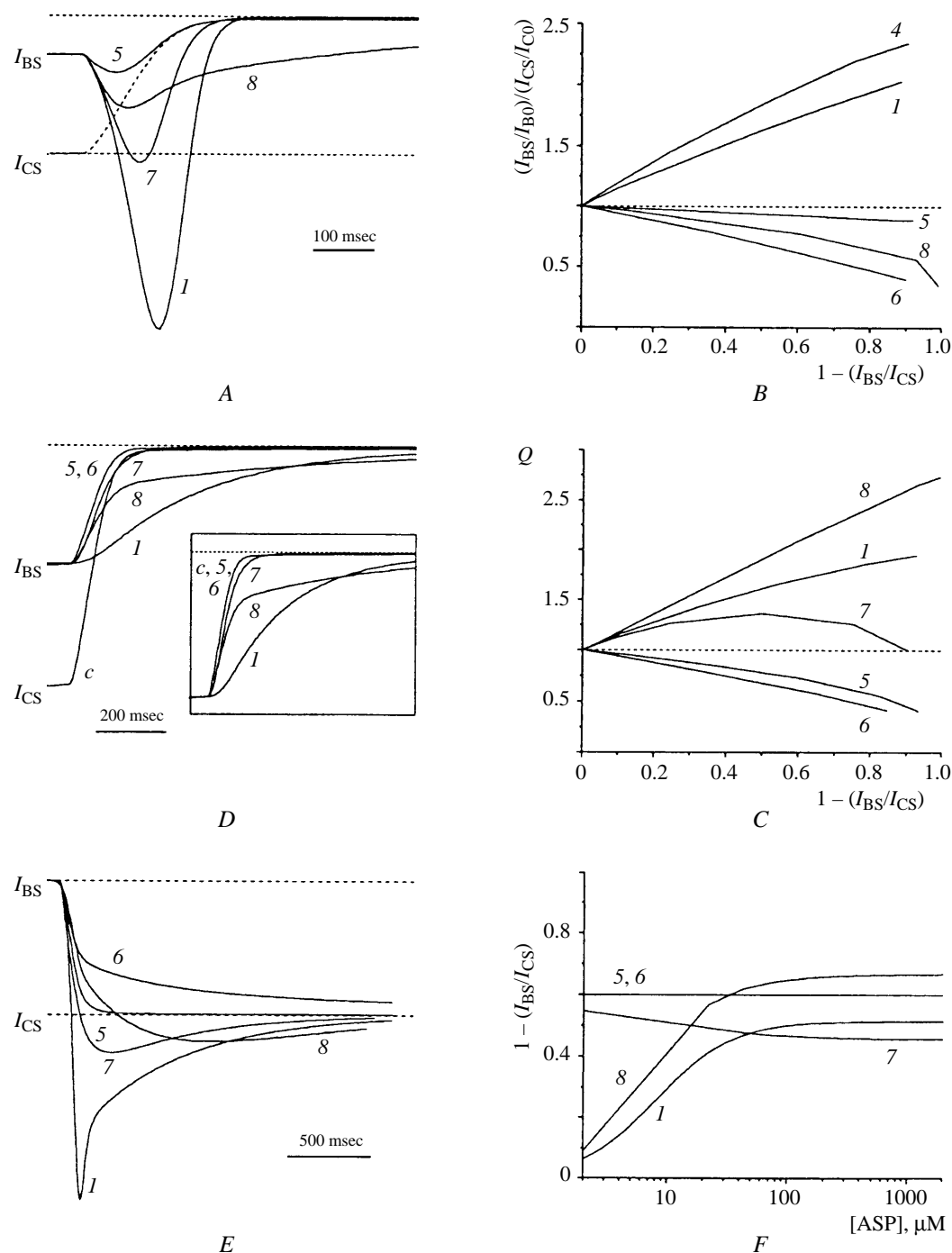


Fig. 7. Predictions of models describing the actions of blockers (identified by numbers). A) Aftercurrents appearing after the end of simultaneously application of blocker and agonist continuous lines) superimposed on control traces (dotted lines); B, C) relationships of control-normalized ratios of stationary current to peak current  $[(I_{BS}/I_{BO})/(I_{CS}/I_{CO})]$  (B) and control-normalized charge transfer during the aftercurrent (Q) (C) with the extent of suppression of the stationary current  $(1 - (I_{BS}/I_{CS}))$ ; D) aftercurrents appearing after the end of application of agonist in the continuous presence of blocker superimposed on control traces (c). The insert shows current curves with normalized stationary levels; E) aftercurrents appearing after the end of exposure to blocker in the continuous presence of agonist; F) relationship between the extent of suppression of the stationary current and the agonist concentration.

TABLE 2. Predictions of Models 1–5 (from [35] with additional data)

Model	Criteria for model 5		Criteria for desensitization		Criteria for channel closure	Criteria for agonist dissociation		
	Probability of $I_P > I_{CS}$	Intersection during coapplication <sup>1</sup>	$(I_{BS}/I_{B0}) / (I_{CS}/I_{C0})$	Overshoot <sup>2</sup>	Rapid phase of overshoot <sup>3</sup>	$Q^4$	Agonist dependence <sup>5</sup>	Intersection in the presence of blocker <sup>6</sup>
1	+	+	>1	+	+	>1	Increasing	+
2	+	+	>1	+	–	>1	Increasing	+
3	+	+	<1	–	–	>1	Increasing	+
4	+	+	>1	+	–	<1	Decreasing	–
5	–	–	<1	–	–	<1	Constant	–

**Notes.** <sup>1</sup>Intersection (on superimposition of traces) of the aftercurrent in controls and the current after coapplication of agonist and blocker. <sup>2</sup>Presence of overshoot of the aftercurrent in the presence of agonist. <sup>3</sup>Probability of the appearance of a rapid component in the overshoot decay phase. <sup>4</sup>Magnitude of control-normalized charge transfer during the aftercurrent. <sup>5</sup>Agonist dependence of the extent of suppression of the stationary current. <sup>6</sup>Intersection (on superimposition of traces) of the control aftercurrent and the current after the end of application of agonist in the continuous presence of blocker.

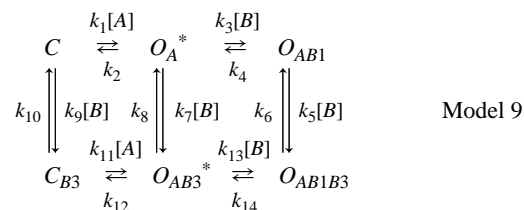
kinetic constants:  $k_1 = 29 \mu\text{M}^{-1}\text{sec}^{-1}$ ,  $k_2 = 1000 \text{ sec}^{-1}$ ,  $k_3 = 0.74 \mu\text{M}^{-1}\text{sec}^{-1}$ ,  $k_4 = 1.54 \text{ sec}^{-1}$ ,  $k_5 = 0.054 \mu\text{M}^{-1}\text{sec}^{-1}$ , and  $k_6 = 0.47 \text{ sec}^{-1}$ .

Thus, description of the kinetics and stationary characteristics of NMDA channel blockade by different substances needed different kinetic models. This suggests that the mechanisms of action of these blockers are different. The first point is that models based on different actions for blockers on the processes of channel closure, channel desensitization, and dissociation of agonist, with identical microscopic equilibrium dissociation constants ( $K_d = k_2/k_1$ ) predict different apparent blocker affinities for channels ( $\text{IC}_{50}$ ). This is an important question, as the microscopic dissociation constant and the half-blocking concentration are often the same, which in turn leads to incorrect interpretation of the data and erroneous comparative analysis.

It follows that the apparent affinity of tetraalkylammonium compounds [ $(1/\text{IC}_{50})$ ,  $(1/K_{0.5}(0))$ ] depend not only on hydrophobic and steric factors (which influence the microscopic  $K_d$ ), but also on interactions with the gating mechanism [affecting the difference between  $\text{IC}_{50}$  values ( $K_{0.5}(0)$  and  $K_d$ )]. The ratio of  $K_d$  and  $\text{IC}_{50}$  depends on the probability of channel opening ( $P_0$ ), on the number of desensitized channels, and also on the concentration of agonist. For model 5,  $\text{IC}_{50}/K_d$  is always unity. For the other models, this ratio is always greater than unity. Thus, with  $P_0 = 0.048$ ,  $\gamma/\varepsilon = 1.5$  and an asparagine concentration of  $2.5 \mu\text{M}$ , model 1 gives  $\text{IC}_{50}/K_d = 1000$ .

**Screening Effect.** A second possible source of differences between the microscopic  $K_d$  and the half-blocking concentration  $\text{IC}_{50}$  is the mechanism of “screening.” Screening means the existence of a non-blocked binding site, such that attachment of one blocker molecule to this site hinders the binding of another blocker molecule to the blocked site (Fig. 8, C). The blocked binding site (1) is deep within the channel pore, while the screening site (3) is in the

wide part of the extracellular vestibule. The screening effect is manifest as a deviation in the value of the Hill coefficient for the relationship between concentration and the extent of suppression of the stationary current from unity, i.e., the value predicted by all eight of the kinetic models analyzed above. Thus, the greater the binding of one blocker molecule to the screening binding site hinders binding of a second blocker molecule to the blocked site, the smaller is the Hill coefficient. It is logical to suppose that the larger the blocker molecule, the greater the screening effect it would have. The significant decrease in the Hill coefficient with blocker molecule size seen for tetraalkylammonium compounds (Table 3) agrees with this hypothesis. The simplest kinetic model describing the screening effect is



The applicability of the screening model hypothesis was assessed by testing model 9 with  $k_1 = k_{11} = 4 \text{ sec}^{-1}\mu\text{M}^{-1}$ ,  $k_2 = k_{12} = 50 \text{ sec}^{-1}$ ,  $k_3 = k_5 = k_7 = k_9 = 100 \text{ sec}^{-1}[\text{B}]^{-1}$ , and  $k_4 = k_6 = k_8 = k_{10} = k_{14} = 100 \text{ sec}^{-1}$ . The rate constant  $k_{13}$  was varied. Calculated curves showing the relationship between the extent of suppression of the stationary current and blocker concentration, expressed as  $K_d = k_4/k_3$  at different  $k_{13}$  values, are shown in Fig. 8, B. When constant  $k_{13}$  was less than  $k_3$  (binding of one blocker molecule to the screening site hinders binding of another blocker molecule to the blocked site), the relationship between the extent of suppression of the stationary current and the blocker concentration was less steep and the Hill coefficient was less than unity (Fig. 8, C). The ratio  $\text{IC}_{50}/K_d$  increased in these conditions and was greater



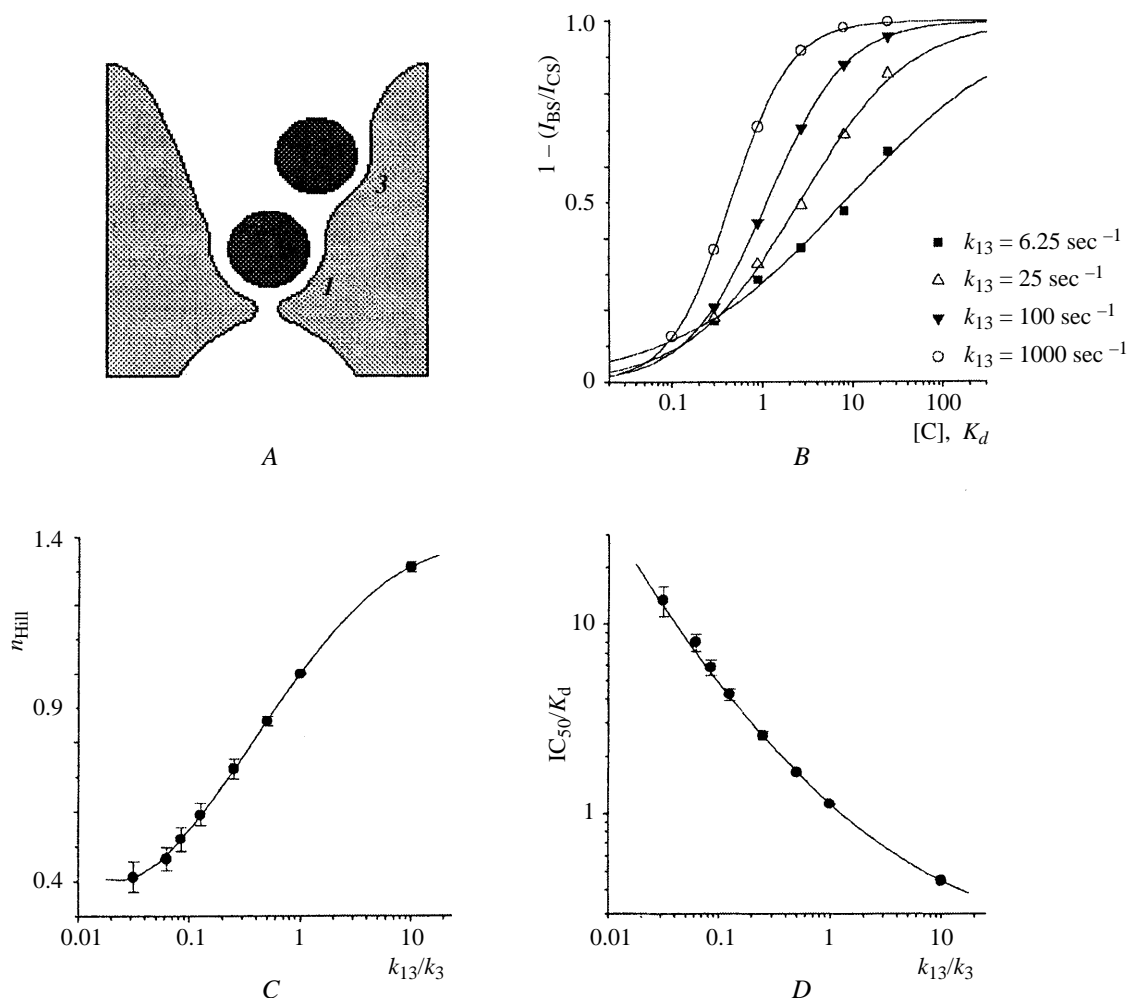


Fig. 8. The "screening" hypothesis. A) Diagram showing the screening hypothesis. The blocker binding sites (1 is the blocking site and 3 is the screening site) are located in the extracellular vestibule of the channel. Circles identify blocker molecules. The narrow part of the channel is just below site 1, the selective filter; B) relationship between the extent of suppression of the stationary current predicted by model 9 at different values of constant  $k_{13}$ . Curves show fitting to the equation; C) relationship between the Hill coefficient and the ratio  $k_{13}/k_3$ ; D) relationship between ratio  $IC_{50}/K_d$  and  $k_{13}/k_3$ .

than unity (Fig. 8, D). Conversely, when  $k_{13}$  was greater than  $k_3$  (binding of one blocker molecule to the screening site facilitated binding of another blocker molecule to the blocked site), the plot showing suppression of the stationary current was steeper and the Hill coefficient was greater than 1 (Fig. 8, C), while  $IC_{50}/K_d$  decreased (Fig. 8, D).

**The Roles of Hydrophobicity and the Size of Tetraalkylammonium Compounds in Their Binding to NMDA Channels.** Having found the coefficients of increase of  $IC_{50}$  as compared with  $K_d$ , due to the interaction with the gating mechanism ( $k_g$ ), and the screening mechanism ( $k_s$ ), values of  $K_{0.5}(0)$  can be used to estimate microscopic equilibrium dissociation constants at  $E_h = 0 \text{ mV}$ :  $k_d(0)_{\text{micro}} = K_{0.5}(0)/k_g/k_s$ . Calculated values of  $k_g$ ,  $k_s$ , and  $k_d(0)_{\text{micro}}$  for tetraalkylammonium compounds are shown in Table 3.

The change in the free binding energy of tetraalkylammonium compounds, per mole of alkyl groups, with NMDA channels, calculated according to

$$\delta G(=CH_2) = -(1/4)RT\delta[\ln(K_d(0)_{\text{micro}})],$$

gave  $\delta G(=CH_2)$  values of 318 cal/mole going from tetraethylammonium to tetrapropylammonium, 569 cal/mole going from tetrapropylammonium to tetrabutylammonium, and 555 cal/mole going from tetrabutylammonium to tetrapentylammonium. Linear fitting of  $\ln[K_d(0)_{\text{micro}}]$  for all tetraalkylammonium compounds gave  $\delta G(=CH_2) = 489 \pm 42 \text{ cal/mole}$  (Fig. 9). This value is half the theoretical change in the free energy of one mole of  $=CH_2=$  groups (1000 cal/mole) for transfer from an aqueous environment to a hydrophobic environment [23]. Con-

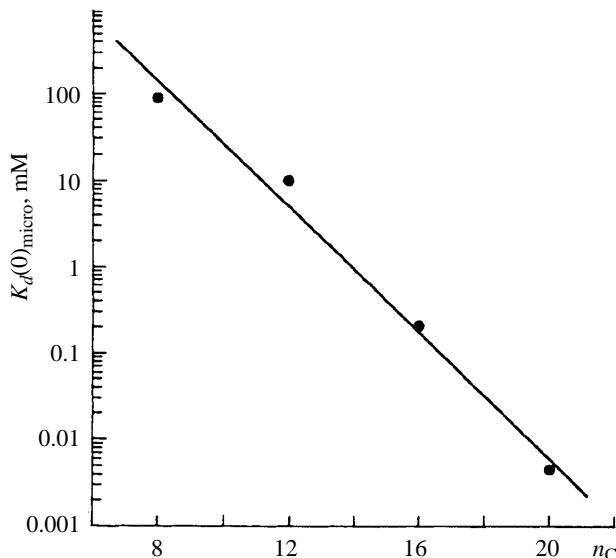


Fig. 9. Relationship between  $K_d(0)_{\text{micro}}$  and the number of carbon atoms ( $n_C$ ) in tetraalkylammonium compounds.

TABLE 3. Values of  $k_g$ ,  $n_{\text{Hill}}$ ,  $k_s$ , and  $K_d(0)_{\text{micro}}$  for Tetraalkylammonium Compounds

Substance	$k_g$	$n_{\text{Hill}}$	$k_s$	$K_d(0)_{\text{micro}}$ , mM
Tetraethylammonium	1	$1.22 \pm 0.08$	0.7	$88.9 \pm 8.6$
Tetrapropylammonium	1	$1.06 \pm 0.04$	1	$10.0 \pm 1.5$
Tetrabutylammonium	16.4	$0.88 \pm 0.09$	1.63	$0.20 \pm 0.01$
Tetrapentylammonium	49	$0.65 \pm 0.02$	8.5	$0.0044 \pm 0.0003$

sidering that the positive charge of the nitrogen atom in all tetraalkylammonium compounds is distributed over the alkyl chain and that the binding regions of these compounds cannot be regarded as ideal non-polar hydrophobic environments, the transfer energy of one mole of  $=\text{CH}_2=$  groups must be less than 1000 cal/mole. Thus, hydrophobic interactions play a large role in the binding of tetraalkylammonium compounds with NMDA channels and it can be suggested that at least half the  $=\text{CH}_2=$  groups of these compounds form hydrophobic bonds when blocking channels. Contradicting the conclusions of a previous study [2], we came to the conclusion that the absence of any significant decrease in  $\delta G(=\text{CH}_2=)$  with increases in the length of the alkyl chain is evidence that the size of the tetraalkylammonium compounds has no effect on their ability to form hydrophobic bonds in NMDA channels.

**A Model for the Gating Mechanism of NMDA Channels.** The difference in the mechanisms of action of blockers is apparent mainly in their effects on channel closure, channel desensitization, and agonist dissociation. Some blockers prevent closure of NMDA channels (tetrapentylammonium), while others (tetrabutylammoni-

um) only decrease the probability that the blocked channel will be in the closed state and, finally, a third group have no effect on closure ( $\text{Mg}^{2+}$ , tetraethylammonium, and tetrapropylammonium). This is evidence for the existence of activatory gates in NMDA channels, on which blockers can act in different ways. The fact that some blockers prevent desensitization of NMDA channels (tetrapentylammonium, tetrabutylammonium, and 9-aminoacridine), while others only have partial effects on NMDA channels ( $\text{Mg}^{2+}$  and tetrapropylammonium), and, finally, a third group has no effect (tetraethylammonium) suggests that the NMDA channel contains some structure responsible for its desensitization and on which different blockers can act in different ways. The existence of a blocker which does not prevent closure of NMDA channels but does prevent desensitization (tetrabutylammonium) shows that the activatory gate of the NMDA channel and the structure responsible for channel desensitization are different from each other. Since all the study substances enter the pore and block the channel, this structure is most likely to be located in the transmembrane pore-forming fragments of the amino-acid sequence of the NMDA channel.

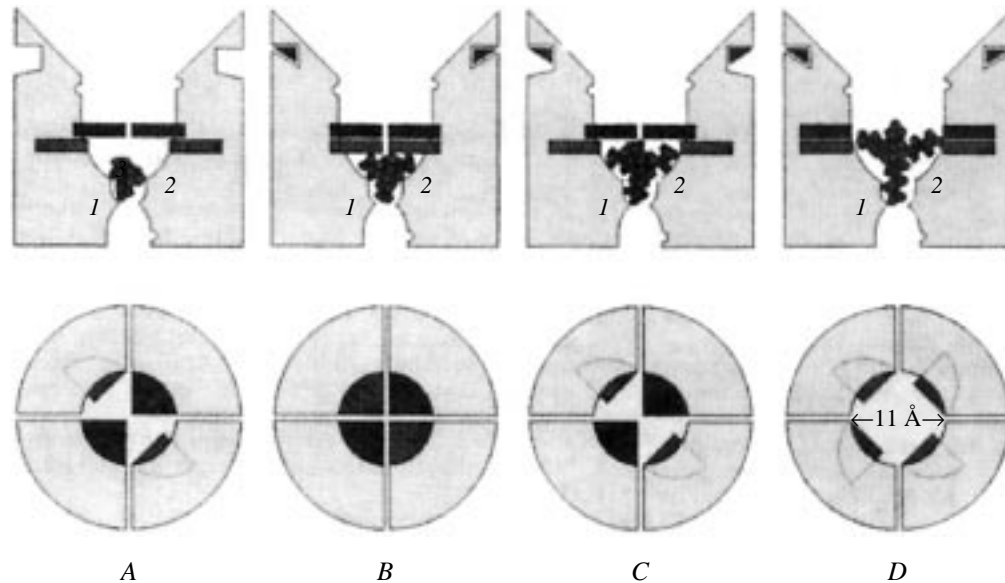


Fig. 10. Explanation of the hypothesis that NMDA channels contain activatory and desensitizing gates, which are different from each other (from [35]). The activatory gates are shown darker than the desensitizing gates and are located closer to the extracellular surface of the membrane. Triangles show agonist molecules. Hemispheres in the channel walls are binding sites for penetrating cations. 1, 2) Blocker binding sites. The upper row shows side views, and the lower row shows views from above. A) An NMDA channel with bound tetraethylammonium in the closed agonist-non-bound blocked state ( $C_B$ ); B) a channel with bound tetrapropylammonium in the desensitized blocked state ( $D_{AAB}$ ); C) a channel with bound tetrabutylammonium in the closed agonist-bound blocked state ( $C_{AAB}$ ); D) a channel with bound tetrapentylammonium in the open blocked state ( $O_{AAB}$ ).

The molecules of blockers which prevent closure or desensitization of the NMDA channel are large in size. Blockers which do not prevent but can hinder these processes are smaller, and blockers which hinder neither closure nor desensitization are the smallest. This is evidence for the suggestion that blocker molecule size plays the key role in the interactions of blockers with the gating structures of the NMDA channel [2]. The fact that the value of  $\delta$  for small-size blockers is significantly greater than  $\delta$  for large blockers (Table 1) is indirect evidence that the former penetrate more deeply into the channel pore than the latter.

According to current concepts, the NMDA channel is a pore with a small intracellular vestibule and a large extracellular vestibule containing a narrowing of length about 6 Å and a diameter of 6.4 Å; the vestibules are separated by a selective filter with a cross-section of 22–26 Å [37, 40]. Figure 10 shows part of the pore of the NMDA channel, containing two blocking regions and binding sites for cations which penetrate the pore. The latter are most likely to be located in the upper part of the ion pore (the extracellular vestibule), because the binding of penetrating cations to them is independent of membrane potential [3, 5]. It is very likely that one or several binding sites for penetrating cations are at the same time screening binding sites (Fig. 8). The structure responsible for opening and closing of the NMDA channel is shown in Fig. 10 as an activatory gate separated from the selective filter by a distance no greater

than the length of the extended IEM-1754 molecule (17 Å), whose terminal ammonium group attaches to site 1 at a membrane potential of –90 mV, while the adamantane head prevents closure of the activatory gates [4, 6, 21].

The structure responsible for desensitization of the NMDA channel is also shown in Fig. 10 as gates. Thus, blockers preventing channel closure or desensitization prevent closure of the corresponding gates. The difference in the depths of the activatory and desensitizing channel gates is determined mainly by the difference in the sizes of tetrapentylammonium and tetrabutylammonium. Since this is small (1–2 Å), it is logical to suppose that the activatory and desensitizing gates are formed from transmembrane fragments of different subunits of the NMDA channel. This suggestion is shown in diagram form as views of the channel from above (Fig. 10, lower row).

There is an alternative suggestion, that only the activatory gates are within the channel pore, while the structure responsible for desensitization is outside the pore-forming channel walls. This structure can be illustrated as “bolts,” which completely lock the closed activatory gates, converting the channel into the non-conducting desensitized state.

Regardless of the actual structure of the “desensitizing gates” of the NMDA channel, the diameter of the channel pore at the activatory gate site has to be taken as essentially the same as the size of the tetrapentylammonium molecule (11 Å), calculated as the mean of the two minimum sizes of

the smallest box containing the tetrapentylammonium molecule (HyperChem) (and which is equal to the cross-sectional size of the 9-aminoacridine molecule). This is in good agreement with data obtained by Koshelev and Khodorov [2], who came to the conclusion that only those blockers whose maximum molecular size is greater than the critical size of the window, 11 Å, have the ability to immobilize the open configuration of the channel. In this case, if the desensitizing mechanism shown in Fig. 10 is correct, the diameter of the channel pore in the region of the desensitizing gates is essentially equal to the size of the tetrabutylammonium ammonium molecule (10 Å).

Thus, the present results lead to the conclusion that blockers are useful tools for studying the functional architecture of receptor-controlled channels in neuron membranes.

This study was supported by the Russian Fund for Basic Research (Grant Nos. 96-15-97866 and 99-04-48770) and a grant from the Physiological Society of Great Britain.

## REFERENCES

1. S. G. Koshelev and B. I. Khodorov, "Tetraethylammonium and tetrabutylammonium as tools for studies of NMDA channels in neuron membranes," *Biol. Membrany*, **9**, 1365–1369 (1992).
2. S. G. Koshelev and B. I. Khodorov, "Tetrabutylammonium, tacrine, and 9-aminoacridine, which block open NMDA channels, prevent channel closure and desensitization," *Biol. Membrany*, **12**, 89–104 (1995).
3. S. M. Antonov, V. E. Gmiro, and J. W. Johnson, "Binding sites for permeant ions in the channel of NMDA receptors and their effects on channel block," *Nat. Neurosci.*, **1**, 451–456 (1998).
4. S. M. Antonov and J. W. Johnson, "Voltage-dependent interaction of open-channel blocking molecules with gating of NMDA receptors in rat cortical neurons," *J. Physiol.*, **493**, 425–445 (1996).
5. S. M. Antonov and J. W. Johnson, "Permeant ion regulation of N-methyl-D-aspartate receptor channel block by  $Mg^{2+}$ ," *Proc. Natl. Acad. Sci. USA*, **96**, 14571–14576 (1999).
6. S. M. Antonov, J. W. Johnson, N. Y. Lukomskaya, N. N. Potapyeve, V. E. Gmiro, and L. G. Magazanik, "Novel adamantane derivatives act as blockers of open ligand-gated channels and as anticonvulsants," *Mol. Pharmacol.*, **47**, 558–567 (1995).
7. P. Ascher, P. Bregestovski, and L. Nowak, "NMDA-activated channels of mouse central neurons in magnesium-free solutions," *J. Physiol.*, **399**, 207–226 (1988).
8. F. Asztely and B. Gustafsson, "Ionotropic glutamate receptors: Their role in the expression of hippocampal synaptic plasticity," *Mol. Neurobiol.*, **12**, 1–11 (1996).
9. M. Benveniste and M. L. Mayer, "Kinetic analysis of antagonist action at N-methyl-D-aspartic acid receptors. Two binding sites each for glutamate and glycine," *Biophys. J.*, **59**, 560–573 (1991).
10. M. Benveniste and M. L. Mayer, "Trapping of glutamate and glycine during open channel block of rat hippocampal neuron NMDA receptors by 9-aminoacridine," *J. Physiol.*, **483**, 367–384 (1995).
11. M. Benveniste, J.-M. Mienville, E. Sernafor, and M. L. Mayer, "Concentration-jump experimental with NMDA antagonists in mouse cultured hippocampal neurons," *J. Neurophysiol.*, **63**, 1373–1384 (1990).
12. T. V. Bliss and G. L. Collingridge, "A synaptic model of memory: long-term potentiation in the hippocampus," *Nature*, **361**, 31–39 (1993).
13. H. T. Cline, E. A. Debski, and M. Constantine-Paton, "The role of NMDA receptor in the development of the frog visual system," *Adv. Exp. Med. Biol.*, **268**, 197–203 (1990).
14. M. Constantine-Paton, "NMDA receptor as a mediator of activity-dependent synaptogenesis in the developing brain," *Cold. Spring Harb. Symp. Quant. Biol.*, **55**, 431–443 (1990).
15. A. C. S. Costa and E. X. Albuquerque, "Dynamics of the actions of tetrahydro-9-aminoacridine and 9-aminoacridine on glutamatergic currents. Concentration-jump studies in cultured rat hippocampal neurons," *J. Pharmacol. Exp. Ther.*, **268**, 503–514 (1994).
16. S. G. Cull-Candy and M. M. Usowich, "On the multiple-conductance single channels activated by excitatory amino acids in large cerebellar neurones of the rat," *J. Physiol.*, **415**, 555–582 (1989).
17. W. Danysz and C. G. Parsons, "Glycine and N-methyl-D-aspartate receptors. Physiological significance and possible therapeutic application," *Pharmacol. Rev.*, **50**, 597–664 (1998).
18. W. Danysz, C. G. Parsons, I. Breskink, and G. Quack, "Glutamate in CNS disorders," *Drug News Perspect.*, **8**, 261–277 (1995).
19. R. Dingledine, K. Borges, D. Bowie, and S. F. Traynelis, "The glutamate receptor ion channels," *Pharmacol. Rev.*, **51**, 7–61 (1999).
20. C. E. Jahr and C. F. Stevens, "A quantitative description of NMDA receptor channel kinetic behavior," *J. Neurosci.*, **10**, 1830–1837 (1990).
21. J. W. Johnson, S. M. Antonov, T. S. Blanpied, and Y. Li-Smerin, "Channel block of NMDA receptor," in: *Excitatory Amino Acids and Synaptic Transmission*, H. V. Wheal (ed.), Academic Press Inc., London (1997), pp. 99–113.
22. J. W. Johnson and P. Ascher, "Glycine potentiates the NMDA response in cultured mouse brain neurons," *Nature*, **325**, 529–531 (1987).
23. W. Kauzmann, "Some factors in the interpretation of protein denaturation," *Adv. Protein Chem.*, **14**, 1–63 (1959).
24. H. Komuro and P. Pakic, "Modulation of neuronal migration by NMDA receptors," *Science*, **260**, 95–97 (1993).
25. R. Lester, J. D. Clements, G. L. Westbrook, and C. E. Jahr, "Channel kinetics determine the time course of NMDA receptor-mediated synaptic currents," *Nature*, **346**, 565–567 (1990).
26. R. A. J. Lester and C. E. Jahr, "NMDA channel behaviour depends on agonist affinity," *J. Neurosci.*, **12**, 635–643 (1992).
27. S. A. Lipton, "Prospects for clinically tolerated NMDA antagonists: open-channel blockers and alternative redox states of nitric oxide," *TINS*, **16**, 527–532 (1993).
28. A. B. MacDermott, M. L. Mayer, G. L. Westbrook, S. J. Smith, and J. L. Baker, "NMDA receptor activation increases cytoplasmic calcium concentration in cultured spinal cord neurones," *Nature*, **321**, 519–522 (1986).
29. S. Maren and M. Baudry, "Properties and mechanisms of long-term synaptic plasticity in the mammalian brain: relationships to learning and memory," *Neurobiol. Learn. Mem.*, **63**, 1–18 (1995).
30. L. Nowak, P. Bregestovski, P. Ascher, A. Herbert, and A. Prochiantz, "Magnesium gates glutamate-activated channels in mouse central neurones," *Nature*, **307**, 462–465 (1984).
31. C. G. Parsons, W. Danysz, and G. Quack, "Glutamate in CNS disorders as a target for drug development: an update," *Drug News Perspect.*, **11**, 523–569 (1998).
32. C. G. Parsons, W. Danysz, and G. Quack, "Memantine is a clinically well tolerated N-methyl-D-aspartate (NMDA) receptor antagonist – a review of preclinical data," *Neuropharmacology*, **38**, 735–767 (1999).
33. A. I. Sobolevsky, "Two-component blocking kinetics of open NMDA channels by organic cations," *Biochim. Biophys. Acta*, **1416**, 69–91 (1999).
34. A. Sobolevsky and S. Koshelev, "Two blocking sites of amino-adamantane derivatives in open N-methyl-D-aspartate channels," *Biophys. J.*, **74**, 1305–1319 (1998).

35. A. I. Sobolevsky, S. G. Koshelev, and B. I. Khodorov, "Probing of NMDA channels with fast blockers," *J. Neurosci.*, **19**, 10611–10626 (1999).
36. H. G. Traven, L. Brodin, A. Lansner, O. Ekeberg, P. Wallens, and S. Grillner, "Computer simulations of NMDA and non-NMDA receptor-mediated synaptic drive: sensory and supraspinal modulation of neurons and small networks," *J. Neurophysiol.*, **70**, 695–709 (1993).
37. A. Villarroel, N. Bernashev, and B. Sakmann, "Dimensions of the narrow portion of a recombinant NMDA receptor channel," *Biophys. J.*, **68**, 866–875 (1995).
38. V. S. Vorobjev, "Vibrodisssection of sliced mammalian nervous tissue," *J. Neurosci. Methods*, **38**, 145–150 (1991).
39. A. M. Woodhull, "Ionic blockage of sodium channels in nerve," *J. Gen. Physiol.*, **61**, 687–708 (1973).
40. M. M. Zarei and J. A. Dani, "Structural basis for explaining open-channel blockade of the NMDA receptor," *J. Neurosci.*, **15**, 1446–1454 (1995).